PANCREAS IMAGING ACROSS THE SPECTRUM

EDITED BY: Amelia K. Linnemann, Vincent Poitout and Guy A. Rutter
PUBLISHED IN: Frontiers in Endocrinology

frontiers Research Topics

ISSN 1664-8714
ISBN 978-2-88974-360-5
DOI 10.3389/978-2-88974-360-5

About Frontiers

Frontiers is more than just an open-access publisher of scholarly articles: it is a pioneering approach to the world of academia, radically improving the way scholarly research is managed. The grand vision of Frontiers is a world where all people have an equal opportunity to seek, share and generate knowledge. Frontiers provides immediate and permanent online open access to all its publications, but this alone is not enough to realize our grand goals.

Frontiers Journal Series

The Frontiers Journal Series is a multi-tier and interdisciplinary set of open-access, online journals, promising a paradigm shift from the current review, selection and dissemination processes in academic publishing. All Frontiers journals are driven by researchers for researchers; therefore, they constitute a service to the scholarly community. At the same time, the Frontiers Journal Series operates on a revolutionary invention, the tiered publishing system, initially addressing specific communities of scholars, and gradually climbing up to broader public understanding, thus serving the interests of the lay society, too.

Dedication to Quality

Each Frontiers article is a landmark of the highest quality, thanks to genuinely collaborative interactions between authors and review editors, who include some of the world's best academicians. Research must be certified by peers before entering a stream of knowledge that may eventually reach the public - and shape society; therefore, Frontiers only applies the most rigorous and unbiased reviews.
Frontiers revolutionizes research publishing by freely delivering the most outstanding research, evaluated with no bias from both the academic and social point of view. By applying the most advanced information technologies, Frontiers is catapulting scholarly publishing into a new generation.

What are Frontiers Research Topics?

Frontiers Research Topics are very popular trademarks of the Frontiers Journals Series: they are collections of at least ten articles, all centered on a particular subject. With their unique mix of varied contributions from Original Research to Review Articles, Frontiers Research Topics unify the most influential researchers, the latest key findings and historical advances in a hot research area! Find out more on how to host your own Frontiers Research Topic or contribute to one as an author by contacting the Frontiers Editorial Office: frontiersin.org/about/contact

PANCREAS IMAGING ACROSS THE SPECTRUM

Topic Editors:
Amelia K. Linnemann, Indiana University, United States
Vincent Poitout, Université de Montréal, Canada
Guy A. Rutter, Imperial College London, United Kingdom

Citation: Linnemann, A. K., Poitout, V., Rutter, G. A., eds. (2022). Pancreas Imaging Across the Spectrum. Lausanne: Frontiers Media SA.
doi: 10.3389/978-2-88974-360-5

Table of Contents

frontiers in Endocrinology

EDITORIAL
published: 03 January 2021
doi: 10.3389/fendo.2021.832519

Editorial: Pancreas Imaging Across the Spectrum

Amelia K. Linnemann[1,2]*, *Vincent Poitout*[3,4] *and Guy A. Rutter*[3,4,5,6]

[1] Department of Pediatrics, Herman B Wells Center for Pediatric Research, Indiana University School of Medicine, Indianapolis, IN, United States, [2] Indiana Center for Diabetes and Metabolic Diseases, Indiana University School of Medicine, Indianapolis, IN, United States, [3] Montreal Diabetes Research Center, Centre hospitalier de l'Université de Montréal, Montreal, QC, Canada, [4] Department of Medicine, Université de Montréal, Montreal, QC, Canada, [5] Department of Metabolism, Digestion and Reproduction, Imperial College London, London, United Kingdom, [6] Lee Kong Chian School of Medicine, Nanyang Technological University, Singapore, Singapore

Keywords: islet, pancreas, imaging, *in vivo* imaging, optical imaging, MRI

Editorial on the Research Topic

Pancreas Imaging Across the Spectrum

The pancreas serves two principal roles: the secretion of digestive enzymes from acinar cells and the release of metabolically critical hormones, notably insulin and glucagon, from the endocrine compartment. The latter is formed of discrete structures, the islets of Langerhans, which usually comprise < 2% of the whole mass of the gland. For many years, the bulk of what we knew and understood about the pancreas, and in particular the endocrine pancreas in situ, was garnered primarily from a combination of *ex vivo* analyses of isolated pancreatic islets and post-mortem tissue analyses of rodent pancreata. Recently, however, unprecedented access to human tissues, combined with an ever-evolving myriad of novel techniques for pancreas visualization, have revolutionized our understanding of the pancreas in both normal and diseased states. The *Pancreas Imaging Across the Spectrum* Research Topic contains a collection of review and original research articles that highlight this revolution, and provides a glimpse into the state-of-the-art advances in our understanding of pancreas morphology and function enabled by these technical innovations.

Magnetic resonance imaging (MRI) has long been used for clinical imaging, and its application to imaging pancreatitis has become routine standard of care in the 21st century. In the first article of the Research Topic, Virostko comprehensively discusses recent advances in quantitative MRI and their application to studying the pancreas of individuals with diabetes. Importantly, he highlights efforts to standardize the imaging and processing pipelines to allow efficient quantitative analysis of pancreas heterogeneity, a necessity as the field continues to develop and as large multi-site clinical trials proceed for diabetes treatment and prevention.

Developing a clear understanding of how the pancreas ultrastructure changes during diabetes pathogenesis requires effective analysis of pancreas structure and function in the *in vivo* setting. Many features of the intact pancreas, including both the vasculature and innervation, are disrupted upon isolation of pancreatic islets for analysis. Some of these components remain relatively intact upon isolation of the entire pancreas, but are then disrupted as only a small section of the tissue is processed in most immunohistochemistry or immunocytochemistry analyses. Therefore, much of what we know about pancreas ultrastructure is based on only a partial picture. The fundamental anatomy of the normal pancreas is outlined in a series of papers within this Research Topic. In the first, Gonçalves and Almaça utilize living human pancreas slices from nondiabetic organ donors to demonstrate responsiveness of the human islet vasculature to a variety of stimuli. They couple these observations to parallel analyses of islet

OPEN ACCESS

Edited by:
Jeff M. P. Holly,
University of Bristol, United Kingdom

***Correspondence:**
Amelia K. Linnemann
aklinnem@iu.edu

Specialty section:
This article was submitted to Diabetes: Molecular Mechanisms, a section of the journal Frontiers in Endocrinology

Received: *09 December 2021*
Accepted: *10 December 2021*
Published: *03 January 2021*

Citation:
Linnemann AK, Poitout V and Rutter GA (2021) Editorial: Pancreas Imaging Across the Spectrum. Front. Endocrinol. 12:832519. doi: 10.3389/fendo.2021.832519

calcium oscillations, thus supporting the utility of this approach for valuable insight into pancreas structure-function relationship. Our understanding of human islet microvasculature is further discussed in a review by Dybala and Hara, highlighting both the advances and limitations in the recent literature, and forecasting where the field may be headed using novel technologies. Finally, pancreatic innervation is also disrupted in many approaches, and structure-function analyses have historically been extraordinarily difficult to perform in intact pancreata. Makhmutova and Caicedo discuss this concept in a review article, alongside what we know regarding the complexity of pancreas innervation. They describe novel optogenetic and pharmacological tools that when combined with newly available imaging modalities, have provided significant insight into our basal understanding of pancreas innervation.

Optical clearing methods have been used broadly to study intact tissues and organs, enabling large scale 3D images of tissues in both normal and diseased states. At the level of the whole pancreas, optical clearing approaches are particularly advantageous, and, as described by Campbell-Thompson and Shiue-Cheng Tang, have been bolstered in recent years by the availability of high-powered microscopes capable of imaging the cleared tissue at incredible depth and resolution. These imaging approaches, described as mesoscopic imaging by Alanentalo et al., have contributed significantly to our understanding of pancreas anatomy at both the cellular and molecular level.

Evaluation of pancreatic islet function and plasticity is critical to our understanding of disease pathogenesis. While live cell imaging in the *in vitro* context enables quantitative analysis of dynamic function, this widely used approach is limited by the removal of the islet from its endogenous niche. Disrupting the extensive network of vasculature, innervation, and exocrine spatial relationship with the islets limits the applicability of the observations to relevant physiologic function. Many have turned to islet xenograft and allograft models, including islet transplants into the anterior chamber of the eye, as discussed by Ilegems and Berggren. This site, in particular, has proven to be an excellent location for islet engraftment, enabling revascularization and innervation of the graft, thus allowing longitudinal imaging of islets over long periods of time and providing an unprecedented window into physiologically relevant functional changes during diabetes development.

Finally, the future of clinical application of advances in the field will only be as good as our ability to monitor the effects of novel therapeutics in the *in vivo* setting. Beta cells contain high levels of Zn^{2+}, an essential element for the proper processing, storage, and release of insulin. Therefore, Zn^{2+} is of significant interest for the spatial and functional identification of beta cells. Two articles in this Research Topic are focused on the use of agents to monitor zinc release from individual beta cells in the *in vivo* setting. The first, by Chen et al., describes the *in vivo* visualization of a systemically delivered fluorescent granule zinc indicator, ZIGIR. Using this approach, the authors are able to visualize oscillatory release of Zn^{2+} from mouse islet beta cells *in vivo* at cellular resolution. Clavijo Jordan et al. further capitalize upon the use of Zn^{2+} for translational studies in non-human primates, a clear advance towards clinical application of this type of indicator. They utilize a Gd-based zinc sensor, Gd-CP027, as a contrast agent and demonstrate its utility for monitoring functional changes in the pancreas non-invasively using MRI-based imaging.

Collectively, the studies presented within this Research Topic highlight the significant advances afforded by the leaps in imaging capabilities that have been made within the last decade. By applying these technologies, we have now begun to gain an understanding of endogenous pancreas structure and how it relates to function in normal and diseased states. Although important hurdles remain – notably the identification of a robust means to image islet cell mass and hormone secretion non-invasively in man – the furious pace of development in this realm holds significant promise for enabling novel approaches to understand the changes leading up to and after the onset of diabetes and other pancreatic diseases. These seem likely to ensure that the next decade will be just as exciting for moving the field forward.

AUTHOR CONTRIBUTIONS

This editorial was written by AL and revised and approved by VP and GR. All authors contributed to the article and approved the submitted version.

Conflict of Interest: The authors declare that the research was conducted in the absence of any commercial or financial relationships that could be construed as a potential conflict of interest.

frontiers in Endocrinology

REVIEW
published: 04 December 2020
doi: 10.3389/fendo.2020.592349

Quantitative Magnetic Resonance Imaging of the Pancreas of Individuals With Diabetes

John Virostko [1,2,3]*

[1] Department of Diagnostic Medicine, University of Texas at Austin, Austin, TX, United States, [2] Livestrong Cancer Institutes, University of Texas at Austin, Austin, TX, United States, [3] Department of Oncology, University of Texas at Austin, Austin, TX, United States

Magnetic resonance imaging (MRI) has the potential to improve our understanding of diabetes and improve both diagnosis and monitoring of the disease. Although the spatial resolution of MRI is insufficient to directly image the endocrine pancreas in people, the increasing awareness that the exocrine pancreas is also involved in diabetes pathogenesis has spurred new MRI applications. These techniques build upon studies of exocrine pancreatic diseases, for which MRI has already developed into a routine clinical tool for diagnosis and monitoring of pancreatic cancer and pancreatitis. By adjusting the imaging contrast and carefully controlling image acquisition and processing, MRI can quantify a variety of tissue pathologies. This review introduces a number of quantitative MRI techniques that have been applied to study the diabetic pancreas, summarizes progress in validating and standardizing each technique, and discusses the need for image analyses that account for spatial heterogeneity in the pancreas.

Keywords: MRI, volume, relaxometry, perfusion, type 2 diabetes, type 1 diabetes, diffusion, radiomic

OPEN ACCESS

Edited by:
Guy A. Rutter, Imperial College London, United Kingdom

Reviewed by:
Amelia K. Linnemann, Indiana University, United States
Marcia Hiriart, National Autonomous University of Mexico, Mexico

***Correspondence:**
John Virostko
jack.virostko@austin.utexas.edu

Specialty section:
This article was submitted to Diabetes: Molecular Mechanisms, a section of the journal Frontiers in Endocrinology

Received: *06 August 2020*
Accepted: *28 October 2020*
Published: *04 December 2020*

Citation:
Virostko J (2020) Quantitative Magnetic Resonance Imaging of the Pancreas of Individuals With Diabetes. Front. Endocrinol. 11:592349. doi: 10.3389/fendo.2020.592349

INTRODUCTION

Recent advances in magnetic resonance imaging (MRI) technology have improved pancreas imaging, surmounting some of the difficulties inherent to the small, irregular shape of the pancreas, and its challenging location and susceptibility to motion. MRI of the pancreas has emerged into a valuable clinical tool for characterizing a number of pancreatic diseases. The staging and diagnosis of both acute (1) and chronic (2) pancreatitis often includes MRI. Furthermore, MRI can detect focal pancreatic lesions, and is employed clinically in both diagnosis of pancreatic cancer (3) and monitoring of therapeutic response (4). However, to date, MRI of the pancreas has had relatively limited impact on the study or management of diabetes. This likely stems in part from the established paradigm that diabetes effects only the endocrine pancreas, or islets, which are too small to be imaged by MRI. However, the involvement of exocrine pancreas in T1D and T2D is of renewed interest, as reviewed by Alexendra-Heymann et al. (5). As glucose, hormones, and other measures of glycemic control can be assessed using blood or urine tests, there may be an assumption that imaging is unnecessary. Indeed, two fields in which imaging has entered standard clinical practice, neurology and oncology, are both characterized by difficulty in directly assaying the tissue of interest and/or the absence of blood biomarkers. But while blood tests will likely always be the cornerstone of diabetes management, they are subject to important limitations. For instance, testing

of A1C is hampered by standardization issues, poor sensitivity, and a lack of correlation with some pathophysiological hallmarks of diabetes (6). In type 1 diabetes (T1D), fasting hyperglycemia presents only after destruction of a majority of beta cells (7), suggesting that blood tests are a lagging indicator of beta cell loss due to a high insulin reserve. Circulating autoantibodies signify risk for T1D, but their presence can be transient and time to progression after autoantibody presentation is highly variable (8). These limitations and other aspects of diabetes care currently not well characterized by blood tests may be addressed in part by medical imaging.

This review focuses on quantitative MRI techniques and their application to study the pancreas in both type 1 and type 2 diabetes (T2D). These techniques are summarized in **Table 1**. Quantitative MRI refers to the objective measurement of parameters derived from digital images that characterize tissue attributes (9). This contrasts with the traditional qualitative assessment typically performed in standard radiology practice. Importantly, quantitative MRI techniques can map the entire pancreas, and thus identify regions of the pancreas with altered properties. This ability to interrogate spatial variation is significant, as histological studies have shown that the insult characteristic of both T1D (10) and T2D (11, 12) can differ across the pancreas. Furthermore, quantitative MRI parameters can be standardized across multiple sites for incorporation into clinical trials, and ultimately used to guide clinical practice. However, in order for quantitative MRI to be adopted to study the diabetic pancreas, the biological underpinnings of imaging results must be validated against gold standard measurements and techniques must be repeatable and reproducible across imaging centers. This review highlights a range of quantitative MRI parameters that may improve our understanding of the diabetic pancreas, benchmarks each technique's progress in validation and standardization, and concludes with a discussion of image analyses that can accurately characterize pancreas heterogeneity.

PANCREAS VOLUME

Owing to its exquisite soft tissue contrast, MRI can delineate pancreas borders from neighboring organs, which can in turn be used to quantify pancreas size. The pancreas has long been known to be smaller in type 1 diabetes (13) and more recently in type 2 diabetes as well (14). A meta-analysis validated these findings across multiple studies and found smaller pancreas size in T1D than T2D (15). Of note, the degree of pancreas reduction in both type T1D and T2D far exceeds the volume of the endocrine pancreas, suggesting exocrine involvement in diabetes pathogenesis. These imaging findings are supported by histological studies of the pancreas from T1D donors which found reduced numbers of acinar cells (16) and altered exocrine cell expression (17) versus controls. Investigations into the temporal dynamics of pancreas size in T1D have found reduced pancreas size at diagnosis (18, 19), in individuals at risk for disease (20, 21), and longitudinal declines over the course of disease (20). Example images demonstrating the longitudinal decline seen in pancreas size in one individual with T1D is shown in **Figure 1**. Taken together, these studies suggest that alterations in pancreas size may be an early hallmark of T1D risk and may correlate with disease progression.

The relationship between pancreas volume and beta cell mass or function remains unclear. An islet transplantation study found a direct correlation between pancreas size and islet yield, and that this relationship was dependent on donor HbA1c (22). This suggests that pancreas size may reflect a combination of islet mass and function. Pancreas volume measurements performed using MRI display high accuracy, repeatability, and reproducibility. Porcine pancreas volume calculated from MRI demonstrated excellent correlation with gold standard water displacement measurements (23), indicating the accuracy of the technique. Furthermore, in human subjects who received MRI scans in quick succession, measurements of pancreas

TABLE 1 | Quantitative magnetic resonance imaging (MRI) techniques.

MRI Technique	Pancreas Pathology Interrogated	Change in T1D	Change in T2D	Biological Confounders	Technical Confounders
Anatomical MRI	Pancreas Volume	↓↓	↓	Age; weight	
Fat Fraction Mapping	Fat infiltration	↔	↑	Age, sex, visceral adiposity	MRI acquisition; pancreas heterogeneity
Longitudinal Relaxation (T1)	Fibrosis	?	?	Age	MRI acquisition; magnetic field strength; pancreas heterogeneity
Extracellular Volume Fraction (ECV)	Fibrosis	?	↑		MRI acquisition; contrast agent administration; magnetic field strength; pancreas heterogeneity
Diffusion-Weighted Imaging (DWI)	Cell density; membrane integrity; fibrosis	↑	?	Age, sex	MRI acquisition; magnetic field strength; pancreas heterogeneity
Dynamic Contrast-Enhanced (DCE)	Perfusion; vascular permeability	?	↑		MRI acquisition; contrast agent administration; processing technique; pancreas heterogeneity
Arterial Spin Labeling (ASL)	Perfusion	?	?		MRI acquisition; pancreas heterogeneity
Incoherent Intravoxel Motion (IVIM)	Microvascular perfusion	?	?		MRI acquisition; processing technique
Blood Oxygen Level Dependent (BOLD)	Perfusion; oxygen consumption	?	?		
Magnetic Resonance Elastography (MRE)	Stiffness; fibrosis	?	↑	Age	MRI acquisition; processing technique

↑ = *increase;* ↓ == *decrease;* ↔ = *no change;* ? = *unknown.*

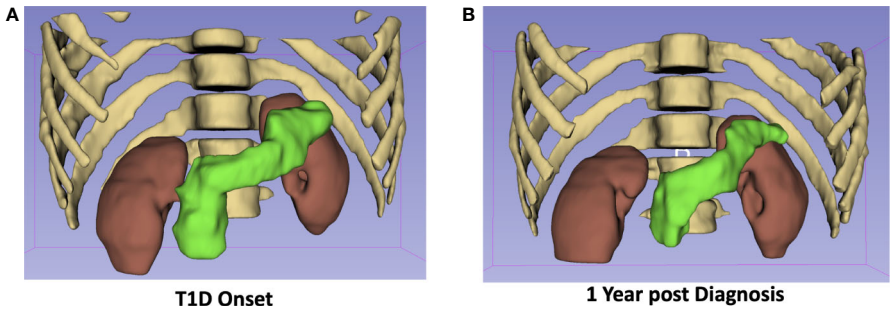

FIGURE 1 | The pancreas of a 19-year-old male at diagnosis with T1D **(A)** is 25% smaller one-year post diagnosis **(B)**. The pancreas is displayed in green with the kidneys, ribs, and spine shown for anatomical context.

volume were highly repeatable (24, 25). Pancreas borders can be difficult to delineate, which may lead to reader subjectivity in pancreas volume measurements. However, reproducibility across multiple readers reveals good agreement between two readers outlining the same image (24, 25). One caveat is that pancreas volume changes over the course of the human lifespan in the absence of disease, with rapid increases in size over childhood and pancreas atrophy in later life (14). Current quantification of pancreas size typically normalizes to body weight or surface area to account for these dynamics in pancreas size over the lifespan. Other factors that account for the large variations in pancreas volume seen between individuals are currently not known, but warrant further investigation.

FAT FRACTION MAPPING

MRI can measure the fat composition of tissue, as protons associated with fat and water spin with slightly different frequencies. Thus, their relative concentrations in a voxel (a portmanteau of "volume element", i.e., a three-dimensional pixel) of interest are relatively easy to separate. The relationship between pancreatic fat deposition and diabetes has been demonstrated in rodent models, in which ectopic fat accumulation leads to beta cell dysfunction (26). Similarly, MRI studies of people with T2D have demonstrated higher pancreatic fat associated with reduced beta cell function (27, 28). However, a number of other studies have failed to find a correlation between T2D and pancreatic fat content (29, 30). MRI may be sensitive to declines in pancreatic fat content. A study of diet-induced reversal of T2D found that diabetes reversal was accompanied by a decline in pancreatic fat fraction (31). Furthermore, pancreatic fat content may be increased in individuals at risk for developing T2D (32, 33) (**Figure 2**). In contrast with studies of T2D, MRI measures of pancreatic fat content are not altered in T1D (34), although some autopsy studies have found fatty infiltrate in the pancreas of T1D donors.

In terms of standardization and validation, fat fraction measurements are relatively advanced, owing in part to the simplicity of the technique and the availability of standard processing tools from MRI vendors. Histological measures of fat content from resected pancreata and MRI quantification of fat fraction demonstrate excellent agreement (35). Furthermore, test-retest measurements of pancreatic fat content calculated using MR spectroscopy were found to be repeatable (36). However, a meta-analysis of five studies of pancreatic fat content in T2D demonstrated high heterogeneity in fat measurements between studies (15). As is typical of MRI techniques, the acquisition and processing used to calculate the

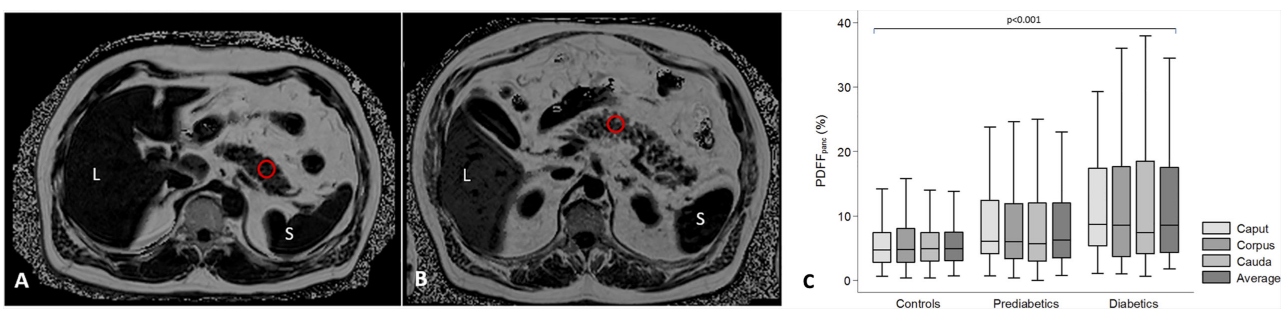

FIGURE 2 | Assessment of pancreatic fat content in subjects with lower **(A)** and higher **(B)** pancreatic fat content. Pancreatic fat content was measured as proton-density fat fraction ($PDFF_{panc}$) in a region of interest (red circle). L = liver; S = spleen. **(C)** Differences of pancreatic fat content between controls, subjects with prediabetes and diabetes displayed by box-and-whisker. Figure adapted from Heber et al. (32) under a Creative Commons License.

fat fraction may impact the measurement (37), and may account for some of the differences seen between studies. Additionally, there exist regional variations in fat fraction throughout the pancreas, with different values in the head, body, and tail (38) (**Figure 2**). Finally, pancreatic fat content can be influenced by age, sex, and visceral adipose tissue (32). These demographic factors must be carefully accounted for when examining pancreatic fat content in individuals with diabetes. Unfortunately, reference standards for pancreatic fat content and its relationship with demographic factors are not well established at present.

RELAXOMETRY

Longitudinal Relaxation (T1)

Generation of an MR image relies on perturbation (or tipping) of protons from the main magnetic field by a radiofrequency pulse. Longitudinal relaxation refers to the return of these perturbed protons to their equilibrium state. The relaxation rate for each voxel within an image is a function of the intrinsic tissue parameters and is quantified by the time constant T1 (not to be confused with T1D). This is the basis for so called T1-weighted images, in which fat, injected contrast agents, and tissues with high protein content appear bright. Of note, the pancreas appears bright on a T1-weighted image, presumably due to the presence of high levels of aqueous protein in the acinar cells (39). In addition to qualitative T1-weighted images, one can employ a variety of techniques to quantify the T1 value characteristic of each voxel (40). Quantitative T1 mapping of the pancreas has demonstrated increased T1 in chronic pancreatitis (41), suggested that T1 may be sensitive to pancreatic inflammation. In studies of individuals with T2D, the T1 value was found to be higher than controls and correlated with HbA1c in one study (42). In contrast, another study found lower T1 values in T2D, although these values were also significantly different than controls (43). The T1 of the pancreas in individuals with prediabetes is also increased (44) (**Figure 3**), suggesting that the alterations responsible for prolonged longitudinal relaxation may occur early in the development of T2D.

Validation and standardization of T1 measurements of the pancreas are underway. The foremost hurdle is determining the specific pancreas pathology reflected by T1 measurements. In the heart, histological measurements of fibrosis have correlated with T1 (45). Similar studies of resected pancreas are limited but have shown correlation of T1 with grade of pancreatic fibrosis (46). Standardization of T1 measurements must take into account known correlations between pancreas T1 values and age (47), although these associations have not been seen in all studies (48). Additionally, there is a known dependence of T1 on magnetic field strength of the MRI scanner (47). Finally, there are a variety of different techniques used to generate T1 maps. These methods display some discrepancies when applied to image the pancreas of the same individual (49). Further work is needed to standardize T1 mapping techniques for application to the pancreas.

Extracellular Volume Fraction (ECV)

Contrast agents are often used to alter tissue enhancement on MR images. These contrast agents are typically paramagnetic agents which shorten T1, thus leading to enhancement of tissues with high contrast agent perfusion. This technique is commonly used in oncological imaging, where well vascularized tumors "light up" after contrast agent administration. By examining changes in T1 maps in both the tissue of interest and blood and coupling it with the hematocrit, the extracellular volume fraction (ECV) can be calculated. ECV has been developed primarily for cardiac MRI applications, and has been found to be sensitive to a number of cardiomyopathies (50). In the pancreas, ECV has been shown to increase with increasing grade of chronic pancreatitis (51). ECV of the pancreas is also higher in individuals with T2D and, similar to native T1 maps, correlates with HbA1c (42).

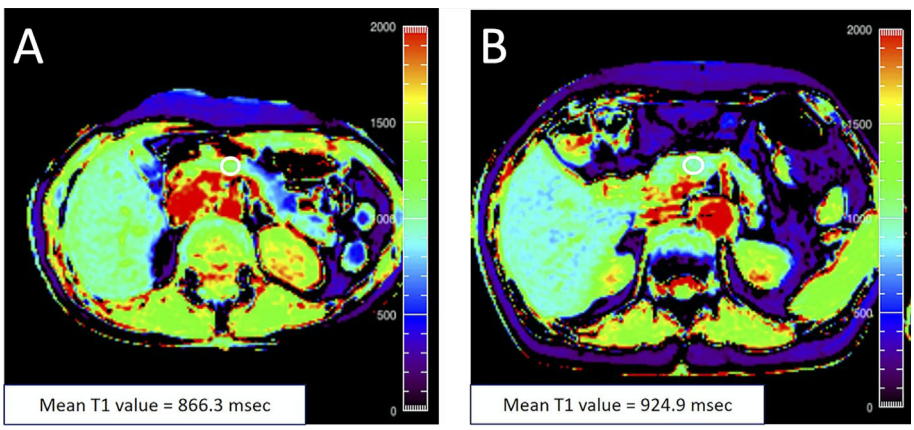

FIGURE 3 | **(A)** A 48-year-old female with an HbA1c value of 5.5% with T1 map displayed in rainbow color shows the mean pancreatic T1 value of 866.3 msec. **(B)** A 76-year-old female with an HbA1c value of 6.0% with T1 map displayed in rainbow color shows the mean pancreatic T1 value of 924.9 msec. The white circle in each panel indicates a regions-of-interest (ROI) manually placed in the pancreas. Figure adapted from reference (44) with permission, © 2020 John Wiley & Sons, Inc.

The biological basis for increased ECV in the pancreas in diabetes is assumed to be due fibrosis. However, while MRI has demonstrated correlation between fibrosis and ECV in the heart (52), similar correlation of imaging and pathology are lacking in the pancreas. ECV values in the pancreas do not appear to be influenced by age or sex (47). The repeatability and reproducibility of ECV measurements have been established in the myocardium. These studies have demonstrated general agreement, although as with non-contrast enhanced T1 measurements, the technique used for quantification can impact the result (53). Of note, ECV requires administration of a contrast agent containing gadolinium, which has been the subject of recent concerns over long term brain retention.

DIFFUSION-WEIGHTED IMAGING (DWI)

Diffusion-weighted imaging (DWI) measures the random Brownian motion of water molecules within a voxel. In biological tissue, DWI reflects an amalgamation of cell density, cell membrane integrity, and viscosity. DWI can be quantified by adjusting the diffusion weighting (commonly referred to as the b-value) of two images and comparing their intensities to yield the apparent diffusion coefficient (ADC). While early applications of DWI were primarily limited to the brain due to long imaging times, advances in MRI hardware and processing have reduced acquisition times for abdominal imaging. In the pancreas, MRI has proven useful for detecting and characterizing malignant pancreatic masses (54), similar to the success of DWI in other oncological applications. Furthermore, in chronic pancreatitis the ADC value has been found to be reduced compared with controls (55). Applications of DWI to study the diabetic pancreas are limited. One study found reduced ADC in individuals with fulminant T1D (55). Our study of individuals with recent onset T1D did not find differences in ADC versus controls when measurements were averaged throughout the pancreas (20). However, we did find altered distributions of ADC in the pancreas in T1D, with an increased number of voxels with high ADC values in T1D. These areas of high ADC (corresponding to areas of increased water diffusion, and presumably inflamed tissue) were found in focal areas in the pancreas in T1D at a greater rate than control pancreas (**Figure 4**). In individuals with suspected pancreatic disease, a negative correlation was found between pancreatic ADC and HbA1c (56). In addition to ADC, DWI can be quantified using other metrics. For instance, diffusion kurtosis can be calculated by assuming non-Gaussian Brownian motion and acquiring DWI with strongly diffusion-weighted images (higher 'b-values'). This kurtosis is thought to reflect the restriction of water diffusion by cell membranes and other tissue microstructure. Similar to ADC, diffusion kurtosis was found to correlate with HbA1c, with higher kurtosis in the group with highest HbA1c (56).

As DWI is a mixed measure that reflects a number of tissue parameters influencing water diffusion, the biological basis in the pancreas is still under investigation. One study of resected pancreas found reduced ADC in more fibrotic tissue (46), presumably reflecting increased cellular density in fibrous tissue. The ADC in healthy pancreas appears to display regional variation over the pancreas, with highest values in the pancreas head and lowest values in the body (57). ADC values are also influenced by age and sex (58). A study across multiple MRI scanners found that ADC measures of the pancreas are generally reproducible, although, similar to T1 measurements, ADC is influenced by magnetic field strength (59). Measurement of ADC in the pancreas is likewise influenced by the acquisition scheme. DWI acquired with higher diffusion weighting (higher b-values) results in a higher calculated ADC (60). Thus, accurately quantifying DWI of the diabetic pancreas requires standardization of image acquisition and normalization for pancreas anatomy and patient demographics.

PERFUSION

The endocrine pancreas is characterized by a dense network of capillaries, which receive a significantly higher rate of blood flow

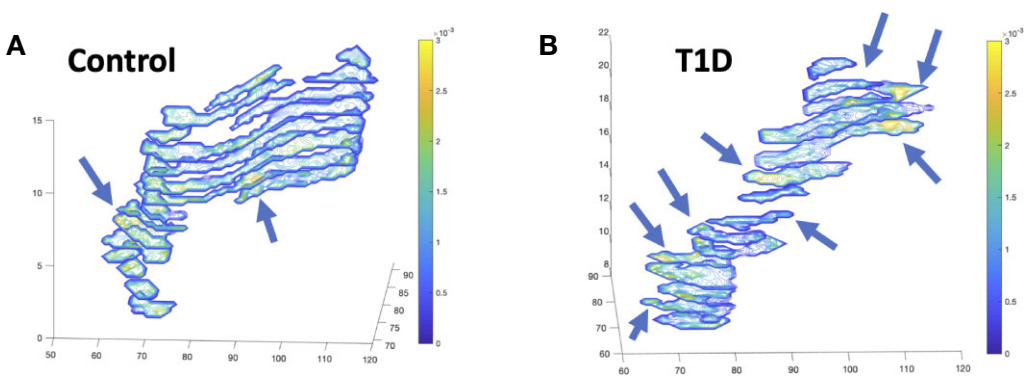

FIGURE 4 | Diffusion-weighted imaging (DWI) of the pancreas of a control **(A)** and individual with recent-onset T1D **(B)** displays focal alterations in the apparent diffusion coefficient (ADC), designated with arrows, with more focal areas of increased diffusion in T1D. Images display contiguous slices spanning the pancreas pseudo colored with contour plots according to the ADC value according to the ADC value in units of mm^2/s.

than exocrine tissue (61). Alterations in islet vasculature have been found in the pancreas of organ donors with both T1D (62) and T2D (63). Thus, there is intense interest in studying islet blood flow and measuring it non-invasively in humans. MRI is widely used clinically to measure cerebral and myocardial perfusion. Four different MRI techniques for measuring perfusion are introduced below along with implications for pancreas imaging.

Dynamic Contrast-Enhanced MRI (DCE-MRI)

Dynamic contrast-enhanced MRI (DCE-MRI) relies upon acquisition of T1-weighted MR images after injection of a paramagnetic contrast agent. For further information on T1-weighting and MR contrast agents, please refer back to *Longitudinal Relaxation (T1)* and *Extracellular Volume Fraction (ECV)*, respectively. These contrast agents traverse through the vascular network and extravasate out of permeable vessels. The "dynamic" nature of this technique is derived from the acquisition of serial images over the time course of contrast agent distribution. The resultant time activity curves for each voxel in the image can be analyzed using pharmacokinetic models to yield estimates of perfusion parameters (64). DCE-MRI has shown promise for imaging pancreatitis (65) and tracking response of pancreatic cancer to therapy (66). A study of DCE-MRI in individuals with T2D found increased vascular permeability but lower plasma volume in the pancreas (**Figure 5**), and that the magnitude of these perfusion changes increased with longer disease duration (67). A later study was unable to replicate these findings, and also did not determine an effect of glucose bolus on DCE-MRI parameters (43).

Correlation of DCE-MRI parameters and pathology has been performed in pancreas sections resected from individuals with pancreatic cancer. This analysis found correlation between DCE parameters and both fibrosis and microvascular density (68). Repeatability and reproducibility of DCE-MRI has been notoriously difficult to both measure and improve, as measurements can be influenced by acquisition parameters, choice of pharmacokinetic model, and contrast agent administration protocol. One study of repeatability in the pancreas found variability of 21% and also measured regional variations in the pancreas head, body, and tail (69). As with ECV measurements, contrast agent safety can be a concern when imaging in young individuals or performing repeat scans.

Arterial Spin Labeling (ASL)

Concerns over contrast agent injection have spurred the development of MRI techniques sensitive to perfusion that do not require exogenous sources of contrast. One such technique is known as arterial spin labeling (ASL) which magnetically labels blood flowing through a plane containing feeding blood vessels and images the resultant distribution of this tagged blood volume. ASL has demonstrated the ability to image increases in pancreas perfusion due to secretin (70), a hormone known to induce pancreatic fluid and bicarbonate secretion. Similarly, ASL of the pancreas has measured increased pancreas perfusion in response to glucose bolus (71). A study performing ASL during hyperglycemic clamp did not detect a difference between individuals with T1D and controls (72). However, ASL has been subject to a number of recent technological advances and continues to rapidly improve.

There have not been studies comparing ASL measurements in the pancreas to pathology. However, comparisons between DCE-MRI derived perfusion with those from ASL display strong agreement (73). Thus, ASL may also reflect microvascular density throughout the pancreas. Of note, this parameter may vary across the pancreas, as ASL measurements found differences in the pancreas heady, body, and tail (74). The repeatability of ASL in the pancreas is moderate (70). Further work is needed to define the reproducibility of ASL across different MRI scanners and establish standardized acquisition and processing schemes.

Intravoxel Incoherent Motion (IVIM)

In previous discussion of diffusion-weighted MRI (Section 5), we noted that Brownian motion can be analyzed as having non-Gaussian distribution. While analyzing high b-value data yields diffusion kurtosis measurements, fitting non-Gaussian diffusion using low b-value data yields intravoxel incoherent motion (IVIM). IVIM is thought to be sensitive to the microscopic perfusion of capillaries (75). In pancreas imaging, IVIM may help characterize benign versus malignant pancreas lesions (76). While we are not aware of studies of IVIM in individuals with diabetes, IVIM has demonstrated correlation with glucose stimulated perfusion increases in porcine models (77). Future

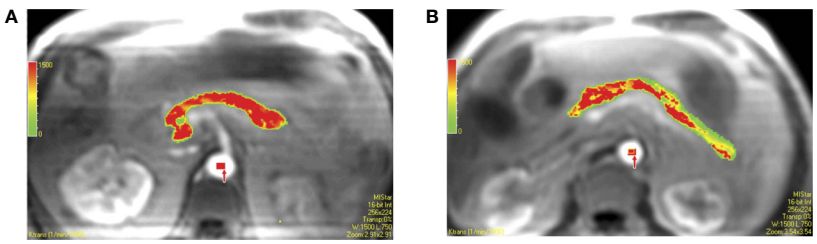

FIGURE 5 | Pixel-by-pixel color maps for transfer constant obtained with region of interest analysis. Calculated values of each pixel in region of interest can be seen in colors (red, yellow, and green are high, middle, and low values, respectively). **(A)** Color map in 61-year-old male coronary artery disease patient with type 2 diabetes shows a mean transfer constant = 1.291 min^{-1}. **(B)** Color map in 54-year-old male coronary artery disease patient without type 2 diabetes shows a mean transfer constant = 0.787 min^{-1}. Figure reproduced from reference (67) with permission, © 2009 RSNA.

studies examining response to glucose in diabetes using IVIM are warranted.

The biological basis of IVIM in the pancreas has been demonstrated to derive from the blood component using blood suppression techniques (78). Furthermore, IVIM parameters agree with PET and microsphere measurements of pancreas perfusion (77). Repeatability and reproducibility of pancreas IVIM is influenced by both image acquisition and processing techniques (79). Currently, acquisition and processing of IVIM are complex techniques which are not well standardized across studies.

Blood Oxygen Level Dependent (BOLD)

BOLD imaging is widely used in neuroscience to image brain activity. BOLD reflects the accumulation of deoxyhemoglobin in response to oxygen consumption (which in the brain is posited to be a surrogate for neural activation). Fewer BOLD applications have been performed outside the central nervous system, although there are studies exploring renal oxygenation using BOLD (80). Similarly to IVIM, studies in individuals with diabetes are lacking, but there is a report showing alterations in BOLD MRI in the pancreas after glucose ingestion (81).

Decades after its first use, the biological basis of BOLD MRI is still under investigation. The biological correlate of BOLD signal in the pancreas, as well as its repeatability and reproducibility are not well characterized.

MAGNETIC RESONANCE ELASTOGRAPHY (MRE)

Magnetic resonance elastography (MRE) consists of imaging performed while a tissue is subjected to high frequency vibrations. MRE interrogates the movement of vibration-induced shear waves through the body; these waves move slower in stiffer tissues. The primary clinical application of MRE currently is detecting fibrosis and cirrhosis in chronic liver disease. Applications to the pancreas are limited by the small size of the pancreas, but have found increased stiffness in chronic pancreatitis (82). Similar to perfusion measurements, MRE has been performed after glucose bolus which led to pancreas stiffening (83). Additionally, individuals with diabetes have been found to have higher pancreas stiffness than controls (84), as shown in **Figure 6**.

Histological studies of resected pancreata found a correlation between MRE-derived stiffness and both fibrosis and acinar atrophy (85). MRE measurements of pancreas stiffness are repeatable in test-retest studies, but are dependent on the vibration frequency used (83) and the age of the individual (86).

RADIOMICS: ACCOUNTING FOR HETEROGENEITY THROUGHOUT THE PANCREAS

MRI of the pancreas interrogates the complex structure of the pancreas encompassing islets, acinar cells, and the ductal network. There are known differences across the pancreas in the relative concentration of these components, with higher relative numbers of islet in the pancreas tail (87). A common theme throughout the MRI techniques introduced in this review is that they were frequently different in the pancreas head, body, and tail of the same individual. This was seen for measurements of fat fraction (38), diffusion (57), and perfusion measured by DCE (69) or ASL (74). Furthermore, spatial heterogeneity of the pancreas is further altered in diabetes, as has long been appreciated in autopsy studies of the pancreas from donors with diabetes (88). In T1D, there is marked spatial heterogeneity in the presence of the immune infiltrate characteristic of T1D (10) as well as individuals at risk for disease (89). Similarly, the islet amyloids and corresponding exocrine fibrosis found in T2D show lobular distribution throughout the pancreas (11, 12). The heterogeneity of quantitative MRI parameters throughout the pancreas is evident in **Figures 2**–**6**.

The spatial heterogeneity in MRI measures of the pancreas in general, and in the diabetic pancreas specifically, has important implications when quantifying MRI parameters. MRI analysis is commonly performed using a regions-of-interest (ROI) placed over a section of the pancreas, as demonstrated in **Figures 2** and **3**. However, in a mosaic tissue such as the pancreas the choice of ROI placement can influence the parameter of interest. An ROI placed in the same individual's pancreas may have significantly different values if it is placed in the pancreas head versus tail.

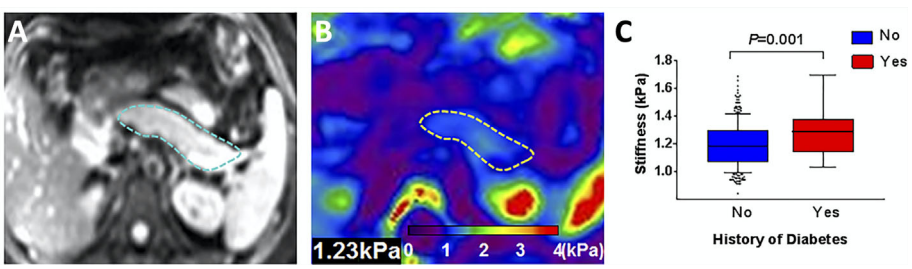

FIGURE 6 | Representative pancreatic axial magnitude images (**A**, pancreas outlined in blue) and elastograms (**B**, pancreas outlined in yellow). Box plot in **(C)** compares pancreas stiffness in individuals with a history of diabetes versus controls. Figure adapted from reference (84) with permission, © 2020 John Wiley & Sons, Inc.

TABLE 2 | Pancreas magnetic resonance imaging (MRI) analysis techniques.

Technique	Advantages	Disadvantages
Region-of-interest	Easy to implement; fast; can avoid ductal structures and organ borders	Placement affects quantification; does not capture anatomical heterogeneity
Whole pancreas averaging	Not subject to reader placement; captures all regions of the pancreas	Averages ductal structures and organ borders; may average out sparse alterations; requires capturing entire pancreas in field of view
Radiomics	Quantifies anatomical heterogeneity; identifies anatomical regions with different properties ("habitats")	Difficult to implement; High dimensionality of data can result in overfitting

Even within the same region of the pancreas, ROI-based calculations may be dependent on the proportion of endocrine, ductal, or fatty infiltrate encompassed in the ROI. A helpful analogy can be found in histology, where analyzing only a single section of a slide induces sampling bias. Averaging measurements over multiple sections and slides gives more robust analysis of histological samples. Similarly, one can average MRI parameters over the entire pancreas, although this technique may be insensitive to sparse alterations, such as those found using DWI in T1D (20). For instance, if only a small portion of the pancreas is affected but the entire pancreas is averaged together, then the preponderance of similar intensity voxels can average out sparse voxels with significantly higher or lower intensities.

The insufficiency of ROI or whole organ-based analyses coupled with advances in high performance computing has led to so-called "radiomic" analysis of medical image data. The field of radiomics, excellently reviewed by Gillies et al. (90), couples high throughput feature extraction from quantitative imaging data with multi-dimensional texture, histogram, shape, and wavelet analysis. These radiomic features are uniquely suited to quantify spatially variant organs, such as the different habitats present in tumors (91). Likewise, radiomic analysis show great promise for characterizing and quantifying the spatial heterogeneity of the diabetic pancreas. For example, we have demonstrated that histogram analysis of the pancreas of individuals with T1D identifies differences in DWI that is not evident when averaging the whole pancreas (20). The relative advantages and disadvantages of image analysis techniques for pancreas MRI are summarized in **Table 2**. Radiomic analysis of the diabetic pancreas has not been well characterized and represents a promising new direction in the field.

CONCLUSION

Quantitative MRI techniques have been rapidly integrated into clinical practice across a number of medical specialties. Their contribution to endocrinology and the study of the pancreas in diabetes is still under investigation. A number of techniques display promise for improving our understanding of diabetes pathogenesis in the pancreas and evaluating response to therapy. The flexibility of MRI, which gives rise to a plethora of techniques interrogating different aspects of disease, is also a hindrance, in that imaging protocols employ different acquisition and processing techniques. Thus, comparing studies across sites can be difficult. Standardized imaging and processing pipelines are needed in order to compare studies and perform multisite clinical trials. Analysis of quantitative MRI studies of the pancreas will be aided by radiomic analysis in order to account for pancreas heterogeneity, especially the heterogeneity characteristic of the diabetic pancreas.

AUTHOR CONTRIBUTIONS

The author confirms being the sole contributor of this work and has approved it for publication.

FUNDING

This work was supported by JDRF International (3-SRA-2019-759-M-B and 3-SRA-2015-102-M-B) and the Cain Foundation.

REFERENCES

1. Miller FH, Keppke AL, Dalal K, Ly JN, Kamler VA, Sica GT. MRI of pancreatitis and its complications: part 1, acute pancreatitis. *AJR Am J Roentgenol* (2004) 183(6):1637–44. doi: 10.2214/ajr.183.6.01831637
2. Miller FH, Keppke AL, Wadhwa A, Ly JN, Dalal K, Kamler VA. MRI of pancreatitis and its complications: part 2, chronic pancreatitis. *AJR Am J Roentgenol* (2004) 183(6):1645–52. doi: 10.2214/ajr.183.6.01831645
3. Tummala P, Junaidi O, Agarwal B. Imaging of pancreatic cancer: An overview. *J Gastrointest Oncol* (2011) 2(3):168–74. doi: 10.3978/j.issn.2078-6891.2011.036
4. Cassinotto C, Sa-Cunha A, Trillaud H. Radiological evaluation of response to neoadjuvant treatment in pancreatic cancer. *Diagn Interv Imaging* (2016) 97 (12):1225–32. doi: 10.1016/j.diii.2016.07.011
5. Alexandre-Heymann L, Mallone R, Boitard C, Scharfmann R, Larger E. Structure and function of the exocrine pancreas in patients with type 1 diabetes. *Rev Endocr Metab Disord* (2019) 20(2):129–49. doi: 10.1007/s11154-019-09501-3
6. Bonora E, Tuomilehto J. The pros and cons of diagnosing diabetes with A1C. *Diabetes Care* (2011) 34:S184–90. doi: 10.2337/dc11-s216
7. Bonner-Weir S, Trent DF, Weir GC. Partial pancreatectomy in the rat and subsequent defect in glucose-induced insulin release. *J Clin Invest* (1983) 71 (6):1544–53. doi: 10.1172/JCI110910
8. Jacobsen LM, Bocchino L, Evans-Molina C, DiMeglio L, Goland R, Wilson DM, et al. The risk of progression to type 1 diabetes is highly variable in individuals with multiple autoantibodies following screening. *Diabetologia* (2020) 63(3):588–96. doi: 10.1007/s00125-019-05047-w
9. Yankeelov TE, Mankoff DA, Schwartz LH, Lieberman FS, Buatti JM, Mountz JM, et al. Quantitative Imaging in Cancer Clinical Trials. *Clin Cancer Res* (2016) 22(2):284–90. doi: 10.1158/1078-0432.CCR-14-3336
10. Willcox A, Richardson SJ, Bone AJ, Foulis AK, Morgan NG. Analysis of islet inflammation in human type 1 diabetes. *Clin Exp Immunol* (2009) 155 (2):173–81. doi: 10.1111/j.1365-2249.2008.03860.x
11. Bell ET. Hyalinization of the islets of Langerhans in nondiabetic individuals. *Am J Pathol* (1959) 35(4):801–5.

12. Clark A, Wells CA, Buley ID, Cruickshank JK, Vanhegan RI, Matthews DR, et al. Islet amyloid, increased A-cells, reduced B-cells and exocrine fibrosis: quantitative changes in the pancreas in type 2 diabetes. *Diabetes Res* (1988) 9 (4):151–9.
13. Gepts W. Pathologic anatomy of the pancreas in juvenile diabetes mellitus. *Diabetes* (1965) 14(10):619–33. doi: 10.2337/diab.14.10.619
14. Saisho Y, Butler AE, Meier JJ, Monchamp T, Allen-Auerbach M, Rizza RA, et al. Pancreas volumes in humans from birth to age one hundred taking into account sex, obesity, and presence of type-2 diabetes. *Clin Anat* (2007) 20 (8):933–42. doi: 10.1002/ca.20543
15. Garcia TS, Rech TH, Leitao CB. Pancreatic size and fat content in diabetes: A systematic review and meta-analysis of imaging studies. *PLoS One* (2017) 12 (7):e0180911. doi: 10.1371/journal.pone.0180911
16. Wright JJ, Saunders DC, Dai C, Poffenberger G, Cairns B, Serreze DV, et al. Decreased pancreatic acinar cell number in type 1 diabetes. *Diabetologia* (2020) 63(7):1418–23. doi: 10.1007/s00125-020-05155-y
17. Kusmartseva I, Beery M, Hiller H, Padilla M, Selman S, Posgai A, et al. Temporal Analysis of Amylase Expression in Control, Autoantibody-Positive, and Type 1 Diabetes Pancreatic Tissues. *Diabetes* (2020) 69(1):60–6. doi: 10.2337/db19-0554
18. Gaglia JL, Harisinghani M, Aganj I, Wojtkiewicz GR, Hedgire S, Benoist C, et al. Noninvasive mapping of pancreatic inflammation in recent-onset type-1 diabetes patients. *Proc Natl Acad Sci U S A* (2015) 112(7):2139–44. doi: 10.1073/pnas.1424993112
19. Williams AJ, Thrower SL, Sequeiros IM, Ward A, Bickerton AS, Triay JM, et al. Pancreatic volume is reduced in adult patients with recently diagnosed type 1 diabetes. *J Clin Endocrinol Metab* (2012) 97(11):E2109–13. doi: 10.1210/jc.2012-1815
20. Virostko J, Williams J, Hilmes M, Bowman C, Wright JJ, Du L, et al. Pancreas Volume Declines During the First Year After Diagnosis of Type 1 Diabetes and Exhibits Altered Diffusion at Disease Onset. *Diabetes Care* (2019) 42 (2):248–57. doi: 10.2337/dc18-1507
21. Campbell-Thompson ML, Filipp SL, Grajo JR, Nambam B, Beegle R, Middlebrooks EH, et al. Relative Pancreas Volume Is Reduced in First-Degree Relatives of Patients With Type 1 Diabetes. *Diabetes Care* (2019) 42 (2):281–7. doi: 10.2337/dc18-1512
22. Nanno Y, Wilhelm JJ, Heller D, Schat R, Freeman ML, Trikudanathan G, et al. Combination of pancreas volume and HbA1c level predicts islet yield in patients undergoing total pancreatectomy and islet autotransplantation. *Clin Transplant* (2020) 34(8):e14008. doi: 10.1111/ctr.14008
23. Szczepaniak EW, Malliaras K, Nelson MD, Szczepaniak LS. Measurement of pancreatic volume by abdominal MRI: a validation study. *PLoS One* (2013) 8 (2):e55991. doi: 10.1371/journal.pone.0055991
24. Williams JM, Hilmes MA, Archer B, Dulaney A, Du L, Kang H, et al. Repeatability and Reproducibility of Pancreas Volume Measurements Using MRI. *Sci Rep* (2020) 10(1):4767. doi: 10.1038/s41598-020-61759-9
25. Williams AJ, Chau W, Callaway MP, Dayan CM. Magnetic resonance imaging: a reliable method for measuring pancreatic volume in Type 1 diabetes. *Diabetes Med* (2007) 24(1):35–40. doi: 10.1111/j.1464-5491.2007.02027.x
26. Lee Y, Hirose H, Ohneda M, Johnson JH, McGarry JD, Unger RH. Beta-cell lipotoxicity in the pathogenesis of non-insulin-dependent diabetes mellitus of obese rats: impairment in adipocyte-beta-cell relationships. *Proc Natl Acad Sci U S A* (1994) 91(23):10878–82. doi: 10.1073/pnas.91.23.10878
27. Heni M, Machann J, Staiger H, Schwenzer NF, Peter A, Schick F, et al. Pancreatic fat is negatively associated with insulin secretion in individuals with impaired fasting glucose and/or impaired glucose tolerance: a nuclear magnetic resonance study. *Diabetes Metab Res Rev* (2010) 26(3):200–5. doi: 10.1002/dmrr.1073
28. Tushuizen ME, Bunck MC, Pouwels PJ, Bontemps S, van Waesberghe JH, Schindhelm RK, et al. Pancreatic fat content and beta-cell function in men with and without type 2 diabetes. *Diabetes Care* (2007) 30(11):2916–21. doi: 10.2337/dc07-0326
29. Kuhn JP, Berthold F, Mayerle J, Volzke H, Reeder SB, Rathmann W, et al. Pancreatic Steatosis Demonstrated at MR Imaging in the General Population: Clinical Relevance. *Radiology* (2015) 276(1):129–36. doi: 10.1148/radiol.15140446
30. Patel NS, Peterson MR, Brenner DA, Heba E, Sirlin C, Loomba R. Association between novel MRI-estimated pancreatic fat and liver histology-determined steatosis and fibrosis in non-alcoholic fatty liver disease. *Aliment Pharmacol Ther* (2013) 37(6):630–9. doi: 10.1111/apt.12237
31. Lim EL, Hollingsworth KG, Aribisala BS, Chen MJ, Mathers JC, Taylor R. Reversal of type 2 diabetes: normalisation of beta cell function in association with decreased pancreas and liver triacylglycerol. *Diabetologia* (2011) 54 (10):2506–14. doi: 10.1007/s00125-011-2204-7
32. Heber SD, Hetterich H, Lorbeer R, Bayerl C, Machann J, Auweter S, et al. Pancreatic fat content by magnetic resonance imaging in subjects with prediabetes, diabetes, and controls from a general population without cardiovascular disease. *PLoS One* (2017) 12(5):e0177154. doi: 10.1371/journal.pone.0177154
33. Nadarajah C, Fananapazir G, Cui E, Gichoya J, Thayalan N, Asare-Sawiri M, et al. Association of pancreatic fat content with type II diabetes mellitus. *Clin Radiol* (2020) 75(1):51–6. doi: 10.1016/j.crad.2019.05.027
34. Regnell SE, Peterson P, Trinh L, Broberg P, Leander P, Lernmark A, et al. Pancreas volume and fat fraction in children with Type 1 diabetes. *Diabetes Med* (2016) 33(10):1374–9. doi: 10.1111/dme.13115
35. Fukui H, Hori M, Fukuda Y, Onishi H, Nakamoto A, Ota T, et al. Evaluation of fatty pancreas by proton density fat fraction using 3-T magnetic resonance imaging and its association with pancreatic cancer. *Eur J Radiol* (2019) 118:25–31. doi: 10.1016/j.ejrad.2019.06.024
36. Lingvay I, Esser V, Legendre JL, Price AL, Wertz KM, Adams-Huet B, et al. Noninvasive quantification of pancreatic fat in humans. *J Clin Endocrinol Metab* (2009) 94(10):4070–6. doi: 10.1210/jc.2009-0584
37. Hu HH, Kim HW, Nayak KS, Goran MI. Comparison of fat-water MRI and single-voxel MRS in the assessment of hepatic and pancreatic fat fractions in humans. *Obes (Silver Spring)* (2010) 18(4):841–7. doi: 10.1038/oby.2009.352
38. Al-Mrabeh A, Hollingsworth KG, Steven S, Tiniakos D, Taylor R. Quantification of intrapancreatic fat in type 2 diabetes by MRI. *PLoS One* (2017) 12(4):e0174660. doi: 10.1371/journal.pone.0174660
39. Manikkavasakar S, AlObaidy M, Busireddy KK, Ramalho M, Nilmini V, Alagiyawanna M, et al. Magnetic resonance imaging of pancreatitis: an update. *World J Gastroenterol* (2014) 20(40):14760–77. doi: 10.3748/wjg.v20.i40.14760
40. Taylor AJ, Salerno M, Dharmakumar R, Jerosch-Herold M. T1 Mapping: Basic Techniques and Clinical Applications. *JACC Cardiovasc Imaging* (2016) 9(1):67–81. doi: 10.1016/j.jcmg.2015.11.005
41. Tirkes T, Lin C, Fogel EL, Sherman SS, Wang Q, Sandrasegaran K. T1 mapping for diagnosis of mild chronic pancreatitis. *J Magn Reson Imaging* (2017) 45(4):1171–6. doi: 10.1002/jmri.25428
42. Noda Y, Goshima S, Tsuji Y, Kajita K, Akamine Y, Kawai N, et al. Pancreatic extracellular volume fraction using T1 mapping in patients with impaired glucose intolerance. *Abdom Radiol (NY)* (2020) 45(2):449–56. doi: 10.1007/s00261-019-02384-7
43. Naish JH, Hutchinson CE, Caunce A, Roberts C, Waterton JC, Hockings PD, et al. Multiple-bolus dynamic contrast-enhanced MRI in the pancreas during a glucose challenge. *J Magn Reson Imaging* (2010) 32(3):622–8. doi: 10.1002/jmri.22281
44. Noda Y, Goshima S, Tsuji Y, Kajita K, Kawada H, Kawai N, et al. Correlation of quantitative pancreatic T1 value and HbA1c value in subjects with normal and impaired glucose tolerance. *J Magn Reson Imaging* (2019) 49(3):711–8. doi: 10.1002/jmri.26242
45. Sibley CT, Noureldin RA, Gai N, Nacif MS, Liu S, Turkbey EB, et al. T1 Mapping in cardiomyopathy at cardiac MR: comparison with endomyocardial biopsy. *Radiology* (2012) 265(3):724–32. doi: 10.1148/radiol.12112721
46. Watanabe H, Kanematsu M, Tanaka K, Osada S, Tomita H, Hara A, et al. Fibrosis and postoperative fistula of the pancreas: correlation with MR imaging findings–preliminary results. *Radiology* (2014) 270(3):791–9. doi: 10.1148/radiol.13131194
47. Tirkes T, Mitchell JR, Li L, Zhao X, Lin C. Normal T1 relaxometry and extracellular volume of the pancreas in subjects with no pancreas disease: correlation with age and gender. *Abdom Radiol (NY)* (2019) 44(9):3133–8. doi: 10.1007/s00261-019-02071-7
48. Damen M, van Leeuwen M, Webb A, Klomp D, de Castro CA. Measurement of T1 and T2 relaxation times of the pancreas at 7 T using a multi-transmit system. *MAGMA* (2019) 32(6):703–8. doi: 10.1007/s10334-019-00768-w

49. Tirkes T, Zhao X, Lin C, Stuckey AJ, Li L, Giri S, et al. Evaluation of variable flip angle, MOLLI, SASHA, and IR-SNAPSHOT pulse sequences for T1 relaxometry and extracellular volume imaging of the pancreas and liver. *MAGMA* (2019) 32(5):559–66. doi: 10.1007/s10334-019-00762-2
50. Haaf P, Garg P, Messroghli DR, Broadbent DA, Greenwood JP, Plein S. Cardiac T1 Mapping and Extracellular Volume (ECV) in clinical practice: a comprehensive review. *J Cardiovasc Magn Reson* (2016) 18(1):89. doi: 10.1186/s12968-016-0308-4
51. Tirkes T, Lin C, Cui E, Deng Y, Territo PR, Sandrasegaran K, et al. Quantitative MR Evaluation of Chronic Pancreatitis: Extracellular Volume Fraction and MR Relaxometry. *AJR Am J Roentgenol* (2018) 210(3):533–42. doi: 10.2214/AJR.17.18606
52. Cui Y, Cao Y, Song J, Dong N, Kong X, Wang J, et al. Association between myocardial extracellular volume and strain analysis through cardiovascular magnetic resonance with histological myocardial fibrosis in patients awaiting heart transplantation. *J Cardiovasc Magn Reson* (2018) 20(1):25. doi: 10.1186/s12968-018-0445-z
53. Roujol S, Weingartner S, Foppa M, Chow K, Kawaji K, Ngo LH, et al. Accuracy, precision, and reproducibility of four T1 mapping sequences: a head-to-head comparison of MOLLI, ShMOLLI, SASHA, and SAPPHIRE. *Radiology* (2014) 272(3):683–9. doi: 10.1148/radiol.14140296
54. Lee SS, Byun JH, Park BJ, Park SH, Kim N, Park B, et al. Quantitative analysis of diffusion-weighted magnetic resonance imaging of the pancreas: usefulness in characterizing solid pancreatic masses. *J Magn Reson Imaging* (2008) 28(4):928–36. doi: 10.1002/jmri.21508
55. Akisik MF, Aisen AM, Sandrasegaran K, Jennings SG, Lin C, Sherman S, et al. Assessment of chronic pancreatitis: utility of diffusion-weighted MR imaging with secretin enhancement. *Radiology* (2009) 250(1):103–9. doi: 10.1148/radiol.2493080160
56. Noda Y, Kanematsu M, Goshima S, Horikawa Y, Takeda J, Kondo H, et al. Diffusion kurtosis imaging of the pancreas for the assessment of HbA1c levels. *J Magn Reson Imaging* (2016) 43(1):159–65. doi: 10.1002/jmri.24982
57. Schoennagel BP, Habermann CR, Roesch M, Hahne JD, Arndt C, Kleibeler L, et al. Diffusion-weighted imaging of the healthy pancreas: apparent diffusion coefficient values of the normal head, body, and tail calculated from different sets of b-values. *J Magn Reson Imaging* (2011) 34(4):861–5. doi: 10.1002/jmri.22743
58. Herrmann J, Schoennagel BP, Roesch M, Busch JD, Derlin T, Doh LK, et al. Diffusion-weighted imaging of the healthy pancreas: ADC values are age and gender dependent. *J Magn Reson Imaging* (2013) 37(4):886–91. doi: 10.1002/jmri.23871
59. Ye XH, Gao JY, Yang ZH, Liu Y. Apparent diffusion coefficient reproducibility of the pancreas measured at different MR scanners using diffusion-weighted imaging. *J Magn Reson Imaging* (2014) 40(6):1375–81. doi: 10.1002/jmri.24492
60. Dale BM, Braithwaite AC, Boll DT, Merkle EM. Field strength and diffusion encoding technique affect the apparent diffusion coefficient measurements in diffusion-weighted imaging of the abdomen. *Invest Radiol* (2010) 45(2):104–8. doi: 10.1097/RLI.0b013e3181c8ceac
61. Henderson JR, Moss MC. A morphometric study of the endocrine and exocrine capillaries of the pancreas. *Q J Exp Physiol* (1985) 70(3):347–56. doi: 10.1113/expphysiol.1985.sp002920
62. Canzano JS, Nasif LH, Butterworth EA, Fu DA, Atkinson MA, Campbell-Thompson M. Islet Microvasculature Alterations With Loss of Beta-cells in Patients With Type 1 Diabetes. *J Histochem Cytochem* (2019) 67(1):41–52. doi: 10.1369/0022155418778546
63. Brissova M, Shostak A, Fligner CL, Revetta FL, Washington MK, Powers AC, et al. Human Islets Have Fewer Blood Vessels than Mouse Islets and the Density of Islet Vascular Structures Is Increased in Type 2 Diabetes. *J Histochem Cytochem* (2015) 63(8):637–45. doi: 10.1369/0022155415573324
64. Tofts PS, Kermode AG. Measurement of the blood-brain barrier permeability and leakage space using dynamic MR imaging. 1. Fundamental concepts. *Magn Reson Med* (1991) 17(2):357–67. doi: 10.1002/mrm.1910170208
65. Coenegrachts K, Van Steenbergen W, De Keyzer F, Vanbeckevoort D, Bielen D, Chen F, et al. Dynamic contrast-enhanced MRI of the pancreas: initial results in healthy volunteers and patients with chronic pancreatitis. *J Magn Reson Imaging* (2004) 20(6):990–7. doi: 10.1002/jmri.20212
66. Akisik MF, Sandrasegaran K, Bu G, Lin C, Hutchins GD, Chiorean EG. Pancreatic cancer: utility of dynamic contrast-enhanced MR imaging in assessment of antiangiogenic therapy. *Radiology* (2010) 256(2):441–9. doi: 10.1148/radiol.10091733
67. Yu CW, Shih TT, Hsu CY, Lin LC, Wei SY, Lee CM, et al. Correlation between pancreatic microcirculation and type 2 diabetes in patients with coronary artery disease: dynamic contrast-enhanced MR imaging. *Radiology* (2009) 252(3):704–11. doi: 10.1148/radiol.2523081615
68. Bali MA, Metens T, Denolin V, Delhaye M, Demetter P, Closset J, et al. Tumoral and nontumoral pancreas: correlation between quantitative dynamic contrast-enhanced MR imaging and histopathologic parameters. *Radiology* (2011) 261(2):456–66. doi: 10.1148/radiol.11103515
69. Bali MA, Metens T, Denolin V, De Maertelaer V, Deviere J, Matos C. Pancreatic perfusion: noninvasive quantitative assessment with dynamic contrast-enhanced MR imaging without and with secretin stimulation in healthy volunteers–initial results. *Radiology* (2008) 247(1):115–21. doi: 10.1148/radiol.2471070685
70. Schawkat K, Ith M, Christe A, Kuhn W, Chittazhathu Y, Bains L, et al. Dynamic non-invasive ASL perfusion imaging of a normal pancreas with secretin augmented MR imaging. *Eur Radiol* (2018) 28(6):2389–96. doi: 10.1007/s00330-017-5227-8
71. Taso M, Papadopoulou F, Smith MP, Tsai LL, Mortele KJ, Alsop DC. Pancreatic perfusion modulation following glucose stimulation assessed by noninvasive arterial spin labeling (ASL) MRI. *J Magn Reson Imaging* (2020) 51(3):854–60. doi: 10.1002/jmri.26899
72. Hirshberg B, Qiu M, Cali AM, Sherwin R, Constable T, Calle RA, et al. Pancreatic perfusion of healthy individuals and type 1 diabetic patients as assessed by magnetic resonance perfusion imaging. *Diabetologia* (2009) 52(8):1561–5. doi: 10.1007/s00125-009-1406-8
73. Cai W, Li F, Wang J, Du H, Wang X, Zhang J, et al. A comparison of arterial spin labeling perfusion MRI and DCE-MRI in human prostate cancer. *NMR Biomed* (2014) 27(7):817–25. doi: 10.1002/nbm.3124
74. Schraml C, Schwenzer NF, Martirosian P, Claussen CD, Schick F. Perfusion imaging of the pancreas using an arterial spin labeling technique. *J Magn Reson Imaging* (2008) 28(6):1459–65. doi: 10.1002/jmri.21564
75. Le Bihan D, Breton E, Lallemand D, Aubin ML, Vignaud J, Laval-Jeantet M. Separation of diffusion and perfusion in intravoxel incoherent motion MR imaging. *Radiology* (1988) 168(2):497–505. doi: 10.1148/radiology.168.2.3393671
76. Kim B, Lee SS, Sung YS, Cheong H, Byun JH, Kim HJ, et al. Intravoxel incoherent motion diffusion-weighted imaging of the pancreas: Characterization of benign and malignant pancreatic pathologies. *J Magn Reson Imaging* (2017) 45(1):260–9. doi: 10.1002/jmri.25334
77. Espes D, Manell E, Ryden A, Carlbom L, Weis J, Jensen-Waern M, et al. Pancreatic perfusion and its response to glucose as measured by simultaneous PET/MRI. *Acta Diabetol* (2019) 56(10):1113–20. doi: 10.1007/s00592-019-01353-2
78. Lemke A, Laun FB, Simon D, Stieltjes B, Schad LR. An *in vivo* verification of the intravoxel incoherent motion effect in diffusion-weighted imaging of the abdomen. *Magn Reson Med* (2010) 64(6):1580–5. doi: 10.1002/mrm.22565
79. Gurney-Champion OJ, Klaassen R, Froeling M, Barbieri S, Stoker J, Engelbrecht MRW, et al. Comparison of six fit algorithms for the intra-voxel incoherent motion model of diffusion-weighted magnetic resonance imaging data of pancreatic cancer patients. *PLoS One* (2018) 13(4):e0194590. doi: 10.1371/journal.pone.0194590
80. Prasad PV, Edelman RR, Epstein FH. Noninvasive evaluation of intrarenal oxygenation with BOLD MRI. *Circulation* (1996) 94(12):3271–5. doi: 10.1161/01.CIR.94.12.3271
81. Chen B, Chen W, Chan Q, Zhou N, He J, Zhou Z. Functional MRI of human pancreas using BOLD contrast: Responses following glucose ingestion. *J Magn Reson Imaging* (2017) 46(3):831–6. doi: 10.1002/jmri.25640
82. Serai SD, Abu-El-Haija M, Trout AT. 3D MR elastography of the pancreas in children. *Abdom Radiol (NY)* (2019) 44(5):1834–40. doi: 10.1007/s00261-019-01903-w
83. Ji R, Li J, Yin Z, Liu Y, Cang L, Wang M, et al. Pancreatic stiffness response to an oral glucose load in obese adults measured by magnetic resonance elastography. *Magn Reson Imaging* (2018) 51:113–9. doi: 10.1016/j.mri.2018.04.019

84. Xu Y, Cai X, Shi Y, Yin M, Lan G, Zhang X, et al. Normative Pancreatic Stiffness Levels and Related Influences Established by Magnetic Resonance Elastography in Volunteers. *J Magn Reson Imaging* (2020) 52(2):448–58. doi: 10.1002/jmri.27052
85. Shi Y, Liu Y, Gao F, Liu Y, Tao S, Li Y, et al. Pancreatic Stiffness Quantified with MR Elastography: Relationship to Postoperative Pancreatic Fistula after Pancreaticoenteric Anastomosis. *Radiology* (2018) 288(2):476–84. doi: 10.1148/radiol.2018170450
86. Kolipaka A, Schroeder S, Mo X, Shah Z, Hart PA, Conwell DL. Magnetic resonance elastography of the pancreas: Measurement reproducibility and relationship with age. *Magn Reson Imaging* (2017) 42:1–7. doi: 10.1016/j.mri.2017.04.015
87. Wittingen J, Frey CF. Islet concentration in the head, body, tail and uncinate process of the pancreas. *Ann Surg* (1974) 179(4):412–4. doi: 10.1097/00000658-197404000-00005
88. Cecil RL. A Study of the Pathological Anatomy of the Pancreas in Ninety Cases of Diabetes Mellitus. *J Exp Med* (1909) 11(2):266–90. doi: 10.1084/jem.11.2.266
89. Rodriguez-Calvo T, Suwandi JS, Amirian N, Zapardiel-Gonzalo J, Anquetil F, Sabouri S, et al. Heterogeneity and Lobularity of Pancreatic Pathology in Type 1 Diabetes during the Prediabetic Phase. *J Histochem Cytochem* (2015) 63(8):626–36. doi: 10.1369/0022155415576543
90. Gillies RJ, Kinahan PE, Hricak H. Radiomics: Images Are More than Pictures, They Are Data. *Radiology* (2016) 278(2):563–77. doi: 10.1148/radiol.2015151169
91. Zhou M, Hall L, Goldgof D, Russo R, Balagurunathan Y, Gillies R, et al. Radiologically defined ecological dynamics and clinical outcomes in glioblastoma multiforme: preliminary results. *Transl Oncol* (2014) 7(1):5–13. doi: 10.1593/tlo.13730

Conflict of Interest: The author declares that the research was conducted in the absence of any commercial or financial relationships that could be construed as a potential conflict of interest.

frontiers in Endocrinology

ORIGINAL RESEARCH
published: 15 January 2021
doi: 10.3389/fendo.2020.602519

Functional Characterization of the Human Islet Microvasculature Using Living Pancreas Slices

*Luciana Mateus Gonçalves and Joana Almaça**

Division of Endocrinology, Diabetes and Metabolism, Department of Medicine, University of Miami Miller School of Medicine, Miami, FL, United States

OPEN ACCESS

Edited by:
Guy A. Rutter, Imperial College London, United Kingdom

Reviewed by:
Elina Akalestou, Imperial College London, United Kingdom
Hung Ping Shih, Beckman Research Institute, City of Hope, United States

***Correspondence:**
Joana Almaça
jalmaca@med.miami.edu

Specialty section:
This article was submitted to Diabetes: Molecular Mechanisms, a section of the journal Frontiers in Endocrinology

Received: *03 September 2020*
Accepted: *23 November 2020*
Published: *15 January 2021*

Citation:
Mateus Gonçalves L and Almaça J (2021) Functional Characterization of the Human Islet Microvasculature Using Living Pancreas Slices. Front. Endocrinol. 11:602519. doi: 10.3389/fendo.2020.602519

Pancreatic islets are clusters of endocrine cells that secrete different hormones to regulate blood glucose levels. Efficient hormone secretion requires a close interaction of endocrine cells with their vascular system. Islets receive blood through feeding arteriole(s) that branch into capillaries made of endothelial cells covered by pericytes. While a lot is known about rodent islet blood vessels, the structure and function of the human islet microvasculature has been less investigated. In this study, we used living pancreas slices from non-diabetic human donors to examine the function of human islet blood vessels. Living human pancreas slices were incubated with a membrane permeant calcium indicator and pericytes/smooth muscle cells were visualized with a fluorescent antibody against the mural cell marker NG2 proteoglycan. By confocal microscopy, we simultaneously recorded changes in the diameter of lectin-labeled blood vessels and cytosolic calcium levels in mural cells in islets. We tested several stimuli with vasoactive properties, such as norepinephrine, endothelin-1 and adenosine and compared human vascular responses with those previously published for mouse islet blood vessels. Norepinephrine and endothelin-1 significantly constricted human islet feeding arterioles, while adenosine dilated them. Islet capillaries were less responsive and only 15–20% of the mouse and human islet capillary network showed vasomotion. Nevertheless, in these responsive regions, norepinephrine and endothelin-1 decreased both mouse and human islet capillary diameter. Changes in islet blood vessel diameter were coupled to changes in cytosolic calcium levels in adjacent mouse and human islet mural cells. Our study shows that mural cells in islets are the targets of different regulatory mechanisms of islet blood perfusion. Several alterations of the human islet microvasculature occur during diabetes progression. Elucidating their functional consequences in future studies will be critical for our understanding of disease pathogenesis.

Keywords: pancreatic islet, microvasculature, pericytes, smooth muscle cells, pancreas slices, vasomotion

INTRODUCTION

Pancreatic islets are endocrine mini-organs rich in blood vessels (1, 2). Close interactions between islet endocrine cells and vascular cells are established early on during development and maintained throughout life, by providing mutual trophic and functional support (2–7). Indeed, as any other endocrine organ, islets depend on their blood vessels to function properly (8). Defects in the islet microvasculature can lead to diabetic phenotypes (9). Several studies have reported structural alterations of the human islet microvasculature and composition of the extracellular matrix during type 1 and type 2 diabetes (10–15). However, the functional consequences of these alterations are hard to assess in humans. In animals, altered islet blood flow, for instance, is observed in different rodent models of disturbed glucose homeostasis (16, 17). Microvascular dysfunction and abnormal regulation of islet blood flow could compromise exchanges between endocrine cells and the circulation, resulting in defective hormone secretion as previously suggested (18, 19).

The mouse is an extensively used and valuable animal model in medical research. However, previous studies have shown that in human islets the microvascular niche differs significantly from that of the mouse. Not only human islets have less and shorter capillaries than mouse islets (13, 20), but also their vessels are surrounded by a double basement membrane (21) and a denser layer of connective tissue exists in their perivascular space (22). Another important difference between human and mouse islets is that human beta cells produce an amyloidogenic peptide (islet amyloid polypeptide, IAPP) that accumulates next to capillaries within the human islet parenchyma (23, 24). These anatomical differences in the islet microcirculation between the two species prompted us to examine whether blood vessels in human islets would also be regulated differently than those in mouse islets.

To examine microvascular function in human islets, we adopted the pancreatic slice technique (25). In pancreas slices, islet vascular networks are preserved, and their function can now be studied within the native pancreatic environment (11, 20). We have previously used this platform to monitor microvascular responses in mouse islets *ex vivo* (11, 22). Similar to mouse pancreas slices, living human pancreas slices can also be produced from small pancreas pieces and used in physiological experiments acutely after slicing (26) or after long-term culture [at least 10 days (27)]. We have recently performed dynamic hormone secretion assays and imaged intracellular calcium levels in living human pancreas slices to characterize endocrine cell function in individuals at different stages of type 1 diabetes (26). Living human pancreas slices have also enabled us to study how endocrine cells communicate with other cells in the human islet microenvironment such as islet resident macrophages (28). In this study, we used living pancreas slices from non-diabetic donors to investigate the cellular mechanisms that control vasomotion in human islets. By confocal imaging, we simultaneously recorded changes in islet blood vessel diameter and cytosolic calcium levels in mural cells. To the best of our knowledge, this is the first functional characterization of human islet blood vessels and comparison with mouse islet vascular responses.

METHODS

Human Organ Donors

We obtained human living pancreas slices from de-identified cadaveric donors (from the head of the pancreas, n = 6 non-diabetic individuals, male and female, ages from 20–59 years old; information on the donors used in this study is provided in **Table S1**) from the Network of Pancreatic Organ Donors with Diabetes (nPOD) or sliced locally at the Diabetes Research Institute (University of Miami). Slices produced by nPOD were shipped overnight from Gainesville to Miami and used 3 h after arrival, while slices produced locally were cultured overnight and used the day after (26, 27).

Tissue Viability

Pancreatic slices were incubated with calcein-AM (to label live cells in green) and ethidium homodimer-1 (labels dead cells in red). Addition of both reagents was done according to the manufacturer's recommendations as part of the Live/Dead viability/cytotoxicity kit for mammalian cells [Invitrogen, Carlsbad, CA, Cat# L3224; (27)]. Endocrine cell calcium responses to KCl depolarization (25 mM; protocol of loading with calcium indicator is below) were used as an additional readout of tissue viability. Only viable and responsive tissue was used in subsequent experiments.

Confocal Imaging of Living Pancreas Slices

Living human pancreas slices were incubated with Fluo4-AM (final concentration 6.3µM, Invitrogen, cat. nr. F14201) and DyLight 649 lectin from *Lycopersicon Esculentum* (final concentration 3.3µg/mL, VectorLabs, cat. nr. DL1178) for 1 h in 3 mM glucose solution prepared in HEPES buffer (125 mmol/l NaCl, 5.9 mmol/l KCl, 2.56 mmol/l $CaCl_2$, 1 mmol/l $MgCl_2$, 25 mmol/l HEPES, and 0.1% BSA [w/v], pH 7.4) supplemented with aprotinin (25 KIU, MilliporeSigma, cat. nr. A6106) at room temperature and in the dark. To identify pericytes *in situ*, slices were incubated for 2 h with a fluorescent-conjugated antibody against NG2 (final dilution 1:50, R&D Systems, cat. nr. Fab2585R). After incubation, living pancreas slices were placed on a coverslip in an imaging chamber (Warner instruments, Hamden, CT, USA) and imaged under an upright confocal microscope (Leica TCS SP5 upright; Leica Microsystems, Wetzlar, Germany). The chamber was continuously perfused with HEPES-buffered solution containing 3 mM glucose and confocal images were acquired with LAS AF software (Leica Microsystems) using a 40X water immersion objective (NA 0.8). We used a resonance scanner for fast image acquisition to produce time-lapse recordings spanning 50–100 µm of the slice (z-step: 5–10 µm, stack of 10–15 confocal images with a size of 512 × 512 pixels) at 5 seconds resolution (xyzt imaging). Fluo-4 fluorescence was excited at 488 nm and emission detected at 510–550 nm, DyLight 649 labeled tomato lectin was excited at 638 nm and emission detected at 648–690 nm.

From each human donor, a group of slices was incubated with Fluo4 and lectin and another group of slices was incubated with Fluo4 and NG2-alexa647, to account for potential effects of

antibody binding and change in cell physiology. Mural cells responded similarly with or without antibody labeling.

We recorded changes in $[Ca^{2+}]_i$ and blood vessel diameter induced by norepinephrine (20 μM; applied for 3 min), endothelin-1 (10 nM, applied for 5 min) and adenosine (50 μM, applied for 4 min). To quantify changes in $[Ca^{2+}]_i$, we drew regions of interest around individual islet pericytes and measured the mean Fluo4 fluorescence intensity using ImageJ software (http://imagej.nih.gov/ij/). Changes in fluorescence intensity were expressed as percentage over baseline (ΔF/F). The baseline was defined as the mean of the three first values of the control period of each recording [i.e., in non-stimulatory, basal glucose concentration conditions (3 mM)]. Blood vessels were labeled with DyLight-649 and we could image vessel borders in slices. Quantification of vessel diameter was done as previously described (11). Briefly, we drew a straight-line transversal to the blood vessel borders (**Figure 3A'** and **A"**) and used the "reslice" z-function in ImageJ to generate a single image showing the changes in vessel diameter over time (xt scan; temporal projections shown in **Figures 3C–E**). Noise from reslice images was removed using a median filter (radius = 1 pixel). We drew another line on the xt scan (resliced) image and, using the "plot profile" function, we determined the position of the pixels with the highest fluorescence intensity and considered these the vessel borders. Vessel diameter was calculated by subtracting these two position values. To determine the extent of constriction/dilation, we pooled data on responsive capillaries from different islets from different donors and calculated the relative change in diameter (as fraction of initial vessel diameter). We estimated the proportion of "responsive capillaries" by dividing the area of the lectin-labeled capillaries that responded to a certain stimulus by the total area of the islet capillary network.

Immunohistochemistry

Small pieces of pancreatic tissue were fixed overnight with 4% PFA and then placed in PBS. Slices were incubated in blocking solution (PBS-Triton X-100 0.3% and Universal Blocker Reagent; Biogenex, San Ramon, CA) for 3 h. Thereafter, slices were incubated for 48 h (20°C) with primary antibodies diluted in blocking solution. We immunostained pericytes (NG2, 1:50–1:100), endothelial cells (CD31, 1:25), smooth muscle cells (αSMA, 1:250), beta cells (insulin, 1:2000). Immunostaining was visualized conjugated secondary antibodies (1:500 in PBS; 16 h at 20°C; Invitrogen, Carlsbad, CA). Cell nuclei were stained with dapi. Slides were mounted with Vectashield mounting medium (Vector Laboratories) and imaged on an inverted laser-scanning confocal microscope (Leica TCS SP5; Leica Microsystems) with LAS AF software using a 63X oil immersion objective (NA 1.4). To quantify colocalization between αSMA and NG2 immunostainings, we calculated Mander's coefficients in confocal images using the ImageJ plugin "JACoP": Just Another Co-localization Plugin.

Statistical Analyses

For statistical comparisons we used Prism 7 (GraphPad software, La Jolla, CA) and performed Student's t tests (paired and unpaired) or One sample t test. p values < 0.05 were considered statistically significant (indicated with an *). Throughout the manuscript we present data as mean ± SEM.

RESULTS

Pericytes Cover Human and Mouse Islet Capillaries and Express αSMA

Pericytes, the mural cells of the microcirculation, are part of the mouse and human islet microenvironment (5, 11, 29, 30). Pericytes are complex cells (31). The unambiguous distinction of pericytes from other perivascular cells requires inspecting their basement membrane at the ultrastructural level (32). However, pericytes can be identified in tissue sections using antibodies against pericyte surface markers, such as neuron-glial antigen 2 (NG2) and platelet-derived growth factor receptor-beta (PDGFRβ). Pericytes have a typical bump-on-a-log morphology: a cell body with a prominent nucleus and cytoplasmic processes on the surface of capillaries (31, 33) (**Figures 1H, I**). Following this classification, we have previously reported that mouse and human islet capillaries are covered with pericytes and estimated an average pericyte: endothelial cell ratio of 1:3–1:2 for mouse and human islets, respectively (11). Pericytes interact closely with islet endothelial cells and are present on straight parts of islet capillaries and at capillary branch points (**Figure 1A**). Interestingly, pericyte density in islets is higher than in the surrounding exocrine tissue [**Figure 1A**; (30)]. Pericytes in mouse and human islets also express PDGFRβ, although expression of this receptor is not limited to pericytes in human islets (10).

Pericytes in mouse islets have contractile properties (11). To determine if pericytes in human islets also help regulating islet capillary diameter, we examined in more detail pericytic expression of α-smooth muscle actin (αSMA). αSMA is expressed by cells of smooth muscle cell lineages, allowing us to visualize arterioles that feed into pancreatic islets (**Figures 1B, C**). In most human islets only one feeding arteriole would be seen, in line with previous findings (34). αSMA positive cells are also present within the human and mouse islet parenchyma (**Figures 1C, D**). The density of αSMA immunostaining inside human islets is higher than what is found in mouse islets (**Figure 1E**), as previously reported (35). Around 50% of the αSMA positive immunostaining colocalizes with NG2 (**Figures 1C, D, F**). This fraction tends to decrease with donor age (data not shown). Importantly, around 60% of the NG2 positive cell population expresses αSMA [**Figures 1C, D, G**; (11)]. In human islets, a subset of these double positive cells are found tightly wrapping the capillary end of the feeding arteriole (**Figures 1C, H**). These pericytes have a different morphology than those found in the islet parenchyma. Indeed, it is known that pericyte morphology depends on their location in the capillary bed: more circumferential cytoplasmic processes at the arteriole end, more longitudinal processes in the middle, and a stellate morphology toward the venule end of the capillary bed (33). Given the circumferential morphology of their cytoplasmic processes and the fact that they are associated with

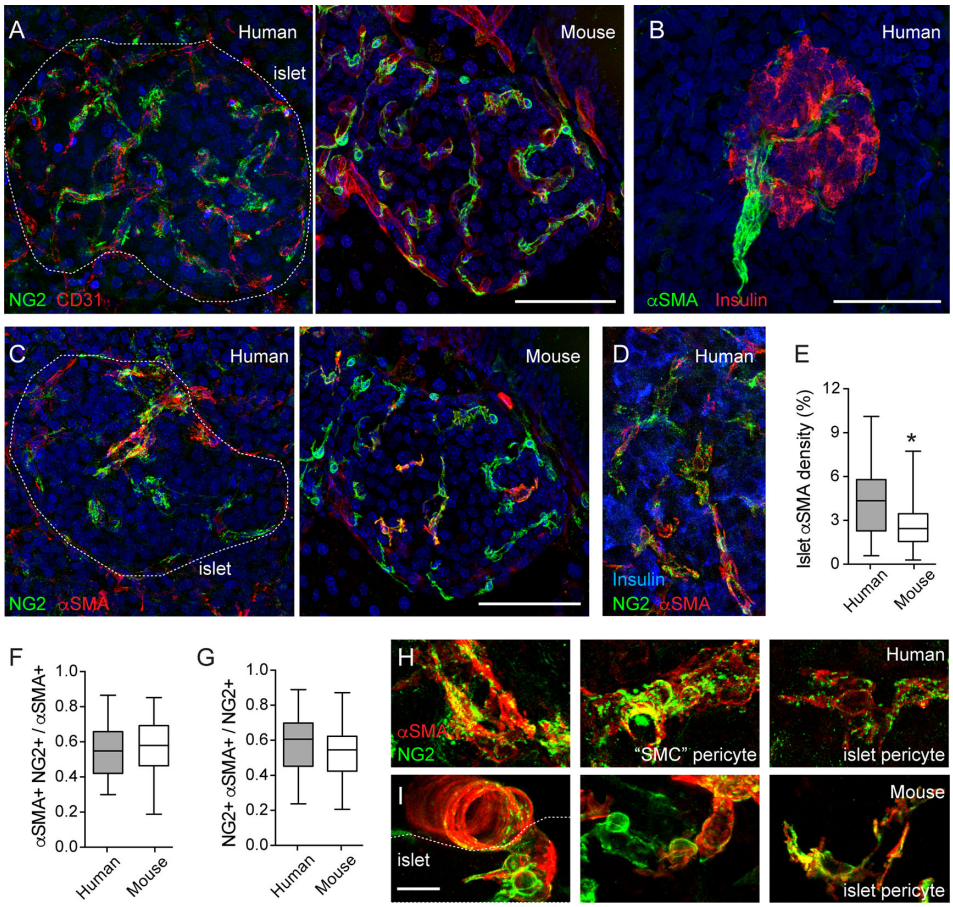

FIGURE 1 | Pericytes cover human and mouse islet capillaries and express αSMA. **(A)** Maximal projection of confocal images of a human (left panel; 16-year-old individual) and a mouse islet (right panel; 2 months old) in pancreatic sections immunostained for pericytes (neuron-glial antigen 2 (NG2), green) and endothelial cells (CD31, red). Pericytes cover mouse and human islet capillaries. Their densities in islets are higher than in surrounding exocrine tissues. **(B)** Maximal projection of confocal images of a human islet immunostained for insulin (red) and smooth muscle actin alpha isoform (αSMA, green). The donor was a 16-year-old individual. Scale bar = 50 µm. **(C)** Maximal projections of confocal images of human (left panel; 16 year old) and a mouse islet (right panel; 2 months old) in pancreatic sections immunostained for pericytes (NG2, green) and αSMA (red). **(D)** Maximal projections of confocal images of a region within a human islet immunostained for NG2 (green), αSMA (red) and insulin (blue). Human donor was a 44-year-old individual. **(E)** Quantification of the islet αSMA density, which is the % of αSMA immunostained area divided the total islet area (N = 24 human islets from 7 non-diabetic human donors (male and female; ages: 15–55 years old); N = 37 mouse islets from 6 C57BL6 mice; 2–18 months old). *p < 0.05 (unpaired t-test). **(F, G)** Mander's (M1 and M2) coefficients reflecting the colocalization between NG2 and αSMA immunostainings. **(F)** is the fraction of αSMA-positive immunostaining that colocalizes with NG2 and **(G)** is the fraction of NG2 -positive immunostaining that colocalizes with αSMA. Panel G has been partially published in (11). We analyzed 21 human islets from 7 non-diabetic human donors (male and female; ages: 15-55 years old) and 31 mouse islets from 6 C57BL6 male mice (2–18 months old). **(H, I)** Zoomed images of NG2 (green) and αSMA (red) labeled cells in human **(H)** and mouse islets **(I)** Different types of pericytes can be found in human islets. We named "SMC" pericytes those cells with more circumferential cytoplasmic processes found on the surface of human islet feeding arterioles (left and middle panels, **H**) to distinguish them from pericytes that were present in the islet parenchyma (islet pericytes, right panels in H and I). "SMC" pericytes and some of human and mouse islet pericytes express αSMA. Scale bars = 50 µm **(A–C)** and 10 µm **(H, I)**.

an arteriole instead of a capillary (vessel diameter of 8–10 µm), this type of islet pericytes resembles more a transitional state toward smooth muscle cells. Therefore, in this study, we named them "SMC" pericytes, while pericytes in the human islet parenchyma and covering capillaries are referred to as human islet pericytes (**Figure 1H**). In mouse islets, the morphology of pericytes (and of blood vessels, see **Figure 2C**) is more homogenous and, thus, we refer to them all as mouse islet pericytes (**Figure 1I**). To summarize, a significant number of mouse and human islet pericytes expresses αSMA, as previously reported for pericytes in the central nervous system (11, 36). These data indicate that pericytes in human and mouse islets may participate in blood flow regulation, but in human islets, they are more heterogenous in terms of morphology and contractile protein expression.

Vascular Trees are Preserved in Living Human and Mouse Pancreas Slices

Isolated islets are the most common research material used to study the physiology of pancreatic islet cells in humans.

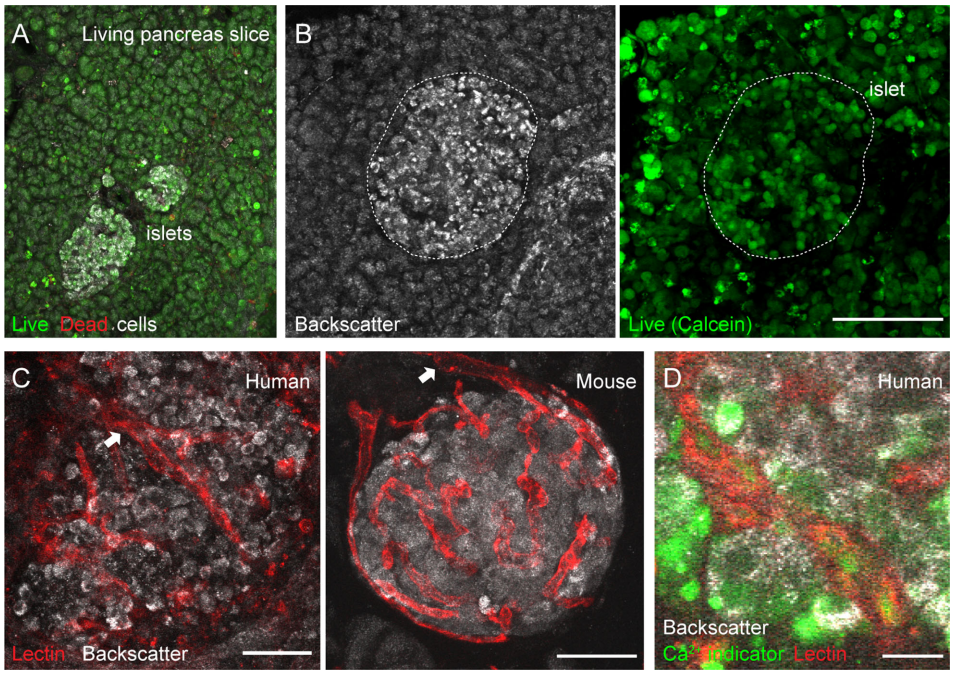

FIGURE 2 | Vascular trees are preserved in living human and mouse pancreas slices. **(A, B)** Maximal projection of confocal images of living human pancreas slices stained with calcein-AM (to visualize live cells, green) and with ethidium homodimer-1 (to visulize dead cells, red). Islet endocrine cells can be seen using the backscatter signal (white, left panel in **B**). The majority of the pancreatic tissue is alive in slices. **(C)** Vascular trees in living human (left panel) and mouse (right panel) living pancreas slices. Human slices were incubated with a fluorescent lectin (from *Lycopersicon esculentum*) to label blood vessels (red), while the lectin was injected intravenously in the mouse before extracting the pancreas. The islet microvasculature is preserved in living pancreas slices. Arrows point to islet feeding arterioles. **(D)** Living human pancreas slices can be incubated with membrane permeable calcium indicators (e.g., Fluo4, green) and fluorescent lectins (red) to simultaneously monitor changes in islet endocrine cell or vascular cell activity. Scale bars = 40 μm **(A–C)** and 10 μm **(D)**.

However, islets, similarly to other endocrine organs (37), lose a significant amount of their vascular cells during the isolation process and with culture (38). To overcome this obstacle and be able to study vascular responses in human islets, we adopted the pancreatic slice technique (25, 39). In pancreas slices, the different cellular components of the islet vascular network are preserved (20), and we have used this platform to perform a detailed functional analysis of mouse islet microvascular responses within the native pancreatic environment (11). Living human pancreas slices produced from fresh tissue samples obtained from the nPOD program have been used by us to compare endocrine cell function in non-diabetics with that of individuals at different stages of type 1 diabetes (26). In the current study, we have used pancreas slices from six organ donors procured either by nPOD or received locally at the Diabetes Research Institute (**Table S1**). Tissue slices were produced within few hours after organ arrival and experiments performed 24 h after slicing. In pancreas slices, the morphology of both exocrine and endocrine tissue compartments is preserved and islet endocrine cells can be distinguished from the surrounding tissue due to the strong light scattering properties of mature secretory granules [**Figure 2B**; (40)]. The vast majority of cells within pancreas slices is viable and, except for the cutting surface, few dead cells are detected (**Figure 2A**). Previous studies had already shown no signs of increased tissue inflammation or immune cell infiltration in islets from non-diabetic organ donors associated with slicing of living tissue (26, 28).

Fluorescent lectins (e.g., from *Lycopersicon esculentum*) that bind to glycoproteins located in the endothelial basement and plasma membranes can be used to visualize blood vessels *ex vivo*. While in mice these lectins can be injected intravenously before sacrificing the animals, living human pancreas slices have to be incubated with them after tissue slicing. In any case, lectin labeling allows us to visualize islet vascular trees (**Figure 2C**). Islet feeding arterioles, which are larger blood vessels that branch off into smaller vessels or capillaries, can be seen penetrating the human islet parenchyma or at the border in mouse islets (**Figure 2C**). Notably, mouse and human islet capillaries do not collapse during slicing, and a lumen is still present in many of them, allowing us to monitor changes in islet vessel diameter by confocal microscopy. Unlike mouse slices, which can be produced from transgenic animals that express genetically encoded fluorescent indicators in specific cell types [e.g., from transgenic mice that express GCaMP3 in pericytes; see **Figure 5** and (11)], human slices have to be incubated with indicators that report on cellular activity. For instance, membrane permeable calcium indicators (such as Fluo4) allow us to monitor changes in cytosolic Ca^{2+} levels ($[Ca^{2+}]_i$) in different cells in human

pancreas slices (e.g., endocrine, vascular, and immune cells; **Figure 2D**). This platform is, thus, very valuable to study intercellular communication in human islets [e.g (28)]. Importantly, we can now simultaneously record changes in vessel diameter and $[Ca^{2+}]_i$ in adjacent vascular cells in the human islet.

Human and Mouse Islet Blood Vessels Constrict and Dilate in Response to Different Vasoactive Substances

As previously published and shown in **Figures 1** and **2**, the human islet microvasculature consists of one (or more) feeding arterioles that penetrate the islet and branch off into a network of capillaries that irrigates the whole islet parenchyma (16). Blood leaves the islet through small venules that often drain directly into capillaries in the exocrine tissue [islet-acinar portal system; (41)]. In this study, we did not examine any postcapillary vessel but focused instead on the arteriolar and capillary segments of the islet microvasculature. In many islets in pancreas slices labeled with lectin, we could distinguish a *feeding arteriole*, that is a vessel with a diameter of around 10 μm (8–12 μm) at the islet border (**Figures 1B** and **3A**) or entering the islet parenchyma (**Figures 1C**, **2C**, and **4C**). We considered *islet capillaries* those lectin-labeled vessels surrounded by endocrine cells (cells with backscatter) with a diameter around 5–7 μm [(42); **Figures 3A** and **3A'**].

Several mechanisms have evolved that regulate islet blood perfusion (8). These include signals from neighboring endothelial cells or metabolically active endocrine cells and extrinsic signals, for instance, from the nervous system (16). We have previously observed that mouse islet capillaries are responsive to these islet intrinsic and extrinsic inputs (11). Using living human pancreas slices, we investigated whether these different signals triggered vasomotion in the human islet. Of note, only a subset of islet capillaries (15–20%) exhibited vasomotion in mouse and human islets and was responsive to applied stimuli *ex vivo* (**Figure 3B**). Norepinephrine is endogenously released by sympathetic nerves that innervate blood vessels in the human islet (35). Exogenous norepinephrine (NE, 20 μM) administration significantly constricted the feeding arteriole in human islets (**Figures 3C, F, G**; average reduction of arteriole diameter ~12%) and a subset of human and mouse islet capillaries (5% reduction in human islet capillary diameter; **Figures 3D–G**). Endothelins are vasoconstrictor peptides endogenously produced by endothelial cells (43). Exogenous administration of endothelin 1 (ET-1, 10 nM) led to powerful constriction of human islet feeding arterioles, as well as of human and mouse islet capillaries (**Figures 3C–E, G**). Interestingly, in human islets, capillary constriction induced by ET-1 occurred before arteriole constriction (**Figures 3C, D**); **Supplementary movie S1**). Adenosine is an important mediator of the metabolic blood flow regulation in many tissues. We had previously published that adenosine, endogenously produced from ATP co-released with insulin, mediates the increase in islet capillary diameter and blood flow upon stimulation of mouse islet beta cells with high glucose (11). Regarding human islets, exogenous adenosine administration (ADO, 50 μM) dilated human islet arterioles by 10% and had no significant effect on human islet capillary diameter (**Figure 3G**).

Vasoactive Substances Change $[Ca^{2+}]_i$ Levels in Human and Mouse Islet Mural Cells

Our next goal was to better characterize the mechanisms that induce vasomotion in human islets, similarly to what we had done in the mouse. An increase or a decrease in $[Ca^{2+}]_i$ in mural cells (vascular smooth muscle cells and pericytes) mediate vasoconstriction or vasodilation, respectively (44). Briefly, initiation of a vasoconstrictor myogenic response, for instance, involves an increase in intracellular free calcium levels in mural cells and calmodulin-dependent activation of myosin light chain kinase. This kinase, in turn, phosphorylates myosin light chain and stimulates the formation of cross bridges between myosin and actin filaments, leading to vasoconstriction (45). By incubating living human pancreas slices with a membrane permeant calcium indicator (Fluo4), we noticed that changes in human islet vessel diameter were accompanied by changes in $[Ca^{2+}]_i$ in neighboring mural cells (**Figure 4**). For instance, NE-mediated arteriole constriction was preceded by an increase in $[Ca^{2+}]_i$ in cells wrapping this vessel (**Figures 4A, B, D**).

Using transgenic mice that express GCaMP3 in pericytes (GCaMP3 expression is controlled by the NG2 promoter), we had previously determined that pericytes control capillary diameter in mouse islets (11). To determine the nature of vascular cells whose activation accompanied vasoconstriction in human islets, we labeled them *in situ* using an anti-NG2 antibody conjugated to a fluorophore (alexa 647; **Figure 5A**). The pattern of labeling using this fluorescent antibody is very similar to the one achieved using a non-conjugated NG2 antibody (used in **Figure 1**; **Figure 5B**). Human islet pericytes can now be visualized *in situ* in living pancreas slices (**Figures 5A, C**). In particular, as described in **Figure 1**, this antibody labels not only pericytes in the islet parenchyma (islet pericytes) but also cells at the islet border that resemble more smooth muscle cells and that we had named "SMC" pericytes (**Figure 5C**). Islet pericytes and "SMC" pericytes incorporated well the calcium indicator, allowing us to compare their physiological responses to different agonists (**Figure 5C**). We recorded changes in $[Ca^{2+}]_i$ induced by norepinephrine, endothelin-1 and adenosine in mural cells in human islets and compared with previously published mouse mural cell $[Ca^{2+}]_i$ data. Norepinephrine (NE) induced a robust and uniform increase in $[Ca^{2+}]_i$ in "SMC" pericytes that coincide with a reduction of the arteriole diameter (**Figures 5D–F** and **Supplementary movie S2**). Indeed, the response of "SMC" pericytes displayed the synchronicity that is needed for vasomotion (46). NE induced a smaller increase in $[Ca^{2+}]_i$ in human and mouse islet pericytes. Interestingly, in human islets, pericytes that responded to NE were located at the islet border and pericytes within the islet parenchyma did not respond to the sympathetic agonist (**Figure 5E**). Endothelin-1 produced a very sharp and significant increase

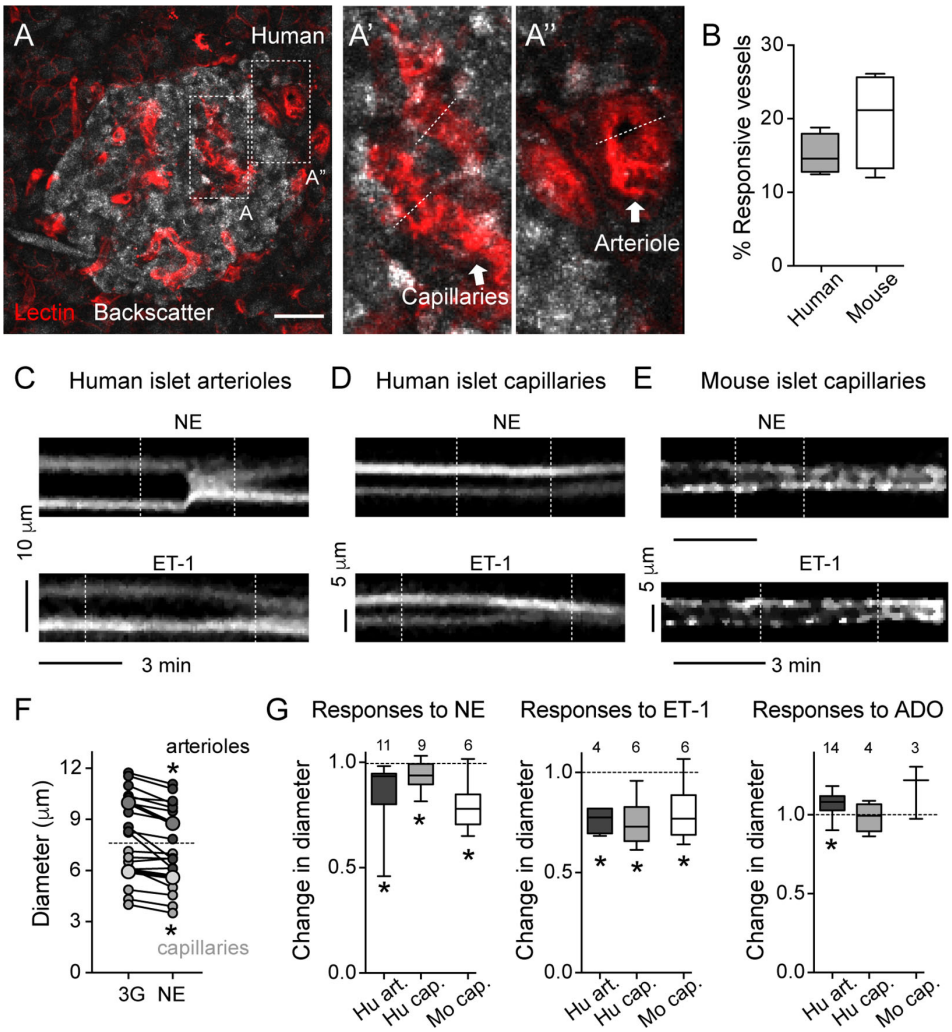

FIGURE 3 | Human and mouse islet blood vessels constrict and dilate in response to different vasoactive substances. **(A)** Maximal projection of confocal images of an islet within a living human pancreas slice. Different types of blood vessels are labeled with a fluorescent lectin (red): capillaries within the islet parenchyma **(A')** and arterioles at the islet border **(A")**. Islet endocrine cells are visualized with backscatter. Dashed lines show vessel regions where temporal projections like those shown in **(C–E)** were taken from. Scale bar = 20 µm. **(B)** Quantification of the percentage of the islet microvasculature that shows vasomotion, calculated as the percentage of responsive vessel area divided by the total islet lectin-labeled vessel area [N = 6 mouse islets (from 4 mice); N = 4 human islets (from 4 donors)]. **(C–E)** Temporal projections showing changes in diameter induced by norepinephrine (20 µM, NE; upper panels) and endothelin-1 (10 nM, ET-1; lower panels) of human islet arterioles [**C**; region A" showed in **(A)**], human islet capillaries [**D**; region A' showed in **(A)**] and mouse islet capillaries **(E)**. Vertical dashed lines indicate when stimuli were applied. Stimuli were applied in 3 mM glucose solutions. Both stimuli are vasoconstrictor. Interestingly, in human islets, ET-1-induced capillary constriction starts before arteriole constriction (arteriole and capillary projections are from the same recording). **(F)** Norepinephrine-induced changes in human islet arterioles (dark gray symbols) and capillary diameters (light gray symbols). Shown are diameter values of different vessels right before (3G) and 3 min after norepinephrine (NE). Bigger symbols show the average vessel diameter. *$p < 0.05$ (paired t-test; N = 9 capillaries, 11 arterioles from 4 different non-diabetic donors). **(G)** Quantification of relative changes in diameter of mouse islet capillaries (white), human islet arterioles (dark gray) and capillaries (light gray box-plot) induced by NE, ET-1 and adenosine (50 µM, ADO) normalized to the initial diameter (after perfusing slices for 3 min with 3 mM glucose solution). Diameter values were taken 3 min after perfusing with norepinephrine (20 µM, NE), 5 min with endothelin-1 (10 nM, ET-1) and 4 min with adenosine (50 µM, ADO). The numbers of vessels analyzed are shown above the box-plots. Data are from 4 different non-diabetic individuals or 3 different mice, at least 1 islet per individual. *$p < 0.05$ [One sample t-test compared to a theoretical mean of 1 (diameter values were normalized to initial vessel diameter)]. Mouse data in this figure were taken from (11, 22).

in $[Ca^{2+}]_i$ in mouse and human islet pericytes, as well as in "SMC" pericytes in human islets (**Figures 5D, F**). In human islets, pericytes at the islet border or in the islet parenchyma responded to endothelin-1 (not shown). Adenosine, in turn, was inhibitory and significantly decreased $[Ca^{2+}]_i$ in mouse islet pericytes, as well as in human islet pericytes and "SMC" pericytes (**Figure 5F**). Our data confirm that pericytes are a very heterogenous population (47) that exhibit various response profiles to different vasoactive substances. The subtype of islet pericyte may be dictated by their location in the islet and differential interactions with other cells within the islet microenvironment, which also differs between mouse and human islets.

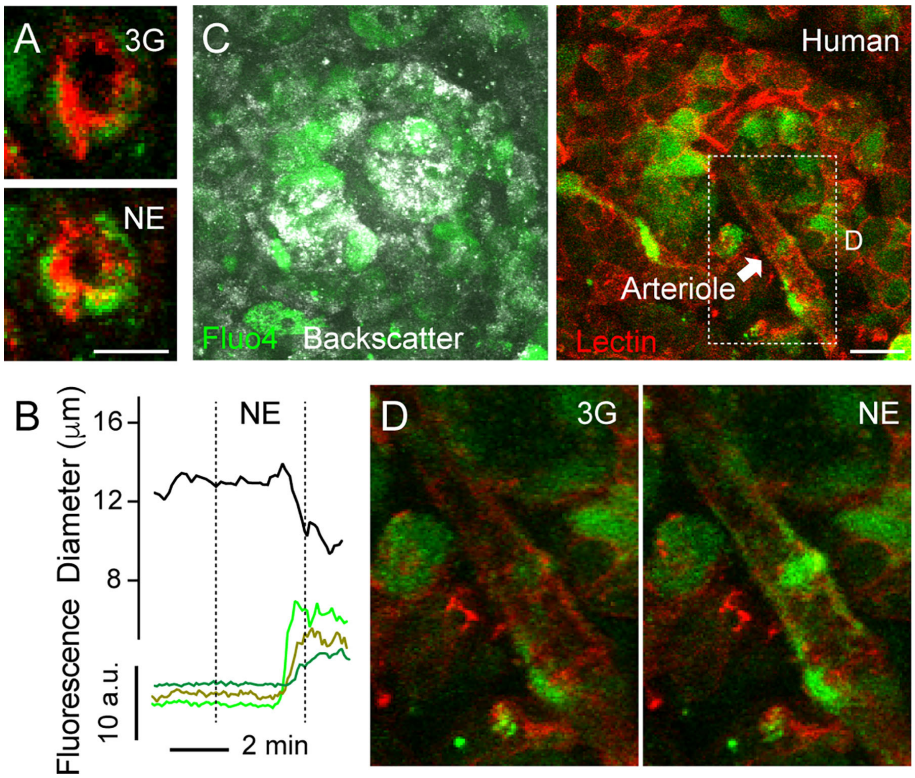

FIGURE 4 | Increases in $[Ca^{2+}]_i$ in mural cells covering human islet arterioles accompanies vasoconstriction. **(A)** Zoomed confocal images of the islet arteriole shown in (A" in **Figure 3**) before (3G; upper panel) and 3 min after NE application (NE, lower panel). Lectin-labeled vessel is shown in red and cells labeled with calcium indicator Fluo4 are shown in green. Scale bar = 10 μm. **(B)** Traces showing absolute changes in diameter and $[Ca^{2+}]_i$ in mural cells of the islet feeding arteriole shown in **(A)**, elicited by NE (20 μM). Curve showing changes in diameter over time was smoothened by averaging 4-neighboring values. **(C)** Maximal projection of confocal images of a human islet in a living pancreas slice labeled with Fluo4 (green) and with a lectin (red). The islet feeding arteriole is indicated with an arrow. Endocrine cells in the islet (seen with backscatter) and mural cells on the surface of the feeding arteriole incorporate the calcium indicator. Scale bar = 20 μm. **(D)** Zoomed images of region within dashed rectangle shown in **(C)** showing an increase in $[Ca^{2+}]_i$ in mural cells covering islet arteriole and vessel constriction triggered by NE.

DISCUSSION

In this study, we performed the first detailed functional characterization of the human islet microvasculature, comparing it side-by-side with what we know about the physiology of mouse islet blood vessels. In human islets, a subset of islet pericytes and smooth muscle cell-like ("SMC") pericytes express the contractile protein αSMA. We measured vasomotion in different types of islet blood vessels in response to exogenous administration of norepinephrine, endothelin-1, and adenosine. We found that islet feeding arterioles and a small subset of capillaries constrict upon norepinephrine and endothelin-1, but only arterioles dilate upon adenosine. We further determined that changes in blood vessel diameter are coupled to changes in cytosolic calcium levels in adjacent pericytes or "SMC" pericytes. Our study points to pericytes as targets of several regulatory mechanisms of islet blood perfusion, similarly to their role in mouse islets.

Our data support that blood flow in the human islet can be regulated locally at the level of the feeding arteriole and of a subset (~15–20%) of islet capillaries, similar to what has been described in rodents (11, 48–50). Here we show that changes in the activity of islet pericytes and "SMC" pericytes mediate vasomotion in human islets and propose that these cells function as local gates. Given recent functional evidence in mice that the islet microcirculation is open and not isolated from that of the surrounding exocrine tissue (51), and the fact that in humans an islet-portal circulatory system is also well developed (41), the existence of such a gating system would allow islet blood flow to be regulated independently of the exocrine tissue under certain conditions, as previously suggested (52).

In this study we perform a functional and anatomical cross comparison of the islet microvasculature between mice and humans. Previous studies had already shown that the architecture and density of islet vascular trees differed significantly between these two species (13, 20). Our analysis has revealed that also the morphology of islet pericytes and blood vessels is more heterogenous in human islets than in mouse islets. Human islets contain a subset of pericytes whose circular cytoplasmic processes give them a smooth muscle cell-like morphology and, therefore, we named them "SMC" pericytes. These type of pericytes localize on

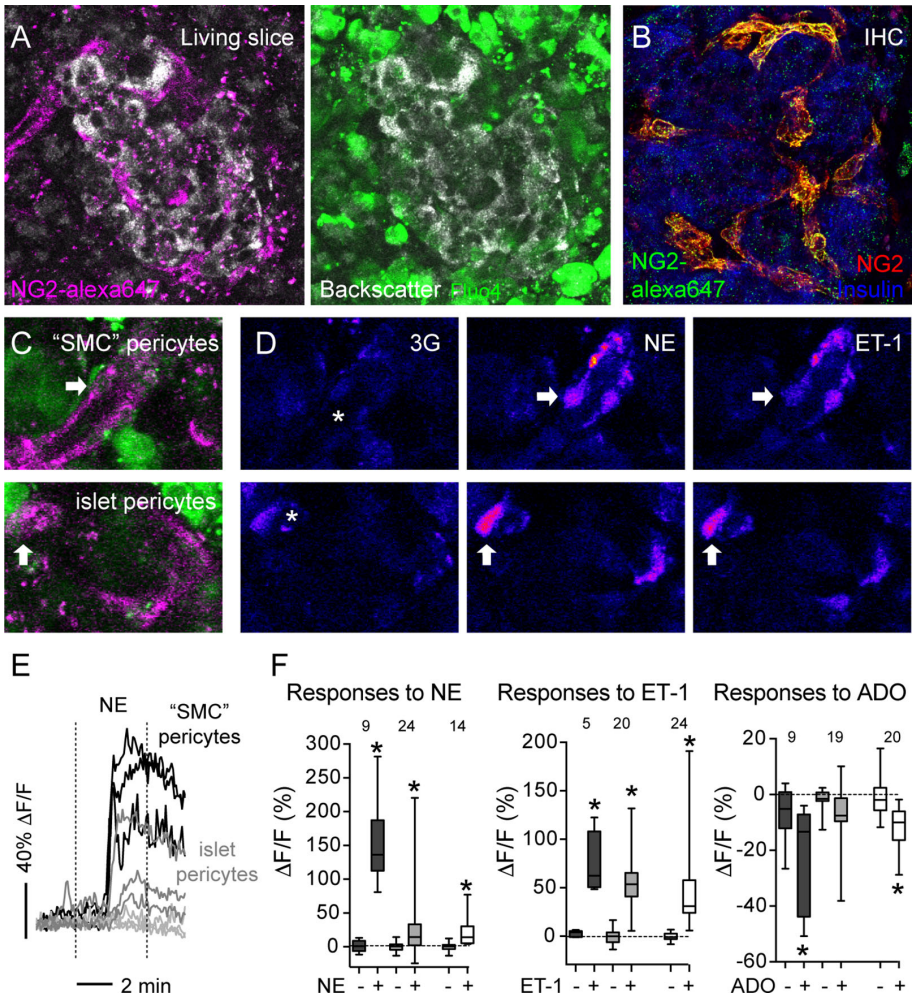

FIGURE 5 | Vasoactive substances change $[Ca^{2+}]_i$ levels in human and mouse islet mural cells. **(A)** Confocal images of a human islet in a living pancreas slice showing fluorescent NG2 antibody (NG2-alexa647; magenta) labeled pericytes *in situ* and fluo-4 loaded cells (green) in living slices. NG2 is a proteoglycan expressed at the plasma membrane of pericytes. Slices Scale bars = 20 µm. **(B)** Maximal projection of confocal images of a human islet in a pancreatic section immunostained for insulin (blue) and pericytes using two different anti-NG2 antibodies: a non-conjugated one (red; used in **Figure 1**) and another conjugated to Alexa647 (green). NG2-alexa647 recognizes pericytes. **(C)** Confocal images of regions within the human islet shown in **(A)**. Different islet mural cells incorporate the calcium indicator Fluo4 (green) and can be visualized with NG2-alexa647 antibody (magenta), such as "SMC" pericytes (upper panel) and islet pericytes (lower panel). **(D)** Changes in Fluo4 fluorescence of cells shown in **(C)** reflecting changes in $[Ca^{2+}]_i$ in "SMC" pericytes (upper panels) and islet pericytes (lower panels) under basal conditions (3 mM glucose concentration, 3G, left panels), after 3 min with NE (middle panels) and 5 min with ET-1 (right panels). Pseudocolor (LUT fire) images are shown to better illustrate absolute changes in fluorescence. Arrows indicate different cells responding to the stimuli, and the * shows the vessel lumen. **(E)** Traces showing relative changes in fluorescence induced by norepinephrine (NE) in individual islet mural cells: "SMC" pericytes (black traces), pericytes at the islet border (dark gray traces) and pericytes in the islet parenchyma (light gray traces). **(F)** Quantification of changes in fluorescence induced by NE, ET-1 or adenosine (ADO) for individual mural cells in human and mouse islets: "SMC" pericytes in human islets (dark gray box-plot), human islet pericytes (light gray box-plot) and mouse islet pericytes (white box-plot). Maximum (peak) amplitude values were taken before (-) and at the end of stimulus application (+). $[Ca^{2+}]_i$ data of mouse islet pericytes was from experiments using mice that expressed the genetically encoded calcium indicator GCaMP3 in pericytes (11). The numbers of cells analyzed are shown above the box-plots. Data are from three different non-diabetic individuals, three different mice, at least one islet per individual. *$p < 0.05$ (paired t-test, comparisons with corresponding values before stimulus application).

the surface of islet feeding arterioles (larger blood vessels that enter the islet parenchyma). Given their location and calcium response profile, "SMC" pericytes resemble precapillary sphincters. The existence of a sphincter-like mechanism had already been reported in monkey islets transplanted into the anterior chamber of the monkey eye (53). Here we show that exogenous norepinephrine induces a stronger activation of islet "SMC" pericytes than of mouse and human islet pericytes and a concomitant and powerful constriction of human islet feeding arterioles. Norepinephrine is a neurotransmitter released at sympathetic nerve terminals. While in mouse islets sympathetic axons equally innervate islet blood vessels and endocrine cells at the periphery, in human islets sympathetic nerves preferentially contact contractile elements around islet blood vessels (35). Thus,

sympathetic modulation of islet hormone secretion in humans may occur in part by affecting islet blood flow (54). Disruption of this mechanism may contribute, for instance, to the impaired glucagon secretion characteristic of type 1 diabetics (55), as loss of islet sympathetic nerves has been seen in mouse models of type 1 diabetes (56) and in type 1 diabetic patients (57).

We further show that mouse and human islet blood vessels and their mural cells are very responsive to the vasoconstrictor peptide endothelin-1. Previous study in rats had shown that endothelin-1 induces a pronounced constriction of islet arterioles and decreased islet blood flow, mainly through ET_A receptors expressed on smooth muscle cells (58). Interestingly, alterations in endothelin-1 release and action have been consistently shown in diabetic patients and animal models of the disease (59). In future studies, we will explore if similar alterations occur at the level of the islet and contribute to impaired hormone secretion during diabetes pathogenesis.

Blood perfusion in the islet is under tight regulatory mechanisms as it can strongly impact the final hormonal output of the islet. Therefore, several mechanisms have evolved that regulate islet blood flow, combining local paracrine signals (e.g., from neighboring endothelial or endocrine cells) with those from the nervous system or the systemic circulation (8, 16). Although *in vivo* studies are critical to understand the physiological context, *ex vivo* functional studies are essential to elucidate the cellular mechanisms responsible for regulating vascular diameter in human islets (46). Using living pancreas slices from donors without diabetes, we have given the first steps exploring what controls vasomotion in human islets. Similar studies can now be performed with tissue from individuals with diabetes and at different disease stages to assess the functional impact of structural alterations of the islet microvasculature that progressively occur, contributing to our understanding of disease pathogenesis.

DATA AVAILABILITY STATEMENT

The raw data supporting the conclusions of this article will be made available by the authors, without undue reservation.

ETHICS STATEMENT

The studies involving human participants were reviewed and approved by IRB approval, University of Miami. Written informed consent for participation was not required for this study in accordance with the national legislation and the institutional requirements.

AUTHOR CONTRIBUTIONS

LG and JA designed the study, and acquired and analyzed data. Both authors discussed the results and interpreted the data. JA wrote the manuscript. All authors contributed to the article and approved the submitted version.

FUNDING

This work was funded by NIH grants K01DK111757 (JA) and by the NIDDK-supported Human Islet Research Network (HIRN, RRID : SCR_014393; https://hirnetwork.org; UC4 DK104162, New Investigator Pilot Award to Joana Almaça).

ACKNOWLEDGMENTS

The authors would like to thank the Network for Pancreatic Organ Donors with Diabetes (nPOD), in particular the organ donors and their families and the whole nPOD slicing team under Dr. Irina Kusmartseva's supervision. We would also like to thank Drs. Fahd Qadir, Jonathan Weitz, and Sirlene Cechin for the help in preparing and culturing human pancreas slices produced locally at the Diabetes Research Institute (Univeristy of Miami).

SUPPLEMENTARY MATERIAL

The Supplementary Material for this article can be found online at: https://www.frontiersin.org/articles/10.3389/fendo.2020.602519/full#supplementary-material

REFERENCES

1. Bonner-Weir S, Orci L. New perspectives on the microvasculature of the islets of Langerhans in the rat. *Diabetes* (1982) 31:883–9. doi: 10.2337/diabetes.31.10.883
2. Brissova M, Shostak A, Shiota M, Wiebe PO, Poffenberger G, Kantz J, et al. Pancreatic islet production of vascular endothelial growth factor–a is essential for islet vascularization, revascularization, and function. *Diabetes* (2006) 55:2974–85. doi: 10.2337/db06-0690
3. Lammert E, Cleaver O, Melton D. Induction of pancreatic differentiation by signals from blood vessels. *Sci (New York NY)* (2001) 294:564–7. doi: 10.1126/science.1064344
4. Lammert E, Gu G, McLaughlin M, Brown D, Brekken R, Murtaugh LC, et al. Role of VEGF-A in vascularization of pancreatic islets. *Curr Biol CB* (2003) 13:1070–4. doi: 10.1016/S0960-9822(03)00378-6
5. Sasson A, Rachi E, Sakhneny L, Baer D, Lisnyansky M, Epshtein A, et al. Islet Pericytes Are Required for beta-Cell Maturity. *Diabetes* (2016) 65:3008–14. doi: 10.2337/db16-0365
6. Epshtein A, Rachi E, Sakhneny L, Mizrachi S, Baer D, Landsman L. Neonatal pancreatic pericytes support beta-cell proliferation. *Mol Metab* (2017) 6:1330–8. doi: 10.1016/j.molmet.2017.07.010
7. Park HS, Kim HZ, Park JS, Lee J, Lee SP, Kim H, et al. beta-Cell-Derived Angiopoietin-1 Regulates Insulin Secretion and Glucose Homeostasis by Stabilizing the Islet Microenvironment. *Diabetes* (2019) 68:774–86. doi: 10.2337/db18-0864
8. Ballian N, Brunicardi FC. Islet vasculature as a regulator of endocrine pancreas function. *World J Surg* (2007) 31:705–14. doi: 10.1007/s00268-006-0719-8
9. Richards OC, Raines SM, Attie AD. The role of blood vessels, endothelial cells, and vascular pericytes in insulin secretion and peripheral insulin action. *Endocrine Rev* (2010) 31:343–63. doi: 10.1210/er.2009-0035

10. Almaça J, Caicedo A, Landsman L. Beta cell dysfunction in diabetes: the islet microenvironment as an unusual suspect. *Diabetologia* (2020) 63:2076–85. doi: 10.1007/s00125-020-05186-5
11. Almaca J, Weitz J, Rodriguez-Diaz R, Pereira E, Caicedo A. The Pericyte of the Pancreatic Islet Regulates Capillary Diameter and Local Blood Flow. *Cell Metab* (2018) 27:630–44.e4. doi: 10.1016/j.cmet.2018.02.016
12. Bogdani M, Johnson PY, Potter-Perigo S, Nagy N, Day AJ, Bollyky PL, et al. Hyaluronan and hyaluronan-binding proteins accumulate in both human type 1 diabetic islets and lymphoid tissues and associate with inflammatory cells in insulitis. *Diabetes* (2014) 63:2727–43. doi: 10.2337/db13-1658
13. Brissova M, Shostak A, Fligner CL, Revetta FL, Washington MK, Powers AC, et al. Human Islets Have Fewer Blood Vessels than Mouse Islets and the Density of Islet Vascular Structures Is Increased in Type 2 Diabetes. *J Histochem Cytochem Off J Histochem Soc* (2015) 63:637–45. doi: 10.1369/0022155415573324
14. Canzano JS, Nasif LH, Butterworth EA, Fu DA, Atkinson MA, Campbell-Thompson M. Islet Microvasculature Alterations With Loss of Beta-cells in Patients With Type 1 Diabetes. *J Histochem Cytochem Off J Histochem Soc* (2019) 67:41–52. doi: 10.1369/0022155418778546
15. Gepts W, Lecompte PM. The pancreatic islets in diabetes. *Am J Med* (1981) 70:105–15. doi: 10.1016/0002-9343(81)90417-4
16. Jansson L, Carlsson PO. Pancreatic Blood Flow with Special Emphasis on Blood Perfusion of the Islets of Langerhans. *Compr Physiol* (2019) 9:799–837. doi: 10.1002/cphy.c160050
17. St Clair JR, Ramirez D, Passman S, Benninger RKP. Contrast-enhanced ultrasound measurement of pancreatic blood flow dynamics predicts type 1 diabetes progression in preclinical models. *Nat Commun* (2018) 9:1742. doi: 10.1038/s41467-018-03953-y
18. Gepts W. *The islet of Langerhans: Biochemistry, Physiology and Pathology*. Academic Press (1981), Chapter 13. doi: 10.1016/B978-0-12-187820-7.50019-X
19. Hayden MR, Karuparthi PR, Habibi J, Lastra G, Patel K, Wasekar C, et al. Ultrastructure of islet microcirculation, pericytes and the islet exocrine interface in the HIP rat model of diabetes. *Exp Biol Med (Maywood NJ)* (2008) 233:1109–23. doi: 10.3181/0709-RM-251
20. Cohrs CM, Chen C, Jahn SR, Stertmann J, Chmelova H, Weitz J, et al. Vessel Network Architecture of Adult Human Islets Promotes Distinct Cell-Cell Interactions In Situ and Is Altered After Transplantation. *Endocrinology* (2017) 158:1373–85. doi: 10.1210/en.2016-1184
21. Virtanen I, Banerjee M, Palgi J, Korsgren O, Lukinius A, Thornell LE, et al. Blood vessels of human islets of Langerhans are surrounded by a double basement membrane. *Diabetologia* (2008) 51:1181–91. doi: 10.1007/s00125-008-0997-9
22. Mateus Gonçalves L, Pereira E, Werneck de Castro JP, Bernal-Mizrachi E, Almaça J. Islet pericytes convert into profibrotic myofibroblasts in a mouse model of islet vascular fibrosis. *Diabetologia* (2020) 63:1564–75. doi: 10.1007/s00125-020-05168-7
23. Westermark P, Engstrom U, Johnson KH, Westermark GT, Betsholtz C. Islet amyloid polypeptide: pinpointing amino acid residues linked to amyloid fibril formation. *Proc Natl Acad Sci U S A* (1990) 87:5036–40. doi: 10.1073/pnas.87.13.5036
24. Westermark P, Wilander E. The influence of amyloid deposits on the islet volume in maturity onset diabetes mellitus. *Diabetologia* (1978) 15:417–21. doi: 10.1007/BF01219652
25. Marciniak A, Cohrs CM, Tsata V, Chouinard JA, Selck C, Stertmann J, et al. Using pancreas tissue slices for in situ studies of islet of Langerhans and acinar cell biology. *Nat Protoc* (2014) 9:2809–22. doi: 10.1038/nprot.2014.195
26. Panzer JK, Hiller H, Cohrs CM, Almaça J, Enos SJ, Beery M, et al. Pancreas tissue slices from organ donors enable in situ analysis of type 1 diabetes pathogenesis. *JCI Insight* (2020) 5(8):e134525. doi: 10.1172/jci.insight.134525
27. Qadir MMF, Álvarez-Cubela S, Weitz J, Panzer JK, Klein D, Moreno-Hernández Y, et al. Long-term culture of human pancreatic slices as a model to study real-time islet regeneration. *Nat Commun* (2020) 11:3265. doi: 10.1038/s41467-020-17040-8
28. Weitz JR, Jacques-Silva C, Fahd Qadir MM, Umland O, Pereira E, Qureshi F, et al. Secretory Functions of Macrophages in the Human Pancreatic Islet are Regulated by Endogenous Purinergic Signaling. *Diabetes* (2020) 69(6):1206–18. doi: 10.2337/db19-0687
29. Houtz J, Borden P, Ceasrine A, Minichiello L, Kuruvilla R. Neurotrophin Signaling Is Required for Glucose-Induced Insulin Secretion. *Dev Cell* (2016) 39:329–45. doi: 10.1016/j.devcel.2016.10.003
30. Tang SC, Jessup CF, Campbell-Thompson M. The Role of Accessory Cells in Islet Homeostasis. *Curr Diabetes Rep* (2018) 18:117. doi: 10.1007/s11892-018-1096-z
31. Bergers G, Song S. The role of pericytes in blood-vessel formation and maintenance. *Neuro-oncology* (2005) 7:452–64. doi: 10.1215/S1152851705000232
32. Krueger M, Bechmann I. CNS pericytes: concepts, misconceptions, and a way out. *Glia* (2010) 58:1–10. doi: 10.1002/glia.20898
33. Attwell D, Mishra A, Hall CN, O'Farrell FM, Dalkara T. What is a pericyte? *J Cereb Blood Flow Metab Off J Int Soc Cereb Blood Flow Metab* (2016) 36:451–5. doi: 10.1177/0271678X15610340
34. Fowler JL, Lee SS, Wesner ZC, Olehnik SK, Kron SJ, Hara M. Three-Dimensional Analysis of the Human Pancreas. *Endocrinology* (2018) 159:1393–400. doi: 10.1210/en.2017-03076
35. Rodriguez-Diaz R, Abdulreda MH, Formoso AL, Gans I, Ricordi C, Berggren PO, et al. Innervation patterns of autonomic axons in the human endocrine pancreas. *Cell Metab* (2011) 14:45–54. doi: 10.1016/j.cmet.2011.05.008
36. Bandopadhyay R, Orte C, Lawrenson JG, Reid AR, De Silva S, Allt G. Contractile proteins in pericytes at the blood-brain and blood-retinal barriers. *J Neurocytol* (2001) 30:35–44. doi: 10.1023/A:1011965307612
37. Parr EL, Bowen KM, Lafferty KJ. Cellular changes in cultured mouse thyroid glands and islets of Langerhans. *Transplantation* (1980) 30:135–41. doi: 10.1097/00007890-198008000-00012
38. Nyqvist D, Köhler M, Wahlstedt H, Berggren PO. Donor islet endothelial cells participate in formation of functional vessels within pancreatic islet grafts. *Diabetes* (2005) 54:2287–93. doi: 10.2337/diabetes.54.8.2287
39. Speier S, Rupnik M. A novel approach to in situ characterization of pancreatic beta-cells. *Pflugers Archiv Eur J Physiol* (2003) 446:553–8. doi: 10.1007/s00424-003-1097-9
40. Ilegems E, van Krieken PP, Edlund PK, Dicker A, Alanentalo T, Eriksson M, et al. Light scattering as an intrinsic indicator for pancreatic islet cell mass and secretion. *Sci Rep* (2015) 5:10740. doi: 10.1038/srep10740
41. Murakami T, Hitomi S, Ohtsuka A, Taguchi T, Fujita T. Pancreatic insulo-acinar portal systems in humans, rats, and some other mammals: scanning electron microscopy of vascular casts. *Microscopy Res Technique* (1997) 37:478–88. doi: 10.1002/(SICI)1097-0029(19970601)37:5/6<478::AID-JEMT10>3.0.CO;2-N
42. Henderson JR, Moss MC. A morphometric study of the endocrine and exocrine capillaries of the pancreas. *Q J Exp Physiol (Cambridge. England)* (1985) 70:347–56. doi: 10.1113/expphysiol.1985.sp002920
43. Davenport AP, Hyndman KA, Dhaun N, Southan C, Kohan DE, Pollock JS, et al. Endothelin. *Pharmacol Rev* (2016) 68:357–418. doi: 10.1124/pr.115.011833
44. Burdyga T, Borysova L. Calcium signalling in pericytes. *J Vasc Res* (2014) 51:190–9. doi: 10.1159/000362687
45. Kamm KE, Stull JT. The function of myosin and myosin light chain kinase phosphorylation in smooth muscle. *Annu Rev Pharmacol Toxicol* (1985) 25:593–620. doi: 10.1146/annurev.pa.25.040185.003113
46. Aalkjær C, Boedtkjer D, Matchkov V. Vasomotion - what is currently thought? *Acta Physiol (Oxford England)* (2011) 202:253–69. doi: 10.1111/j.1748-1716.2011.02320.x
47. Shepro D, Morel NM. Pericyte physiology. *FASEB J Off Publ Fed Am Societies Exp Biol* (1993) 7:1031–8. doi: 10.1096/fasebj.7.11.8370472
48. Brunicardi FC, Stagner J, Bonner-Weir S, Wayland H, Kleinman R, Livingston E, et al. Microcirculation of the islets of Langerhans. Long Beach Veterans Administration Regional Medical Education Center Symposium. *Diabetes* (1996) 45:385–92. doi: 10.2337/diab.45.4.385
49. Liu YM, Guth PH, Kaneko K, Livingston EH, Brunicardi FC. Dynamic in vivo observation of rat islet microcirculation. *Pancreas* (1993) 8:15–21. doi: 10.1097/00006676-199301000-00005
50. McCuskey RS, Chapman TM. Microscopy of the living pancreas in situ. *Am J Anat* (1969) 126:395–407. doi: 10.1002/aja.1001260402
51. Dybala MP, Kuznetsov A, Motobu M, Hendren-Santiago BK, Philipson LH, Chervonsky AV, et al. Integrated Pancreatic Blood Flow: Bidirectional

Microcirculation Between Endocrine and Exocrine Pancreas. *Diabetes* (2020) 69:1439–50. doi: 10.2337/db19-1034
52. Almaça J, Caicedo A. Blood Flow in the Pancreatic Islet: Not so Isolated Anymore. *Diabetes* (2020) 69:1336–8. doi: 10.2337/dbi20-0016
53. Diez JA, Arrojo EDR, Zheng X, Stelmashenko OV, Chua M, Rodriguez-Diaz R, et al. Pancreatic Islet Blood Flow Dynamics in Primates. *Cell Rep* (2017) 20:1490–501. doi: 10.1016/j.celrep.2017.07.039
54. Brunicardi FC, Sun YS, Druck P, Goulet RJ, Elahi D, Andersen DK. Splanchnic neural regulation of insulin and glucagon secretion in the isolated perfused human pancreas. *Am J Surg* (1987) 153:34–40. doi: 10.1016/0002-9610(87)90198-X
55. Bolli G, de Feo P, Compagnucci P, Cartechini MG, Angeletti G, Santeusanio F, et al. Abnormal glucose counterregulation in insulin-dependent diabetes mellitus. Interaction of anti-insulin antibodies and impaired glucagon and epinephrine secretion. *Diabetes* (1983) 32:134–41. doi: 10.2337/diabetes.32.2.134
56. Taborsky GJ Jr, Mei Q, Hackney DJ, Figlewicz DP, LeBoeuf R, Mundinger TO. Loss of islet sympathetic nerves and impairment of glucagon secretion in the NOD mouse: relationship to invasive insulitis. *Diabetologia* (2009) 52:2602–11. doi: 10.1007/s00125-009-1494-5
57. Mundinger TO, Mei Q, Foulis AK, Fligner CL, Hull RL, Taborsky GJ Jr. Human Type 1 Diabetes Is Characterized by an Early, Marked, Sustained, and Islet-Selective Loss of Sympathetic Nerves. *Diabetes* (2016) 65:2322–30. doi: 10.2337/db16-0284
58. Lai EY, Persson AE, Bodin B, Kallskog O, Andersson A, Pettersson U, et al. Endothelin-1 and pancreatic islet vasculature: studies in vivo and on isolated, vascularly perfused pancreatic islets. *Am J Physiol Endocrinol Metab* (2007) 292:E1616–23. doi: 10.1152/ajpendo.00640.2006
59. Hopfner RL, Gopalakrishnan V. Endothelin: emerging role in diabetic vascular complications. *Diabetologia* (1999) 42:1383–94. doi: 10.1007/s001250051308

Conflict of Interest: The authors declare that the research was conducted in the absence of any commercial or financial relationships that could be construed as a potential conflict of interest.

frontiers in Endocrinology

MINI REVIEW
published: 04 March 2021
doi: 10.3389/fendo.2021.633063

Mesoscopic Optical Imaging of the Pancreas—Revisiting Pancreatic Anatomy and Pathophysiology

Tomas Alanentalo, Max Hahn, Stefanie M. A. Willekens and Ulf Ahlgren *

Umeå Centre for Molecular Medicine, Umeå University, Umeå, Sweden

The exocrine-endocrine multipart organization of the pancreas makes it an exceedingly challenging organ to analyze, quantitatively and spatially. Both in rodents and humans, estimates of the pancreatic cellular composition, including beta-cell mass, has been largely relying on the extrapolation of 2D stereological data originating from limited sample volumes. Alternatively, they have been obtained by low resolution non-invasive imaging techniques providing little detail regarding the anatomical organization of the pancreas and its cellular and/or molecular make up. In this mini-review, the state of the art and the future potential of currently existing and emerging high-resolution optical imaging techniques working in the mm-cm range with μm resolution, here referred to as mesoscopic imaging approaches, will be discussed regarding their contribution toward a better understanding of pancreatic anatomy both in normal conditions and in the diabetic setting. In particular, optical projection tomography (OPT) and light sheet fluorescence microscopy (LSFM) imaging of the pancreas and their associated tissue processing and computational analysis protocols will be discussed in the light of their current capabilities and future potential to obtain more detailed 3D-spatial, quantitative, and molecular information of the pancreas.

Keywords: mesoscopic imaging, optical projection tomography, light sheet fluorescence microscopy, pancreas, diabetes

OPEN ACCESS

Edited by:
Vincent Poitout,
Université de Montréal, Canada

Reviewed by:
Susan Bonner-Weir,
Joslin Diabetes Center and Harvard Medical School, United States
Tom Jetton,
University of Vermont, United States

***Correspondence:**
Ulf Ahlgren
Ulf.Ahlgren@umu.se

Specialty section:
This article was submitted to Diabetes: Molecular Mechanisms, a section of the journal Frontiers in Endocrinology

Received: *24 November 2020*
Accepted: *07 January 2021*
Published: *04 March 2021*

Citation:
Alanentalo T, Hahn M, Willekens SMA and Ahlgren U (2021) Mesoscopic Optical Imaging of the Pancreas—Revisiting Pancreatic Anatomy and Pathophysiology. Front. Endocrinol. 12:633063. doi: 10.3389/fendo.2021.633063

INTRODUCTION

Both in rodents and humans, the compound organization of the pancreas renders analyses of its cellular and molecular make up exceedingly challenging. Until recently, studies of pancreatic anatomy/pathophysiology have largely relied on traditional immunohistochemical analyses. However, these usually only cover a very limited tissue volume and their results inevitably represent extrapolations of a limited amount of 2-dimensional (2D) data. This not only entails challenges for putting the resultant data into a 3-dimensional (3D) context, but it may also involve a wide range of assumptions regarding structural shapes (e.g., islets) or organ homogeneity of the object to study. Albeit stereological assessments obviously are of great importance; the development of modern optical imaging techniques provides a whole new set of tools to better assess and understand cellular and molecular pancreatic features in both a 3D spatial and quantitative context. By high resolution mesoscopic imaging techniques working in the mm-cm range, such as: optical projection tomography (OPT) (1) and light sheet fluorescence microscopy (LSFM) (2–4), highly

detailed images of the pancreatic cellular composition can be obtained in a broader anatomical context, even within the framework of the entire gland. Furthermore, they offer powerful possibilities to assess various and specific quantitative and spatial pancreatic features in the diabetic setting, including ß-cell mass (BCM), distribution and plasticity, organ heterogeneities, rare event screening, cellular ratios, immune-cell infiltration, vascularization, innervation, and many more. When using advanced image analysis software, they also offer new ways to display the obtained data and perform advanced statistical assessments. In this mini-review, we will give a brief overview of how these techniques have been applied in basic diabetes research, elaborate on recent developments in the field and propose how they may be implemented in the future.

OPT AND LSFM: COMPLEMENTARY APPROACHES FOR *EX VIVO* 3D IMAGING OF THE PANCREAS

Although 3D imaging techniques, such as: micro-computed tomography (μCT) and micro-magnetic resonance imaging (μMRI), provide high resolution images of tissue morphology in complete organs, or even entire animals, they cannot take advantage of the molecule-specific labeling techniques available for fluorescence microscopy imaging. OPT and LSFM are optical 3D imaging techniques for mesoscopic sized samples (i.e., on the mm-cm scale), enabling assessments on the mm-scale. In principle, OPT could simply be described as the optical analogue of X-ray CT, using light instead of X-rays. Hence, by acquiring a series of 2D projections, obtained from different angles, the 3D structure of the investigated tissue is generated as a stack of cross-sectional image slices using a reconstruction algorithm, commonly a filtered-back projection. In contrast to OPT, wherein sample illumination and detection are performed in one direction (for each projection), LSFM acquires data by performing these processes in two distinct optical paths, orthogonally to each other. Most commonly, a light sheet is generated by a (Gaussian) laser and the specimen is scanned either by moving the light sheet or by moving the specimen in relation to a static light sheet in order to produce optical sections through the specimen. For both techniques, registration is performed by a digital camera. Whereas OPT and LSFM have several common features, including labeling techniques and the need for tissue clearing, allowing light propagation through the tissue sample, they also have a number of distinct features, rendering both of them optimal for different imaging tasks. Most importantly, LSFM provides a higher lateral but lower axial resolution as compared to OPT (5), resulting in non-isotropic voxels, which may result in ambiguities for 3D analysis. Nonetheless, it should be noted that both hardware and software development is advancing rapidly in this field. A recent significant example is cleared-tissue axially swept light-sheet microscopy (ctASLM), which enables imaging with significantly increased z-axial resolution in mm-sized specimen (6), thereby approaching isotropic voxels. However, due to its respective detection principle, OPT does provide true isotropic spatial resolution (i.e., voxels with identical dimensions along the x, y, and z axes). For imaging of murine and human pancreatic tissue, it is our experience that OPT is more suited for larger samples at lower magnification and for larger tissue cohorts, in relation to scan times and data volumes, while LSFM is preferred for higher resolution images of specific regions of interest (ROIs), or smaller sample cohorts. Still, both techniques are often interchangeable and can in many cases substitute or complement each other (5).

Methods for rendering tissues transparent were already described as early as in 1914 (7) F and represent a key feature in mesoscopic 3D imaging to allow the propagation of light through the investigated specimen. Another very important aspect is to assure penetration of labeling agents, commonly antibodies. For certain tissues, quenching of autofluorescence (AF) is also required to increase the signal to noise ratio. Due to the limited available methods to overcome these obstacles, fluorescent immunohistochemistry has remained, for a long period of time, restricted to thin tissue sections or embryonic scale specimen. In 2007, Alanentalo et al., developed an approach enabling clearing and whole-mount immunohistochemistry for OPT-based assessments of the BCM distribution in the complete mouse pancreas (8). Afterward, the protocol was successfully applied to other organs, such as livers containing islet grafts (9). Ever since, there has been an explosion in this particular field and at present, numerous powerful clearing, and whole-mount immunohistochemistry protocols exist [for review see (10–12)]. Clearing methods are commonly divided into organic-, aqueous-, and hydrogel-based clearing techniques (13). These have in common that they use liquids to match the refractive index (RI) of the cellular constituents to reduce light scattering within the sample. Organic clearing methods usually dehydrate and delipidate the tissue before homogenization of the RI. The choice of the optimal clearing agent for a specific tissue should be based on the sample size, the need to prevent fluorescence quenching of the labeling reagent (like transgenically expressed proteins), and its potential tissue shrinkage or expansion effects.

MESOSCOPIC IMAGING OF THE PANCREAS—SO FAR

Pancreatic development has been well studied (14), but given the complex morphogenesis of the pancreatic buds in relation to one another and to the surrounding tissues, several aspects of its development are difficult to interpret by traditional 2D stereological imaging techniques. Therefore, OPT was originally used for 3D mapping of RNA and protein expression in developmental biology studies. The possibility of OPT to produce interactive 3D data, such as: blow-up views and tiltable section planes, highlighting distinct tissue components, has contributed to reveal new aspects of the interrelationship between the pancreatic epithelium and the spleno-pancreatic mesenchyme (15–17). Indeed, OPT imaging played an instrumental role in demonstrating that the

gastric lobe of the murine pancreas forms by perpendicular growth from the dorsal pancreatic bud and, that its morphogenesis is dependent on formation of the spleen (18). Furthermore, these particular studies prompted for a designated nomenclature of the murine pancreatic regions, based on their developmental origins (14). After optimization of the OPT hardware, tissue clearing/labeling protocols and processing schemes for the murine pancreas, the complete BCM distribution within the intact gland, revealing significant heterogeneities in both islet size and number throughout the pancreatic lobes was presented (19).By further technical refinements (9, 20, 21), OPT has been proven a very useful approach for ß-cell/islet mass distribution assessments in murine diabetes models, by omitting the need for extrapolation of 2D data through direct assessments of the islet's numbers, volumes, and spatial coordinates throughout the entire gland. Noteworthy, OPT analyses demonstrated significant heterogeneities in BCM distribution and islet density between the primary pancreatic lobes (21), emphasizing the need for careful considerations regarding the origin of the investigated tissue for sampled analyses (see **Figures 1A–C**). Working with tomographic data provides the possibility to perform combined 3D-spatial, quantitative, and statistical analyses of the BCM distribution (see **Figures 1D, E**). As such, OPT has significantly contributed to a range of studies investigating BCM dynamics, islet plasticity, and ß-cell function in diverse rodent models (22, 23, 25–33). For example, by pseudocoloring islets of different size categories, patterns of selective islet vulnerability of different sized islets were revealed in models of ß-cell destruction. It was demonstrated that smaller islets are more susceptible to destruction in models of naturally induced diabetes (22, 28), whereas in streptozotocin induced diabetes primarily larger islets are affected (25). Furthermore, a global view of the pancreatic constitution may reveal novel features, even in previously well studied diabetes models. OPT analyses of the leptin deficient *Ob/Ob* mouse, a model used in thousands of investigations, demonstrated significant internal islet hemorrhaging, a feature overlooked in previous stereological assessments (23). Of note, in conjunction with this study, tomographic data of the complete pancreatic islet distribution between 4 and 52 weeks in cohorts of both lean and obese mice were made publicly available (24). These studies exemplify how OPT imaging of large animal cohorts can be employed to identify ROIs for higher resolution imaging by LSFM, in order to study disturbed islet morphology in more detail. Obviously mesoscopic imaging techniques like OPT and LSFM are not limited to studies of BCM. In particular LSFM techniques, taking advantage of its normally higher resolution, have been recently applied to study aspects of e.g., pancreatic innervation, immune cell infiltration, and proliferation, in various mouse models of diabetes using specific antibody markers for these features (34, 35).

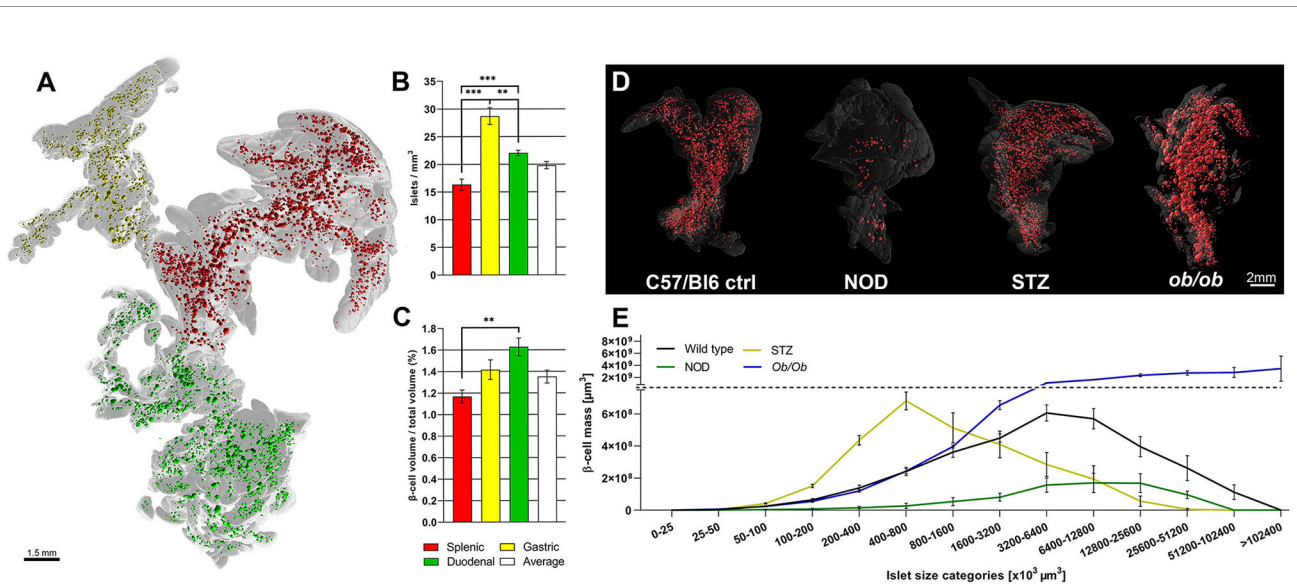

FIGURE 1 | Optical projection tomography enables isotropic resolution imaging and quantification of antibody labeled features throughout the volume of the rodent pancreas. Montage illustrating the variance in islet mass distribution between different disease models as determined by OPT. **(A)** Optical projection tomography (OPT) generated 3D reconstruction of the isolated pancreas from a C57Bl/6 mouse (8 weeks) labeled for insulin. The islets of the splenic, gastric, and duodenal lobe are pseudocolored; red, yellow, and red respectively. The lobular compartments (gray) are delineated based on their developmental origins [see Hörnblad et al. (14)]. **(B, C)** Graphs showing the lobar distribution of insulin$^+$ islets per mm (3) **(B)** and ß-cell volume per total lobular volume **(C)**, illustrating that the lobular compartments of the rodent pancreas display significant different differences in islet ß-cell mass (BCM) densities. **(D)** Images depicting (from left to right) OPT based iso-surface reconstructions of adult mouse pancreas (splenic lobe), from a healthy C57Bl/6 mouse (8 weeks), a non-obese diabetic (NOD) mouse (T1D model at 16 weeks), streptozotocin (STZ) induced diabetic (C57Bl/6 mice at 9 weeks, 2 weeks post-single high dose STZ administration), and an *ob/ob* mouse (at 26 weeks), respectively. The islet β-cell volumes (red) are reconstructed based on insulin specific antibody signal and the outline of the pancreas (gray) is based on the tissues autofluorescence. **(E)** Graph depicting ß-cell volumes per islet size category of the models depicted in **(D)**, illustrating the possibility to obtain detailed assessments of BCM distribution in the pancreas by OPT. Data is obtained from Hörnblad et al. (21), Alanentalo et al. (22), Parween et al. (23, 24), and Hahn et al. (25).

Ex vivo OPT or LSFM imaging of the pancreas also provides a powerful complemental approach for studies of islet plasticity, destruction etc., conducted by *in vivo* assessments of islets grafts in the anterior chamber of the eye (ACE) (36) (see separate article Ilegems et al.). Since islets transplanted to this site have been reported to provide a mirror image of the endogenous islets, phenotypical *in vivo* observations in the ACE may therefore be confirmed on the pancreatic level by end point *ex vivo* mesoscopic imaging (23, 25, 37, 38). Additionally, mesoscopic optical imaging also offers the possibility to serve as an evaluating tool for other *in vivo* imaging technologies. Since they offer an "absolute" quantitative and spatial account of specifically labeled cells within the entire volume, OPT or LSFM data sets could serve as a "gold" standard against which other imaging modalities could be compared and potentially provide additional complementary information. In this respect, OPT has been demonstrated advantageous for validating radiotracer uptake for ß-cell imaging (39). Interestingly, this study demonstrated a superior linear correlation between the single photon emission computed tomography (SPECT) and OPT, as compared to SPECT *versus* histology. Another example comes from studies of islets with a technology diametrically different from SPECT. Ilegems et al., demonstrated that the transplanted islet volume to the ACE can be measured *in vivo* based on the backscatter from the insulin secretory granules. When the grafted eyes were examined by OPT *ex vivo*, the islet volumes could be plotted against each other, islet by islet, showing a nearly perfect correlation (40).

MESOSCOPIC IMAGING OF THE PANCREAS—WHAT LIES AHEAD

In combination with a vast number of potent tissue-clearing protocols, mesoscopic optical imaging technologies have undergone dramatic developments during the past decade. We anticipate that the next, and very important, technological/methodological development for mesocopic imaging will involve improved procedures for penetration of fluorescent labeling reagents with high molecular binding specificity (e.g., antibodies). Such optimizations will help addressing one of the greatest limitations of these high-resolution 3D imaging approaches for diabetes research by allowing the possibility to analyze larger volumes of human pancreatic tissue. Albeit a small number of studies have demonstrated the possibility to label human pancreatic tissue by antibodies *ex vivo*, these studies are confined to relatively small tissue preparations [see e.g. (34, 41)]. Furthermore, clearing protocols, such as SHANEL (42), have been demonstrated to enable clearing of intact human organs (and the pig pancreas). Still the human pancreas presents significant challenges for antibody-based labeling procedures caused by insufficient reagent penetration and endogenous AF disturbances. The possibility to study any protein expression pattern throughout the human pancreas, in mm resolution, would have significant implications in this research field. It is likely that a holistic view of the human pancreatic anatomy, implementing high resolution optical 3D images, using specific molecular markers, will contribute to a greatly enhanced understanding of the pancreatic constitution. As previously exemplified in the mouse (8, 14, 18), it may not only contribute to unravel novel features of its normal anatomical organization. Such methodological advances may obviously also contribute to address a wide range of pathological/mechanistical features, on a molecular level, related to diabetes. For example, by offering the possibility to screen for and to perform "absolute" quantifications of e.g., islet mass distribution, immune-cell infiltration, amyloid deposition, endocrine cell maturity/function, or cellular ratios etc. Furthermore, they may provide a powerful approach to identify ROI´s or rare cell niches which would be much more challenging with the currently available technologies. Recently, Zhao et al. used purpose-built LSFM setups to demonstrate that this type of investigation would already be possible given that sufficient labeling could be acquired (42). Probably, future labeling protocols utilizing cameloid or shark nanobodies (43), which have much lower molecular weight as compared to common antibodies (approximately 12–15 *vs*. 150–160 kDa in size), will contribute to such developments. In view of the above, it is likely that advances in computational tools will be required for our possibilities to statistically assess and to visualize the gradually increasing data sets that are/will be possible to obtain by mesoscopic imaging techniques. Powerful computers running specific programs using algorithms for machine learning and/or deep learning may significantly contribute to facilitate analyses of complicated expression patterns and cellular distribution patterns in large organs preparations analyzed by high resolution OPT or LSFM. In this respect, these tools could enable greatly improved analyses of e.g., vascularization and innervation (44, 45), cellular responses, gene activation (46), automated and unbiased volumetric quantification of labeled features, such as islets or infiltrating immune-cells (47).

As mentioned before, the AF properties of the pancreas, and in particular the human pancreas, may significantly obstruct fluorescent 3D imaging assessments when using OPT and LSFM. However, the pancreatic AF properties differ significantly in distinct parts of the spectrum. By using narrow wavelength bands in a wide range of the spectrum (400–700nm), we could recently demonstrate that e.g., blood vessels, islets and even pancreatic malignancies could be visualized and segmented individually based solely on their AF properties both by OPT and LSFM (48) (see **Figure 2**). In this study, the far red to near infrared spectrum provided sufficient signal to noise ratio to enable quantitative 3D assessments of the islet mass distribution in >cm (3) sized pancreatic biopsies, based on the AF signal caused by the accumulation of, most likely, lipofuscin-like pigments in the islets. It should be noted however, that the accumulation of this lysosomal digestion product may differ between individuals of various ages and disease history. Therefore, specific molecular labeling would be advantageous for standardized assessments of islet mass.

Like SPECT and PET, OPT, and LSFM represent functional imaging techniques, designed to visualize specific cells or processes in a certain target tissue, normally using specific antibodies. The most important advantage of these functional techniques is that they exert great sensitivity and specificity for their target. On the

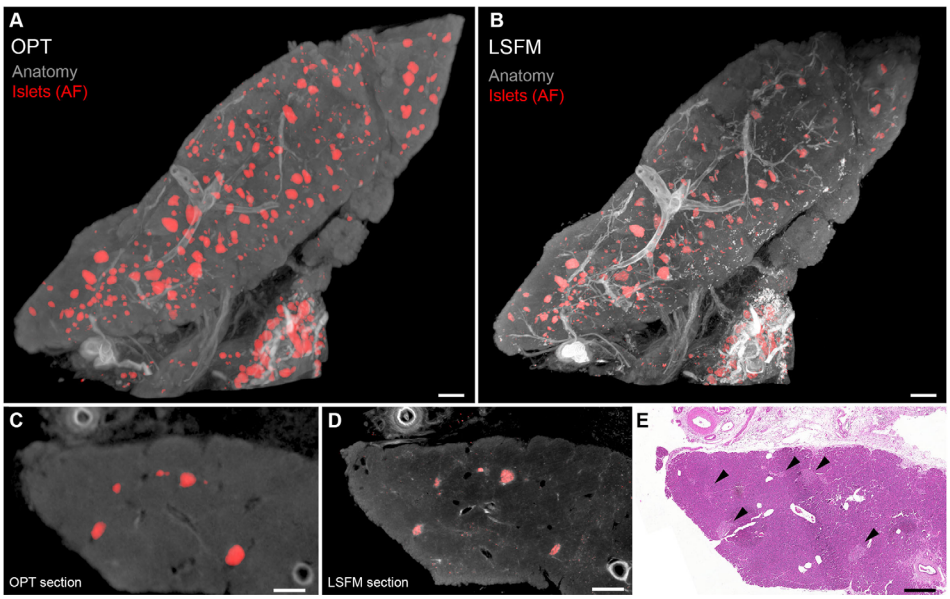

FIGURE 2 | Optical projection tomography (OPT) and light sheet fluorescence microscopy (LSFM) imaging of human islets of Langerhans based on islet autofluorescence. **(A, B)** OPT **(A)** and LSFM **(B)** 3D reconstruction of human pancreatic tissue. The islets (red) are reconstructed based on their AF properties in the near infrared part of the spectrum and the "anatomy" and vessels (gray) in the visible part of the spectrum (GFP-channel). **(C, D)** Tomographic slices of the specimen seen in **(A, B)**. **(E)** Hematoxylin/Eosin staining of a tissue section obtained post-mesoscopic imaging corresponding to **(C, D)**. Islets are indicated by black arrowheads. As outlined in the text, OPT and LSFM are complementary techniques with pros and cons for different imaging scenarios, and most usually applied tissue processing protocols render them fully interchangeable. Data is obtained from Hahn et al. (48). Scale bar in **(A, B)** is 500µm and in **(C–E)** 400µm.

other hand, however, they usually provide limited anatomical information. Although some anatomical reference information can be obtained from tissue autofluorescence in mesoscopic imaging, the anatomical detail remains limited for certain tissues. In nuclear images, this problem is often overcome by co-registering them with CT or MR images to create so called fusion images, providing an image that displays the specifically targeted signal onto the detailed anatomy of the tissue of interest. In theory, creating fusion images would also be possible for mesoscopic images of the pancreas, when co-registering them to *ex vivo* CT or MRI images of the target tissue, acquired after clearing. In the future, the possibility of creating mesoscopic fusion images might significantly contribute to the clinical significance of these imaging modalities in pancreatic disease since it would allow to visualize their specific high-resolution signal in its anatomical environment. Indeed, similar analyses with LSFM imaging as a functional modality have already been created for the brain (49).

CONCLUDING REMARKS

During the past decade, mesoscopic imaging technologies have undergone dramatic developments. As such, they have opened the door for a wide range of highly specific molecular 3D analyses of the pancreatic anatomy and its constitution both in health and disease. Already now, they provide the possibility to perform holistic µm-resolution 3D imaging and accurate quantitative assessments of distinct cellular features of the rodent pancreas, a possibility that may be enabled in the human pancreas in the near future. It is our expectation that these rapidly evolving imaging technologies will soon contribute significantly to a better understanding of both the anatomical and molecular features of the normal and diseased pancreas as well as other tissues involved in endocrinological disorders.

AUTHOR CONTRIBUTIONS

TA, MH, SW, and UA wrote the manuscript. UA and MH made the figures. All authors contributed to the article and approved the submitted version.

FUNDING

This work and the data from which figures 1 and 2 are derived was supported by the Swedish Research Council (grant no. 2017-01307), Barndiabetesfonden, the Diabetes Wellness Foundation (Sverige), Umeå University, The Novo Nordisk Foundation (grant no. NNF17OC0026794), the Juvenile Diabetes Fundation, the Kempe Foundations and the People Programme (Marie Curie Actions) of EU FP7/2007–2013/ under grant agreement no. 289932 by grants to UA.

REFERENCES

1. Sharpe J, Ahlgren U, Perry P, Hill B, Ross A, Hecksher-Sorensen J, et al. Optical projection tomography as a tool for 3D microscopy and gene expression studies. *Science* (2002) 296:541–5. doi: 10.1126/science.1068206
2. Dodt HU, Leischner U, Schierloh A, Jahrling N, Mauch CP, Deininger K, et al. Ultramicroscopy: three-dimensional visualization of neuronal networks in the whole mouse brain. *Nat Methods* (2007) 4:331–6. doi: 10.1038/nmeth1036
3. Huisken J, Swoger J, Del Bene F, Wittbrodt J, Stelzer EH. Optical sectioning deep inside live embryos by selective plane illumination microscopy. *Science* (2004) 305(5686):1007–9. doi: 10.1126/science.1100035
4. Keller PJ, Schmidt AD, Wittbrodt J, Stelzer EH. Reconstruction of zebrafish early embryonic development by scanned light sheet microscopy. *Science* (2008) 322:1065–9. doi: 10.1126/science.1162493
5. Liu A, Xiao W, Li R, Liu L, Chen L. Comparison of optical projection tomography and light-sheet fluorescence microscopy. *J Microsc* (2019) 275 (1):3–10. doi: 10.1111/jmi.12796
6. Chakraborty T, Driscoll MK, Jeffery E, Murphy MM, Roudot P, Chang BJ, et al. Light-sheet microscopy of cleared tissues with isotropic, subcellular resolution. *Nat Methods* (2019) 16:1109–13. doi: 10.1038/s41592-019-0615-4
7. Spalteholz W. *Über das Durchsichtigmachen von menschlichen und tierischen Präparaten und seine theoretischen Bedingungen, nebst Anhang: Über Knochenfärbung*. Leipzig: S. Hirzel (1914).
8. Alanentalo T, Asayesh A, Morrison H, Loren CE, Holmberg D, Sharpe J, et al. Tomographic molecular imaging and 3D quantification within adult mouse organs. *Nat Methods* (2007) 4:31–3. doi: 10.1038/nmeth985
9. Eriksson AU, Svensson C, Hornblad A, Cheddad A, Kostromina E, Eriksson M, et al. Near infrared optical projection tomography for assessments of beta-cell mass distribution in diabetes research. *J Vis Exp* (2013) (71):e50238. doi: 10.3791/50238
10. Ariel P. A beginner's guide to tissue clearing. *Int J Biochem Cell Biol* (2017) 84:35–9. doi: 10.1016/j.biocel.2016.12.009
11. Ueda HR, Erturk A, Chung K, Gradinaru V, Chedotal A, Tomancak P, et al. Tissue clearing and its applications in neuroscience. *Nat Rev Neurosci* (2020) 21(2):61–79. doi: 10.1038/s41583-019-0250-1
12. Hong SM, Jung D, Kiemen A, Gaida MM, Yoshizawa T, Braxton AM, et al. Three-dimensional visualization of cleared human pancreas cancer reveals that sustained epithelial-to-mesenchymal transition is not required for venous invasion. *Mod Pathol* (2019). doi: 10.1038/s41379-019-0409-3
13. Costa EC, Silva DN, Moreira AF, Correia IJ. Optical clearing methods: An overview of the techniques used for the imaging of 3D spheroids. *Biotechnol Bioeng* (2019) 116:2742–63. doi: 10.1002/bit.27105
14. Hörnblad A, Nord C, S P, Ahnfeldt-Rønne J, Ahlgren U. "The Pancreas". In: *Kaufman´s Atlas of Mouse Development Supplement: With Coronal Images*. R Baldock, J Bard, DR Davidson, G Moriss-Kay, editors. London: Academic Press/ Elsevier (2016) p. 85–94.
15. Asayesh A, Sharpe J, Watson RP, Hecksher-Sorensen J, Hastie ND, Hill RE, et al. Spleen versus pancreas: strict control of organ interrelationship revealed by analyses of Bapx1-/- mice. *Genes Dev* (2006) 20:2208–13. doi: 10.1101/gad.381906
16. Burn SF, Boot MJ, de Angelis C, Doohan R, Arques CG, Torres M, et al. The dynamics of spleen morphogenesis. *Dev Biol* (2008) 318:303–11. doi: 10.1016/j.ydbio.2008.03.031
17. Hecksher-Sorensen J, Watson RP, Lettice LA, Serup P, Eley L, De Angelis C, et al. The splanchnic mesodermal plate directs spleen and pancreatic laterality, and is regulated by Bapx1/Nkx3.2. *Development* (2004) 131(19):4665–75. doi: 10.1242/dev.01364
18. Hornblad A, Eriksson AU, Sock E, Hill RE, Ahlgren U. Impaired spleen formation perturbs morphogenesis of the gastric lobe of the pancreas. *PLoS One* (2011) 6(6):e21753. doi: 10.1371/journal.pone.0021753
19. Alanentalo T, Chatonnet F, Karlen M, Sulniute R, Ericson J, Andersson E, et al. Cloning and analysis of Nkx6.3 during CNS and gastrointestinal development. *Gene Expr Patterns* (2006) 6:162–70. doi: 10.1016/j.modgep.2005.06.012
20. Cheddad A, Svensson C, Sharpe J, Georgsson F, Ahlgren U. Image processing assisted algorithms for optical projection tomography. *IEEE Trans Med Imaging* (2012) 31:1–15. doi: 10.1109/TMI.2011.2161590
21. Hornblad A, Cheddad A, Ahlgren U. An improved protocol for optical projection tomography imaging reveals lobular heterogeneities in pancreatic islet and beta-cell mass distribution. *Islets* (2011) 3(4):204–8.
22. Alanentalo T, Hornblad A, Mayans S, Karin Nilsson A, Sharpe J, Larefalk A, et al. Quantification and three-dimensional imaging of the insulitis-induced destruction of beta-cells in murine type 1 diabetes. *Diabetes* (2010) 59:1756–64. doi: 10.2337/db09-1400
23. Parween S, Kostromina E, Nord C, Eriksson M, Lindstrom P, Ahlgren U, et al. Intra-islet lesions and lobular variations in beta-cell mass expansion in ob/ob mice revealed by 3D imaging of intact pancreas. *Sci Rep* (2016) 6:34885. doi: 10.1038/srep34885
24. Parween S, Eriksson M, Nord C, Kostromina E, Ahlgren U. Spatial and quantitative datasets of the pancreatic beta-cell mass distribution in lean and obese mice. *Sci Data* (2017) 4:170031. doi: 10.1038/sdata.2017.31
25. Hahn M, van Krieken P, Nord C, Alanentalo T, Morini F, Xiong Y, et al. Topologically selective islet vulnerability and self-sustained downregulation of markers for beta-cell maturity in streptozotocin-induced diabetes. *Commun Biol* (2020) 3(1):541. doi: 10.1038/s42003-020-01243-2
26. Grong E, Kulseng B, Arbo IB, Nord C, Eriksson M, Ahlgren U, et al. Sleeve gastrectomy, but not duodenojejunostomy, preserves total beta-cell mass in Goto-Kakizaki rats evaluated by three-dimensional optical projection tomography. *Surg Endosc* (2016) 30(2):532–42. doi: 10.1007/s00464-015-4236-4
27. Grong E, Nord C, Arbo IB, Eriksson M, Kulseng BE, Ahlgren U, et al. The effect of hypergastrinemia following sleeve gastrectomy and pantoprazole on type 2 diabetes mellitus and beta-cell mass in Goto-Kakizaki rats. *J Endocrinol Invest* (2018) 41(6):691–701. doi: 10.1007/s40618-017-0793-9
28. Medina A, Parween S, Ullsten S, Vishnu N, Siu YT, Quach M, et al. Early deficits in insulin secretion, beta cell mass and islet blood perfusion precede onset of autoimmune type 1 diabetes in BioBreeding rats. *Diabetologia* (2018) 61(4):896–905. doi: 10.1007/s00125-017-4512-z
29. Mitchell RK, Mondragon A, Chen L, McGinty JA, French PM, Ferrer J, et al. Selective disruption of Tcf7l2 in the pancreatic beta cell impairs secretory function and lowers beta cell mass. *Hum Mol Genet* (2015) 24(5):1390–9. doi: 10.1093/hmg/ddu553
30. Pardo FN, Altirriba J, Pradas-Juni M, Garcia A, Ahlgren U, Barbera A, et al. The role of Raf-1 kinase inhibitor protein in the regulation of pancreatic beta cell proliferation in mice. *Diabetologia* (2012) 55(12):3331–40. doi: 10.1007/s00125-012-2696-9
31. Sun G, Tarasov AI, McGinty J, McDonald A, da Silva Xavier G, Gorman T, et al. Ablation of AMP-activated protein kinase alpha1 and alpha2 from mouse pancreatic beta cells and RIP2.Cre neurons suppresses insulin release in vivo. *Diabetologia* (2010) 53:924–36. doi: 10.1007/s00125-010-1692-1
32. Sun G, Tarasov AI, McGinty JA, French PM, McDonald A, Leclerc I, et al. LKB1 deletion with the RIP2.Cre transgene modifies pancreatic beta-cell morphology and enhances insulin secretion in vivo. *Am J Physiol Endocrinol Metab* (2010) 298 (6):E1261–1273. doi: 10.1152/ajpendo.00100.2010
33. Van de Casteele M, Leuckx G, Baeyens L, Cai Y, Yuchi Y, Coppens V, et al. Neurogenin 3+ cells contribute to beta-cell neogenesis and proliferation in injured adult mouse pancreas. *Cell Death Dis* (2013) 4:e523. doi: 10.1038/cddis.2013.52
34. Alvarsson A, Jimenez-Gonzalez M, Li R, Rosselot C, Tzavaras N, Wu Z, et al. A 3D atlas of the dynamic and regional variation of pancreatic innervation in diabetes. *Sci Adv* (2020) 6(41). doi: 10.1126/sciadv.aaz9124
35. Roostalu U, Skytte JL, Salinas CG, Klein T, Vrang N, Jelsing J, et al. 3D quantification of changes in pancreatic islets in mouse models of diabetes type I and II. *Dis Model Mech* (2020). doi: 10.1242/dmm.045351
36. Speier S, Nyqvist D, Cabrera O, Yu J, Molano RD, Pileggi A, et al. Noninvasive in vivo imaging of pancreatic islet cell biology. *Nat Med* (2008) 14(5):574–8. doi: 10.1038/nm1701
37. van Krieken PP, Dicker A, Eriksson M, Herrera PL, Ahlgren U, Berggren PO, et al. Kinetics of functional beta cell mass decay in a diphtheria toxin receptor mouse model of diabetes. *Sci Rep* (2017) 7(1):12440. doi: 10.1038/s41598-017-12124-w
38. Ilegems E, Dicker A, Speier S, Sharma A, Bahow A, Edlund PK, et al. Reporter islets in the eye reveal the plasticity of the endocrine pancreas. *Proc Natl Acad Sci U S A* (2013) 110(51):20581–6. doi: 10.1073/pnas.1313696110

39. Eter WA, Parween S, Joosten L, Frielink C, Eriksson M, Brom M, et al. SPECT-OPT multimodal imaging enables accurate evaluation of radiotracers for beta-cell mass assessments. *Sci Rep* (2016) 6:24576. doi: 10.1038/srep24576
40. Ilegems E, van Krieken PP, Edlund PK, Dicker A, Alanentalo T, Eriksson M, et al. Light scattering as an intrinsic indicator for pancreatic islet cell mass and secretion. *Sci Rep* (2015) 5:10740. doi: 10.1038/srep10740
41. Noe M, Rezaee N, Asrani K, Skaro M, Groot VP, Wu PH, et al. Immunolabeling of Cleared Human Pancreata Provides Insights into Three-Dimensional Pancreatic Anatomy and Pathology. *Am J Pathol* (2018) 188(7):1530–5. doi: 10.1016/j.ajpath.2018.04.002
42. Zhao S, Todorov MI, Cai R, Maskari RA, Steinke H, Kemter E, et al. Cellular and Molecular Probing of Intact Human Organs. *Cell* (2020) 180:796–812 e719. doi: 10.1016/j.cell.2020.01.030
43. Muyldermans S. Nanobodies: natural single-domain antibodies. *Annu Rev Biochem* (2013) 82:775–97. doi: 10.1146/annurev-biochem-063011-092449
44. Kirst C, Skriabine S, Vieites-Prado A, Topilko T, Bertin P, Gerschenfeld G, et al. Mapping the Fine-Scale Organization and Plasticity of the Brain Vasculature. *Cell* (2020) 180(4):780–95.e725. doi: 10.1016/j.cell.2020.01.028
45. Todorov MI, Paetzold JC, Schoppe O, Tetteh G, Shit S, Efremov V, et al. Machine learning analysis of whole mouse brain vasculature. *Nat Methods* (2020) 17(4):442–9. doi: 10.1038/s41592-020-0792-1
46. Renier N, Adams EL, Kirst C, Wu Z, Azevedo R, Kohl J, et al. Mapping of Brain Activity by Automated Volume Analysis of Immediate Early Genes. *Cell* (2016) 165(7):1789–802. doi: 10.1016/j.cell.2016.05.007
47. Pan C, Schoppe O, Parra-Damas A, Cai R, Todorov MI, Gondi G, et al. Deep Learning Reveals Cancer Metastasis and Therapeutic Antibody Targeting in the Entire Body. *Cell* (2019) 179(7):1661–76.e1619. doi: 10.1016/j.cell.2019.11.013
48. Hahn M, Nord C, Franklin O, Alanentalo T, Mettavainio MI, Morini F, et al. Mesoscopic 3D imaging of pancreatic cancer and Langerhans islets based on tissue autofluorescence. *Sci Rep* (2020) 10(1):18246. doi: 10.1038/s41598-020-74616-6
49. Perens J, Salinas CG, Skytte JL, Roostalu U, Dahl AB, Dyrby TB, et al. An Optimized Mouse Brain Atlas for Automated Mapping and Quantification of Neuronal Activity Using iDISCO+ and Light Sheet Fluorescence Microscopy. *Neuroinformatics* (2020). doi: 10.1007/s12021-020-09490-8

Conflict of Interest: The authors declare that the research was conducted in the absence of any commercial or financial relationships that could be construed as a potential conflict of interest.

frontiers in Endocrinology

METHODS
published: 09 March 2021
doi: 10.3389/fendo.2021.613964

In Vivo ZIMIR Imaging of Mouse Pancreatic Islet Cells Shows Oscillatory Insulin Secretion

*Shiuhwei Chen[1,2,3], ZhiJiang Huang[1], Harrison Kidd[1], Min Kim[2,3,4], Eul Hyun Suh[5], Shangkui Xie[1], Ebrahim H. Ghazvini Zadeh[1], Yan Xu[1], A. Dean Sherry[5,6,7], Philipp E. Scherer[2,3] and Wen-hong Li[1]**

[1] Departments of Cell Biology and of Biochemistry, University of Texas Southwestern Medical, Dallas, TX, United States, [2] Touchstone Diabetes Center, University of Texas Southwestern Medical Center, Dallas, TX, United States, [3] Department of Cell Biology, University of Texas Southwestern Medical Center, Dallas, TX, United States, [4] Department of Biological Sciences, School of Life Sciences, Ulsan National Institute of Science and Technology, Ulsan, South Korea, [5] Advanced Imaging Research Center, University of Texas Southwestern Medical Center, Dallas, TX, United States, [6] Department of Chemistry and Biochemistry, University of Texas Dallas, Richardson, TX, United States, [7] Department of Radiology, University of Texas Southwestern Medical Center, Dallas, TX, United States

OPEN ACCESS

Edited by:
Guy A. Rutter,
Imperial College London,
United Kingdom

Reviewed by:
Guoqiang Gu,
Vanderbilt University, United States
Marcia Hiriart,
National Autonomous University of Mexico, Mexico

***Correspondence:**
Wen-hong Li
wen-hong.li@utsouthwestern.edu

Specialty section:
This article was submitted to Diabetes: Molecular Mechanisms, a section of the journal Frontiers in Endocrinology

Received: 04 October 2020
Accepted: 26 January 2021
Published: 09 March 2021

Citation:
Chen S, Huang Z, Kidd H, Kim M, Suh EH, Xie S, Ghazvini Zadeh EH, Xu Y, Sherry AD, Scherer PE and Li W-h (2021) In Vivo ZIMIR Imaging of Mouse Pancreatic Islet Cells Shows Oscillatory Insulin Secretion. Front. Endocrinol. 12:613964. doi: 10.3389/fendo.2021.613964

Appropriate insulin secretion is essential for maintaining euglycemia, and impairment or loss of insulin release represents a causal event leading to diabetes. There have been extensive efforts of studying insulin secretion and its regulation using a variety of biological preparations, yet it remains challenging to monitor the dynamics of insulin secretion at the cellular level in the intact pancreas of living animals, where islet cells are supplied with physiological blood circulation and oxygenation, nerve innervation, and tissue support of surrounding exocrine cells. Herein we presented our pilot efforts of ZIMIR imaging in pancreatic islet cells in a living mouse. The imaging tracked insulin/Zn^{2+} release of individual islet β-cells in the intact pancreas with high spatiotemporal resolution, revealing a rhythmic secretion activity that appeared to be synchronized among islet β-cells. To facilitate probe delivery to islet cells, we also developed a chemogenetic approach by expressing the HaloTag protein on the cell surface. Finally, we demonstrated the application of a fluorescent granule zinc indicator, ZIGIR, as a selective and efficient islet cell marker in living animals through systemic delivery. We expect future optimization and integration of these approaches would enable longitudinal tracking of beta cell mass and function *in vivo* by optical imaging.

Keywords: insulin oscillation, ZIMIR, ZIGIR, HaloTag, intravital microscopy (IVM), beta cell mass, imaging insulin secretion, beta cell imaging

INTRODUCTION

The islet of Langerhans plays essential roles in controlling metabolism and glucose homeostasis through the release of peptide hormones. The islet beta cell, in particular, is crucial for maintaining euglycemia *via* insulin secretion. In healthy subjects, insulin secretion is tightly regulated, and beta cells release insulin in response to nutrient fluctuations to clamp blood glucose within a narrow range. There has been growing interests in characterizing insulin release dynamics and studying

its physiological regulation *in vivo*. By sampling the total insulin output from the pancreas, a number of studies have revealed the dynamic feature of insulin release in live animals, including rodents, dogs, and human (1, 2).

At the cellular and subcellular level, our understanding of insulin secretion *in vivo* is still limited. The lack of imaging assays capable of tracking insulin release of single cells or individual islets in live animals remains to be a roadblock towards functional analysis of islet beta cells *in vivo* (3). Previously, we developed a fluorescent, cell-surface targeted zinc indicator for monitoring induced exocytotic release (ZIMIR) (4). Exploiting Zn^{2+} elevation at the cell surface as a surrogate marker of insulin release, we applied laser scanning confocal microscopy to image ZIMIR and to map the spatiotemporal characteristics of insulin release in isolated islets. Herein we report our efforts of extending ZIMIR imaging to living mice. We developed a surgery procedure to label islet cells with ZIMIR through the celiac artery. Confocal ZIMIR imaging revealed oscillatory and synchronized insulin release among islet beta cells in a living mouse. Moreover, to facilitate probe delivery to islet cells, we exploited the HaloTag labeling technology and developed a chemogenetic approach for the targeted probe delivery to the plasma membrane of beta cells. Finally, we presented data to demonstrate the utility of a recently developed granule Zn^{2+} indicator, ZIGIR, as a selective and efficient marker of islet beta cells *in vivo via* systemic delivery.

MATERIAL AND METHODS

Mouse Maintenance and Surgery

All protocols for mouse use and euthanasia were reviewed and approved by the Institutional Animal Care and Use Committee of the University of Texas Southwestern Medical Center. All mice, including C57Bl/6J, MIP-GFP (Jackson Laboratory stock No. 006864), MIP-DsRed (Jackson No. 006866), MIP-rtTA (5), TRE-pDisplay-HaloTag-Myc were maintained in 12-h dark/light cycles, with *ad libitum* access to diet (Teklad 2016) and water. Mice 10–15 weeks old were used for the experiments. The TRE-pDisplay-HaloTag-Myc mouse was generated by the UTSW transgenic mouse core facility by cloning the pDisplay-HaloTag-Myc sequence (6) downstream of a TRE vector (5). Sprague Dawley rats were from Charles River.

Intravital Imaging of Exteriorized Pancreas in Mice

To image islets in the exteriorized mouse pancreas, we customized an imaging platform containing a flexible stand to facilitate accessing pancreatic islets, and a home-made stabilizer to constrain mouse movement. During image acquisition, animals were laid on top of a heating pad to maintain body temperature. The entire imaging platform was enclosed within a temperature and humidity-controlled chamber. The exteriorized pancreas of an anesthetized mouse was carefully placed on the imaging platform, and islets close to the pancreas surface were identified and centered beneath the objective. Vaseline was applied to the sides of pancreas, which was sandwiched between two pedals of the stabilizer. We then applied a vacuum grease (Dow Corning) to adhere the two pedals and to seal the opening of the top pedal with a No. 1 glass coverslip. A small volume of saline was placed on top of the glass coverslip, through which the islets underneath were imaged by a dipping lens (20x objective). To image islet blood flow, we injected Texas-Red labeled dextran (70 KDa, 0.2 mg in 0.1 ml DPBS) to a MIP-GFP mouse through a catheter installed at the jugular vein 3 days earlier. To test bolus dye loading of pancreatic cells, we micro-injected Cy3-C12 (20 μM) to the mouse pancreas under a dissection scope.

To label pancreatic islets with amphipathic dyes (Cy3-C12 or ZIMIR) through the splenic artery, we temporarily blocked blood circulation to the celiac artery with a micro vessel clip, and infused 0.2 ml of dye solution (20 μM of Cy3-C12, or 100 μM of ZIMIR in DPBS) through the splenic artery using a 31 gauge needle. We removed the micro vessel clip 5 min later to restore the blood circulation and started confocal imaging within the next 10–15 min. Prior to imaging the ZIMIR signal, the mouse received an infusion of dextrose (50% in water) through the jugular vein catheter for 30 s at a rate of 25 μl/min.

Confocal imaging was performed on an upright LSM510-Meta system (Zeiss). ZIMIR and GFP were excited with 488 nm laser and detected at 500–560 nm. Dextran-Texas Red and Cy3-C12 were excited with 561 nm laser and detected at 570–625 nm.

HaloTag Labeling of Islet Beta Cells

Expression of HaloTag-Myc in islet beta cells was confirmed by immunofluorescence. After feeding a transgenic mouse (*MIP-rtTA::TRE-pDisplay-HaloTag-Myc*) with Dox200 chow (Envigo) for 1 week, we harvested the pancreas and prepared formalin fixed paraffin embedded (FFPE) tissue section (10 μm). The tissue section was labeled with antibodies against insulin (Agilent, A0564) and Myc (Upstate, 06-549), and stained with the corresponding secondary antibodies (Jackson Immunoresearch, 706-545-148 and 711-165-152, respectively). To label beta cells *in vivo via* systemic dye delivery, we injected Fluo-HaloTag-2 (40 μM x 0.2 ml) through the tail vein of a transgenic mouse that had been on Dox200 for a week. We then sacrificed the mouse 30 min later and performed transcardial perfusion with ice-cold PBS buffer for 10 min at a flow rate of 1 ml/min. The pancreas was harvested immediately afterwards. A piece of pancreatic tissue containing both islets and exocrine cells was micro-dissected and imaged by confocal microscopy (Ex 488 nm, Em 500–550 nm).

To label HEK293 cells with ZIMIR-HaloTag, we infected the cells with a pDisplay-HaloTag plasmid and Lipofectamine for 48 h. Cells were then washed with a secretion assay buffer (SAB) containing 114 mM NaCl, 4.7 mM KCl, 1.2 mM KH_2PO_4, 2.5 mM $CaCl_2$, 1.16 mM $MgSO_4$, 3 mM glucose, and 20 mM Hepes (pH 7.4). Cells were then incubated with ZIMIR-HaloTag (2 μM) in the SAB buffer for 30 min at RT, washed and imaged by epifluorescence (Zeiss Axiovert 200). A high Zn^{2+} buffer (1 μM free Zn^{2+}, buffered by 8.1 mM l-histidine, 2.6 mM ZnO in 10 mM Hepes, 5 mM KCl, 140 mM NaCl, pH 7.4) was added at the end to enhance ZIMIR-HaloTag signal.

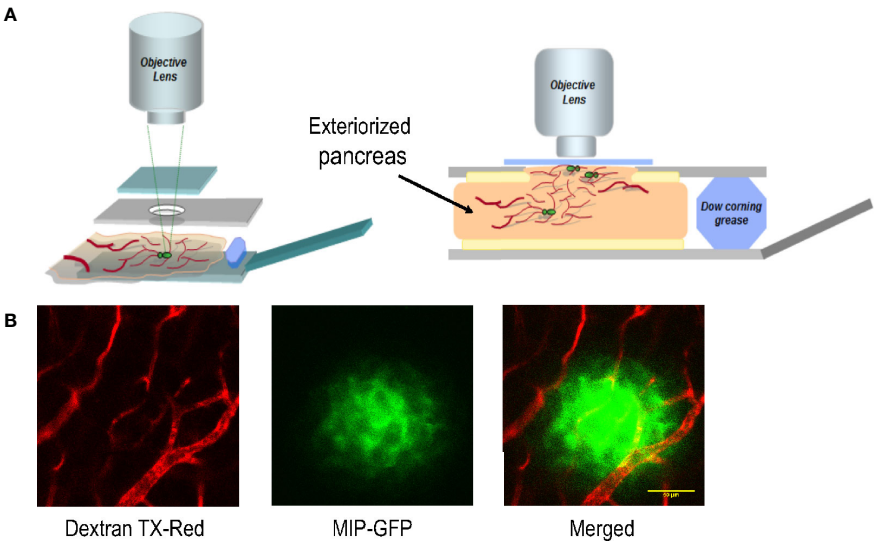

FIGURE 1 | The platform for imaging islet cells in the intact pancreas of a live mouse. **(A)** Schematic of the customized imaging reservoir for housing the exteriorized pancreas for intravital imaging. **(B)** Example images showing blood vessels surrounding and within an islet of a MIP-GFP mouse. Dextran TX-Red was delivered through tail vein injection to label the vasculature.

To label mouse islets with ZIMIR-HaloTag, we fed a transgenic mouse (*MIP-rtTA::TRE-pDisplay-HaloTag-Myc*) with Dox200 chow (Envigo) for 2 weeks. During the last 3 days of the 2-week feeding period, we gave the mouse 0.5 ml doxycycline (2 mg/ml) three times a day *via* oral gavage to boost doxycycline dosing and to further enhance HaloTag expression. We then isolated mouse islets following the standard protocol of collagenase digestion (4). The isolated mouse islets were cultured in RPMI medium for 2 h to allow recovery, and subsequently incubated with ZIMIR HaloTag (2 μM) in the SAB buffer (with 3 mM glucose, 10 μM EDTA and 2 μM DPAS (4)) for 30 min at room temperature. Islets were then washed once and imaged by confocal microscopy at either basal (3 mM) or elevated glucose (20 mM) in SAB.

ZIGIR Labeling of Islets *In Vitro* and *In Vivo*

To label islet cells with ZIGIR *in vivo*, we injected a PBS solution (0.2 ml for mouse, 2 ml for rat) containing ZIGIR (400 nmol/Kg) *via* the tail vein. The animal was sacrificed 30 min later for the islet isolation. The isolated islets were imaged by confocal microscopy exciting at 561 nm (Em 570–620 nm). To label islets with ZIGIR *in vitro*, hand-picked mouse islets (C57Bl6/J) were incubated in the SAB solution with ZIGIR (1 μM, diluted from 1 mM stock in DMF) for 15 min at 37°C. Islets were then washed once with SAB and imaged by confocal microscopy.

RESULTS

Imaging Platform

To establish and optimize an imaging platform for monitoring islet cells in the intact pancreas, we implemented a minimally invasive surgical procedure for exteriorizing the mouse pancreas for intravital imaging. A similar procedure has been successfully applied to track immune cells during pancreas inflammation in a mouse model of type 1 diabetes (7). In this protocol, we surgically exposed the pancreas of a mouse under anesthesia, and placed it in a customized reservoir containing a heated physiological saline (**Figure 1**). The top of the reservoir was covered with a glass coverslip which was gently pressed against the tissue underneath.

Dye Loading to Cells in the Pancreas *via* Microinjection

When applied to isolated islets, ZIMIR diffuses through interstitial space to label individual islet cells (4). To label islet cells with ZIMIR in the intact pancreas, we initially considered a multicell bolus loading method previously developed for loading fluorescent indicators to a population of cells in brain slices (8). The bolus loading involves injecting a concentrated DMSO dye stock solution into the tissue. The injected dye solution then diffuses to nearby areas, where the cells take up the dye.

To adopt this method for labeling pancreatic islet cells, we applied an amphipathic fluorophore, Cy3-C12, to label islet cells in MIP-GFP mice. Cy3-C12, like ZIMIR, contains a pair of dodecyl alkyl chains for membrane anchoring (**Figure 2A**). Since it has two sulfonate anions and one quaternary ammonium cation, Cy3-C12 is impermeant to the cell membrane. It labels the outer leaflet of the plasma membrane similarly as ZIMIR. Cy3-C12 emits bright orange fluorescence, so it spectrally complements MIP-GFP expressed in the beta cell, enabling dual color imaging to assess dye labeling of the islet cell after dye injection.

After locating an islet near the surface of the exteriorized pancreas, we microinjected Cy3-C12 into the exocrine tissue

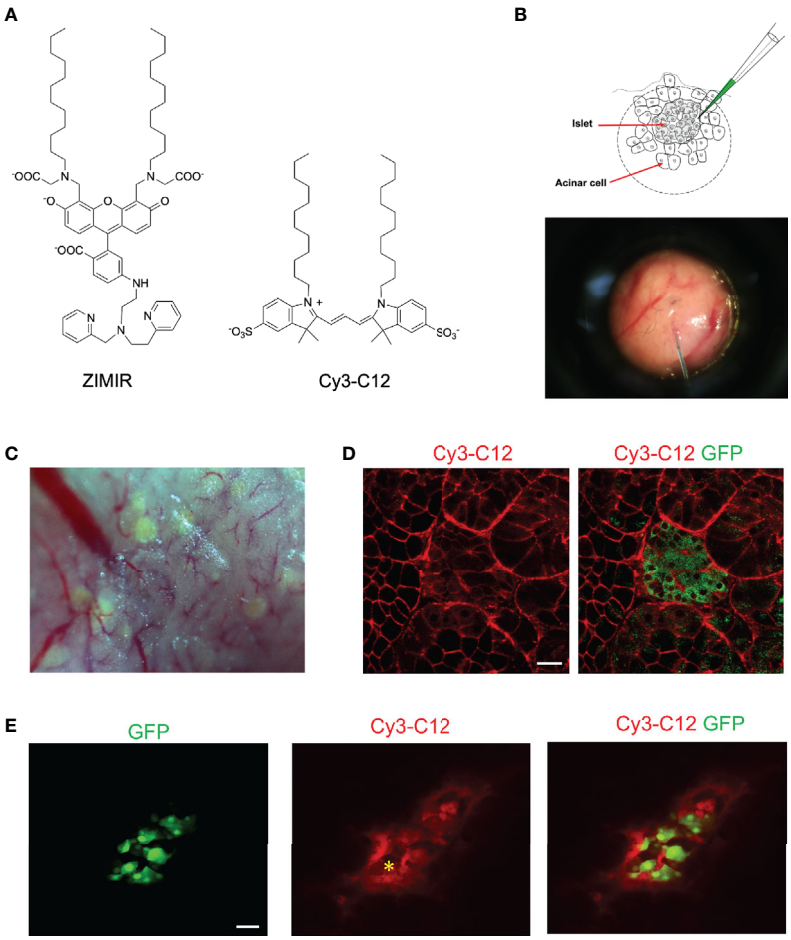

FIGURE 2 | Labeling mouse islet cells in the intact pancreas *via* microinjection of dye solutions. **(A)** Chemical structures of ZIMIR and Cy3-C12. **(B)** Schematic of bolus loading of pancreatic cells *via* microinjection. The picture showed a needle filled with a dye solution piercing into the exocrine tissue near an islet. **(C)** A bright field image of the pancreatic tissue of a MIP-GFP mouse. Islets near the surface presented as light green puncta arising from GFP expression. **(D)** Confocal fluorescence images of a pancreas (MIP-GFP) post-injecting Cy3-C12 into the exocrine tissue. **(E)** Confocal fluorescence images of a pancreas (MIP-GFP) where an islet was injected with Cy3-C12. The yellow asterisk indicates the site of injection. Scale bar = 20 μm.

near the islet (**Figures 2B, C**). We then imaged dye distribution and cellular dye uptake by confocal microscopy. The injected Cy3-C12 yielded an intense membrane labeling of pancreatic acinar cells near the site of injection (**Figure 2D**). However, Cy3-C12 labeling within the islet was much dimmer, and it appeared to be largely restricted to the intra-islet capillaries. We attributed this weak islet labeling to the retardation of dye diffusion across the peri-islet capsule. The peri-islet capsule was thought to function as a barrier between the endocrine and exocrine compartments (9, 10). To circumvent the problem, we attempted to deliver the dye to islet cells by positioning the injection needle within the islet. The intra-islet injection did confine the dye delivery to the islet (**Figure 2E**). However, unlike the membrane-specific labeling observed in the acinar cells (**Figure 2D**), we observed promiscuous distribution of Cy3-C12 throughout islet cells with a prominent intracellular staining.

Dye Loading of Islet Cells *via* Pancreas Perfusion Through the Splenic Artery

Given the obstacles encountered with the bolus loading of pancreatic islet cells, we explored an alternative approach of delivering small amphipathic dyes to the islet. The splenic artery is a branch of celiac artery that supplies blood to the neck, body and tail regions of the pancreas. After exteriorizing a pancreas, we blocked blood flow of the celiac artery briefly by clamping the vessel with a micro-clip. We then infused a small volume of Cy3-C12 solution (0.2 ml) through the splenic artery to deliver the dye to the pancreas. After 5 min, we removed the micro-clip to restore the circulation. Confocal imaging of the dye-perfused pancreas confirmed that the plasma membranes of both endocrine and exocrine cells were labeled with Cy3-C12 (**Figure 3A**). Similarly, delivery of ZIMIR solution through the splenic artery also labeled pancreatic islet cells (**Figure 3B**). Hence, this dye infusion procedure through the vasculature

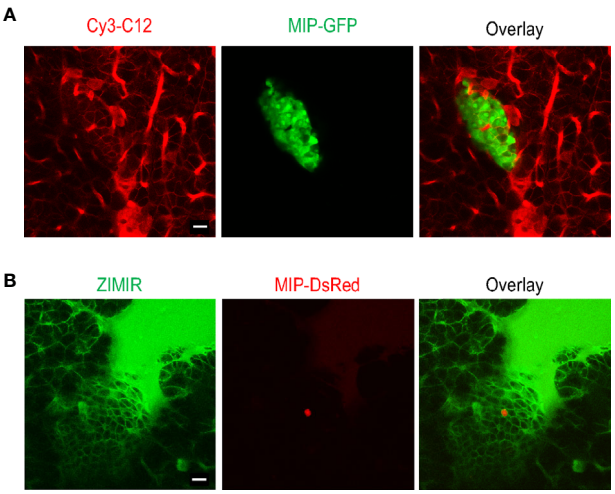

FIGURE 3 | Labeling mouse islet cells in the intact pancreas *via* dye infusion through the splenic artery. **(A)** Confocal fluorescence images of a pancreas (MIP-GFP) post-infusing Cy3-C12 for 5 min into the exocrine tissue. **(B)** Confocal fluorescence images of a pancreas (MIP-DsRed) post-infusing ZIMIR. The scarce DsRed labeling was likely due to the low penetrance of MIP-DsRed transgene in this mouse. Scale bar = 20 μm.

yielded sufficient labeling of both endocrine and exocrine pancreatic cells for imaging applications.

Intravital ZIMIR Imaging Revealed Oscillatory Insulin/Zn^{2+} Secretion *In Vivo*

Having established the imaging platform and a procedure for labeling islet cells in the intact pancreas, we applied the method to image insulin secretion in a living mouse. After labeling a mouse pancreas with ZIMIR through the splenic artery, we located an islet near the surface and centered it below the objective. We then challenged the mouse with a bolus of glucose through the jugular vein infusion. Subsequent confocal ZIMIR imaging showed a highly rhythmic insulin/Zn^{2+} secretion among a cluster of neighboring cells (**Figure 4**). Quantification of cell surface ZIMIR signal established a time course and an oscillation period of 32.48 ± 8.06 s (mean ± stdev).

Targeted Dye Delivery to Islet Beta Cells *In Vivo* Through HaloTag Labeling

The success of capturing oscillatory insulin/Zn^{2+} secretion *in vivo* at the cellular resolution demonstrated the versatility and the potential of ZIMIR imaging. To facilitate labeling islet beta cells in live animals while minimizing animal stress, we explored an alternative strategy of targeted dye delivery through systemic circulation and tail vein injection. In this approach, we expressed a self-labeling enzyme, HaloTag (11), at the cell surface of islet beta cells. The HaloTag enzyme reacts with small molecules containing a haloalkane moiety to form a covalent bond between the protein itself and the small molecule. We bred a transgenic mouse that harbored two transgenes: *MIP-rtTA* and *TRE-pDisplay-HaloTag-Myc* (**Figure 5A**). *MIP-rtTA* drives the expression of reverse tetracycline transactivator (*rtTA*) in beta cells under the control of the mouse insulin promoter (*MIP*) (5). Addition of tetracycline activates the transactivator, which then binds to the tetracycline responsive element (*TRE*) to induce the expression of HaloTag protein selectively in beta cells. The HaloTag protein with a Myc tag was targeted to the cell surface by fusing with a PDGFR transmembrane domain (pDisplay construct) (6). After feeding a transgenic *MIP-rtTA::*

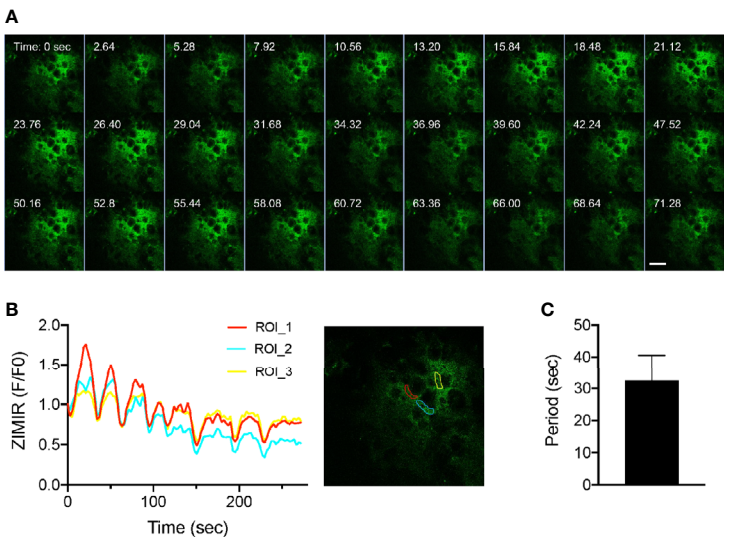

FIGURE 4 | Intravital ZIMIR imaging showed oscillatory insulin/Zn^{2+} release of mouse islet cells. **(A)** Time lapse confocal ZIMIR images of pancreatic islet cells of a mouse under anesthesia. The mouse received a glucose injection just before the imaging session. Scale bar = 20 μm. **(B)** Time course of ZIMIR signal in three regions of interest (ROI) as indicated in the image to the right. **(C)** Average oscillation period of insulin/Zn^{2+} release (mean ± stdev) calculated from the time course shown in **(B)**.

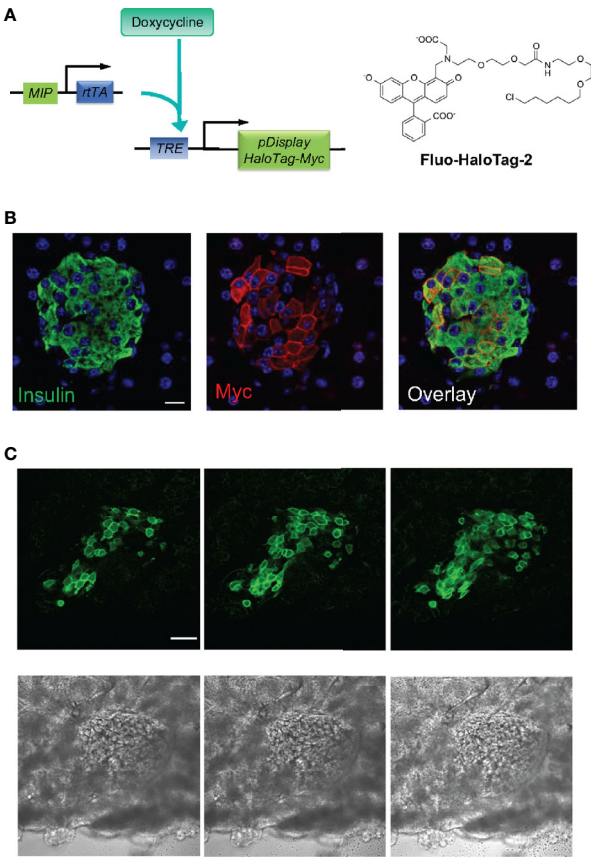

FIGURE 5 | *In vivo* dye labeling of islet beta cells expressing HaloTag. **(A)** Transgenic mice harboring two transgenes express the HaloTag-Myc protein in beta cells upon doxycycline (Dox) induction. HaloTag labels itself by reacting with its ligands such as Fluo HaloTag-2. **(B)** Confirmation of HaloTag-Myc protein expression in islet beta cells by immunofluorescence. The pancreatic tissue section of a transgenic mouse (*MIP-rtTA::TRE-pDisplay-HaloTag-Myc*) fed on Dox200 for 1 week was stained with antibodies against insulin and Myc. Scale bar = 10 μm. **(C)** Confocal images of a dissected pancreas from a transgenic mouse fed with doxycycline for 1 week. The mouse received Fluo HaloTag-2 through tail vein injection 30 min before pancreas harvest. Three consecutive confocal sections 10 μm apart along the z-axis were shown. The bottom row shows the corresponding bright field images. Scale bar = 50 μm.

TRE-pDisplay-HaloTag-Myc mouse doxycycline for a week, we confirmed the expression of HaloTag-Myc selectively at the beta cell surface by immunofluorescence (**Figure 5B**). Consistently, tail vein injection of a fluorescent HaloTag substrate, Fluo-HaloTag-2 (6), selectively labeled islet beta cells in a live transgenic mouse (**Figure 5C**). This *in vivo* labeling through systemic delivery of Fluo-HaloTag-2 was remarkably efficient, and it yielded a strong labeling of islet beta cells in just 30 min after tail vein injection of Fluo-HaloTag-2.

Having established the feasibility of *in vivo* beta cell labeling using this chemogenetic approach, we went on to test ZIMIR-HaloTag for imaging insulin/Zn^{2+} release in beta cells expressing HaloTag. ZIMIR-HaloTag contains the same Zn^{2+} binding motif and fluorophore as ZIMIR (**Figure 6A**). It binds Zn^{2+} with an affinity of 0.13 μM and displays a 15-fold fluorescence enhancement upon Zn^{2+} binding (6). In cultured HEK293 cells infected with a pDisplay-HaloTag-Myc plasmid, ZIMIR-HaloTag labeled the cell plasma membrane and showed a robust fluorescence increase in response to Zn^{2+} elevation in the extracellular medium (**Figure 6B**). However, when we attempted to label islet beta cells with ZIMIR-HaloTag in a living transgenic mouse after doxycycline induction, we only observed a rather low fluorescence signal similar to the background intensity in beta cells following the same procedure as we had used for Fluo-HaloTag-2. After isolating mouse islets, we were nonetheless able to label the islet beta cells *in vitro* with ZIMIR-HaloTag (**Figure 6C**), confirming HaloTag expression in beta cells. Moreover, glucose stimulation promoted insulin/Zn^{2+} secretion and increased ZIMIR-HaloTag intensity in a number of regions in the islet, demonstrating an intact functionality of the isolated islets in glucose sensing and hormone release. Adding Zn^{2+} to the medium further raised ZIMIR-HaloTag intensity to a supramaximal level throughout the entire islet (**Figure 6C**).

In Vivo Labeling of Dense Core Granules and Islet Cells With ZIGIR

In parallel to our efforts of imaging beta cell function, we are also exploring new approaches for tagging native islet cells based on their intrinsic properties for evaluating islet cell mass. Recently, we have developed a zinc granule indicator, ZIGIR, as a specific, brightly fluorescent label of zinc rich secretory granules (12). ZIGIR is cell membrane permeable and accumulates in the dense core granules of islet cells, exhibiting the highest fluorescence intensity in the insulin granule owing to its high Zn^{2+} content. Moreover, ZIGIR exhibits no cytotoxicity and does not affect cell proliferation or cell function (insulin secretion) *in vitro* (12). To evaluate the potential of ZIGIR as an islet cell label *in vivo*, we delivered ZIGIR to a rat through the tail vein injection. We sacrificed the animal 30 min later and isolated the islets after a limited collagenase digestion of the pancreas. We randomly picked a piece of digested pancreatic tissue that contained both endocrine and exocrine cells. Confocal imaging of the tissue revealed exclusive ZIGIR labeling of the islet, and null fluorescence signal in the surrounding acinar tissue (**Figure 7A**). This result demonstrated the exquisite labeling specificity of ZIGIR towards pancreatic endocrine cells *in vivo*, likely attributing to the intrinsic property of high zinc level in the granular compartments of islet cells, most notably beta cells. We also compared ZIGIR labeling of isolated islets *in vitro vs.* islet labeling *in vivo* through systemic delivery. Compared to the *in vivo* ZIGIR labeling, where ZIGIR signal was seen throughout the entire islet (**Figures 7A, B**), ZIGIR labeling in the isolated islets was restricted to the outer cell layers (**Figure 7C**). The difference likely reflects the trapping of ZIGIR *in vitro* by the superficial cell layers which limit the diffusion of ZIGIR to the islet interior. In contrast, *in vivo*, ZIGIR is transported through the circulation and delivered to all islet cells through the rich vasculature within the islet. Notwithstanding the difference, for both *in vitro* and *in vivo* labeling, a subset of cells along the islet mantle exhibited lower

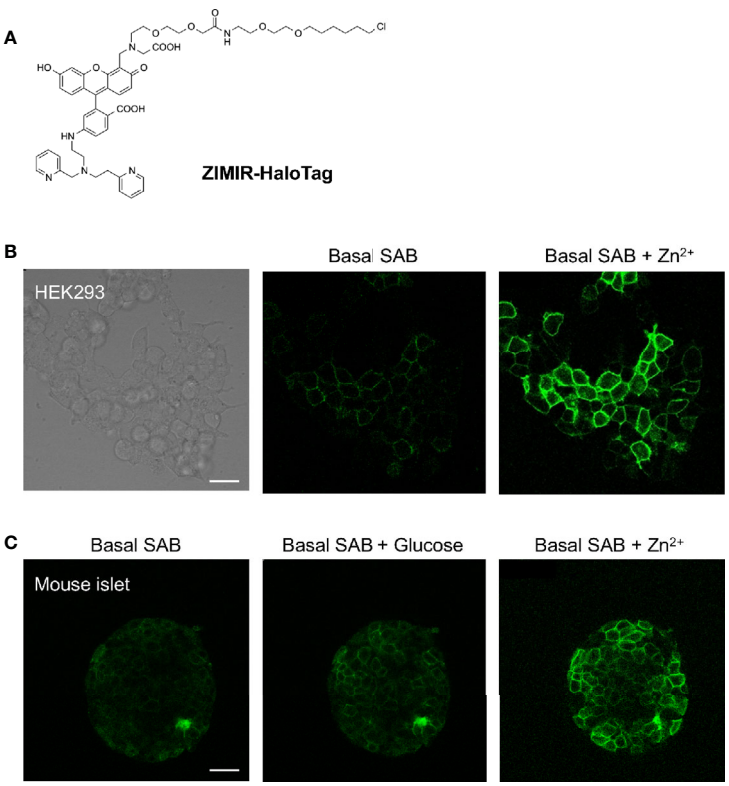

FIGURE 6 | Imaging insulin/Zn^{2+} secretion in isolated mouse islets with ZIMIR-HaloTag. **(A)** Chemical structure of ZIMIR-HaloTag. **(B)** ZIMIR-HaloTag labeled the plasma membrane of HEK293 cells expressing pDisplay-HaloTag and responded to Zn^{2+} elevation in the medium. **(C)** Confocal imaging of insulin/Zn^{2+} secretion in an isolated islet from a MIP-rtTA::TRE-pDisplay-HaloTag-Myc mouse (doxycycline induced). The islet was labeled with ZIMIR-HaloTag (2 μM for 30 min) *in vitro*. After glucose challenge, a high Zn^{2+} buffer (1 μM Zn^{2+}) was added. Scale bar = 20 μm.

ZIGIR signal intensity than the surrounding beta cells. These cells corresponded to mouse alpha cells and delta cells with relatively low granular Zn^{2+} content, as we previously demonstrated by the flow cytometry analysis of ZIGIR labeled mouse islet cells (12).

DISCUSSION

There have been growing interests in studying islet cells in their native habitat. The islet of Langerhans is a highly vascularized mini-organ amply supplied with blood circulation and oxygen (13, 14). In the pancreas, islets are encapsulated by the peri-islet capsule which separates the endocrine compartment from the exocrine cells (9, 10). In addition to sensing and responding to nutrient fluctuations in the circulation, islet cells also receive neuronal inputs that modulate their hormone release activity (15, 16). Studies on the regulated insulin secretion thus far have been largely relying on cultured beta cells or isolated islets. While these systems have yielded valuable insights into the molecular mechanisms governing stimulus-secretion coupling *in vitro*, our understanding on how islet cells behave *in vivo* and how they tune their secretion dynamics moment by moment in response to physiological cues is relatively limited. Imaging assays capable of tracking hormone release activity of islet cells in live animals would be invaluable for studying islet cell physiology, for monitoring the declining of islet cell function during diabetes progression, and for assessing the efficacy of therapeutics intended for maintaining or restoring beta cell function.

ZIMIR imaging tracks insulin/Zn^{2+} release at the cellular and subcellular resolution and has been applied to cultured cells and isolated islets (4, 17–20). To image insulin/Zn^{2+} release *in vivo*, we attempted several methods for loading ZIMIR to islet cells in the intact pancreas. The bolus dye loading is an established method for labeling neurons in the brain. In our hands, dye microinjection into the exocrine tissue was rather inefficient in labeling nearby islets, while intra-islet dye injection turned out to be challenging, likely due to the miniature size and cellular compactness of an islet. Compared to the microinjection, pancreas perfusion through the splenic artery turned out to be more effective in labeling endocrine cells with amphipathic dyes such as Cy3-C12 and ZIMIR (**Figure 3**). Among the three approaches that we have explored, the chemogenetic method of tagging the plasma membrane of islet cells with a HaloTag probe turned out to be most facile and selective, and it holds the promise for the routine application through systemic delivery in

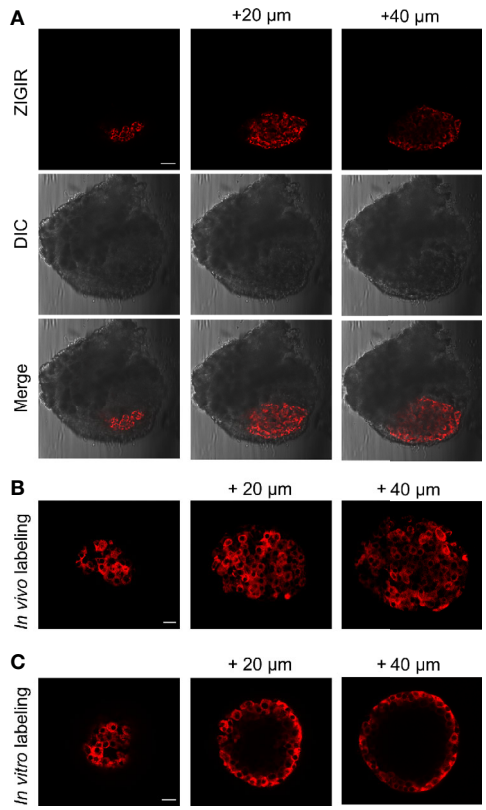

FIGURE 7 | *In vivo* systemic delivery of ZIGIR selectively labeled pancreatic endocrine cells throughout entire islets. **(A)** ZIGIR selectively labeled rat islet cells after tail vein injection. Confocal images of a pancreatic tissue from a rat injected with ZIGIR. Three consecutive confocal sections 20 μm apart along the z-axis were shown. ZIGIR signal was seen only in the islet but not the exocrine cells. Scale bar = 100 μm. **(B, C)** ZIGIR labeled mouse islet cells throughout the islet after tail vein injection **(B)**, but only labeled the outer cell layer when it was applied to the isolated mouse islets *in vitro* **(C)**. Three consecutive confocal sections of ZIGIR-labeled islets were shown. Scale bar = 20 μm.

the future. After inducible expression of HaloTag protein in the transgenic mouse, we were able to achieve efficient and selective labeling of beta cells after tail vein injection of Fluo-HaloTag-2 (**Figure 5**). However, adopting this strategy to deliver ZIMIR-HaloTag to beta cells turned out to be less efficient compared with Fluo-HaloTag-2. The difference probably reflected a variation in biodistribution and pharmacokinetics (PK) of these two probes *in vivo*, such that ZIMIR-HaloTag in the circulation falls off too rapidly to react with the HaloTag protein expressed on the beta cell surface. Efforts of engineering ZIMIR derivatives to improve their PK and islet distribution are underway and, if successful, such probes are expected to boost the labeling efficiency of beta cells of the transgenic mouse.

In a pilot experiment of *in vivo* ZIMIR imaging, we observed synchronized, oscillatory insulin/Zn^{2+} releases among a cluster of mouse islet beta cells (**Figure 4**). These rhythmic oscillations exhibited a period of ~ 32 s. To our knowledge, this represents the first report of insulin release at the cellular resolution in the intact pancreas *in vivo*. Insulin oscillation has been documented in the isolated islets *in vitro*, and in the blood circulation *in vivo* (21, 22). A number of studies have shown rhythmic behavior of hormone secretion in isolated islets, with oscillating periods ranging from ~ 20 s to several minutes (21, 23, 24). Insulin oscillation is thought to be coupled with intracellular Ca^{2+} oscillation, bursting electrical activity and cellular metabolic rhythm (25). It has been proposed that oscillatory insulin release is important to normal glucose homeostasis, and disturbance of oscillations could be detrimental and play a major role in type 2 diabetes (1). The *in vivo* imaging technique that we have been developing and its future enhancements should enable investigating this important phenomenon at the cellular level and to address its regulation in live animals. The recent development of abdominal imaging window (AIW) has made it possible to track internal organs by high resolution fluorescence microscopy for a prolonged period of time (26, 27). Under favorable conditions, an animal could be imaged repeatedly up to several weeks. Even though our work described herein focuses on probe delivery as a proof of principle for the *in vivo* ZIMIR imaging, we anticipate that future probe engineering and integration with AIW would eventually lead to an imaging platform for the longitudinal monitoring of insulin release of individual islets *in vivo*. In additional to optical imaging, recent advancements in magnetic resonance imaging (MRI) of Zn^{2+} release provides yet another imaging platform for monitoring the secretory activity of cells *in vivo* (28, 29). Integration of these different imaging modalities is expected to enhance our ability to track islet beta cell function in the intact pancreas spanning a broader range of spatial and temporal scales.

Besides beta cell function, another parameter of importance to islet biology and diabetes research is beta cell mass. As we have shown here, ZIGIR represents a promising *in vivo* imaging probe of islet cell mass. ZIGIR is brightly fluorescent and can be applied at a rather low concentration to label beta cells *in vivo*. We routinely injected ZIGIR through tail vein at 10 nmol/mouse. Based on a blood volume of ~ 2 ml, this is equivalent to ~ 5 μM ZIGIR in the blood circulation immediately after injection. At this dosage, ZIGIR labeled islet cells efficiently and selectively without showing any detectable signal in the exocrine tissue (**Figure 7**). Given the bright signal we observed in the labeled islets, we speculate that even lower doses of ZIGIR can be used for the *in vivo* labeling and imaging applications. Zinc chelating agents such as dithizone (DTZ) have long been used to stain pancreatic islets (30). However, DTZ is a rather poor fluorophore for fluorescence imaging, and is limited by its cytotoxicity (31). In fact, DTZ reduces insulin secretion and causes islet cell death, and DTZ has been used as a diabetogenic agent in animal studies (32). In contrast, at micromolar concentration, ZIGIR shows no cytotoxicity, and does not affect cell proliferation or insulin secretion (12). Future molecular engineering of ZIGIR analogues emitting at longer wavelengths up to near-infrared, or incorporating radioisotopes (^{18}F, ^{11}C, ^{125}I, etc) presents new opportunities for engineering whole body imaging platforms of interrogating islet cell physiology *in vivo*.

DATA AVAILABILITY STATEMENT

The raw data supporting the conclusions of this article will be made available by the authors, without undue reservation.

AUTHOR CONTRIBUTIONS

W-hL and PES designed the experiments. SC, ZH, HK, MK, ES, SX, EG, and YX conducted the experiments and analyzed the data. W-hL and SC wrote the paper. W-hL, PES, and ADS provided supervision and funding. All authors contributed to the article and approved the submitted version.

FUNDING

This work was supported by grant awards from JDRF (1-SRA-2018-675-S-B to W-hL) and NIH (R01-GM132610 to W-hL, R01-DK55758 and R01-DK099110 to PES, and R01-DK095416 to ADS).

ACKNOWLEDGMENTS

We thank the Live Cell Imaging Core Facility of UT Southwestern for providing the confocal imaging equipment.

REFERENCES

1. Satin LS, Butler PC, Ha J, Sherman AS. Pulsatile insulin secretion, impaired glucose tolerance and type 2 diabetes. *Mol Aspects Med* (2015) 42:61–77. doi: 10.1016/j.mam.2015.01.003
2. Porksen N, Hollingdal M, Juhl C, Butler P, Veldhuis JD, Schmitz O. Pulsatile insulin secretion: detection, regulation, and role in diabetes. *Diabetes* (2002) 51 Suppl 1:S245–54. doi: 10.2337/diabetes.51.2007.S245
3. Li WH. Functional analysis of islet cells in vitro, in situ, and in vivo. *Semin Cell Dev Biol* (2020) 103:14–9. doi: 10.1016/j.semcdb.2020.02.002
4. Li D, Chen S, Bellomo EA, Tarasov AI, Kaut C, Rutter GA, et al. Imaging dynamic insulin release using a fluorescent zinc indicator for monitoring induced exocytotic release (ZIMIR). *Proc Natl Acad Sci USA* (2011) 108:21063–68. doi: 10.1073/pnas.1109773109
5. Kusminski CM, Chen S, Ye R, Sun K, Wang QA, Spurgin SB, et al. MitoNEET-Parkin Effects in Pancreatic alpha- and beta-Cells, Cellular Survival, and Intrainsular Cross Talk. *Diabetes* (2016) 65:1534–55. doi: 10.2337/db15-1323
6. Li D, Liu L, Li WH. Genetic Targeting of a Small Fluorescent Zinc Indicator to Cell Surface for Monitoring Zinc Secretion. *ACS Chem Biol* (2015) 10:1054–63. doi: 10.1021/cb5007536
7. Coppieters K, Martinic MM, Kiosses WB, Amirian N, von Herrath M. A novel technique for the in vivo imaging of autoimmune diabetes development in the pancreas by two-photon microscopy. *PloS One* (2010) 5:e15732. doi: 10.1371/journal.pone.0015732
8. Stosiek C, Garaschuk O, Holthoff K, Konnerth A. In vivo two-photon calcium imaging of neuronal networks. *Proc Natl Acad Sci USA* (2003) 100:7319–24. doi: 10.1073/pnas.1232232100
9. van Deijnen JH, Hulstaert CE, Wolters GH, van Schilfgaarde R. Significance of the peri-insular extracellular matrix for islet isolation from the pancreas of rat, dog, pig, and man. *Cell Tissue Res* (1992) 267:139–46. doi: 10.1007/BF00318700
10. Korpos E, Kadri N, Kappelhoff R, Wegner J, Overall CM, Weber E, et al. The Peri-islet Basement Membrane, a Barrier to Infiltrating Leukocytes in Type 1 Diabetes in Mouse and Human. *Diabetes* (2013) 62:531–42. doi: 10.2337/db12-0432
11. Los GV, Encell LP, McDougall MG, Hartzell DD, Karassina N, Zimprich C, et al. HaloTag: a novel protein labeling technology for cell imaging and protein analysis. *ACS Chem Biol* (2008) 3:373–82. doi: 10.1021/cb800025k
12. Ghazvini Zadeh EH, Huang Z, Xia J, Li D, Davidson HW, Li WH. ZIGIR, a Granule-Specific Zn(2+) Indicator, Reveals Human Islet alpha Cell Heterogeneity. *Cell Rep* (2020) 32:107904. doi: 10.1016/j.celrep.2020.107904
13. Lifson N, Lassa CV, Dixit PK. Relation between blood flow and morphology in islet organ of rat pancreas. *Am J Physiol* (1985) 249:E43–8. doi: 10.1152/ajpendo.1985.249.1.E43
14. Carlsson PO, Liss P, Andersson A, Jansson L. Measurements of oxygen tension in native and transplanted rat pancreatic islets. *Diabetes* (1998) 47:1027–32. doi: 10.2337/diabetes.47.7.1027
15. Schwartz MW, Seeley RJ, Tschop MH, Woods SC, Morton GJ, Myers MG, et al. Cooperation between brain and islet in glucose homeostasis and diabetes. *Nature* (2013) 503:59–66. doi: 10.1038/nature12709
16. Pozo M, Claret M. Hypothalamic Control of Systemic Glucose Homeostasis: The Pancreas Connection. *Trends Endocrinol Metab* (2018) 29:581–94. doi: 10.1016/j.tem.2018.05.001
17. Hodson DJ, Mitchell RK, Marselli L, Pullen TJ, Brias SG, Semplici F, et al. ADCY5 couples glucose to insulin secretion in human islets. *Diabetes* (2014) 63:3009–21. doi: 10.2337/db13-1607
18. Hodson DJ, Mitchell RK, Bellomo EA, Sun G, Vinet L, Meda P, et al. Lipotoxicity disrupts incretin-regulated human beta cell connectivity. *J Clin Invest* (2013) 123:4182–94. doi: 10.1172/JCI68459
19. Mitchell RK, Hu M, Chabosseau PL, Cane MC, Meur G, Bellomo EA, et al. Molecular Genetic Regulation of Slc30a8/ZnT8 Reveals a Positive Association With Glucose Tolerance. *Mol Endocrinol* (2016) 30:77–91. doi: 10.1210/me.2015-1227
20. Li D, Huang Z, Chen S, Hu Z, Li WH. GLP-1 Receptor Mediated Targeting of a Fluorescent Zn2+ Sensor to Beta Cell Surface for Imaging Insulin/Zn2+ Release. *Bioconjug Chem* (2015) 26:1443–50. doi: 10.1021/acs.bioconjchem.5b00332
21. Gilon P, Ravier MA, Jonas JC, Henquin JC. Control mechanisms of the oscillations of insulin secretion in vitro and in vivo. *Diabetes* (2002) 51 Suppl 1:S144–51. doi: 10.2337/diabetes.51.2007.S144
22. Song SH, McIntyre SS, Shah H, Veldhuis JD, Hayes PC, Butler PC. Direct measurement of pulsatile insulin secretion from the portal vein in human subjects. *J Clin Endocrinol Metab* (2000) 85:4491–9. doi: 10.1210/jc.85.12.4491
23. Li X, Hu J, Easley CJ. Automated microfluidic droplet sampling with integrated, mix-and-read immunoassays to resolve endocrine tissue secretion dynamics. *Lab Chip* (2018) 18:2926–35. doi: 10.1039/C8LC00616D
24. Bandak B, Yi L, Roper MG. Microfluidic-enabled quantitative measurements of insulin release dynamics from single islets of Langerhans in response to 5-palmitic acid hydroxy stearic acid. *Lab Chip* (2018) 18:2873–82. doi: 10.1039/C8LC00624E
25. Nunemaker CS, Satin LS. Episodic hormone secretion: a comparison of the basis of pulsatile secretion of insulin and GnRH. *Endocrine* (2014) 47:49–63. doi: 10.1007/s12020-014-0212-3
26. Ritsma L, Steller EJ, Ellenbroek SI, Kranenburg O, Borel Rinkes IH, van Rheenen J. Surgical implantation of an abdominal imaging window for intravital microscopy. *Nat Protoc* (2013) 8:583–94. doi: 10.1038/nprot.2013.026
27. Reissaus CA, Pineros AR, Twigg AN, Orr KS, Conteh AM, Martinez MM, et al. Portable Intravital Microscopy Platform for Studying Beta-cell Biology In Vivo. *Sci Rep* (2019) 9:8449. doi: 10.1038/s41598-019-44777-0
28. Clavijo Jordan MV, Lo ST, Chen S, Preihs C, Chirayil S, Zhang S, et al. Zinc-sensitive MRI contrast agent detects differential release of Zn(II) ions from the healthy vs. *Malignant Mouse Prostate Proc Natl Acad Sci USA* (2016) 113:E5464–71. doi: 10.1073/pnas.1609450113
29. Martins AF, Clavijo Jordan V, Bochner F, Chirayil S, Paranawithana N, Zhang S, et al. Imaging Insulin Secretion from Mouse Pancreas by MRI Is Improved by Use of a Zinc-Responsive MRI Sensor with Lower Affinity for Zn(2+) Ions. *J Am Chem Soc* (2018) 140:17456–64. doi: 10.1021/jacs.8b07607
30. Bonnevie-Nielsen V, Skovgaard LT, Lernmark A. beta-Cell function relative to islet volume and hormone content in the isolated perfused mouse pancreas. *Endocrinology* (1983) 112:1049–56. doi: 10.1210/endo-112-3-1049

31. Conget JI, Sarri Y, Gonzalez-Clemente JM, Casamitjana R, Vives M, Gomis R. Deleterious effect of dithizone-DMSO staining on insulin secretion in rat and human pancreatic islets. *Pancreas* (1994) 9:157–60. doi: 10.1097/00006676-199403000-00003
32. Monago CC, Onwuka F, Osaro E. Effect of combined therapy of diabinese and nicotinic acid on liver enzymes in rabbits with dithizone-induced diabetes. *J Exp Pharmacol* (2010) 2:145–53. doi: 10.2147/JEP.S11490

Conflict of Interest: W-hL and EG are co-inventors of a US patent concerning ZIGIR.

The remaining authors declare that the research was conducted in the absence of any commercial or financial relationships that could be construed as a potential conflict of interest.

frontiers in Endocrinology

MINI REVIEW
published: 23 April 2021
doi: 10.3389/fendo.2021.652853

The Eye as a Transplantation Site to Monitor Pancreatic Islet Cell Plasticity

Erwin Ilegems[1*] *and Per-Olof Berggren*[1,2,3,4,5*]

[1] *The Rolf Luft Research Center for Diabetes and Endocrinology, Karolinska Institute, Stockholm, Sweden,* [2] *Diabetes Research Institute, Miller School of Medicine, University of Miami, Miami, FL, United States,* [3] *Lee Kong Chian School of Medicine, Nanyang Technological University, Singapore, Singapore,* [4] *Center for Diabetes and Metabolism Research, Department of Endocrinology and Metabolism, West China Hospital, Sichuan University, Chengdu, China,* [5] *School of Biomedical Sciences, Ulster University, Coleraine, United Kingdom*

OPEN ACCESS

Edited by:
Guy A. Rutter, Imperial College London, United Kingdom

Reviewed by:
Guoqiang Gu, Vanderbilt University, United States
Amelia K. Linnemann, Indiana University, United States

***Correspondence:**
Erwin Ilegems
erwin.ilegems@ki.se
Per-Olof Berggren
per-olof.berggren@ki.se

Specialty section:
This article was submitted to Diabetes: Molecular Mechanisms, a section of the journal Frontiers in Endocrinology

Received: *13 January 2021*
Accepted: *26 March 2021*
Published: *23 April 2021*

Citation:
Ilegems E and Berggren P-O (2021) The Eye as a Transplantation Site to Monitor Pancreatic Islet Cell Plasticity. Front. Endocrinol. 12:652853. doi: 10.3389/fendo.2021.652853

The endocrine cells confined in the islets of Langerhans are responsible for the maintenance of blood glucose homeostasis. In particular, beta cells produce and secrete insulin, an essential hormone regulating glucose uptake and metabolism. An insufficient amount of beta cells or defects in the molecular mechanisms leading to glucose-induced insulin secretion trigger the development of diabetes, a severe disease with epidemic spreading throughout the world. A comprehensive appreciation of the diverse adaptive procedures regulating beta cell mass and function is thus of paramount importance for the understanding of diabetes pathogenesis and for the development of effective therapeutic strategies. While significant findings were obtained by the use of islets isolated from the pancreas, *in vitro* studies are inherently limited since they lack the many factors influencing pancreatic islet cell function *in vivo* and do not allow for longitudinal monitoring of islet cell plasticity in the living organism. In this respect a number of imaging methodologies have been developed over the years for the study of islets *in situ* in the pancreas, a challenging task due to the relatively small size of the islets and their location, scattered throughout the organ. To increase imaging resolution and allow for longitudinal studies in individual islets, another strategy is based on the transplantation of islets into other sites that are more accessible for imaging. In this review we present the anterior chamber of the eye as a transplantation and imaging site for the study of pancreatic islet cell plasticity, and summarize the major research outcomes facilitated by this technological platform.

Keywords: pancreatic islet imaging, islet transplantation, anterior chamber of the eye, confocal microscopy, islet cell plasticity, beta cell, islet imaging, novel imaging methods

INTRODUCTION

Diabetes mellitus is presently affecting large and growing segments of the population, especially the elderly, and represents a major socio-economic hurdle (1, 2). Constitutively high blood glucose is a symptom of this disease and causes a number of severe pathologies in multiple organs and cell types. Under normal conditions plasma insulin levels typically increase when blood glucose levels rise, and insulin serves as a signal for tissues throughout the body to take up glucose, thereby maintaining blood glucose levels within a narrow, physiologically optimal window. In the majority of cases, diabetes results from a progressive dysfunction in the supply of insulin secreted from the beta cells within the pancreatic islets, caused either by an insufficient number of these endocrine cells or by their failure to release adequate amounts of insulin in response to an increase in blood glucose concentration. In this respect it is necessary to further investigate the fine mechanisms linking glucose sensing to insulin release and how pancreatic islets can adapt to different circumstances to cope with varying insulin demands.

A major challenge in the longitudinal studies of islets is related to the fact that these small structures only represent about 1.5% of the total volume of the pancreas (3). Additionally, the pancreas itself is located deep in the abdomen between other organs and therefore not easily accessible for *in vivo* functional imaging. Although *in vitro* studies based on islets isolated from the pancreas brought significant advances to the understanding of islet biology, these are unfortunately inherently limited since they lack the many factors influencing pancreatic islet cell function *in vivo*, e.g. the effects of hormones secreted from a crosstalk with other organs such as liver, adipose tissue, brain, and gut (4, 5). Therefore, studies under the complex *in vivo* conditions present in the living organism are primordial for the longitudinal appreciation of islet function in health and disease.

A number of different advanced imaging techniques have been developed over the years for the study of pancreatic islets, with a particular focus on their ability to estimate beta cell mass, i.e. a volumetric measurement of insulin-positive cells (6). In particular, magnetic resonance imaging (MRI), positron emission tomography (PET), computer tomography (CT) and bioluminescence imaging (BLI) are the main imaging modalities used for *in vivo* noninvasive studies of islets in the pancreas. However, while these techniques offer appropriate imaging penetration for animal studies, they are still limited in terms of sensitivity and resolution and often require additional labeling for the detection of beta cells. Other techniques to image *in situ* pancreatic islets at higher resolution include optical projection tomography (OPT), light sheet fluorescence microscopy (LSFM), optical coherence tomography (OCT) and confocal microscopy, but require exteriorization or removal of the pancreas and therefore are not suitable for longitudinal imaging at single islet level. Alternatively, abdominal imaging windows have been installed with the aim of imaging islets *in situ* without delocalizing the pancreas (7, 8). While this solution allows for a repetitive optical assessment of individual islets, the number of imaging sessions is still limited and the procedure is technically very challenging.

Due to difficulties in imaging islets longitudinally in the intact pancreas, another strategy is based on transplantation of islets into other sites that are more accessible for imaging. One important aspect in this case, in addition to the possibility to image the islets at high resolution, is the proper engraftment and survival of transplanted islets. Revascularization and reinnervation are indeed primordial factors determining the outcome of islet transplantation due to their critical role in the maintenance of islet functionality and survival (9–11). In particular, intra-islet vessels require a fast formation for tissue oxygenation, and furthermore their endothelial cells have been shown to be involved in local interactions with beta cells that are of particular importance for islet function (12).

Multiple sites have been explored for islet transplantation (13). In particular the kidney subcapsular space, the spleen and the portal vein have been widely used for the *in vivo* evaluation of islet mass and function, albeit with varying levels of engraftment success (14, 15) and of accessibility for high resolution imaging. Another approach is based on the transplantation of pancreatic islets into the anterior chamber of the eye (ACE). Because of its optical and structural properties, the eye is optimally suited as a natural body-window for non-invasive and longitudinal imaging of single islet grafts and their vascularization. Islets transplanted into the ACE have been shown to be functional and various aspects of beta cell function and survival can be readily imaged in this environment. Furthermore, imaging islets at this site can be performed at relatively high speed and at resolutions allowing for single cell functional investigations, essential requirements for the assessment of beta cell heterogeneity and dynamics of intra-islet cellular communications (16). In the following we will review findings obtained by the use of the ACE as a transplantation/imaging site for longitudinal *in vivo* appreciation of pancreatic islet cell mass and function.

THE ACE AS A TRANSPLANTATION SITE AND THE CORNEA AS A NATURAL BODY WINDOW FOR IMAGING PANCREATIC ISLET CELLS

The anterior chamber of the eye has been used as a transplantation site for about 150 years (17) and was shown in a number of studies to allow for the adequate engraftment of tissues from various origins, such as heart, brain, muscle, pituitary gland, liver, prostate, or tumors (18–23). The dense vascular network in the iris is contributing to rapid revascularization of the tissues (23, 24), providing essential nutrients and oxygenation for graft survival. In particular, pancreas tissue has been shown to benefit from proper survival after transplantation into the ACE (24–27). First seen as a convenient location for *in vivo* tissue culture and observation, this transplantation site has since been combined with high resolution microscopy for the assessment of islet morphology and function at individual islet and single cell level (28, 29). In addition to the benefits of this transplantation site for islet

engraftment and imaging, the surgical procedure is particularly straightforward and is not causing pain nor affecting the vision of the recipient animal (30).

After their introduction into the ACE through a small perforation in the cornea, the islets attach to the iris, initiating their engraftment. A few days after transplantation, revascularization of the tissue starts by the appearance of large blood vessels, followed progressively by smaller capillaries (31). Approximately 4 weeks after transplantation islet grafts are completely vascularized and present a similar vascular density as compared to islets in the pancreas (28). Interestingly, it has been shown that the newly-formed vascular network originates from the combination of endothelial cells still residing within the transplanted islet and of endothelial cells emanating from the iris (32). It is important to note that, even when using islets or pseudoislets completely devoid of endothelial cells for transplantation, capillaries emanating from revascularization comprise fenestrations (32, 33), similar to those from islets in the pancreas and required for the optimal transit of compounds between endocrine cells and blood flow. The eye also benefits from a dense innervation, contributing to the supply of sympathetic and parasympathetic fibers to the transplanted tissue (18). Reinnervation of islets starts within a few days and reaches a plateau 3 months after transplantation, with a pattern dictated by the transplanted islet (34). Thus both the innervation, of importance for the modulation of insulin release (35), and the connection of the islet grafts to blood circulation are occurring in the ACE, a prerequisite for any comprehensive investigation of islet biology.

There are basically two transplantation strategies, each giving different information on islet function (**Figure 1**). Firstly, the transplantation of a small number of islets, so-called "reporter islets", will serve to indicate the function of islets in the pancreas without affecting overall blood glucose homeostasis. Secondly, the transplantation of a large number of islets ("metabolic transplantation") into the ACE of mice rendered diabetic by the destruction of their pancreatic beta cells will regulate overall blood glucose homeostasis by secreting sufficient amounts of insulin in response to high glycemic levels, thereby taking over the role of islets in the pancreas. While the success of this latter procedure depends on the number of transplanted islets (37), it is interesting to note that only about 100 islets are required for complete recovery of blood glucose handling. Both transplantation strategies can be combined by the use of both eyes for transplantation, increasing the possibilities for scientific investigations.

A wide range of parameters related to islet function under normal and pathological conditions can be investigated by the use of the ACE as an *in vivo* transplantation/imaging platform (see **Table 1**). To start with, information on the morphology of the islet as well as its volume can be obtained by image acquisition of light scattering from islet cells. Indeed, secretory granules in beta cells are densely packed with crystallized insulin, forming microscopic spherical mirrors that are major contributors to the islet intrinsic scattering properties and permit to obtain volumetric information at cellular resolution without extrinsic labeling (39). Moreover, due to this biological origin, the intensity of light scattering is thereby directly indicative of insulin secretory capacity in islets. The recorded signal will thus be diminished both in cases of hypersecretion (36, 39) and of degranulation following autoimmune attack (53–55), thereby giving valuable insights into the functional status of transplanted islets.

Imaging strategies and probes for the investigation of cellular function are being continuously developed, many of which can be directly applied to the study of islet function *in vivo* after

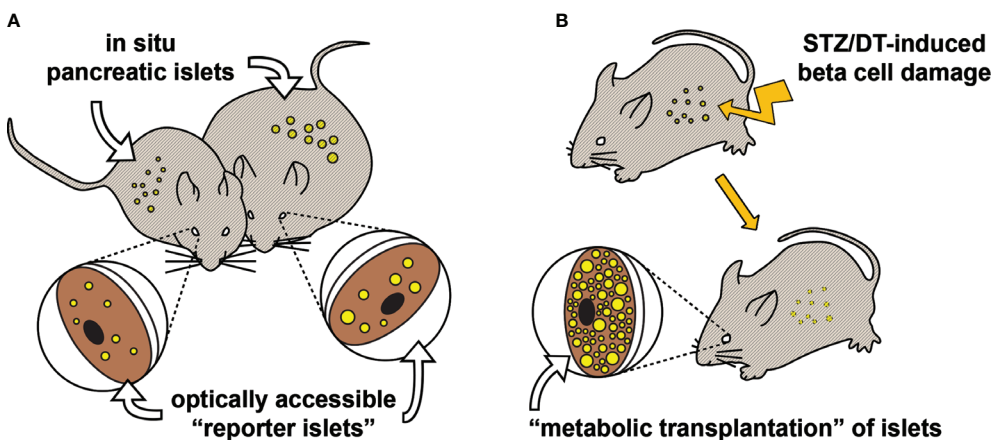

FIGURE 1 | Two transplantation strategies for *in vivo* study of pancreatic islet function and plasticity. **(A)** Various aspects of pancreatic islet function and morphology have been shown to be mirrored in "reporter islets" in the eye (36). This illustrative example shows that changes occurring to the *in situ* pancreatic islets of an obese mouse (right), for instance beta cell hyperplasia, are similarly occurring to the islets transplanted into the ACE. **(B)** Mice rendered hyperglycemic, e.g. by streptozotocin (37) or diphteria toxin (38), can be recovered by "metabolic transplantation" of a large number of islets, taking over the function of damaged pancreatic islets.

TABLE 1 | Morphological and functional parameters acquired in various studies from islets transplanted into the ACE.

Parameters indicative of islet function and morphology	References
Beta cell mass	(36, 39–41)
Intra-islet vascular density and morphology	(32, 42)
Blood flow dynamics	(43)
Innervation	(34)
Biochemical composition	(44)
Beta cell-specific protein expression and localization	(45)
Beta cell $[Ca^{2+}]_i$ mobilization	(33, 41, 46, 47)
NAD(P)H response	(40, 48)
Insulin secretion status	(39)
Beta cell insulin resistance	(49)
Proteomic/metabolomic profile of islet microenvironment	(50–52)
Autoimmune-induced damage	(53–57)
Allorejection	(51, 52, 58)
Cell death	(38, 55, 59)

transplantation into the ACE. Many aspects, from glucose intake to insulin secretion, can now be readily imaged at various temporal resolutions (33, 39–41, 46–48). Probably the most studied signal in the beta cell signaling pathway is the change in cytoplasmic free Ca^{2+} concentrations ($[Ca^{2+}]_i$), for its central role in the secretion of insulin (60). This signal was first studied in islets engrafted into the ACE after intraocular incubation with a $[Ca^{2+}]_i$-sensitive fluorescent dye prior to *in vivo* activation with glibenclamide (28). Transgenic mice expressing genetically encoded fluorescent $[Ca^{2+}]_i$ indicators were later used to record beta cell responses to intravenous administration of glucose (41, 46, 47) and of vasopressin, an agonist for the beta cell expressed V1b receptor (a G protein-coupled receptor, GPCR) (33). Whereas the response to the GPCR agonist was immediate, glucose initiated a slightly slower increase in $[Ca^{2+}]_i$ that culminated about 50s after administration, followed by smaller oscillating signals that gradually disappeared in parallel to the subsequent decrease in blood glucose levels. These experiments showcase how *in vivo* experiments take into account the many factors (e.g. circulating glucose and hormone levels) whose complexity cannot be faithfully reproduced under *in vitro* conditions.

Although the ACE was previously thought to be an immune privileged site (61), as aforementioned it has been shown that islets could be subjected to autoimmune attack at this location (58). Moreover, the infiltration of T lymphocytes into islet grafts is supportive of the notion that the immune privilege is somehow lost during the transplantation/engraftment procedure, and that the ACE is well-suited for longitudinal *in vivo* studies of autoimmunity and allograft rejection. This also implies that rejection of islets originating from another genetic background/species will occur in unmatched recipient mice, but this can be circumvented by the use of immune-deficient mice. This is particularly attractive for the study of human islets and thereby for appreciating to which extent studies performed in rodents can be translated to humans. For instance human islets indeed differ from rodent islets in their endocrine cell content and architecture (62, 63) as well as in their innervation pattern and density (64), thereby displaying functional differences that can now be assessed *in vivo* using the ACE platform (65, 66). Furthermore, the possibility to study human islets longitudinally represents an important asset in that it allows to evaluate short- and long-term effects of pharmacological treatment strategies for diabetes. This has been done for evaluating long-term effects of the beta cell targeting antidiabetic drug liraglutide (65). In this study mice were rendered diabetic by administration of streptozotocin (STZ), followed by a "metabolic transplantation" of human islets. Mice treated systemically with liraglutide returned to normoglycemic levels in a shorter period of time than their controls, indicating a beneficial short-term effect. However, upon prolonged treatment the transplanted islets became dysfunctional, unable to maintain sufficient insulin release to sustain normal glucose levels. These findings indicate that an excessive stimulation of beta cells with liraglutide leads to beta cell exhaustion and failure, which may be of immediate relevance for the outcome of long-term treatment of type 2 diabetes patients with this kind of drugs.

It is therefore possible to study in detail the effect of a pharmacological treatment on beta cell function and survival by systemic administration using this methodological platform. Interestingly, due to the specific location of the transplanted islets it is also possible to proceed with topical drug delivery, targeting more directly the engrafted tissue. In particular, compounds can be administrated locally by the application of eye drops (66) or by the slow release of compounds from co-transplanted micro-containers (67), thereby circumventing potential systemic adverse effects and reducing the overall treatment dosage. Finally, in addition to the advantages of using the ACE for islet transplantation and assessment, this accessible site can be used for analyzing compounds accumulating in the islet micro-environment (50–52). Microliter-size aqueous samples can be obtained in the immediate vicinity of the engrafted tissue, allowing for the analysis of islet-related metabolites and proteins. In particular, this strategy has been used with the aim to define early predictive markers of type 1 diabetes by detecting changes in the metabolic profile (50), and to predict the risk of allograft rejection to allow for a timely therapeutic intervention (51, 52). As a whole, these methodologies using the ACE platform are perfectly suited for the study of islet plasticity in health and disease under *in vivo* conditions.

LONGITUDINAL IMAGING OF PANCREATIC ISLET CELL PLASTICITY: VALIDATION STUDIES AND SCIENTIFIC ADVANCES

Under various physiological circumstances islets can display a certain degree of adaptation, for instance an increased demand for insulin can lead to an increase in beta cell mass (68). The modulation of beta cell function, either in some individual beta cells within islets or in the entire population of beta cells, can also serve as an adaptive biological mechanism of importance for the maintenance of normoglycemia. Both physiological and pathological states may cause changes in these adaptive

mechanisms, which can lead to the incapacity in maintaining normoglycemia and to the development of diabetes. One of the major assets of the ACE as a transplantation/imaging platform is to allow for the investigation of islet plasticity over a period of several months, and thereby for the study of the diverse adaptive procedures and circulating factors involved in the regulation of beta cell mass and function.

Increase and Decrease in Beta Cell Mass

Longitudinal changes in beta cell mass have first been reported for islets transplanted into the ACE of the ob/ob mouse model (36). This mouse model lacks functional leptin and therefore its uncontrolled appetite quickly leads to obesity. The study showed that islets transplanted into the eye rapidly grow as a consequence of beta cell hyperplasia, similarly to what has been previously been reported for islets in their pancreas (69). Islet volume doubled in a period of one month as a consequence of beta cell proliferation, a result corroborating with the impressive beta cell mass expansion seen in the pancreas by OPT (70). Although the islets transplanted into the ACE cannot fully represent the entire range of islets that are existing in the pancreas, due to the different size distribution among isolated islets as compared to *in situ* pancreatic islets (33, 59), we could show that reporter islets in the ACE served as a representative sample that displayed identical beta cell replication as compared to *in situ* pancreatic islets. Also, the dilation of intra-islet blood capillaries, suggested to be due to increased parasympathetic innervation and endothelial nitric oxide production in ob/ob mouse islets (71), was observed in the reporter islets. Interestingly, both islet growth and enlarged capillaries were shown to be dependent on the recipient mouse and not on the origin of the transplanted islets, illustrating the importance of circulating factors for these morphological phenotypes. In addition, reporter islets in the ACE could be used to visualize the efficiency of a treatment. For example, by daily intraperitoneal injections of leptin, the appetite of ob/ob mice was reduced and the growth of their islets was halted, both in the ACE and *in situ* in the pancreas (36). Reporter islets were similarly used in other studies for investigating changes in beta cell mass when mice were fed a high fat diet (HFD) (40, 41). Interestingly, islet growth was relatively modest under HFD-induced prediabetes conditions (islet volumes were doubled after a period of 4 month on HFD), and it was shown that the major compensatory mechanism to cope with insulin resistance was a change in islet function to increase insulin secretion from individual beta cells (41).

A decrease in beta cell mass has also been documented with islets transplanted into the ACE using various mouse models for the study of diabetes. For instance, autoimmune destruction of beta cells was assessed in the NOD mouse model, showing both the infiltration of fluorescently-labelled immune cells and the progressive and rapid destruction of islet cells following diabetes onset (55). Interestingly, this study showed that during the short pre-diabetes period, islet volumes were temporarily increased and their scattering properties were five-fold reduced, indicative of insulin hyper-secretion (39). These findings show that reporter islets in the ACE allow for the early detection of the pathogenesis of type 1 diabetes, with the potential to provide a therapeutic intervention on a timely manner, before the full development of diabetes. Beta cell ablation was also monitored in other widely used mouse models for the study of diabetes and hyperglycemia. The kinetics and extent of toxin-mediated beta cell destruction were monitored both in the RIP-DTR (38) and in the STZ-diabetic models (59), and validated by OPT image analysis of islets in the pancreas. The destruction of islets in the RIP-DTR mouse model was almost total after only a few days, due to an immediate effect of the toxin fully occurring during the day of administration and leading to the inhibition of beta cell protein synthesis (72), and subsequently to beta cell death. Interestingly, glucose handling started to be affected only 2 days after toxin administration despite a discontinuation in the expression of all proteins required for glucose sensing/metabolism and insulin granule secretion. This fact highlights the over-capacity in terms of pancreatic islet function, displaying a surprising functional reserve for the maintenance of blood glucose levels. In mice rendered hyperglycemic by STZ, beta cell mass was much less affected as compared to the RIP-DTR mouse model. Beta cell ablation occurred mainly during the first week after STZ administration, and mice became hyperglycemic with more than half of their beta cell mass remaining (59). This study demonstrated that STZ was mainly affecting the function of pancreatic beta cells rather than beta cell mass. Interestingly, when proceeding with a metabolic transplantation of islets into the ACE following STZ-induced hyperglycemia, supporting the remaining beta cells in the islets within the pancreas in their efforts to regulate blood glucose homeostasis and thereby reducing their metabolic stress, they partially recovered in terms of function and maturity. Jointly, the results from this study indicate that hyperglycemia in itself sustains a negative feedback loop restraining the recovery of islet function, and highlight the impressive plasticity of the endocrine pancreas, even after STZ-induced damage (59).

Functional Plasticity of Pancreatic Islets

Although plasticity in beta cell function can be indirectly inferred by the acquisition of physiological parameters, different imageable indicators can be used to more specifically report on beta cell function using islets engrafted into the ACE. For instance in mice fed a HFD, beta cell $[Ca^{2+}]_i$ dynamics were monitored during the development of prediabetes by the use of the GCaMP3 fluorescent indicator (41). In this study it was shown that glucose-induced increase in beta cell $[Ca^{2+}]_i$ was already reduced after one week of HFD, and basal non-stimulated levels of $[Ca^{2+}]_i$ were increased progressively to a significant level two months after introduction of the diet. Combined with longitudinal imaging of beta cell mass, these results demonstrate that alterations in beta cell function and efficacy in terms of glucose-induced insulin release prevail over the increase in beta cell mass to compensate for insulin resistance in HFD-induced prediabetes (41). This study further showed that, after 4 months of HFD, beta cell $[Ca^{2+}]_i$ responses to glucose could be reverted by refeeding mice a normal diet for 2

weeks only, in parallel with a reversal of the prediabetes status. Altogether these findings support the notion that beta cell function should be the primary target for the treatment of diet-induced diabetes rather than beta cell mass.

Glucose-induced $[Ca^{2+}]_i$ responses were later investigated at the single beta cell level in islets transplanted into the ACE of ob/ob mice (46). While intravenously injected glucose was shown to reach all beta cells simultaneously, both in control and ob/ob mice, this resulted in the activation of only about 20% beta cells in the hyperglycemic ob/ob mouse as compared to about 80% in control mice, at 2 months of age. In another study using islets transplanted into the ACE, it was shown that the number of responding beta cells depends on their connectivity within the islet, which under normal conditions increases when glucose levels are elevated (47). This implies that beta cells are less coordinated in ob/ob as compared to control mice. Interestingly, the percentage of responding beta cells increased over time and became identical to control mice when they reached 10 months of age (46). These findings illustrate the functional plasticity occurring in islets of the ob/ob mouse over time, and how reporter islets in the ACE allow for the investigation of beta cell functional heterogeneity at single islet level.

Although beta cell connectivity was increased in the 10-month-old ob/ob mice, not all aspects of their islet function were improved. Indeed, it was shown using vibrational microscopy and multivariate analysis, that reporter islets transplanted into the ACE of ob/ob mice had a higher content of collagen (44). This technique allows to register changes in the chemical composition of tissues and in this case reported on an increase in blood vessel fibrosis in ob/ob mouse islets. Electron microscopy studies confirmed the strong deposit of collagen fibers surrounding intra-islet endothelial cells, both in islets in the pancreas and in islets engrafted into the ACE. Fibrosis of islet blood vessels has been similarly detected in old mice by *ex vivo* analysis of islets transplanted into the ACE (31), altogether pointing to a natural, progressive and irreversible increase of fibrosis over time that is exacerbated by diabetic conditions.

DISCUSSION

Over the years, *in vivo* imaging of islets transplanted into the ACE has proven to be a remarkably valuable tool for the study of pancreatic islet biology and plasticity. Despite the numerous scientific findings obtained from its use, a few limitations have however to be acknowledged. First and foremost, islets engrafted into the ACE might not reflect in all respects the function and plasticity of islets *in situ* in the pancreas, simply due to their different location. For instance, even though engrafted islets are properly innervated both by sympathetic and parasympathetic neurons, they likely are not connected by circuits emanating from the hypothalamic regions as is the case for *in situ* pancreatic islets (73). The potentiating effect of light on insulin secretion from islets engrafted into the ACE (34) is indicative of connections from the grafts to the visual cortex instead, as demonstrated for other tissues engrafted into the ACE (18). Also, the relative location of the engrafted islets with regard to other organs contributing to blood glucose homeostasis is different from that of islets in the pancreas, which may have functional implications. For example, while the liver is the first organ exposed to insulin released from islets in the pancreas and is the main contributor to insulin clearance (74–77), insulin released from engrafted islets will first encounter other organs before reaching the liver at a progressively diminished concentration. Although it would imply that islets transplanted into the ACE might not utterly mirror *in situ* pancreatic islets in their functionality, this very fact can potentially shed light on the importance of a stepwise presentation of insulin at different concentrations to different organs for the normal function of the endocrine pancreas. In this respect, it is interesting to note that only about 100 islets are required to be transplanted into the ACE of a mouse devoid of functional *in situ* pancreatic islets (37, 59, 66), which suggests a seemingly more efficient insulin signaling between engrafted islets and peripheral organs. Finally, potential endocrine-exocrine interactions in the pancreas, of beneficial or detrimental nature for islet function, will not apply to islets transplanted into the ACE. It is therefore of importance to keep these differences in mind when studying islets engrafted into the ACE, and possibly even make use of these to reveal specific aspects related to the function of *in situ* pancreatic islets and to inter-organ communication in health and disease.

Contrasting to the use of the ACE to study transplanted islets as "reporters", mirroring as accurately as possible pancreatic islet function and plasticity, the ACE can also be a valuable transplantation site to investigate in detail the role of specific genes and signaling pathways on islet function. For instance, islet-expressed ApoCIII was shown by longitudinal *in vivo* imaging and *ex vivo* functional assessment to have a major role in islet growth and signaling (48). Also, transplantation of islets from different species (mouse, human, monkey) into the ACE of mice revealed that intra-islet paracrine interactions are major determinants of the resting glycemic set point *in vivo* (66). The accumulation of such discoveries can serve as the basis for the establishment of all fundamental parameters required for proper islet function. Moreover, and in addition to establishing this optimal repertoire, a further possible "enhancement" of islet function could prove to be beneficial for future clinical transplantation, which suffer to this day from poor islet quality and survival (78). This transplantation and imaging platform has indeed already been successfully used to assess functional enhancement of synthetically engineered islet-derived pseudoislets (33). It could similarly be used in the relatively near future to study potentially beneficial effects of modifying GPCR signaling pathways and/or intra-islet paracrine interactions (79), incorporating supporting structures or accessory cells in islets (80), or using stem cells as a new source of mature islet cells (81–83), altogether supporting the development of promising strategies to improve the outcome of clinical transplantations. In conclusion, the ACE has been a remarkable research platform that is being adopted by an increasing number of scientists for the study of islet function and survival, and without doubt will continue to support novel findings in the field of islet biology and innovative therapeutic approaches for diabetes treatment.

AUTHOR CONTRIBUTIONS

EI wrote the review article. P-OB revised and edited the review article. All authors contributed to the article and approved the submitted version.

FUNDING

Own work discussed in this review was supported by funding from Karolinska Institutet, the Strategic Research Program in Diabetes at Karolinska Institutet, the Swedish Research Council, the Novo Nordisk Foundation, the Swedish Diabetes Association, the Family Knut and Alice Wallenberg Foundation, Diabetes Research and Wellness Foundation, the Stichting af Jochnick Foundation, the Family Erling-Persson Foundation, Berth von Kantzow's Foundation, ERC-2018-AdG 834860 EYELETS, the European Union's Seventh Framework Programme under grant agreements No 289932 and 613879, and the European Diabetes Research Programme in Cellular Plasticity Underlying the Pathophysiology of Type 2 Diabetes.

REFERENCES

1. World Health Organization G. *Global status report on noncommunicable diseases 2010*. (2011). Geneva, Switzerland:World Health Organization
2. Mathers CD, Loncar D. Projections of global mortality and burden of disease from 2002 to 2030. *PloS Med* (2006) 3(11):e442. doi: 10.1371/journal.pmed.0030442
3. Bonner-Weir S. Anatomy of the islet of Langerhans. In: E Samols, editor. *The Endocrine Pancreas*. New York: Raven Press (1991). p. 15–27.
4. Shirakawa J, De Jesus DF, Kulkarni RN. Exploring inter-organ crosstalk to uncover mechanisms that regulate beta-cell function and mass. *Eur J Clin Nutr* (2017) 71(7):896–903. doi: 10.1038/ejcn.2017.13
5. Tanabe K, Amo-Shiinoki K, Hatanaka M, Tanizawa Y. Interorgan Crosstalk Contributing to beta-Cell Dysfunction. *J Diabetes Res* (2017) 2017:3605178. doi: 10.1155/2017/3605178
6. Ahlgren U, Gotthardt M. Approaches for imaging islets: recent advances and future prospects. *Adv Exp Med Biol* (2010) 654:39–57. doi: 10.1007/978-90-481-3271-3_3
7. Ritsma L, Steller EJ, Ellenbroek SI, Kranenburg O, Borel Rinkes IH, van Rheenen J. Surgical implantation of an abdominal imaging window for intravital microscopy. *Nat Protoc* (2013) 8(3):583–94. doi: 10.1038/nprot.2013.026
8. Park I, Hong S, Hwang Y, Kim P. A Novel Pancreatic Imaging Window for Stabilized Longitudinal In Vivo Observation of Pancreatic Islets in Murine Model. *Diabetes Metab J* (2020) 44(1):193–8. doi: 10.4093/dmj.2018.0268
9. Andersson A, Carlsson PO, Carlsson C, Olsson R, Nordin A, Johansson M, et al. Promoting islet cell function after transplantation. *Cell Biochem Biophys* (2004) 40(3 Suppl):55–64. doi: 10.1385/CBB:40:3:55
10. Korsgren O, Jansson L, Andersson A, Sundler F. Reinnervation of transplanted pancreatic islets. A comparison among islets implanted into the kidney, spleen, and liver. *Transplantation* (1993) 56(1):138–43. doi: 10.1097/00007890-199307000-00026
11. Jansson L, Carlsson PO. Graft vascular function after transplantation of pancreatic islets. *Diabetologia* (2002) 45(6):749–63. doi: 10.1007/s00125-002-0827-4
12. Mazier W, Cota D. Islet Endothelial Cell: Friend and Foe. *Endocrinology* (2017) 158(2):226–8. doi: 10.1210/en.2016-1925
13. van der Windt DJ, Echeverri GJ, Ijzermans JNM, Cooper DKC. The Choice of Anatomical Site for Islet Transplantation. *Cell Transpl* (2008) 17(9):1005–14. doi: 10.3727/096368908786991515
14. Kim HI, Yu JE, Park CG, Kim SJ. Comparison of four pancreatic islet implantation sites. *J Korean Med Sci* (2010) 25(2):203–10. doi: 10.3346/jkms.2010.25.2.203
15. Stokes RA, Cheng K, Lalwani A, Swarbrick MM, Thomas HE, Loudovaris T, et al. Transplantation sites for human and murine islets. *Diabetologia* (2017) 60(10):1961–71. doi: 10.1007/s00125-017-4362-8
16. Nasteska D, Hodson DJ. The role of beta cell heterogeneity in islet function and insulin release. *J Mol Endocrinol* (2018) 61(1):R43–60. doi: 10.1530/JME-18-0011
17. Dooremaal JC. Die Entwickelung der in fremden Grund versetzten lebenden Gewebe. *Albrecht von Græfe's Archiv für Ophthalmol* (1873) 19(3):359–73. doi: 10.1007/BF01693910
18. Taylor D, Seiger A, Freedman R, Olson L, Hoffer B. Electrophysiological analysis reinnervation of transplants in the anterior chamber of the eye by the autonomic ground plexus of the iris. *Proc Natl Acad Sci U S A* (1978) 75 (2):1009–12. doi: 10.1073/pnas.75.2.1009
19. Malmfors T, Furness JB, Campbell GR, Burnstock G. Re-innervation of smooth muscle of the vas deferens transplanted into the anterior chamber of the eye. *J Neurobiol* (1971) 2(3):193–207. doi: 10.1002/neu.480020302
20. Haterius H, Schweizer M, Charipper H. Anterior pituitary. III. Observations on the persistence of hypophyseal transplants in the anterior eye chamber. *Endocrinology* (1935) 19(6):673–81. doi: 10.1210/endo-19-6-673
21. Böck J, Popper H. Über Lebertransplantation in die Vorderkammer des Auges. *Virchows Arch Path Anat* (1937) 299:219–34. doi: 10.1007/BF02084471
22. Benjamin J, Belt E, Krichesky B. Total Prostatectomy in the Rabbit and Intraocular Transplantation of Prostatic Tissue: Anatomic-Surgical Procedure. *J Urol* (1940) 44(1):109–15. doi: 10.1016/S0022-5347(17)71250-5
23. Morris DS, Mc DJ, Mann FC. Intra-ocular transplantation of heterologous tissues. *Cancer Res* (1950) 10(1):36–48.
24. Hultquist GT. The ultrastructure of pancreatic tissue from duct-ligated rats implanted into anterior chamber of rat eyes. *Ups J Med Sci* (1972) 77(1):8–18. doi: 10.1517/03009734000000002
25. Browning H, Resnik P. Homologous and heterologous transplantation of pancreatic tissue in normal and diabetic mice. *Yale J Biol Med* (1951) 24(2):140–52.
26. Adeghate E, Donath T. Morphological findings in long-term pancreatic tissue transplants in the anterior eye chamber of rats. *Pancreas* (1990) 5(3):298–305. doi: 10.1097/00006676-199005000-00009
27. Adeghate E. Host-graft circulation and vascular morphology in pancreatic tissue transplants in rats. *Anat Rec* (1998) 251(4):448–59. doi: 10.1002/(SICI)1097-0185(199808)251:4<448::AID-AR4>3.0.CO;2-O
28. Speier S, Nyqvist D, Cabrera O, Yu J, Molano RD, Pileggi A, et al. Noninvasive in vivo imaging of pancreatic islet cell biology. *Nat Med* (2008) 14(5):574–8. doi: 10.1038/nm1701
29. Yang S-N, Berggren P-O. The eye as a novel imaging site in diabetes research. *Pharmacol Ther* (2019) 197:103–21. doi: 10.1016/j.pharmthera.2019.01.005
30. Speier S, Nyqvist D, Kohler M, Caicedo A, Leibiger IB, Berggren PO. Noninvasive high-resolution in vivo imaging of cell biology in the anterior chamber of the mouse eye. *Nat Protoc* (2008) 3(8):1278–86. doi: 10.1038/nprot.2008.118
31. Almaca J, Molina J, Arrojo EDR, Abdulreda MH, Jeon WB, Berggren PO, et al. Young capillary vessels rejuvenate aged pancreatic islets. *Proc Natl Acad Sci USA*. (2014) 111(49):17612–7. doi: 10.1073/pnas.1414053111
32. Nyqvist D, Speier S, Rodriguez-Diaz R, Molano RD, Lipovsek S, Rupnik M, et al. Donor islet endothelial cells in pancreatic islet revascularization. *Diabetes* (2011) 60(10):2571–7. doi: 10.2337/db10-1711
33. van Krieken PP, Voznesenskaya A, Dicker A, Xiong Y, Park JH, Lee JI, et al. Translational assessment of a genetic engineering methodology to improve islet function for transplantation. *EBioMedicine* (2019) 45:529–41. doi: 10.1016/j.ebiom.2019.06.045
34. Rodriguez-Diaz R, Speier S, Molano RD, Formoso A, Gans I, Abdulreda MH, et al. Noninvasive in vivo model demonstrating the effects of autonomic innervation on pancreatic islet function. *Proc Natl Acad Sci USA* (2012) 109 (52):21456–61. doi: 10.1073/pnas.1211659110

35. Ahren B. Autonomic regulation of islet hormone secretion–implications for health and disease. *Diabetologia* (2000) 43(4):393–410. doi: 10.1007/s001250051322
36. Ilegems E, Dicker A, Speier S, Sharma A, Bahow A, Edlund PK, et al. Reporter islets in the eye reveal the plasticity of the endocrine pancreas. *Proc Natl Acad Sci USA* (2013) 110(51):20581–6. doi: 10.1073/pnas.1313696110
37. Mojibian M, Harder B, Hurlburt A, Bruin JE, Asadi A, Kieffer TJ. Implanted islets in the anterior chamber of the eye are prone to autoimmune attack in a mouse model of diabetes. *Diabetologia* (2013) 56(10):2213–21. doi: 10.1007/s00125-013-3004-z
38. van Krieken PP, Dicker A, Eriksson M, Herrera PL, Ahlgren U, Berggren PO, et al. Kinetics of functional beta cell mass decay in a diphtheria toxin receptor mouse model of diabetes. *Sci Rep* (2017) 7(1):12440. doi: 10.1038/s41598-017-12124-w
39. Ilegems E, van Krieken PP, Edlund PK, Dicker A, Alanentalo T, Eriksson M, et al. Light scattering as an intrinsic indicator for pancreatic islet cell mass and secretion. *Sci Rep* (2015) 5(1):10740. doi: 10.1038/srep10740
40. Li G, Wu B, Ward MG, Chong AC, Mukherjee S, Chen S, et al. Multifunctional in vivo imaging of pancreatic islets during diabetes development. *J Cell Sci* (2016) 129(14):2865–75. doi: 10.1242/jcs.190843
41. Chen C, Chmelova H, Cohrs CM, Chouinard JA, Jahn SR, Stertmann J, et al. Alterations in beta-Cell Calcium Dynamics and Efficacy Outweigh Islet Mass Adaptation in Compensation of Insulin Resistance and Prediabetes Onset. *Diabetes* (2016) 65(9):2676–85. doi: 10.2337/db15-1718
42. Xiong Y, Scerbo MJ, Seelig A, Volta F, O'Brien N, Dicker A, et al. Islet vascularization is regulated by primary endothelial cilia via VEGF-A-dependent signaling. *Elife* (2020) 9:e56914. doi: 10.7554/eLife.56914
43. Berclaz C, Szlag D, Nguyen D, Extermann J, Bouwens A, Marchand PJ, et al. Label-free fast 3D coherent imaging reveals pancreatic islet micro-vascularization and dynamic blood flow. *BioMed Opt Express* (2016) 7(11):4569–80. doi: 10.1364/BOE.7.004569
44. Nord C, Eriksson M, Dicker A, Eriksson A, Grong E, Ilegems E, et al. Biochemical profiling of diabetes disease progression by multivariate vibrational microspectroscopy of the pancreas. *Sci Rep* (2017) 7(1):6646. doi: 10.1038/s41598-017-07015-z
45. Saunders DC, Brissova M, Phillips N, Shrestha S, Walker JT, Aramandla R, et al. Ectonucleoside Triphosphate Diphosphohydrolase-3 Antibody Targets Adult Human Pancreatic beta Cells for In Vitro and In Vivo Analysis. *Cell Metab* (2019) 29(3):745–54.e4. doi: 10.1016/j.cmet.2018.10.007
46. Jacob S, Kohler M, Troster P, Visa M, Garcia-Prieto CF, Alanentalo T, et al. In vivo Ca(2+) dynamics in single pancreatic beta cells. *FASEB J* (2020) 34(1):945–59. doi: 10.1096/fj.201901302RR
47. Salem V, Silva LD, Suba K, Georgiadou E, Neda Mousavy Gharavy S, Akhtar N, et al. Leader beta-cells coordinate Ca(2+) dynamics across pancreatic islets in vivo. *Nat Metab* (2019) 1(6):615–29. doi: 10.1038/s42255-019-0075-2
48. Avall K, Ali Y, Leibiger IB, Leibiger B, Moede T, Paschen M, et al. Apolipoprotein CIII links islet insulin resistance to beta-cell failure in diabetes. *Proc Natl Acad Sci USA* (2015) 112(20):E2611–9. doi: 10.1073/pnas.1423849112
49. Paschen M, Moede T, Valladolid-Acebes I, Leibiger B, Moruzzi N, Jacob S, et al. Diet-induced beta-cell insulin resistance results in reversible loss of functional beta-cell mass. *FASEB J* (2019) 33(1):204–18. doi: 10.1096/fj.201800826R
50. Alcazar O, Hernandez LF, Tschiggfrie A, Muehlbauer MJ, Bain JR, Buchwald P, et al. Feasibility of Localized Metabolomics in the Study of Pancreatic Islets and Diabetes. *Metabolites* (2019) 9(10):207. doi: 10.3390/metabo9100207
51. Alcazar O, Hernandez LF, Nakayasu ES, Piehowski PD, Ansong C, Abdulreda MH, et al. Longitudinal proteomics analysis in the immediate microenvironment of islet allografts during progression of rejection. *J Proteomics* (2020) 223:103826. doi: 10.1016/j.jprot.2020.103826
52. Ceballos GA, Hernandez LF, Paredes D, Betancourt LR, Abdulreda MH. A machine learning approach to predict pancreatic islet grafts rejection versus tolerance. *PloS One* (2020) 15(11):e0241925. doi: 10.1371/journal.pone.0241925
53. Chmelova H, Cohrs CM, Chouinard JA, Petzold C, Kuhn M, Chen C, et al. Distinct roles of beta-cell mass and function during type 1 diabetes onset and remission. *Diabetes* (2015) 64(6):2148–60. doi: 10.2337/db14-1055
54. Berclaz C, Schmidt-Christensen A, Szlag D, Extermann J, Hansen L, Bouwens A, et al. Longitudinal three-dimensional visualisation of autoimmune diabetes by functional optical coherence imaging. *Diabetologia* (2016) 59(3):550–9. doi: 10.1007/s00125-015-3819-x
55. Abdulreda MH, Molano RD, Faleo G, Lopez-Cabezas M, Shishido A, Ulissi U, et al. In vivo imaging of type 1 diabetes immunopathology using eye-transplanted islets in NOD mice. *Diabetologia* (2019) 62(7):1237–50. doi: 10.1007/s00125-019-4879-0
56. Miska J, Abdulreda MH, Devarajan P, Lui JB, Suzuki J, Pileggi A, et al. Real-time immune cell interactions in target tissue during autoimmune-induced damage and graft tolerance. *J Exp Med* (2014) 211(3):441–56. doi: 10.1084/jem.20130785
57. Schmidt-Christensen A, Hansen L, Ilegems E, Fransen-Pettersson N, Dahl U, Gupta S, et al. Imaging dynamics of CD11c(+) cells and Foxp3(+) cells in progressive autoimmune insulitis in the NOD mouse model of type 1 diabetes. *Diabetologia* (2013) 56(12):2669–78. doi: 10.1007/s00125-013-3024-8
58. Abdulreda MH, Faleo G, Molano RD, Lopez-Cabezas M, Molina J, Tan Y, et al. High-resolution, noninvasive longitudinal live imaging of immune responses. *Proc Natl Acad Sci USA* (2011) 108(31):12863–8. doi: 10.1073/pnas.1105002108
59. Hahn M, van Krieken PP, Nord C, Alanentalo T, Morini F, Xiong Y, et al. Topologically selective islet vulnerability and self-sustained downregulation of markers for beta-cell maturity in streptozotocin-induced diabetes. *Commun Biol* (2020) 3(1):541. doi: 10.1038/s42003-020-01243-2
60. Henquin JC, Ravier MA, Nenquin M, Jonas JC, Gilon P. Hierarchy of the beta-cell signals controlling insulin secretion. *Eur J Clin Invest* (2003) 33(9):742–50. doi: 10.1046/j.1365-2362.2003.01207.x
61. Taylor AW. Ocular immune privilege. *Eye (Lond)* (2009) 23(10):1885–9. doi: 10.1038/eye.2008.382
62. Cabrera O, Berman DM, Kenyon NS, Ricordi C, Berggren PO, Caicedo A. The unique cytoarchitecture of human pancreatic islets has implications for islet cell function. *Proc Natl Acad Sci U S A* (2006) 103(7):2334–9. doi: 10.1073/pnas.0510790103
63. Steiner DJ, Kim A, Miller K, Hara M. Pancreatic islet plasticity Interspecies comparison of islet architecture and composition. *Islets* (2010) 2(3):135–45. doi: 10.4161/isl.2.3.11815
64. Rodriguez-Diaz R, Abdulreda MH, Formoso AL, Gans I, Ricordi C, Berggren PO, et al. Innervation patterns of autonomic axons in the human endocrine pancreas. *Cell Metab* (2011) 14(1):45–54. doi: 10.1016/j.cmet.2011.05.008
65. Abdulreda MH, Rodriguez-Diaz R, Caicedo A, Berggren PO. Liraglutide Compromises Pancreatic beta Cell Function in a Humanized Mouse Model. *Cell Metab* (2016) 23(3):541–6. doi: 10.1016/j.cmet.2016.01.009
66. Rodriguez-Diaz R, Molano RD, Weitz JR, Abdulreda MH, Berman DM, Leibiger B, et al. Paracrine Interactions within the Pancreatic Islet Determine the Glycemic Set Point. *Cell Metab* (2018) 27(3):549–58.e4. doi: 10.1016/j.cmet.2018.01.015
67. Fan Y, Zheng X, Ali Y, Berggren PO, Loo SCJ. Local release of rapamycin by microparticles delays islet rejection within the anterior chamber of the eye. *Sci Rep* (2019) 9(1):3918. doi: 10.1038/s41598-019-40404-0
68. Collombat P, Xu X, Heimberg H, Mansouri A. Pancreatic beta-cells: from generation to regeneration. *Semin Cell Dev Biol* (2010) 21(8):838–44. doi: 10.1016/j.semcdb.2010.07.007
69. Wrenshall GA, Andrus SB, Mayer J. High levels of pancreatic insulin coexistent with hyperplasia and degranulation of beta cells in mice with the hereditary obese-hyperglycemic syndrome. *Endocrinology* (1955) 56(3):335–40. doi: 10.1210/endo-56-3-335
70. Parween S, Kostromina E, Nord C, Eriksson M, Lindstrom P, Ahlgren U. Intra-islet lesions and lobular variations in beta-cell mass expansion in ob/ob mice revealed by 3D imaging of intact pancreas. *Sci Rep* (2016) 6:34885. doi: 10.1038/srep34885
71. Dai C, Brissova M, Reinert RB, Nyman L, Liu EH, Thompson C, et al. Pancreatic islet vasculature adapts to insulin resistance through dilation and not angiogenesis. *Diabetes* (2013) 62(12):4144–53. doi: 10.2337/db12-1657
72. Yamaizumi M, Mekada E, Uchida T, Okada Y. One molecule of diphtheria toxin fragment A introduced into a cell can kill the cell. *Cell* (1978) 15(1):245–50. doi: 10.1016/0092-8674(78)90099-5

73. Rosario W, Singh I, Wautlet A, Patterson C, Flak J, Becker TC, et al. The Brain-to-Pancreatic Islet Neuronal Map Reveals Differential Glucose Regulation From Distinct Hypothalamic Regions. *Diabetes* (2016) 65 (9):2711–23. doi: 10.2337/db15-0629
74. Asare-Bediako I, Paszkiewicz RL, Kim SP, Woolcott OO, Kolka CM, Burch MA, et al. Variability of Directly Measured First-Pass Hepatic Insulin Extraction and Its Association With Insulin Sensitivity and Plasma Insulin. *Diabetes* (2018) 67(8):1495–503. doi: 10.2337/db17-1520
75. Kryshak EJ, Butler PC, Marsh C, Miller A, Barr D, Polonsky K, et al. Pattern of postprandial carbohydrate metabolism and effects of portal and peripheral insulin delivery. *Diabetes* (1990) 39(2):142–8. doi: 10.2337/diabetes.39.2.142
76. Najjar SM, Perdomo G. Hepatic Insulin Clearance: Mechanism and Physiology. *Physiol (Bethesda)* (2019) 34(3):198–215. doi: 10.1152/physiol.00048.2018
77. Polonsky KS, Given BD, Hirsch L, Shapiro ET, Tillil H, Beebe C, et al. Quantitative study of insulin secretion and clearance in normal and obese subjects. *J Clin Invest* (1988) 81(2):435–41. doi: 10.1172/JCI113338
78. Barton FB, Rickels MR, Alejandro R, Hering BJ, Wease S, Naziruddin B, et al. Improvement in outcomes of clinical islet transplantation: 1999-2010. *Diabetes Care* (2012) 35(7):1436–45. doi: 10.2337/dc12-0063
79. Kato I, Suzuki Y, Akabane A, Yonekura H, Tanaka O, Kondo H, et al. Enhancement of glucose-induced insulin secretion in transgenic mice overexpressing human VIP gene in pancreatic beta cells. *Ann N Y Acad Sci* (1996) 805(1):232–42; discussion 42-3. doi: 10.1111/j.1749-6632.1996.tb17486.x
80. Staels W, De Groef S, Heremans Y, Coppens V, Van Gassen N, Leuckx G, et al. Accessory cells for beta-cell transplantation. *Diabetes Obes Metab* (2016) 18 (2):115–24. doi: 10.1111/dom.12556
81. Kroon E, Martinson LA, Kadoya K, Bang AG, Kelly OG, Eliazer S, et al. Pancreatic endoderm derived from human embryonic stem cells generates glucose-responsive insulin-secreting cells in vivo. *Nat Biotechnol* (2008) 26 (4):443–52. doi: 10.1038/nbt1393
82. Pagliuca FW, Millman JR, Gurtler M, Segel M, Van Dervort A, Ryu JH, et al. Generation of functional human pancreatic beta cells in vitro. *Cell* (2014) 159 (2):428–39. doi: 10.1016/j.cell.2014.09.040
83. Millman JR, Xie C, Van Dervort A, Gurtler M, Pagliuca FW, Melton DA. Generation of stem cell-derived beta-cells from patients with type 1 diabetes. *Nat Commun* (2016) 7:11463. doi: 10.1038/ncomms11463

Conflict of Interest: P-OB is founder and CEO of Biocrine AB. EI is consultant for Biocrine AB.

frontiers in Endocrinology

MINI REVIEW
published: 26 April 2021
doi: 10.3389/fendo.2021.644826

Pancreas Optical Clearing and 3-D Microscopy in Health and Diabetes

Martha Campbell-Thompson[1*] *and Shiue-Cheng Tang*[2*]

[1] Department of Pathology, Immunology and Laboratory Medicine, College of Medicine, University of Florida, Gainesville, FL, United States, [2] Department of Medical Science and Institute of Biotechnology, National Tsing Hua University, Hsinchu, Taiwan

Although first described over a hundred years ago, tissue optical clearing is undergoing renewed interest due to numerous advances in optical clearing methods, microscopy systems, and three-dimensional (3-D) image analysis programs. These advances are advantageous for intact mouse tissues or pieces of human tissues because samples sized several millimeters can be studied. Optical clearing methods are particularly useful for studies of the neuroanatomy of the central and peripheral nervous systems and tissue vasculature or lymphatic system. Using examples from solvent- and aqueous-based optical clearing methods, the mouse and human pancreatic structures and networks will be reviewed in 3-D for neuro-insular complexes, parasympathetic ganglia, and adipocyte infiltration as well as lymphatics in diabetes. Optical clearing with multiplex immunofluorescence microscopy provides new opportunities to examine the role of the nervous and circulatory systems in pancreatic and islet functions by defining their neurovascular anatomy in health and diabetes.

Keywords: islet, autonomic (vegetative) nervous system, lightsheet microscopy, CLARITY, adipocyte, Schwann cell, confocal 3-D microscopy, organoid

OPEN ACCESS

Edited by:
Vincent Poitout, Université de Montréal, Canada

Reviewed by:
Holger Andreas Russ, University of Colorado Anschutz Medical Campus, United States
Senta Georgia, Children's Hospital of Los Angeles, United States
Rebecca Hull, University of Washington, United States

***Correspondence:**
Martha Campbell-Thompson
mct@ufl.edu
Shiue-Cheng Tang
sctang@life.nthu.edu.tw

Specialty section:
This article was submitted to Diabetes: Molecular Mechanisms, a section of the journal Frontiers in Endocrinology

Received: *21 December 2020*
Accepted: *08 April 2021*
Published: *26 April 2021*

Citation:
Campbell-Thompson M and Tang S-C (2021) Pancreas Optical Clearing and 3-D Microscopy in Health and Diabetes. Front. Endocrinol. 12:644826. doi: 10.3389/fendo.2021.644826

INTRODUCTION

Goals

Heterogeneity of the human pancreas is well accepted in terms of islet endocrine cell proportions and mass in healthy people and for lobularity in islet beta-cell losses and frequency of infiltrated islets in patients in type 1 diabetes (T1D) (1–7). Patients with type 2 diabetes (T2D) show similar heterogeneity in islet amyloidosis, fatty infiltration, fibrosis and inflammatory infiltrates (4, 8–10). Morphology-based studies of the human pancreas have been key to understanding regional heterogeneity yet examinations of the pancreas in its natural three-dimensional (3-D) configuration have been limited to laborious serial sectioning with subsequent reconstruction. Islets occupy only ~2% of the entire pancreas volume and sampling of multiple blocks is recommended to maximize islet analyzes by 2-D microscopy (11). Recent applications of optical clearing methods to the human and mouse pancreas provide new details for structure-function relationships in health and subsequent abnormalities in diabetes (12–15). This review provides an overview of recent optical clearing methods used in human and mouse pancreas studies and examples of pancreas optical clearing to define several components of the pancreas endocrine and exocrine compartments.

TECHNIQUES

Although basic optical clearing to render tissues transparent was first described by the German anatomist Walter Spalteholz over 100 years ago, the recent decade has seen a rapid growth in advanced clearing methods applicable for whole body or organ imaging to single cell resolution (16, 17). Optical clearing is readily accomplished in a standard laboratory and new procedures can be found nearly weekly in the literature for different organs and species (**Table 1**). Optical clearing methods are based on obtaining a high degree of tissue transparency and matching of the sample refractive index (RI) to that of the imaging media to remove light scattering (54). Most tissues are comprised of ~80% water (RI=1.33), 10% proteins (RI>1.44), and 10% lipids (RI>1.45) (55). Methods are broadly based on physical or chemical strategies with organic solvents or aqueous solutions used for the latter. Several excellent reviews are available that detail each optical clearing method advantages and disadvantages (45, 56–59). Early optical clearing methods used organic chemicals [e.g., benzyl alcohol–methyl salicylate, benzyl alcohol–benzyl benzoate (BABB), and solvents used in 3-D imaging of solvent-cleared organs (3DISCO)] (27). Generally these methods achieve high transparency within a few days by removing lipids and homogenizing refractive indices (RIs) of the samples, and they are compatible with whole-mount immunolabeling (48, 60). Solvent based clearing methods may use toxic chemicals and steps should be performed using a fume hood and suitable personal protective equipment. Recent methods have been named with acronyms such as immunolabeling-enabled imaging of solvent-cleared organs (iDISCO) (60), clear, unobstructed brain/body imaging cocktails and computational analysis (CUBIC) (17, 27, 61, 62), clear lipid-exchanged acrylamide-hybridized rigid imaging/immunostaining/*in situ* hybridization-compatible tissue hydrogel (CLARITY), and passive CLARITY technique (PACT) (38, 63–65).

The original CLARITY manuscript by Chung et al. (65) described four key steps: (1) hydrogel tissue embedding using a ratio of 4% acrylamide monomer to 0.05% bis-acrylamide followed by polymerization; (2) clearing secondary to lipid removal using 4% sodium dodecyl sulfate (SDS) detergent buffer within a custom built electrophoretic tissue clearing system (ETC); (3) immunostaining; and (4) tissue RI matching and imaging. Several modifications were subsequently published in favor of "passive clearing" without the use of ETC to avoid oxidative tissue artifacts with several variations in the amount of paraformaldehyde (0-4%), acrylamide monomer (1-4%) and bis-acrylamide in the hydrogel mixture depending on target organ (63, 66, 67).

Despite their differences in chemical and/or optical properties, the organic solvent, aqueous reagent, and electrophoresis-assisted clearing methods all extend our view of neurovascular networks (>>100 μm) with 3-D microscopy compared with the images acquired from classic IHC and H&E histology (3-5 μm in thickness). To apply tissue clearing, the key question is whether a specific clearing technique changes the sample chemical and/or cellular environment that causes artifacts in signal detection. For example, in CLARITY, the use of sodium dodecyl sulfate (SDS) treatment and electrophoresis to remove cellular membranes is likely to disturb membrane receptor proteins. Thus, studies of the nerve-receptor association in space will be better accepted if a passive aqueous-based clearing method (e.g., sugar reagent) is employed compared with CLARITY. Likewise, leukocytes and their vascular receptor association in space will be better examined in an aqueous environment, because disturbing the membranes for 3-D imaging may create false negative results in signal detection. However, we need to stress that the false negative result may also come from scattering in deep-tissue imaging. Thus, adding a positive control in the specimen (e.g., nuclear staining) can help investigators monitor the resolving power (e.g., resolving two adjacent nuclei in an islet) across the optical depth in deep-tissue pancreatic and islet imaging.

Volumetric microscopy has also paralleled optical clearing methods with advancements in confocal, multiphoton and lightsheet microscopes. Advantages of the lightsheet microscopes are faster scanning speeds, reduced photobleaching, and good resolution at high tissue penetration depths. When access to lightsheet microscopes is not feasible, confocal microscopy provides an excellent alternative with single-cell resolution. While any type of fluorescent microscope can be used to image optically-cleared tissue, the microscope imaging chamber must be able to accommodate the size of the sample and the stage configuration and imaging depth are dependent on the working distance of the objective. Most images can be obtained with regular air objectives between ×2 and ×20 magnifications. Specialized objectives for optically cleared samples over larger distances are available from multiple vendors such as Olympus and Zeiss. Users of optical clearing methods and advanced microscopy need also consider data storage requirements for both image acquisition and analysis. Additional storage space for the imaging microscope is required as well as additional memory and processing speed for image analysis workstations. The opensource software Fiji/ImageJ can be used for 2-D stitching and basic 3-D adjustments (68). Zeiss Zen software will also provide stitching and maximum intensity projections. Commercial software packages are available for advanced 3-D volume rendering and reconstruction such as Neurolucida360/Vesselucida (MBF), Arivis (FEI), and Imaris (Bitplane, Concord MA). Consideration of sample size and existing microscopes and image analysis software may thus dictate which optical clearing method is most suitable for a given laboratory. For those without sufficient local resources, the growing popularity of optical clearing methods generated several commercial sources services for clearing, microscopy, and analysis services (Visikol, ClearLight, LifeCanvas).

CHALLENGES

Challenges related to optical clearing are relatively few. Acquisition of high-quality samples is important as for any down-stream application based on fixed samples. Fixation with 4% paraformaldehyde or 10% formalin is commonly employed in many laboratories. Cardiac perfusion is recommended for rodent studies in most part to remove red blood cells and their

TABLE 1 | Optical clearing references in human and mouse pancreas.

Species	First Author	Year	Journal	Title	Method	Reference
Mouse	Kim	2010	JoVE	In situ quantification of pancreatic beta-cell mass in mice	Sucrose	(18)
Mouse	Fu	2010	Gastroenterology	At the movies: 3-dimensional technology and gastrointestinal histology	FocusClear	(19)
Mouse	Fu	2010	Journal of Biomedical Optics	Three-dimensional optical method for integrated visualization of mouse islet microstructure and vascular network with subcellular-level resolution	FocusClear	(20)
Rat	Li	2010	J Cell Science	Activation of pancreatic-duct-derived progenitor cells during pancreas regeneration in adult rats	BABB	(21)
Mouse	Chiu	2012	Diabetologia	3-D imaging and illustration of the perfusive mouse islet sympathetic innervation and its remodeling in injury	FocusClear	(22)
Mouse	Tang	2013	Diabetologia	Plasticity of Schwann cells and pericytes in response to islet injury in mice	FocusClear	(23)
Mouse	Juang	2014	AJP	Three-dimensional islet graft histology: panoramic imaging of neural plasticity in sympathetic reinnervation of transplanted islets under the kidney capsule	FocusClear	(24)
Mouse	Tang	2014	Diabetes, Obesity and Metabolism	Imaging of the islet neural network	FocusClear	(25)
Mouse	Lee	2014	BMC Developmental Biology	Improved application of the electrophoretic tissue clearing technology, CLARITY, to intact solid organs including brain, pancreas, liver, kidney, lung, and intestine	CLARITY	(26)
Mouse	Susako	2015	Nature Protocols	Advanced CUBIC protocols for whole-brain and whole-body clearing and imaging	CUBIC	(27)
Mouse	Juang	2015	EBioMedicine	3-D imaging reveals participation of donor islet Schwann cells and pericytes in islet transplantation and graft neurovascular regeneration	FocusClear/ RapiClear	(28)
Human	Treweek	2015	Nature Protocols	Whole-body tissue stabilization and selective extractions *via* tissue-hydrogel hybrids for high-resolution intact circuit mapping and phenotyping	PACT	(29)
Mouse	Chien	2016	International Journal of Obesity	3-D imaging of islets in obesity: formation of the islet-duct complex and neurovascular remodeling in young hyperphagic mice	RapiClear	(30)
Mouse	Lin	2016	AJP	PanIN-associated pericyte, glial, and islet remodeling in mice revealed by 3-D pancreatic duct lesion histology	RapiClear	(31)
Mouse	Simon	2017	J Autoimmunity	Inhibition of effector antigen-specific T cells by intradermal administration of heme oxygenase-1 inducers	3DISCO	(32)
Mouse	Vlahos	2017	PNAS	Modular tissue engineering for the vascularization of subcutaneously transplanted pancreatic islets	CLARITY	(33)
Mouse	Wong	2017	Current Protocols Cell Biology	Simple and Rapid Tissue Clearing Method for Three-Dimensional Histology of the Pancreas	CLARITY	(34)
Mouse	Yamamoto	2017	Nat Comm	Neuronal signals regulate obesity induced β-cell proliferation by FoxM1 dependent mechanism	CUBIC	(35)
Mouse	Pauerstein	2017	Development	A radial axis defined by semaphorin-to-neuropilin signaling controls pancreatic islet morphogenesis	CLARITY	(36)
Mouse	Chen	2017	Scientific Reports	UbasM: An effective balanced optical clearing method for intact biomedical imaging	UbasM	(37)
Mouse, Human	Hsueh	2017	Nature Protocols	Pathways to clinical CLARITY	CLARITY	(38)
Mouse	Tang	2018	Diabetologia	Pancreatic neuro-insular network in young mice revealed by 3-D panoramic histology	RapiClear	(39)
Mouse	Nishimura	2018	Islets	Optical clearing of the pancreas for visualization of mature b-cells and vessels in mice	Sca/eS	(40)
Human	Noë	2018	American Journal of Pathology	Immunolabeling of Cleared Human Pancreata Provides Insights into Three-Dimensional Pancreatic Anatomy and Pathology	iDISCO	(41)
Human	Tang	2018	Diabetologia	Human pancreatic neuro-insular network in health and fatty infiltration	RapiClear	(42)
Human	Tang	2018	Current Diabetes Reports	The role of accessory cells in islet homeostasis	RapiClear, PACT	(14)
Human	Fowler	2018	Endocrinology	Three-Dimensional Analysis of the Human Pancreas	T3	(43)
Human	Butterworth	2018	JoVE	High resolution 3D imaging of the Human Pancreas Neuro-insular network	PACT	(15)
Human, Mouse	Shen	2019	EBioMedicine	Lymphatic vessel remodeling and invasion in pancreatic cancer progression	RapiClear	(44)
Human	Chien	2019	AJP	Human pancreatic afferent and efferent nerves: mapping and 3-D illustration of exocrine, endocrine, and adipose innervation	RapiClear	(13)
Human	Dybala	2019	Diabetes	Heterogeneity Human Pancreatic Islet	T3	(2)
Human	Hong	2019	Advances in Anatomic Pathology	A "Clearer" View of Pancreatic Pathology: A Review of Tissue Clearing and Advanced Microscopy Techniques	iDISCO	(45)
Mouse	Tokumoto	2020	Diabetes	Generation and Characterization of a Novel Mouse Model That Allows Spatiotemporal Quantification of Pancreatic β-Cell Proliferation	CUBIC	(46)
Mouse	Hahn	2020	Communications Biology	Topologically selective islet vulnerability and self-sustained downregulation of markers for β-cell maturity in streptozotocin-induced diabetes	BABB	(47)
Mouse	Maldonado	2020	Stem Cells Tissue Repair	Painting the Pancreas in Three Dimensions: Whole-Mount Immunofluorescence Method	BABB	(48)

(Continued)

TABLE 1 | Continued

Species	First Author	Year	Journal	Title	Method	Reference
(49) Human, Mouse	Alvarsson	2020	Science Advances	3D atlas of the dynamic and regional variation of pancreatic innervation in diabetes	iDISCO (modified), ECi	(12)
Human	Hong	2020	Mod Pathology	Three-dimensional visualization of cleared human pancreas cancer reveals that sustained epithelial-to-mesenchymal transition is not required for venous invasion	iDISCO	(50)
Human	Heuckeroth	2020	Gastroenterology	Robust, 3-Dimensional Visualization of Human Colon Enteric Nervous System Without Tissue Sectioning	BABB	(51)
Mouse, Human	Chen	2021	EMBO	Decreased blood vessel density and endothelial cell subset dynamics during ageing of the endocrine system	PEGASOS	(52)
Human	Campbell-Thompson	2021	Scientific Reports	Islet Sympathetic Innervation and Islet Neuropathology in Patients with Type 1 Diabetes	iDISCO, PACT	(53)

inherent high autofluorescence. However, immersion fixation is a reasonable alternative for rodents and the only method available for human biosamples. As for traditional immunolocalization, the duration of fixation is ideally kept to a minimum to avoid over-fixation of tissue antigens. Many primary antibodies utilized for formalin-fixed paraffin embedded samples work well for optical clearing and those tested in our laboratory are provided as a reference (**Table 2**). A pre-testing step is advised for new primary antibodies and can be accomplished with fixed frozen thick sections (40μm) utilizing similar conditions as those for

TABLE 2 | Primary antibodies for optical clearing.

Antigen	Cell type	Host	Vendor	Cat. #	Dilution	Comments
Endocrine Markers						
Glucagon	Alpha-cells	Mouse	BD Biosciences	565891	1:50	Worked
Glucagon	Alpha-cells	Rabbit	Cell Signaling	2760S	1:200	Did not work
Glucagon	Alpha-cells	Mouse	Abcam	ab10988	1:200	Worked
Insulin	Beta-cells	Guinea Pig	DAKO	A0564	1:200	Worked
Secretogranin 3	Neuroendocrine cells	Rabbit	Sigma	HPA006880	1:200	Worked
Somatostatin	Delta-cells	Goat	Santa Cruz	sc-7819	1:500	Worked
Neural Markers						
GFAP	Glial cells	Rabbit	DAKO	Z0334	1:200	Worked
NCAM (CD56)	Pan-neural	Mouse	DAKO	M730429-2 (also FITC-conjugate)	1:50	Did not work (both)
Peripherin	Pan-neural	Rabbit	EnCor	RPCA-Peri	1:200	Worked
PGP9.5/UCHL1	Pan-neural	Rabbit	DAKO	Z5116	1:50	Did not work
PGP9.5/UCHL1	Pan-neural	Chicken	EnCor	CPCA-UCHL1	1:100	Worked
PGP9.5/UCHL1	Pan-neural	Rabbit	Abcam	ab108986	1:200	Worked
β-Tubulin	Pan-neural	Mouse	EnCor	MCA-4E4	1:100	Worked
Substance P	Sensory nerves	Rat	BioRad	8450-0505	1:200	Worked
Tyrosine Hydroxylase	Sympathetic neurons	Rabbit	Millipore	AB152	1:200	Worked
Tyrosine Hydroxylase	Sympathetic neurons	Chicken	Abcam	Ab76442	1:50	Worked, weak staining
Vasoactive Intestinal Peptide	Autonomic neurons	Rabbit	Immunostar	20077	1:200	Worked
Vesicular acetylcholine transporter	Cholinergic neurons	Rabbit	Synaptic Systems	139103	1:200	Worked
Vascular Markers						
CD31 (PECAM)	Endothelial cells	Rabbit	Abcam	Ab28364	1:30	Worked
CD31 (PECAM)	Endothelial cells	Mouse	ThermoFisher	MS-353-S1	1:50	Worked, weak staining
CD34	Endothelial cells	Mouse	ThermoFisher	MA1-10202	1:50	Did not work
Collagen IV	Basal lamina (blood vessels)	Mouse	Abcam	ab6311	1:200	Did not work
Collagen IV	Basal lamina (blood vessels)	Rabbit	Abcam	ab6586	1:200	Worked
Smooth muscle actin	Smooth muscle (arteries)	Mouse	Sigma	A5228; C6198 (Cy5)	1:200; 1:200	Worked; Conjugated better

Primary antibodies tested for immunolocalization in human pancreas samples cleared by passive CLARITY (PACT) are shown by major headings for endocrine markers, neural markers, and vasculature. Comments include whether successful immunostaining was achieved. These antibodies are expected to work using similar clearing methods and may also work in other species as indicated by the vendor or literature.

permeabilization before immunostaining and optical clearing. Wide applicability of primary antibodies remains an issue, particularly for immune markers. While some methods have successfully employed preconjugated primary antibodies (43), the majority of optical clearing methods employ standard rounds of primary antibodies followed by secondary antibodies to promote antibody penetration. A reported benefit of CLARITY was the ability to reiteratively strip antibodies and reprobe a sample several times (65). In practice, we have been unsuccessful in fully stripping samples from human pancreas cleared using CLARITY and also found limited antigenicity and/or diffusion of subsequent primary antibodies (Campbell-Thompson, unpublished results). As such, our more recent studies employ single clearing methods with multiplex immunostaining on 500μm sections rather than several mm sized pieces to extend use of a given sample, particularly those from rare organ donors with diabetes.

Equipment utilized in optical clearing is generally found in any modern molecular pathology laboratory and include access to fume hoods, refrigeration or ovens, rocker plates, and other ancillary small equipment for immunostaining and clearing steps. Microscope and image analysis software are two aspects to be considered before conducting clearing studies as this will influence sample size and numbers of channels for multiplex staining and analysis. As costs for multiphoton and lightsheet microscopes decrease, access to these microscopes will increase whether through institutional shared resources, subcontract, or collaboration. Image analysis expertise is also limited and laboratory staff become proficient in the software available to them. Expense of commercial 3-D software analysis programs is high. Finally, the greatest hurdle may be the large image file sizes achieved by these methods. Here too, limiting the number of antigens needs to be balanced with the rarity of the sample since reiterative staining is difficult.

OPTICAL CLEARING EXAMPLES

This introduction on optical clearing and imaging provides a basic starting point for studies on human and mouse pancreas in health and diabetes. We will now show examples of application of different clearing methods to demonstrate the versatility of optical clearing in human and mouse pancreas for determination of normal states and changes found with diabetes.

SAMPLE PROCESSING

Human pancreata not suitable for clinical purposes were collected from nondiabetic, brain-dead organ donors after written informed consent from legal representative or next of kin and were processed by the Network for Pancreatic Organ donors with Diabetes (nPOD) program at the University of Florida (UF) Diabetes Institute using methods previously reported (69). The nPOD samples used in this specific study were approved as nonhuman by the UF IRB (IRB201902530). Collection and use of human pancreatectomy specimens were approved by the Institutional Review Board of National Taiwan University Hospital (201703131RIND). All UF animal studies were conducted using published guidelines and regulations of the National Institutes of Health for the care and use of laboratory animals. The protocol was approved by the UF Institutional Animal Care and Use Committee (IACUC 202009976). All animal studies conducted at the National Tsing Hua University were reviewed and approved by the institutional animal use review board.

Pancreatic Islet Schwann Cells

Passive CLARITY (PACT) provides for good tissue transparency and multiplex immunolabeling is quite feasible with image analysis such as using the open software Neurite tracer program in ImageJ (**Figure 1**) (15). Schwann cells are the peripheral counterpart to central nervous system oligodendrocytes and provide support to both myelinated and unmyelinated axons of motor and sensory neurons (70, 71). In addition to providing physical support, nonmyelinating Schwann cells are essential for maintenance and regeneration of damaged axons by production of neurotrophins and acting as "first responders" to injury (72, 73). Unlike the dense mesh-like network formed by islet Schwann cells in mouse islets, Schwann cells provide support for autonomic

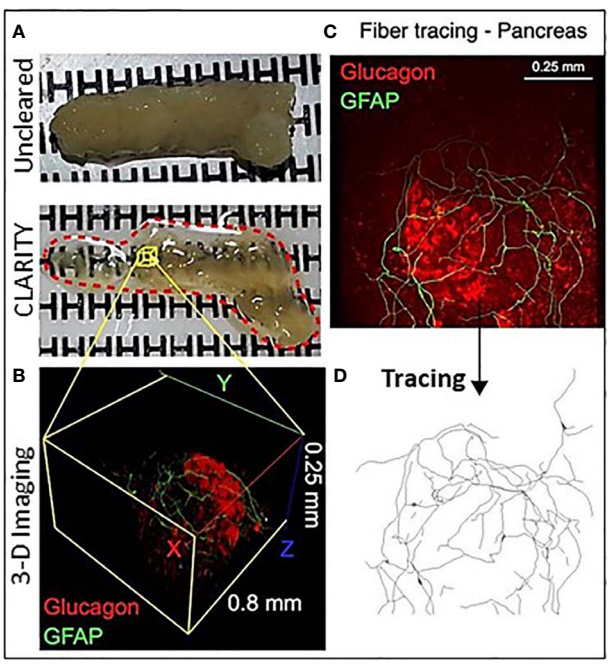

FIGURE 1 | Optical clearing of human pancreas by PACT and iDISCO. **(A)** Fixed pancreas sample from a control donor before and after clearing using passive CLARITY (PACT) showing the degree of sample transparency achieved with this method. **(B)** Representative example of 2-photon imaging for a 0.8 mm x 0.8 mm x 0.25 mm region (X, Y, Z axes) containing an islet immunostained for glucagon (red) and glial fibrillary acidic protein (GFAP, green). **(C)** GFAP-stained Schwann cells overlay an islet and cell projects were analyzed using the ImageJ neurite tracer program. **(D)** The traced Schwann cells are shown by Neurite tracer skeleton diagram.

nerves in human islets in a loose formation (**Figure 2**) (70). Schwann cells are also of particular interest in T1D as they have a role in antigen presentation, interact with the complement system, and secrete factors involved in immune interactions (74, 75) and animal studies report reactive Schwann cells in diabetes and islet injury (23, 76–78). Furthermore, glial fibrillary acidic protein (GFAP) is expressed in peri-islet Schwann cells and is reported to be an autoantigen for T1D with potential use as a biomarker (79).

Pancreatic Ganglia and Neuroinsular Complexes

Intrapancreatic ganglia represent the post-ganglionic neurons of the parasympathetic efferent network (80). They are widely distributed and in relatively low density throughout the human and rodent pancreas and thus optical clearing and 3-D imaging provides a greater opportunity to detect these ganglia (13). At low magnifications, interconnections of intrapancreatic ganglia and to islets are visualized in a human pancreas cleared using

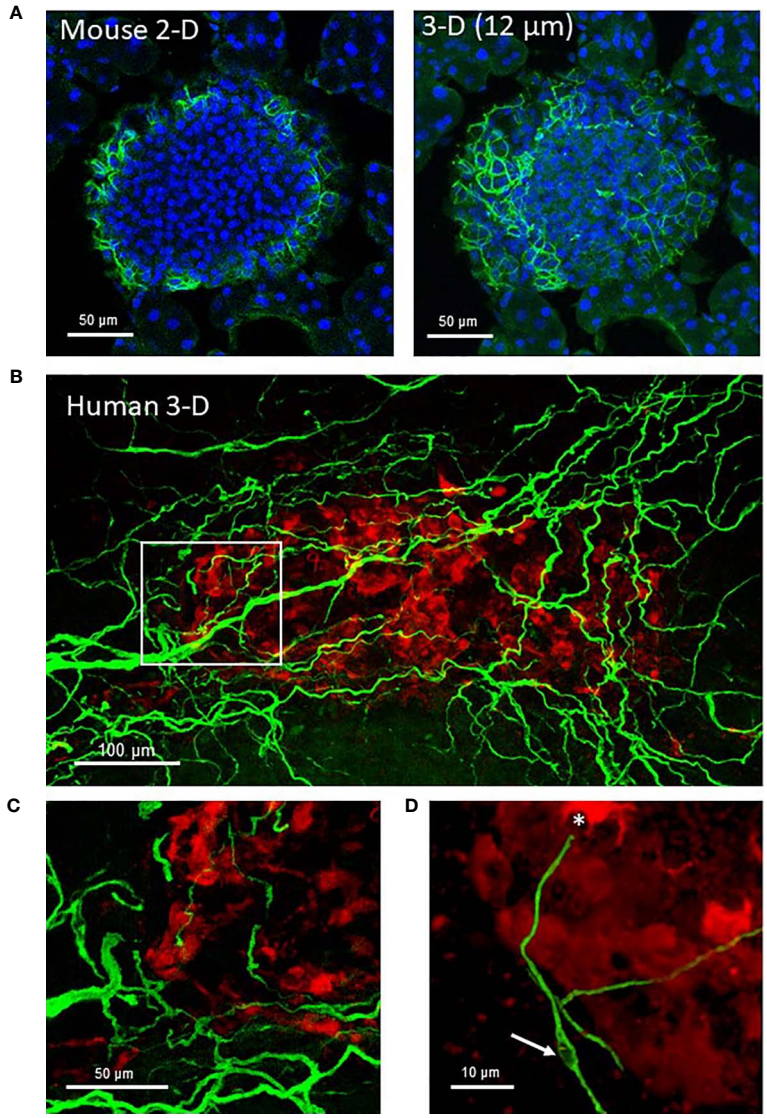

FIGURE 2 | Mouse and human islet Schwann cells. **(A)** A fixed frozen section (40µm) from a C57BL/6 mouse pancreas was stained for GFAP (green) using whole mount staining. A single 2-D slice (7th of 13 slices) and the 3-D maximum intensity projection (MIP, 12 µm stack) are shown to demonstrate the increase in cellular information obtained with a z-stack. **(B)** A human control pancreas sample (~1 mm^3) was cleared by iDISCO and immunolabeling with glucagon (red) and GFAP (green) before confocal 3-D imaging (maximum intensity projection 50 µm). **(C)** The region identified by white box in **(A)** shows Schwann cells at the periphery of the islet that extended along nerves to islet interiors traveling along afferent vessels. **(D)** A single Schwann cell shows a clear nuclear region (white arrow) and numerous extensions with a termination at an alpha-cell (asterisk). See also **Supplementary Video 1** for **(A)**.

PACT (15) (**Figures 3A, B**). Such interconnections likely contribute to the synchronization of islet hormone secretions particularly during the cephalic phase of digestion (81). The intrapancreatic ganglia vary in numbers of neurons and also observed are small clusters of neurons (**Figure 3C**) or small clusters of neurons with islet β-cells and α-cells can also be observed, so-called neuroinsular complex type II (**Figure 3D**) (82). These type II structures have not been previously reported in adult human pancreas and were found only in fetal pancreas. The lack of detection in adults could be due to limitations of 2-D microscopy in finding small structures compared to 3-D microscopy as demonstrated here (83).

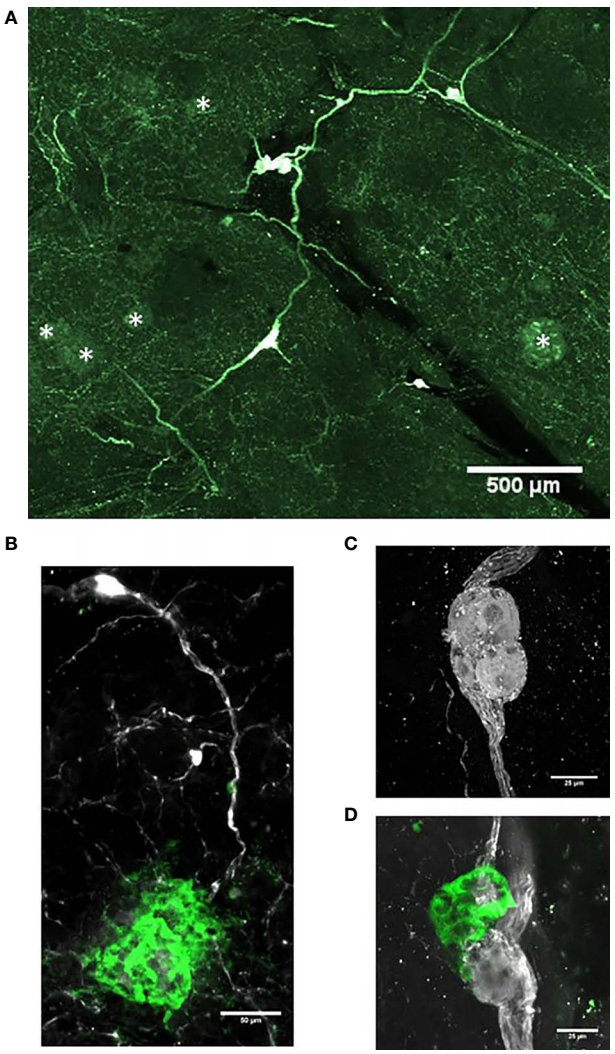

FIGURE 3 | Intrapancreatic ganglia and neuroinsular complexes in adult human pancreas. Pancreas samples were studied in control donors using passive CLARITY (PACT) and immunostaining with primary antibodies for PGP9.5 (white) and GFAP (green) to delineate nerve fibers and supporting Schwann cells, respectively (**Table 2**). PGP9.5 also stained islet endocrine cells although with much less intensity (asterisks). Intrapancreatic ganglia represent post-ganglionic neurons and fibers of the parasympathetic efferent system and 3-D imaging shows how ganglia are interconnected **(A)** and also extend to islets **(B)**. **(C)** Intrapancreatic ganglia contained varying numbers of neurons and small collections of neurons were also found widely scattered with efferent and afferent axons in both interlobular and intralobular regions. **(D)** Imaging for PGP9.5 and islet alpha-cells (GCG, green) demonstrate close association of clustered alpha-cells with neurons at a small ganglion, also known as a neuro-insular complex II. Scale bars: 500µm **(A)**, 50µm **(B)**, 25 µm **(C, D)**. See also **Supplementary Video 2** for **(D)**.

Pancreatic Vasculature

The pancreatic vasculature in health and diabetes has been studied with newer studies showing detection of the Sars-CoV-2 receptor, ACE2, in pancreatic micovasculature, rather than islet endocrine cells, adding additional importance to understanding factors regulating islet blood flow in health and diabetes (84–87). The use of optical clearing provides an unprecedented opportunity to better examine structural-functional relationships of the islet microvasculature in the context of islet heterogeneity and inter-relationship to the surrounding acinar cells. Studies performed in rodents can be achieved by perfusion with fluorescent compounds including lectins or conjugated primary antibodies such as CD31. For human samples, the vasculature can be readily labeled using CD31 or CD34 followed by multiplex immunofluorescence with islet endocrine cell markers and the high vascular density can be appreciated throughout 3-D microscopy (**Figure 4**) (53).

Pancreatic Acinar Ductal Metaplasia

Pancreatic cancer is one of the deadliest tumors and seminal studies showed that early lesions likely arise from acinar-ductal metaplasia forming so-called pancreatic intraductal neoplasia (PanIN) (88). Optical clearing studies in human and mice have shown characteristics of ductal lesions through 3-D imaging (31, 50). Cell culture models of human pancreatic cancer can also benefit from use of optical clearing and 3-D microscopy. Single cell details are apparent in an *in vitro* human primary acinar culture model showing duct formation following optical clearing using HISTO-M, a commercial product similar to iDISCO clearing (**Figure 5**) (Visikol) (T. Schmittgen, personal communication) (89).

Pancreatic Fatty Infiltration

Unlike the fatty liver, in which lipid droplets accumulate in the cytoplasm in the hepatocytes, pancreatic fatty infiltration involves the fat cells (adipocytes) ectopically developing and accumulating in and around the pancreatic lobules alongside the exocrine and endocrine tissues. The fat content in the pancreas increases with age (90) and is detectable as early as in adolescence (91), and the degree is linked with obesity (92–94). In the progression from obesity to type 2 diabetes, the state of hyperinsulinemia is likely to accelerate the pancreatic fat accumulation due to the organ's high insulin concentration. Insulin is a potent factor to induce adipogenesis, in which preadipocytes (e.g., fibroblasts and myofibroblasts in the pancreatic stroma) differentiate into adipocytes (95, 96), and stimulate the proliferation of adipocytes (97). Thus, it is not surprising that multiple studies documented the correlation between type 2 diabetes and pancreatic fats and implicated the negative influence of these fats on the islet microenvironment and function (98–100).

Clinically, magnetic resonance imaging (MRI) and computed tomography (CT) are the preferred imaging modalities to detect

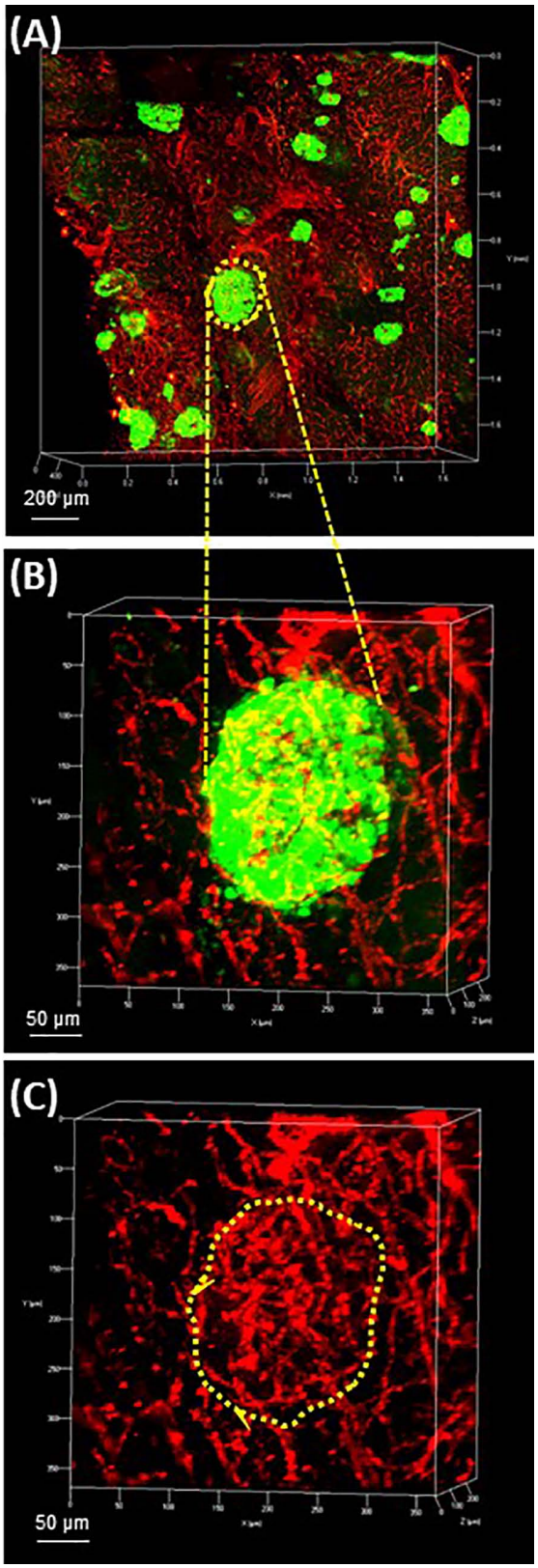

FIGURE 4 | Continued

FIGURE 4 | Human pancreas vasculature. 3-D extended projection of human pancreas exocrine and endocrine vasculature are shown with X, Y and Z axes in mm (Scale bar 200 µm). **(A)** The extensive nature of the human pancreas vascular system is demonstrated by immunolabeling with monoclonal anti-CD31 (red) and islets are shown stained with monoclonal anti-glucagon (green) antibodies. **(B)** An islet identified by yellow-dotted line in **(A)** is shown at higher resolution in **(B)** (Scale bar 50 µm). **(C)** The islet microvasculature is shown without the glucagon overlay (Scale bar 50 µm). See also **Supplementary Video 3** for **(A–C)**.

and quantify the pancreatic fats (90–92, 94, 98–102). While these two methods provide valuable *in vivo* information for cross-sectional or longitudinal studies, they cannot resolve the cellular structures of fats and the pancreatic exocrine and endocrine tissues. At the cellular level, the classic microtome-based histology with H&E staining can identify the adipocytes and their association with blood vessels, acini, ducts, and islets with µm-level resolution. However, due to the hydrophobicity of fats and their weak mechanical connection with the pancreatic lobules, both microtome slicing and dewaxing (xylene wash) of the paraffin-embedded pancreas may create artifacts on the locations of adipocytes, affecting the analysis of the peri- and/or intra-lobular adipocyte association.

Modern 3-D histology with aqueous-based optical clearing alleviates the abovementioned technical concern by maintaining the native hydrophilicity of the tissue and avoiding the microtome slicing in sample preparation (42). This is particularly important in examination of the type 2 diabetic pancreas and the surgical

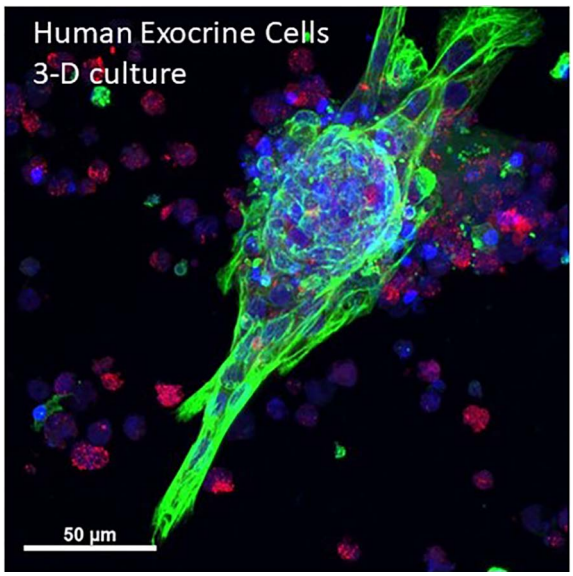

FIGURE 5 | 3-D projection human primary pancreas exocrine cells in culture. Isolated human exocrine cells were obtained from a pancreas donor non-islet fractions and following filtration to remove islets and clumps, exocrine cells were plated in 1:1 DMEM:F12 and Matrigel and grown for 6 days. A maximum projection image shows ductal cells (cytokeratin 19, green), acinar cells (amylase, red) and nuclei (blue). Cells were kindly provided by Dr. Thomas Schmittgen, College of Pharmacy, University of Florida. See also **Supplementary Video 4** for entire 3-D z-stack (12 µm).

biopsy of pancreatic cancer [patient may have developed type 3c diabetes (103, 104)]. In both situations, investigators will likely encounter moderate-to-severe fatty infiltration, in which adipocytes generally or locally become a component of the pancreas (**Figure 6**). To investigate the pancreas in this condition, we advise careful comparison between the modern 3-D and the classic 2-D tissue images to confirm the adipocytes in and around the remodeled pancreatic lobules to avoid misrepresentation of the disease condition.

Pancreatic Lymphatic Network

The lymphatic drainage of pancreas is achieved by an intricate network of lymphatic vessels and nodes, in which the immune cells reside. The open-ended lymphatic network collects the

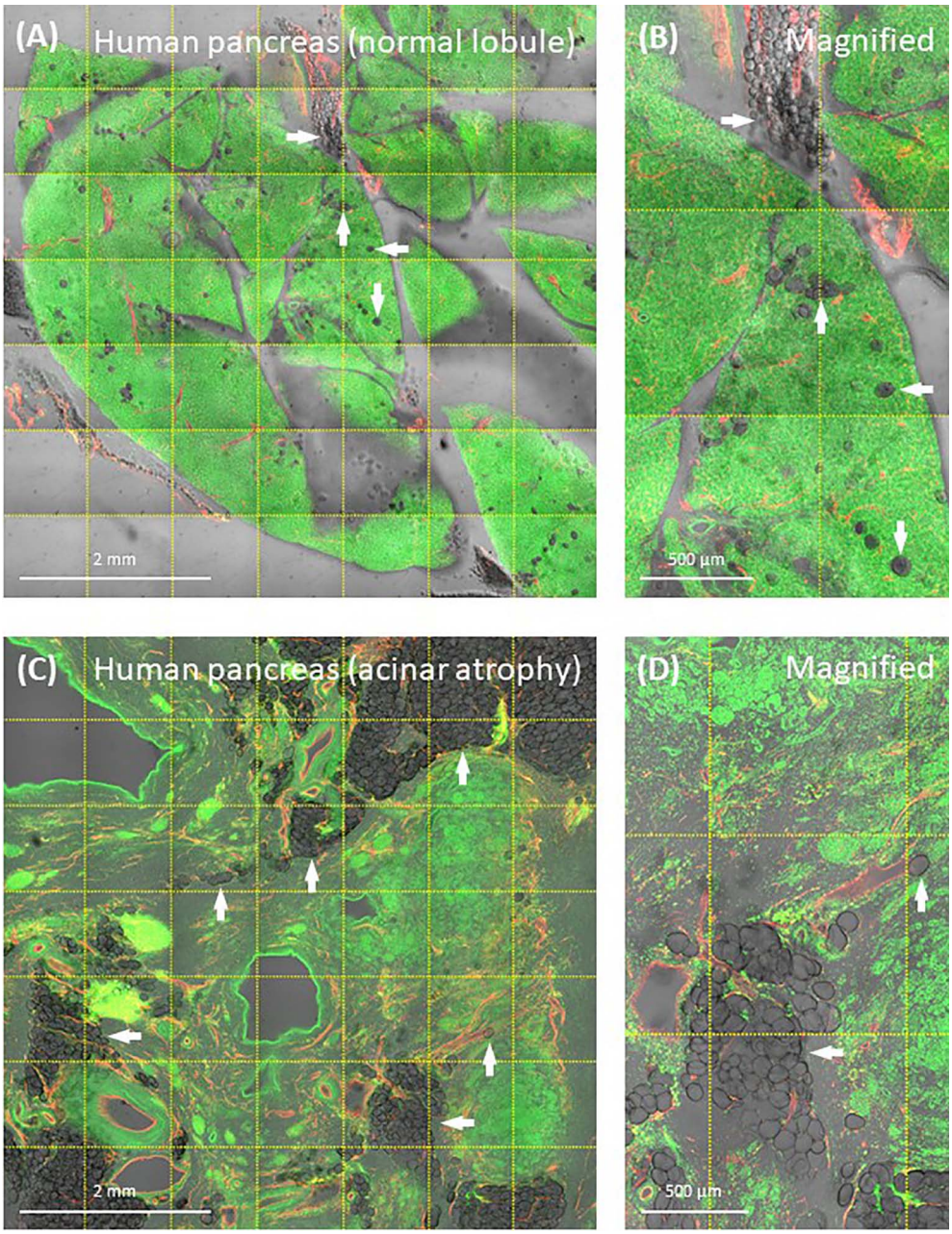

FIGURE 6 | Human pancreatic fatty infiltration. Images were derived from tile scanning of optically cleared pancreatic specimens. **(A, B)** Normal lobule of human pancreas. Adipocytes are clearly seen around the blood vessel and inside the lobule (magnified, arrows). Green, nuclear staining; red, CD31. **(C, D)** Acinar atrophy of diseased lobule. This view was acquired 2-cm distal to the pancreatic ductal adenocarcinoma. Overlay of transmitted light and fluorescence signals identifies the fatty infiltration.

interstitial fluids for water and lipid absorption and recycling (which balances the tissue osmatic pressure) and for immune surveillance (105). When pancreatic injury or disease occurs, the lymphatic system plays a central role in reaction to the exocrine [pancreatitis (44, 106)] and endocrine tissue inflammation. For example, in the nonobese diabetic (NOD) mice, the progression of type 1 diabetes features the migration of T lymphocytes from the circulatory system to the islet, attacking the β-cells (107, 108). In the process, the microtome-based 2-D histology has been used to evaluate the degree of islet inflammation, in which early,

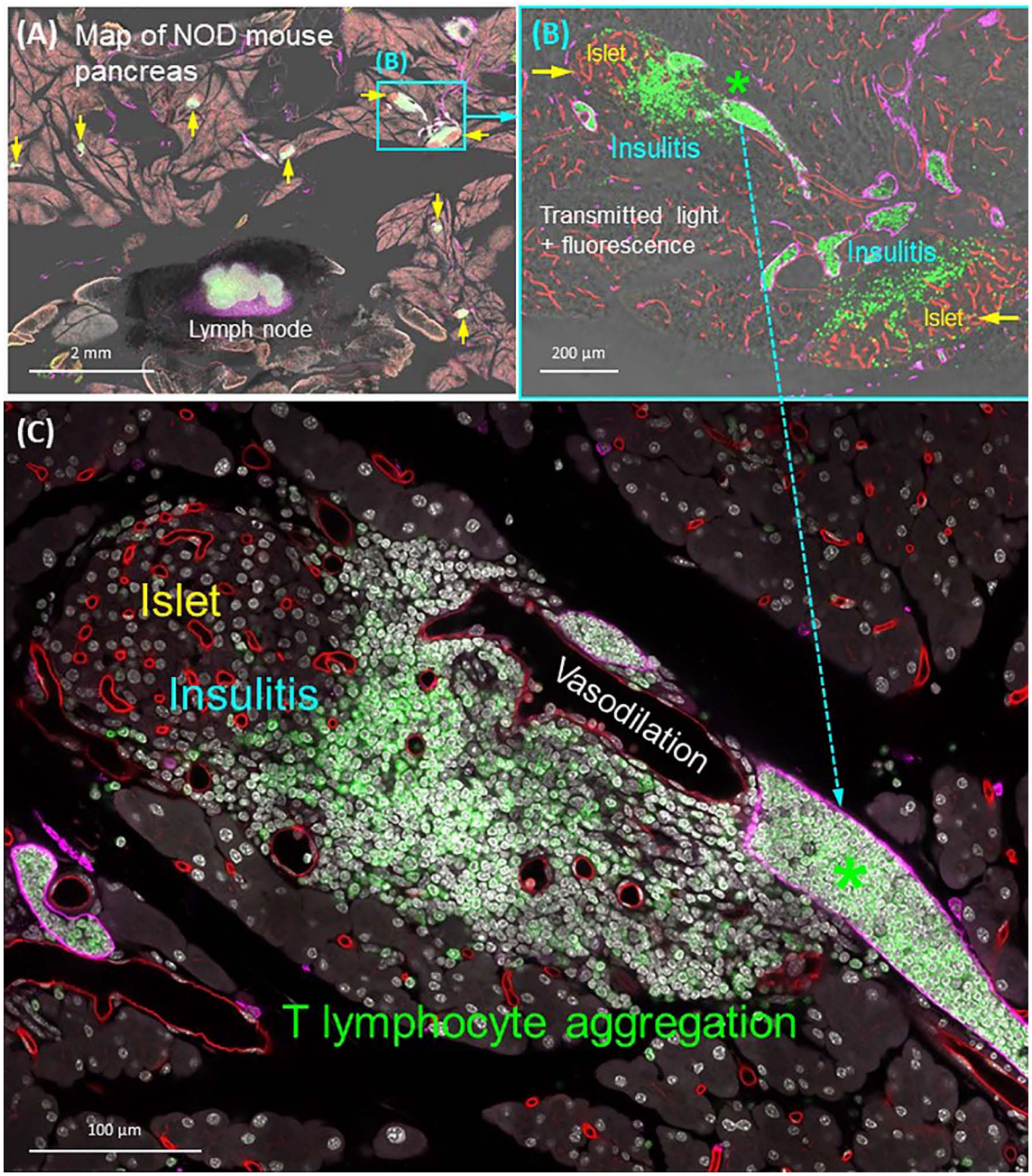

FIGURE 7 | Panoramic and high-resolution images of optically cleared NOD mouse pancreas with insulitis. **(A)** Map of 8-week NOD mouse pancreas. Overlay of transmitted light and fluorescence signals identifies the Lyve1$^+$ lymph node (filled with CD3$^+$ T lymphocytes and surrounded by fats) and locations of insulitic islets (yellow arrows). Two islets (cyan box) are magnified in **(B)**. **(B)** Islets with insulitis are shown with blood vessels (red), lymphatic vessels (magenta), and nuclei (white). CD3$^+$ T lymphocytes are identified around the islets and congregated in the lymphatic vessels (asterisk; vascular compartment vs. extravascular domain). This feature is further magnified in **(C)**. **(C)** Peri-islet aggregation of T lymphocytes and their vascular association shown as well as the peri-islet vasodilation and lymphocytic infiltration. See also **Supplementary Video 5** for **(B)**.

moderate, and severe insulitis are assigned to evaluate the progression of the disease (109). However, due to the dispersed nature of lymphatic vessels, the classic 2-D histology cannot provide a global assessment of lymphatic endothelial remodeling in response to insulitis. To understand the associated lymphatic and immune response to insulitis, panoramic and in-depth imaging of the pancreas is needed to characterize the lymphatic network and T-cell migration in a global and integrated fashion.

As can be seen in **Figure 7**, the optically cleared NOD mouse pancreas provides an experimental setting to investigate the lymphatic and T-lymphocyte association in insulitis. Using the panoramic image (**Figure 7A**), we can detect the $CD3^+$ T lymphocytes in the lymph node (positive control) and around the islets. The latter provides a clear target for examination of the islet under immune attack, featuring vasodilation and the packing of T lymphocytes in the lymphatic vessels (**Figures 7B, C**). Overall, the quadruple signals of tissue microstructure (nuclear staining), vasculature (blood and lymphatic vessels), and $CD3^+$ T lymphocytes in the transparent pancreas provide an optimized condition to visualize the islet vascular remodeling and immune attack in insulitis. They also demonstrate the different scales of tissue information (from interlobular to subcellular features of islets under immune attack) that can be acquired from optically cleared pancreas samples to investigate experimental insulitis.

CONCLUSIONS

Both standard and modified optical clearing methods are well suited for studies of 3-D structure-function relationships for human and mouse pancreas and use readily available chemicals and imaging equipment. These methods are particularly advantageous for studies of diabetes due to known islet heterogeneity requiring examination of numerous islets and pancreas regions. Optical clearing methods can also be used in investigations of pancreatic cancer using patient or rodent samples or *in vitro* experiments examining acinar-ductal metaplasia. Advances in understanding failure of islet beta-cells in diabetes requires a wholistic examination of islets in their native environment as afforded by optical clearing and new findings are anticipated related to the role of the nervous, immune, and vascular systems in beta-cell biology from such studies.

AUTHOR CONTRIBUTIONS

MC-T and S-CT designed the studies, performed experiments, prepared figures, and edited and revised the manuscript. All authors contributed to the article and approved the submitted version.

FUNDING

Funding provided by NIH 1R01DK122160, UC4 DK104155, U54 DK127823 and OT2 OD023861, Helmsley Charitable Trust 2015PG-T1D052 and JDRF 47-2014-1 and 2-SRA-2019-697-S-B to MC-T and Taiwan National Health Research Institutes (NHRI-EX109-10922EI) and Ministry of Science and Technology (MOST 108-2314-B-007-006-MY2) to S-CT.

ACKNOWLEDGMENTS

The authors thank past and current members of their laboratories for their assistance in optical clearing and microscopy. We thank the organ donor families for research organ donations. Organ Procurement Organizations (OPO) partnering with nPOD to provide research resources are listed at http://www.jdrfnpod.org/for-partners/npod-partners/. Human sample research was supported by nPOD (RRID : SCR_014641), a collaborative type 1 diabetes research project sponsored by JDRF (5-SRA-2018-557-Q-R) and the Leona M. & Harry B. Helmsley Charitable Trust (2018PG-T1D053). Imaging with the Zeiss 710 was performed with support from the UF Center for Immunology and Transplantation. Imaging with the Zeiss 800 was performed with support from Taiwan Ministry of Science and Technology (MOST 108-2731-M-007-001).

SUPPLEMENTARY MATERIAL

The Supplementary Material for this article can be found online at: https://www.frontiersin.org/articles/10.3389/fendo.2021.644826/full#supplementary-material

REFERENCES

1. Campbell-Thompson M, Fu A, Kaddis JS, Wasserfall C, Schatz DA, Pugliese A, et al. Insulitis and β-Cell Mass in the Natural History of Type 1 Diabetes. *Diabetes* (2016) 65(3):719–31. doi: 10.2337/db15-0779
2. Dybala MP, Hara M. Heterogeneity of the Human Pancreatic Islet. *Diabetes* (2019) 68(6):1230–9. doi: 10.2337/db19-0072
3. Benninger RKP, Dorrell C, Hodson DJ, Rutter GA. The Impact of Pancreatic Beta Cell Heterogeneity on Type 1 Diabetes Pathogenesis. *Curr Diabetes Rep* (2018) 18(11):112. doi: 10.1007/s11892-018-1085-2
4. Nasteska D, Hodson DJ. The Role of Beta Cell Heterogeneity in Islet Function and Insulin Release. *J Mol Endocrinol* (2018) 61(1):R43–60. doi: 10.1530/JME-18-0011
5. Pipeleers D, De Mesmaeker I, Robert T, Van Hulle F. Heterogeneity in the Beta-Cell Population: A Guided Search Into its Significance in Pancreas and in Implants. *Curr Diabetes Rep* (2017) 17(10):86. doi: 10.1007/s11892-017-0925-9
6. Dorrell C, Schug J, Canaday PS, Russ HA, Tarlow BD, Grompe MT, et al. Human Islets Contain Four Distinct Subtypes of β Cells. *Nat Commun* (2016) 7:11756. doi: 10.1038/ncomms11756
7. Roscioni SS, Migliorini A, Gegg M, Lickert H. Impact of Islet Architecture on β-Cell Heterogeneity, Plasticity and Function. *Nat Rev Endocrinol* (2016) 12(12):695–709. doi: 10.1038/nrendo.2016.147
8. Hunter CS, Stein RW. Evidence for Loss in Identity, De-Differentiation, and Trans-Differentiation of Islet β-Cells in Type 2 Diabetes. *Front Genet* (2017) 8:35. doi: 10.3389/fgene.2017.00035
9. Aguayo-Mazzucato C, van Haaren M, Mruk M, Lee TB, Crawford C, Hollister-Lock J, et al. β Cell Aging Markers Have Heterogeneous Distribution and Are Induced by Insulin Resistance. *Cell Metab* (2017) 25 (4):898–910.e5. doi: 10.1016/j.cmet.2017.03.015
10. Garcia TS, Rech TH, Leitão CB. Pancreatic Size and Fat Content in Diabetes: A Systematic Review and Meta-Analysis of Imaging Studies. *PloS One* (2017) 12(7):e0180911. doi: 10.1371/journal.pone.0180911

11. Poudel A, Fowler JL, Zielinski MC, Kilimnik G, Hara M. Stereological Analyses of the Whole Human Pancreas. *Sci Rep* (2016) 6:34049. doi: 10.1038/srep34049
12. Alvarsson A, Jimenez-Gonzalez M, Li R, Rosselot C, Tzavaras N, Wu Z, et al. A 3D Atlas of the Dynamic and Regional Variation of Pancreatic Innervation in Diabetes. *Sci Adv* (2020) 6(41):eaaz9124. doi: 10.1126/sciadv.aaz9124
13. Chien HJ, Chiang TC, Peng SJ, Chung MH, Chou YH, Lee CY, et al. Human Pancreatic Afferent and Efferent Nerves: Mapping and 3-D Illustration of Exocrine, Endocrine, and Adipose Innervation. *Am J Physiol Gastrointest Liver Physiol* (2019) 317(5):G694–706. doi: 10.1152/ajpgi.00116.2019
14. Tang SC, Jessup CF, Campbell-Thompson M. The Role of Accessory Cells in Islet Homeostasis. *Curr Diabetes Rep* (2018) 18(11):117. doi: 10.1007/s11892-018-1096-z
15. Butterworth E, Dickerson W, Vijay V, Weitzel K, Cooper J, Atkinson EW, et al. High Resolution 3d Imaging of the Human Pancreas Neuro-insular Network. *J Vis Exp* (2018) 131:56859–66. doi: 10.3791/56859
16. Azaripour A, Lagerweij T, Scharfbillig C, Jadczak AE, Willershausen B, Van Noorden CJ. A Survey of Clearing Techniques for 3D Imaging of Tissues With Special Reference to Connective Tissue. *Prog Histochem Cytochem* (2016) 51(2):9–23. doi: 10.1016/j.proghi.2016.04.001
17. Susaki EA, Shimizu C, Kuno A, Tainaka K, Li X, Nishi K, et al. Versatile Whole-Organ/Body Staining and Imaging Based on Electrolyte-Gel Properties of Biological Tissues. *Nat Commun* (2020) 11(1):1982. doi: 10.1038/s41467-020-15906-5
18. Kim A, Kilimnik G, Hara M. In Situ Quantification of Pancreatic Beta-Cell Mass in Mice. *J Vis Exp* (2010) 40:1970–3. doi: 10.3791/1970
19. Fu YY, Tang SC. At the Movies: 3-Dimensional Technology and Gastrointestinal Histology. *Gastroenterology* (2010) 139(4):1100–5, 5.e1. doi: 10.1053/j.gastro.2010.08.025
20. Fu YY, Lu CH, Lin CW, Juang JH, Enikolopov G, Sibley E, et al. Three-Dimensional Optical Method for Integrated Visualization of Mouse Islet Microstructure and Vascular Network With Subcellular-Level Resolution. *J BioMed Opt* (2010) 15(4):046018. doi: 10.1117/1.3470241
21. Li WC, Rukstalis JM, Nishimura W, Tchipashvili V, Habener JF, Sharma A, et al. Activation of Pancreatic-Duct-Derived Progenitor Cells During Pancreas Regeneration in Adult Rats. *J Cell Sci* (2010) 123(Pt 16):2792–802. doi: 10.1242/jcs.065268
22. Chiu YC, Hua TE, Fu YY, Pasricha PJ, Tang SC. 3-D Imaging and Illustration of the Perfusive Mouse Islet Sympathetic Innervation and its Remodelling in Injury. *Diabetologia* (2012) 55(12):3252–61. doi: 10.1007/s00125-012-2699-6
23. Tang SC, Chiu YC, Hsu CT, Peng SJ, Fu YY. Plasticity of Schwann Cells and Pericytes in Response to Islet Injury in Mice. *Diabetologia* (2013) 56(11):2424–34. doi: 10.1007/s00125-013-2977-y
24. Juang JH, Peng SJ, Kuo CH, Tang SC. Three-Dimensional Islet Graft Histology: Panoramic Imaging of Neural Plasticity in Sympathetic Reinnervation of Transplanted Islets Under the Kidney Capsule. *Am J Physiol Endocrinol Metab* (2014) 306(5):E559–70. doi: 10.1152/ajpendo.00515.2013
25. Tang SC, Peng SJ, Chien HJ. Imaging of the Islet Neural Network. *Diabetes Obes Metab* (2014) 16 Suppl 1:77–86. doi: 10.1111/dom.12342
26. Lee H, Park JH, Seo I, Park SH, Kim S. Improved Application of the Electrophoretic Tissue Clearing Technology, CLARITY, to Intact Solid Organs Including Brain, Pancreas, Liver, Kidney, Lung, and Intestine. *BMC Dev Biol* (2014) 14:48. doi: 10.1186/s12861-014-0048-3
27. Susaki EA, Tainaka K, Perrin D, Yukinaga H, Kuno A, Ueda HR. Advanced CUBIC Protocols for Whole-Brain and Whole-Body Clearing and Imaging. *Nat Protoc* (2015) 10(11):1709–27. doi: 10.1038/nprot.2015.085
28. Juang JH, Kuo CH, Peng SJ, Tang SC. 3-D Imaging Reveals Participation of Donor Islet Schwann Cells and Pericytes in Islet Transplantation and Graft Neurovascular Regeneration. *EBioMedicine* (2015) 2(2):109–19. doi: 10.1016/j.ebiom.2015.01.014
29. Treweek JB, Chan KY, Flytzanis NC, Yang B, Deverman BE, Greenbaum A, et al. Whole-Body Tissue Stabilization and Selective Extractions Via Tissue-Hydrogel Hybrids for High-Resolution Intact Circuit Mapping and Phenotyping. *Nat Protoc* (2015) 10(11):1860–96. doi: 10.1038/nprot.2015.122
30. Chien HJ, Peng SJ, Hua TE, Kuo CH, Juang JH, Tang SC. 3-D Imaging of Islets in Obesity: Formation of the Islet-Duct Complex and Neurovascular Remodeling in Young Hyperphagic Mice. *Int J Obes (Lond)* (2016) 40(4):685–97. doi: 10.1038/ijo.2015.224
31. Lin PY, Peng SJ, Shen CN, Pasricha PJ, Tang SC. PanIN-associated Pericyte, Glial, and Islet Remodeling in Mice Revealed by 3D Pancreatic Duct Lesion Histology. *Am J Physiol Gastrointest Liver Physiol* (2016) 311(3):G412–22. doi: 10.1152/ajpgi.00071.2016
32. Simon T, Pogu J, Remy S, Brau F, Pogu S, Maquigneau M, et al. Inhibition of Effector Antigen-Specific T Cells by Intradermal Administration of Heme Oxygenase-1 Inducers. *J Autoimmun* (2017) 81:44–55. doi: 10.1016/j.jaut.2017.03.005
33. Vlahos AE, Cober N, Sefton MV. Modular Tissue Engineering for the Vascularization of Subcutaneously Transplanted Pancreatic Islets. *Proc Natl Acad Sci USA* (2017) 114(35):9337–42. doi: 10.1073/pnas.1619216114
34. Wong HS, Yeung PKK, Lai HM, Lam KSL, Wutian W, Chung SK. Simple and Rapid Tissue Clearing Method for Three-Dimensional Histology of the Pancreas. *Curr Protoc Cell Biol* (2017) 77:19.20.1–19.20.10. doi: 10.1002/cpcb.34
35. Yamamoto J, Imai J, Izumi T, Takahashi H, Kawana Y, Takahashi K, et al. Neuronal Signals Regulate Obesity Induced β-Cell Proliferation by FoxM1 Dependent Mechanism. *Nat Commun* (2017) 8(1):1930. doi: 10.1038/s41467-017-01869-7
36. Pauerstein PT, Tellez K, Willmarth KB, Park KM, Hsueh B, Efsun Arda H, et al. A Radial Axis Defined by Semaphorin-to-Neuropilin Signaling Controls Pancreatic Islet Morphogenesis. *Development* (2017) 144(20):3744–54. doi: 10.1242/dev.148684
37. Chen L, Li G, Li Y, Li Y, Zhu H, Tang L, et al. Ubasm: An Effective Balanced Optical Clearing Method for Intact Biomedical Imaging. *Sci Rep* (2017) 7(1):12218. doi: 10.1038/s41598-017-12484-3
38. Hsueh B, Burns VM, Pauerstein P, Holzem K, Ye L, Engberg K, et al. Pathways to Clinical CLARITY: Volumetric Analysis of Irregular, Soft, and Heterogeneous Tissues in Development and Disease. *Sci Rep* (2017) 7(1):5899. doi: 10.1038/s41598-017-05614-4
39. Tang SC, Shen CN, Lin PY, Peng SJ, Chien HJ, Chou YH, et al. Pancreatic Neuro-Insular Network in Young Mice Revealed by 3D Panoramic Histology. *Diabetologia* (2018) 61(1):158–67. doi: 10.1007/s00125-017-4408-y
40. Nishimura W, Sakaue-Sawano A, Takahashi S, Miyawaki A, Yasuda K, Noda Y. Optical Clearing of the Pancreas for Visualization of Mature β-Cells and Vessels in Mice. *Islets* (2018) 10(3):e1451282. doi: 10.1080/19382014.2018.1451282
41. Noë M, Rezaee N, Asrani K, Skaro M, Groot VP, Wu PH, et al. Immunolabeling of Cleared Human Pancreata Provides Insights Into Three-Dimensional Pancreatic Anatomy and Pathology. *Am J Pathol* (2018) 188(7):1530–5. doi: 10.1016/j.ajpath.2018.04.002
42. Tang SC, Baeyens L, Shen CN, Peng SJ, Chien HJ, Scheel DW, et al. Human Pancreatic Neuro-Insular Network in Health and Fatty Infiltration. *Diabetologia* (2018) 61(1):168–81. doi: 10.1007/s00125-017-4409-x
43. Fowler JL, Lee SS, Wesner ZC, Olehnik SK, Kron SJ, Hara M. Three-Dimensional Analysis of the Human Pancreas. *Endocrinology* (2018) 159(3):1393–400. doi: 10.1210/en.2017-03076
44. Shen CN, Goh KS, Huang CR, Chiang TC, Lee CY, Jeng YM, et al. Lymphatic Vessel Remodeling and Invasion in Pancreatic Cancer Progression. *EBioMedicine* (2019) 47:98–113. doi: 10.1016/j.ebiom.2019.08.044
45. Hong SM, Noe M, Hruban CA, Thompson ED, Wood LD, Hruban RH. A "Clearer" View of Pancreatic Pathology: A Review of Tissue Clearing and Advanced Microscopy Techniques. *Adv Anat Pathol* (2019) 26(1):31–9. doi: 10.1097/PAP.0000000000000215
46. Tokumoto S, Yabe D, Tatsuoka H, Usui R, Fauzi M, Botagarova A, et al. Generation and Characterization of a Novel Mouse Model That Allows Spatiotemporal Quantification of Pancreatic β-Cell Proliferation. *Diabetes* (2020) 69(11):2340–51. doi: 10.2337/db20-0290
47. Hahn M, van Krieken PP, Nord C, Alanentalo T, Morini F, Xiong Y, et al. Topologically Selective Islet Vulnerability and Self-Sustained Downregulation of Markers for β-Cell Maturity in Streptozotocin-Induced Diabetes. *Commun Biol* (2020) 3(1):541. doi: 10.1038/s42003-020-01243-2
48. Maldonado M, Serrill JD, Shih HP. Painting the Pancreas in Three Dimensions: Whole-Mount Immunofluorescence Method. *Methods Mol Biol* (2020) 2155:193–200. doi: 10.1007/978-1-0716-0655-1_16
49. Roostalu U, Lercke Skytte J, Gravesen Salinas C, Klein T, Vrang N, Jelsing J, et al. 3D Quantification of Changes in Pancreatic Islets in Mouse Models of

Diabetes Type I and II. *Dis Model Mech* (2020) 13(12):dmm045351. doi: 10.1242/dmm.045351
50. Hong SM, Jung D, Kiemen A, Gaida MM, Yoshizawa T, Braxton AM, et al. Three-Dimensional Visualization of Cleared Human Pancreas Cancer Reveals That Sustained Epithelial-to-Mesenchymal Transition is Not Required for Venous Invasion. *Mod Pathol* (2020) 33(4):639–47. doi: 10.1038/s41379-019-0409-3
51. Graham KD, Lopez SH, Sengupta R, Shenoy A, Schneider S, Wright CM, et al. Robust, 3-Dimensional Visualization of Human Colon Enteric Nervous System Without Tissue Sectioning. *Gastroenterology* (2020) 158(8):2221–35 e5. doi: 10.1053/j.gastro.2020.02.035
52. Chen J, Lippo L, Labella R, Tan SL, Marsden BD, Dustin ML, et al. Decreased Blood Vessel Density and Endothelial Cell Subset Dynamics During Ageing of the Endocrine System. *EMBO J* (2021) 40(1):e105242. doi: 10.15252/embj.2020105242
53. Campbell-Thompson M, Butterworth EA, Boatwright JL, Nair MA, Nasif LH, Nasif K, et al. Islet Sympathetic Innervation and Islet Neuropathology in Patients With Type 1 Diabetes. *Sci Rep* (2021) 11(1):6562–78. doi: 10.1038/s41598-021-85659-8
54. Costantini I, Cicchi R, Silvestri L, Vanzi F, Pavone FS. In-Vivo and Ex-Vivo Optical Clearing Methods for Biological Tissues: Review. *BioMed Opt Express* (2019) 10(10):5251–67. doi: 10.1364/BOE.10.005251
55. Schega Y, Flinner N, Hansmann ML. Quantitative Assessment of Optical Clearing Methods on Formalin-Fixed Human Lymphoid Tissue. *Pathol Res Pract* (2020) 216(11):153136. doi: 10.1016/j.prp.2020.153136
56. Richardson DS, Lichtman JW. Clarifying Tissue Clearing. *Cell* (2015) 162 (2):246–57. doi: 10.1016/j.cell.2015.06.067
57. Orlich M, Kiefer F. A Qualitative Comparison of Ten Tissue Clearing Techniques. *Histol Histopathol* (2018) 33(2):181–99. doi: 10.14670/HH-11-903
58. Ariel P. A Beginner's Guide to Tissue Clearing. *Int J Biochem Cell Biol* (2017) 84:35–9. doi: 10.1016/j.biocel.2016.12.009
59. Liu CY, Polk DB. Cellular Maps of Gastrointestinal Organs: Getting the Most From Tissue Clearing. *Am J Physiol Gastrointest Liver Physiol* (2020) 319(1):G1–G10. doi: 10.1152/ajpgi.00075.2020
60. Renier N, Wu Z, Simon DJ, Yang J, Ariel P, Tessier-Lavigne M. iDISCO: A Simple, Rapid Method to Immunolabel Large Tissue Samples for Volume Imaging. *Cell* (2014) 159(4):896–910. doi: 10.1016/j.cell.2014.10.010
61. Matsumoto K, Mitani TT, Horiguchi SA, Kaneshiro J, Murakami TC, Mano T, et al. Advanced CUBIC Tissue Clearing for Whole-Organ Cell Profiling. *Nat Protoc* (2019) 14(12):3506–37. doi: 10.1038/s41596-019-0240-9
62. Susaki EA, Tainaka K, Perrin D, Kishino F, Tawara T, Watanabe TM, et al. Whole-Brain Imaging With Single-Cell Resolution Using Chemical Cocktails and Computational Analysis. *Cell* (2014) 157(3):726–39. doi: 10.1016/j.cell.2014.03.042
63. Yang B, Treweek JB, Kulkarni RP, Deverman BE, Chen CK, Lubeck E, et al. Single-Cell Phenotyping Within Transparent Intact Tissue Through Whole-Body Clearing. *Cell* (2014) 158(4):945–58. doi: 10.1016/j.cell.2014.07.017
64. Tomer R, Ye L, Hsueh B, Deisseroth K. Advanced CLARITY for Rapid and High-Resolution Imaging of Intact Tissues. *Nat Protoc* (2014) 9(7):1682–97. doi: 10.1038/nprot.2014.123
65. Chung K, Deisseroth K. CLARITY for Mapping the Nervous System. *Nat Methods* (2013) 10(6):508–13. doi: 10.1038/nmeth.2481
66. Gradinaru V, Treweek J, Overton K, Deisseroth K. Hydrogel-Tissue Chemistry: Principles and Applications. *Annu Rev Biophys* (2018) 47:355–76. doi: 10.1146/annurev-biophys-070317-032905
67. Treweek JB, Gradinaru V. Extracting Structural and Functional Features of Widely Distributed Biological Circuits With Single Cell Resolution Via Tissue Clearing and Delivery Vectors. *Curr Opin Biotechnol* (2016) 40:193–207. doi: 10.1016/j.copbio.2016.03.012
68. Schindelin J, Arganda-Carreras I, Frise E, Kaynig V, Longair M, Pietzsch T, et al. Fiji: An Open-Source Platform for Biological-Image Analysis. *Nat Methods* (2012) 9(7):676–82. doi: 10.1038/nmeth.2019
69. Campbell-Thompson ML, Montgomery EL, Foss RM, Kolheffer KM, Phipps G, Schneider L, et al. Collection Protocol for Human Pancreas. *J Vis Exp* (2012) 63):e4039. doi: 10.3791/4039
70. Sunami E, Kanazawa H, Hashizume H, Takeda M, Hatakeyama K, Ushiki T. Morphological Characteristics of Schwann Cells in the Islets of Langerhans of the Murine Pancreas. *Arch Histol Cytol* (2001) 64(2):191–201. doi: 10.1679/aohc.64.191
71. Kidd GJ, Ohno N, Trapp BD. Biology of Schwann Cells. *Handb Clin Neurol* (2013) 115:55–79. doi: 10.1016/B978-0-444-52902-2.00005-9
72. Reinisch CM, Traxler H, Piringer S, Tangl S, Nader A, Tschachler E. Rarefaction of the Peripheral Nerve Network in Diabetic Patients is Associated With a Pronounced Reduction of Terminal Schwann Cells. *Diabetes Care* (2008) 31(6):1219–21. doi: 10.2337/dc07-1832
73. Griffin JW, Thompson WJ. Biology and Pathology of Nonmyelinating Schwann Cells. *Glia* (2008) 56(14):1518–31. doi: 10.1002/glia.20778
74. Wekerle H, Schwab M, Linington C, Meyermann R. Antigen Presentation in the Peripheral Nervous System: Schwann Cells Present Endogenous Myelin Autoantigens to Lymphocytes. *Eur J Immunol* (1986) 16(12):1551–7. doi: 10.1002/eji.1830161214
75. Tzekova N, Heinen A, Küry P. Molecules Involved in the Crosstalk Between Immune- and Peripheral Nerve Schwann Cells. *J Clin Immunol* (2014) 34 Suppl 1:S86–104. doi: 10.1007/s10875-014-0015-6
76. Tsui H, Chan Y, Tang L, Winer S, Cheung RK, Paltser G, et al. Targeting of Pancreatic Glia in Type 1 Diabetes. *Diabetes* (2008) 57(4):918–28. doi: 10.2337/db07-0226
77. Winer S, Tsui H, Lau A, Song A, Li X, Cheung RK, et al. Autoimmune Islet Destruction in Spontaneous Type 1 Diabetes is Not Beta-Cell Exclusive. *Nat Med* (2003) 9(2):198–205. doi: 10.1038/nm818
78. Teitelman G, Guz Y, Ivkovic S, Ehrlich M. Islet Injury Induces Neurotrophin Expression in Pancreatic Cells and Reactive Gliosis of Peri-Islet Schwann Cells. *J Neurobiol* (1998) 34(4):304–18. doi: 10.1002/(SICI)1097-4695(199803)34:4<304::AID-NEU2>3.0.CO;2-A
79. Pang Z, Kushiyama A, Sun J, Kikuchi T, Yamazaki H, Iwamoto Y, et al. Glial Fibrillary Acidic Protein (GFAP) is a Novel Biomarker for the Prediction of Autoimmune Diabetes. *FASEB J* (2017) 31(9):4053–63. doi: 10.1096/fj.201700110R
80. Li W, Yu G, Liu Y, Sha L. Intrapancreatic Ganglia and Neural Regulation of Pancreatic Endocrine Secretion. *Front Neurosci* (2019) 13:21. doi: 10.3389/fnins.2019.00021
81. Gylfe E, Tengholm A. Neurotransmitter Control of Islet Hormone Pulsatility. *Diabetes Obes Metab* (2014) 16 Suppl 1:102–10. doi: 10.1111/dom.12345
82. Serizawa Y, Kobayashi S, Fujita T. Neuro-Insular Complex Type I in the Mouse. Re-evaluation of the Pancreatic Islet as a Modified Ganglion. *Arch Histol Jpn* (1979) 42(3):389–94. doi: 10.1679/aohc1950.42.389
83. Proshchina AE, Krivova YS, Barabanov VM, Saveliev SV. Ontogeny of Neuro-Insular Complexes and Islets Innervation in the Human Pancreas. *Front Endocrinol (Lausanne)* (2014) 5:57. doi: 10.3389/fendo.2014.00057
84. Dybala MP, Kuznetsov A, Motobu M, Hendren-Santiago BK, Philipson LH, Chervonsky AV, et al. Integrated Pancreatic Blood Flow: Bi-Directional Microcirculation Between Endocrine and Exocrine Pancreas. *Diabetes* (2020) 69(7):1439–50. doi: 10.2337/db19-1034
85. Canzano JS, Nasif LH, Butterworth EA, Fu DA, Atkinson MA, Campbell-Thompson M. Islet Microvasculature Alterations With Loss of Beta-cells in Patients With Type 1 Diabetes. *J Histochem Cytochem* (2019) 67(1):41–52. doi: 10.1369/0022155418778546
86. Kusmartseva I, Wu W, Syed F, Van Der Heide V, Jorgensen M, Joseph P, et al. Expression of SARS-CoV-2 Entry Factors in the Pancreas of Normal Organ Donors and Individuals With COVID-19. *Cell Metab* (2020) 32 (6):1041–51.e6. doi: 10.1016/j.cmet.2020.11.005
87. Coate KC, Cha J, Shrestha S, Wang W, Gonçalves LM, Almaça J, et al. SARS-Cov-2 Cell Entry Factors ACE2 and TMPRSS2 are Expressed in the Microvasculature and Ducts of Human Pancreas But Are Not Enriched in β Cells. *Cell Metab* (2020) 32(6):1028–40.e4. doi: 10.1016/j.cmet.2020.11.006
88. Abbruzzese JL, Andersen DK, Borrebaeck CAK, Chari ST, Costello E, Cruz-Monserrate Z, et al. The Interface of Pancreatic Cancer With Diabetes, Obesity, and Inflammation: Research Gaps and Opportunities: Summary of a National Institute of Diabetes and Digestive and Kidney Diseases Workshop. *Pancreas* (2018) 47(5):516–25. doi: 10.1097/MPA.0000000000001037
89. Bray JK, Elgamal OA, Jiang J, Wright LS, Sutaria DS, Badawi M, et al. Loss of RE-1 Silencing Transcription Factor Accelerates Exocrine Damage From Pancreatic Injury. *Cell Death Dis* (2020) 11(2):138. doi: 10.1038/s41419-020-2269-7
90. Saisho Y, Butler AE, Meier JJ, Monchamp T, Allen-Auerbach M, Rizza RA, et al. Pancreas Volumes in Humans From Birth to Age One Hundred Taking

Into Account Sex, Obesity, and Presence of Type-2 Diabetes. *Clin Anat* (2007) 20(8):933–42. doi: 10.1002/ca.20543

91. Chiyanika C, Chan DFY, Hui SCN, So HK, Deng M, Yeung DKW, et al. The Relationship Between Pancreas Steatosis and the Risk of Metabolic Syndrome and Insulin Resistance in Chinese Adolescents With Concurrent Obesity and non-Alcoholic Fatty Liver Disease. *Pediatr Obes* (2020) 15(9):e12653. doi: 10.1111/ijpo.12653
92. Kovanlikaya A, Mittelman SD, Ward A, Geffner ME, Dorey F, Gilsanz V. Obesity and Fat Quantification in Lean Tissues Using Three-Point Dixon MR Imaging. *Pediatr Radiol* (2005) 35(6):601–7. doi: 10.1007/s00247-005-1413-y
93. Tirkes T, Jeon CY, Li L, Joon AY, Seltman TA, Sankar M, et al. Association of Pancreatic Steatosis With Chronic Pancreatitis, Obesity, and Type 2 Diabetes Mellitus. *Pancreas* (2019) 48(3):420–6. doi: 10.1097/MPA.0000000000001252
94. Pienkowska J, Brzeska B, Kaszubowski M, Kozak O, Jankowska A, Szurowska E. MRI Assessment of Ectopic Fat Accumulation in Pancreas, Liver and Skeletal Muscle in Patients With Obesity, Overweight and Normal BMI in Correlation With the Presence of Central Obesity and Metabolic Syndrome. *Diabetes Metab Syndr Obes* (2019) 12:623–36. doi: 10.2147/DMSO.S194690
95. Sorisky A. From Preadipocyte to Adipocyte: Differentiation-Directed Signals of Insulin From the Cell Surface to the Nucleus. *Crit Rev Clin Lab Sci* (1999) 36(1):1–34. doi: 10.1080/10408369991239169
96. Klemm DJ, Leitner JW, Watson P, Nesterova A, Reusch JE, Goalstone ML, et al. Insulin-Induced Adipocyte Differentiation. Activation of CREB Rescues Adipogenesis From the Arrest Caused by Inhibition of Prenylation. *J Biol Chem* (2001) 276(30):28430–5. doi: 10.1074/jbc.M103382200
97. Geloen A, Collet AJ, Guay G, Bukowiecki LJ. Insulin Stimulates In Vivo Cell Proliferation in White Adipose Tissue. *Am J Physiol* (1989) 256(1 Pt 1): C190–6. doi: 10.1152/ajpcell.1989.256.1.C190
98. Ishibashi C, Kozawa J, Hosakawa Y, Yoneda S, Kimura T, Fujita Y, et al. Pancreatic Fat is Related to the Longitudinal Decrease in the Increment of C-peptide in Glucagon Stimulation Test in Type 2 Diabetes Patients. *J Diabetes Investig* (2020) 11(1):80–7. doi: 10.1111/jdi.13108
99. Sakai NS, Taylor SA, Chouhan MD. Obesity, Metabolic Disease and the pancreas-Quantitative Imaging of Pancreatic Fat. *Br J Radiol* (2018) 91 (1089):20180267. doi: 10.1259/bjr.20180267
100. Ou HY, Wang CY, Yang YC, Chen MF, Chang CJ. The Association Between Nonalcoholic Fatty Pancreas Disease and Diabetes. *PloS One* (2013) 8(5): e62561. doi: 10.1371/journal.pone.0062561
101. Tirkes T, Shah ZK, Takahashi N, Grajo JR, Chang ST, Venkatesh SK, et al. Reporting Standards for Chronic Pancreatitis by Using Ct, MRI, and MR Cholangiopancreatography: The Consortium for the Study of Chronic Pancreatitis, Diabetes, and Pancreatic Cancer. *Radiology* (2019) 290 (1):207–15. doi: 10.1148/radiol.2018181353
102. Macauley M, Percival K, Thelwall PE, Hollingsworth KG, Taylor R. Altered Volume, Morphology and Composition of the Pancreas in Type 2 Diabetes. *PloS One* (2015) 10(5):e0126825. doi: 10.1371/journal.pone.0126825
103. Hart PA, Bellin MD, Andersen DK, Bradley D, Cruz-Monserrate Z, Forsmark CE, et al. Type 3c (Pancreatogenic) Diabetes Mellitus Secondary to Chronic Pancreatitis and Pancreatic Cancer. *Lancet Gastroenterol Hepatol* (2016) 1(3):226–37. doi: 10.1016/S2468-1253(16)30106-6
104. Molina-Montes E, Coscia C, Gomez-Rubio P, Fernandez A, Boenink R, Rava M, et al. Deciphering the Complex Interplay Between Pancreatic Cancer, Diabetes Mellitus Subtypes and Obesity/BMI Through Causal Inference and Mediation Analyses. *Gut* (2020) 70(2):319–29. doi: 10.1136/gutjnl-2019-319990
105. Santambrogio L. The Lymphatic Fluid. *Int Rev Cell Mol Biol* (2018) 337:111–33. doi: 10.1016/bs.ircmb.2017.12.002
106. Cesmebasi A, Malefant J, Patel SD, Du Plessis M, Renna S, Tubbs RS, et al. The Surgical Anatomy of the Lymphatic System of the Pancreas. *Clin Anat* (2015) 28(4):527–37. doi: 10.1002/ca.22461
107. Anderson MS, Bluestone JA. The NOD Mouse: A Model of Immune Dysregulation. *Annu Rev Immunol* (2005) 23:447–85. doi: 10.1146/annurev.immunol.23.021704.115643
108. Wallberg M, Cooke A. Immune Mechanisms in Type 1 Diabetes. *Trends Immunol* (2013) 34(12):583–91. doi: 10.1016/j.it.2013.08.005
109. Eizirik DL, Colli ML, Ortis F. The Role of Inflammation in Insulitis and Beta-Cell Loss in Type 1 Diabetes. *Nat Rev Endocrinol* (2009) 5(4):219–26. doi: 10.1038/nrendo.2009.21

Conflict of Interest: The authors declare that the research was conducted in the absence of any commercial or financial relationships that could be construed as a potential conflict of interest.

frontiers in Endocrinology

REVIEW
published: 27 April 2021
doi: 10.3389/fendo.2021.663022

Optical Imaging of Pancreatic Innervation

Madina Makhmutova * *and Alejandro Caicedo* *

Division of Endocrinology, Diabetes and Metabolism, Department of Medicine, University of Miami Miller School of Medicine, Miami, FL, United States

At the time of Ivan Pavlov, pancreatic innervation was studied by looking at pancreas secretions in response to electrical stimulation of nerves. Nowadays we have ways to visualize neuronal activity in real time thanks to advances in fluorescent reporters and imaging techniques. We also have very precise optogenetic and pharmacogenetic approaches that allow neuronal manipulations in a very specific manner. These technological advances have been extensively employed for studying the central nervous system and are just beginning to be incorporated for studying visceral innervation. Pancreatic innervation is complex, and the role it plays in physiology and pathophysiology of the organ is still not fully understood. In this review we highlight anatomical aspects of pancreatic innervation, techniques for pancreatic neuronal labeling, and approaches for imaging pancreatic innervation *in vitro* and *in vivo*.

Keywords: innervation, pancreatic ganglia, parasympathetic, sympathetic, vagus, nodose ganglia (ng), fluorescence imaging

OPEN ACCESS

Edited by:
Vincent Poitout,
Université de Montréal, Canada

Reviewed by:
Valentine S. Moullé,
INRAE UMR PhAN 1280, France
Christophe Magnan,
Université Paris Diderot, France
Gabriela Da Silva Xavier,
University of Birmingham,
United Kingdom

***Correspondence:**
Madina Makhmutova
m.makhmutova@med.miami.edu
Alejandro Caicedo
acaicedo@med.miami.edu

Specialty section:
This article was submitted to Diabetes: Molecular Mechanisms, a section of the journal Frontiers in Endocrinology

Received: *02 February 2021*
Accepted: *08 April 2021*
Published: *27 April 2021*

Citation:
Makhmutova M and Caicedo A (2021) Optical Imaging of Pancreatic Innervation. Front. Endocrinol. 12:663022. doi: 10.3389/fendo.2021.663022

THE STATUS QUO OF PANCREATIC INNERVATION IS STILL BASED ON EARLY FINDINGS

First accounts of pancreatic innervation go back to the times of Paul Langerhans, who described pancreatic islets as richly innervated clusters of cells (1869), Santiago Ramon y Cajal, who delineated the innervation of the exocrine acinar tissue (1891), and Ivan Pavlov, who showed the role of innervation in pancreas secretion (1887) (1). An understanding of pancreatic innervation came quite far by the first half of the twentieth century. A paper published in 1945 already gave a detailed description of parasympathetic, sympathetic, and afferent innervation, as well as its potential targets and physiological effects in both endocrine and exocrine pancreas (2). Most of the postulates in that review came from studying the effects of neuronal stimulation on endocrine and exocrine secretion and anatomical studies of neuronal degeneration, which were confirmed later with more modern techniques, such as tracing, immunohistochemistry, and electrophysiology.

Although our understanding of innervation patterns, neuronal chemical phenotype, innervation targets, and interspecies differences has advanced over time, conceptually it does not go far beyond of what was known in 1945. The scientific and clinical community still perceives pancreatic innervation as a classical autonomic network of robust competing sympathetic-parasympathetic efferent inputs and a still mysterious afferent sensory branch. The intricate details of peripheral transduction mechanisms, as well as the big picture of the neural circuitry of the pancreas and its role in the physiology of endocrine and exocrine pancreas are still elusive. Modern techniques of optical imaging have answered many questions in the neuroscience field and brought our

understanding of neural circuity and connectivity in the brain to a completely different level. This review discusses approaches and challenges of structural and functional optical imaging of pancreatic innervation.

STRUCTURAL AND FUNCTIONAL FEATURES OF PANCREATIC INNERVATION

As the details of pancreatic innervation have been reviewed elsewhere (3–7), here we briefly go over some structural and functional features of innervation relevant for imaging, with an emphasis on neuroanatomical circuitry and neuronal phenotypes. The most intuitive way to segregate pancreatic innervation for practical imaging purposes is by the location of the neuronal soma: inside (intrinsic) or outside (extrinsic) of the pancreas (**Figure 1**).

Intrinsic Pancreatic Innervation

The intrinsic pancreatic innervation is a network of pancreatic neurons that cluster to form pancreatic ganglia and send unmyelinated projections to their targets in the endocrine and exocrine pancreas (8). Ganglia are dispersed throughout the pancreatic parenchyma and interlobular spaces, but are also present around some pancreatic islets, where they form neuroinsular complexes (9, 10). Anatomical heterogeneity and interspecies differences have been reported for pancreatic ganglia. The physiological significance of these differences, however, remains elusive (9, 11). Although the majority of pancreatic neurons is immunoreactive for cholinergic markers (ACh, VAChT, ChAT) and are thought to be postganglionic parasympathetic neurons (5, 12), only a fraction of them actually receives primary parasympathetic input (12, 13). In addition to cholinergic parasympathetic input, pancreatic ganglia also receive input from noradrenergic sympathetic neurons, substance P (SP)- and calcitonin gene-related peptide (CGRP)- positive sensory neurons, and serotonergic and cholinergic enteric neurons (12, 14–18). Thus, intrinsic neurons in pancreatic ganglia represent neuronal hubs that integrate multimodal extrinsic neuronal input and send an integrated message throughout the pancreas primarily *via* unmyelinated cholinergic projections (**Figure 2**). The histological and electrophysiological properties of pancreatic ganglia and their responsiveness to neurotransmitters, endocrine, and paracrine substances have been studied thoroughly [for a review, see (3, 5, 6)].

Most cholinergic terminals observed throughout the pancreas are thought to be projections of intrinsic pancreatic neurons (**Figure 2**). These fibers travel in the perivascular space and branch out to innervate the vasculature, endocrine cells of

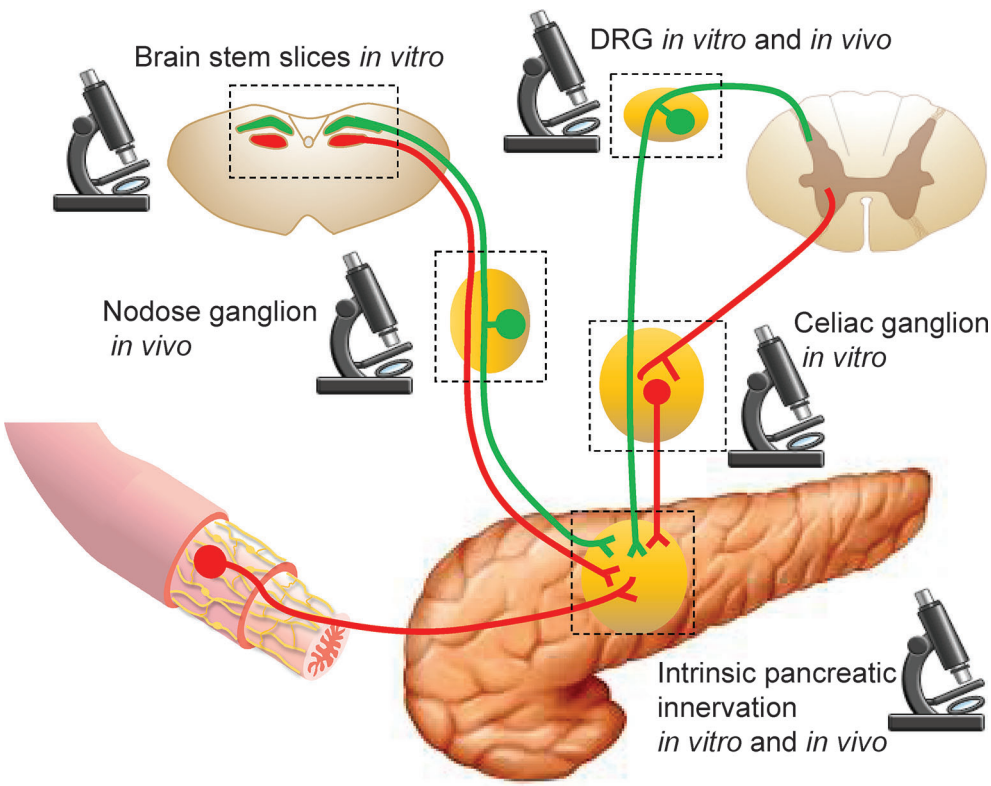

FIGURE 1 | Sites for imaging pancreatic innervation. Schematic representation of extrinsic sources of pancreatic innervation that converge on intrinsic pancreatic ganglia. Microscope icons indicate imaging sites.

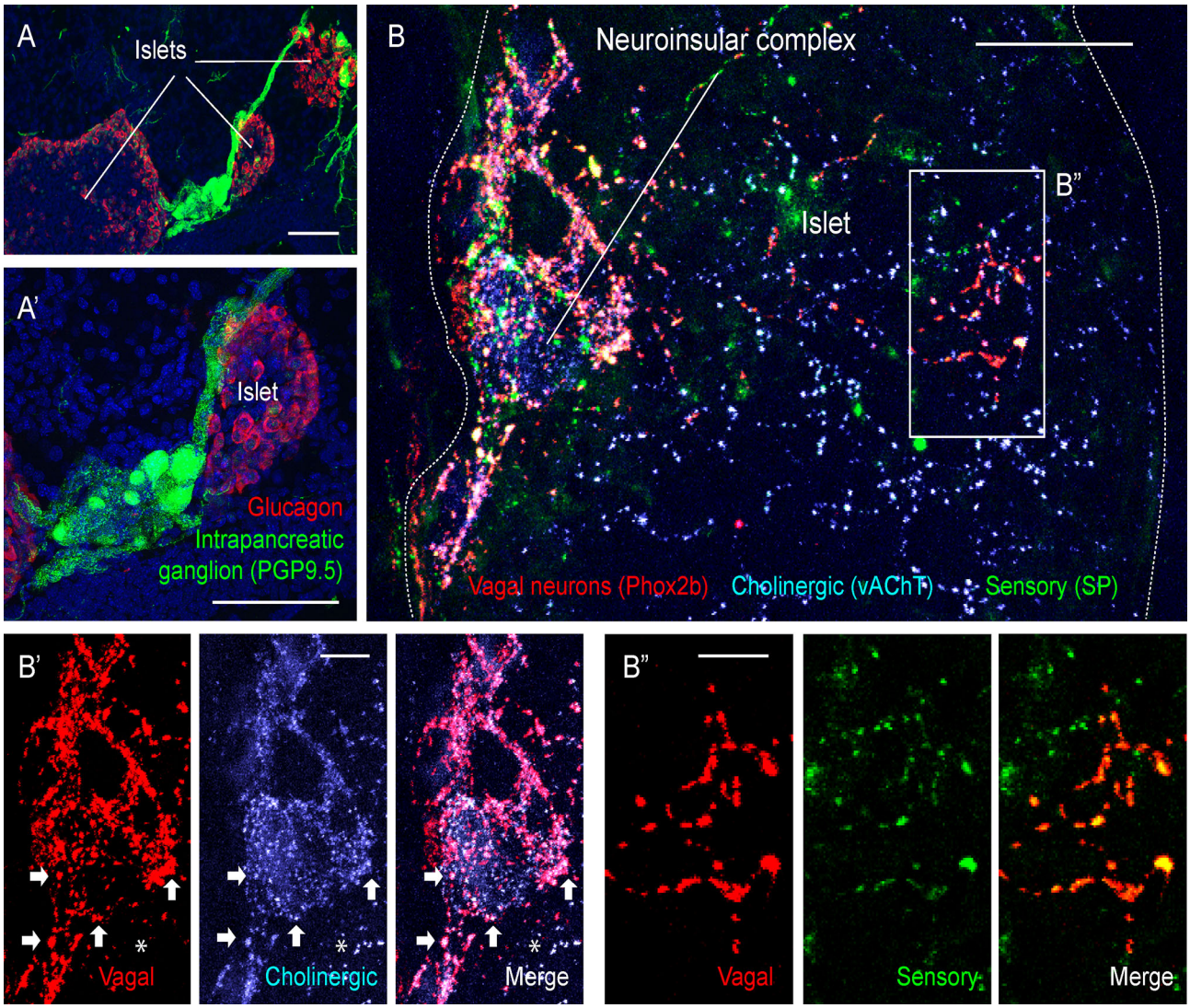

FIGURE 2 | Extrinsic and intrinsic cholinergic innervation of the endocrine pancreas (figure adapted and modified from Supplementary Figures 4, 5 in Makhmutova et al, 2020). **(A, A')** Mouse pancreatic section immunostained for the pan-neuronal marker PGP9.5 (green) and glucagon (red); scale bar 50 μm. **(B, B")** Pancreatic section of a Phox2b-Cre-tdTomato^{floxed} transgenic mouse, immunostained for red fluorescent protein (red), the sensory neuronal marker substance P (SP, green), and the cholinergic neuronal marker vesicular acetylcholine transporter (vAChT, blue). Inside the neuroinsular ganglion, Phox2b-positive varicosities colocalize with vAChT (**B'**, *arrows*), indicating terminals of vagal preganglionic neurons; scale bar 20 μm. Outside of the neuroinsular ganglion (inside the islet), Phox2b-positive fibers colocalize with SP **(B")** but not with vAChT (**B'**, *asterisks*), indicating vagal origin of sensory fibers and non-vagal origin of intrinsic cholinergic fibers; scale bar 5 μm.

pancreatic islets, exocrine acini, and the ductal system. Innervation of endocrine islets varies between species. In mouse islets, cholinergic fibers target α and β-cells, while in human islets endocrine cells are rarely contacted directly (9, 19). Interspecies differences raise many questions about postsynaptic targets, molecular mechanisms, and the physiological role of this innervation branch in the human endocrine pancreas.

Overall, stimulation of the intrinsic cholinergic system *via* multimodal extrinsic input is thought to activate the digestive state of the endocrine and exocrine pancreas by promoting vasodilation and increased secretion of insulin and exocrine enzymes. In parallel to its "rest and digest effects", cholinergic innervation is also an important player in mediating inflammatory responses in exocrine and endocrine pancreas (20, 21).

Extrinsic Pancreatic Innervation

Extrinsic neural input into the pancreas is composed of five autonomic branches: two efferent pathways – parasympathetic and sympathetic; two afferent pathways - vagal and spinal; and the entero-pancreatic axis. While primary parasympathetic neurons project exclusively to intrinsic ganglia, the other extrinsic branches also target pancreatic structures directly (12).

Parasympathetic Innervation

Primary parasympathetic neurons with cell bodies in the dorsal motor nucleus of vagus (DMV) (12) travel in the vagus nerve and synapse exclusively in the pancreatic ganglia without targeting acinar or endocrine structures directly (12). Both primary parasympathetic and intrinsic pancreatic neurons are cholinergic. These different neural populations have distinct embryological origins and can be distinguished by embryonic markers. Vagal neurons (both afferent and efferent) are derived from the neurogenic placodes and can be visualized and accessed using the placodal-specific Phox2b-Cre mouse line (**Figure 2**). The neural crest derived neurons (intrinsic pancreatic, splanchnic, and enteric) can be visualized and accessed using the neural crest-specific Wnt1-Cre line (22, 23). It is generally assumed that parasympathetic innervation brings strong excitatory input to the intrinsic pancreatic neurons, presumably *via* nicotinic cholinergic receptors (13, 16, 24–30). This input is intensely modulated by abundant extrinsic pathways at the level of the ganglia (31–35). Activation of the parasympathetic system facilitates the secretion of digestive enzymes and glucose-lowering insulin and is thought to be responsible for preparing the organ for an increased digestive demand during the cephalic phase (24, 28, 36–42).

Sympathetic Innervation

Primary sympathetic neurons reside in the intermediolateral column of the spinal cord and send projections to postsynaptic neurons of the perivertebral column and celiac ganglia *via* splanchnic nerves (36, 43). Noradrenergic projections of secondary sympathetic neurons enter the pancreas *via* mesenteric nerves and innervate pancreatic ganglia, vasculature, endocrine islets, ducts, and lymph nodes (**Figure 3**). Sympathetic activation leads to vasoconstriction, reduces exocrine secretion, and shifts endocrine secretion to the hyperglycemic state by lowering insulin and increasing glucagon levels (44, 45). In addition to this canonical sympathetic effect on pancreatic secretory function, several recent studies report an important interaction of sympathetic innervation

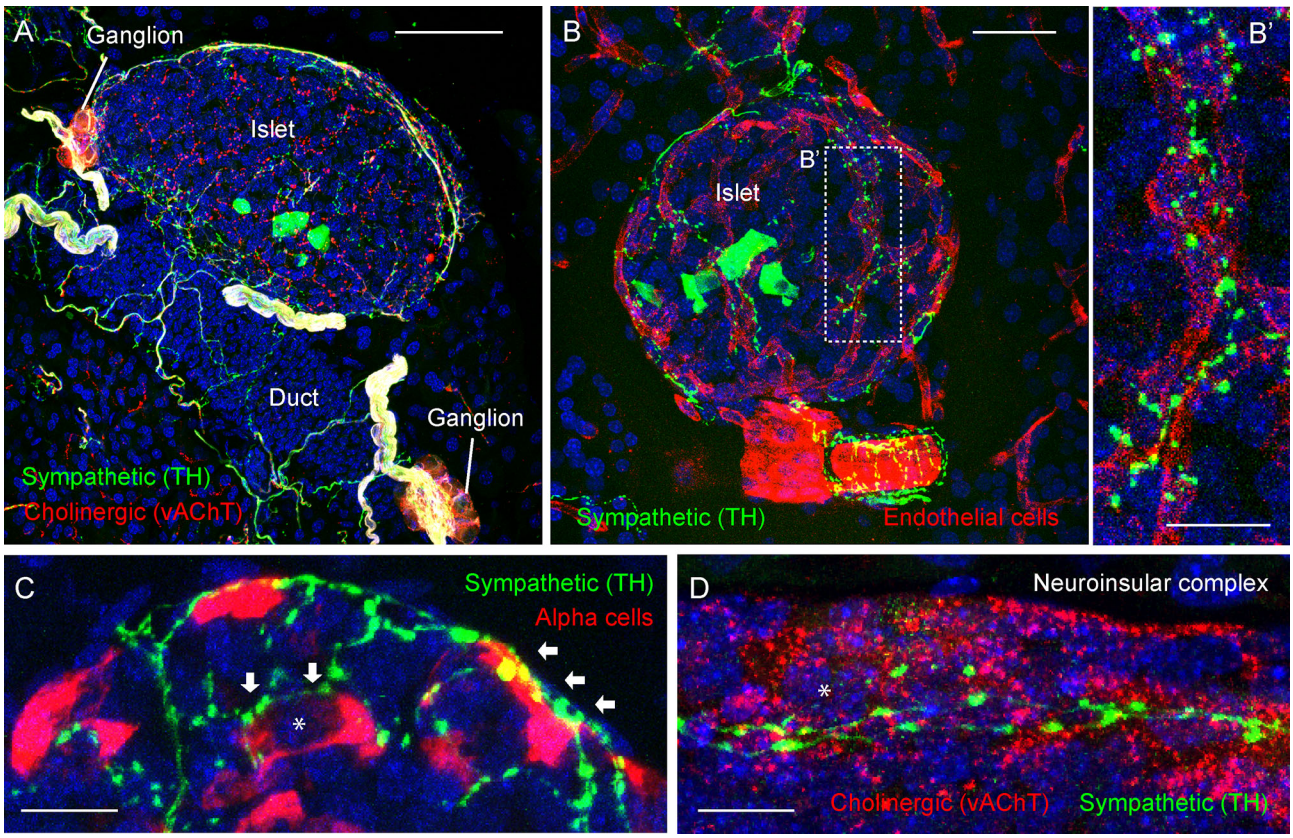

FIGURE 3 | Adrenergic innervation of the endocrine pancreas (photomicrographs are from experiments conducted by Dr. Joana Almaca, unpublished data). **(A)** Mouse pancreatic section immunostained for the sympathetic marker tyrosine hydroxylase (TH, green), the cholinergic marker vesicular acetylcholine transporter (vAChT, red), and DAPI (blue); scale bar 50 μm. **(B-B')** Mouse pancreatic section immunostained for TH (green), endothelial marker CD31 (red), and DAPI (blue); scale bars 20 μm **(B)** and 10 μm **(B')**. **(C)** Mouse pancreatic section immunostained for TH (green), glucagon (red), and DAPI (blue); scale bar 10 μm. **(D)** Mouse pancreatic section immunostained for TH (green), vAChT (red), and DAPI (blue); scale bar 10 μm. TH-positive fibers can be seen along the perivascular space of a large blood vessel **(B)** and intra-islet capillaries **(B')**. TH-positive varicosities contact endothelial vascular cells **(B')**, endocrine α-cells (*arrows* in **C**), and neurons within a neuroinsular complex **(D)**. Asterisks denote an alpha cell (in **C**) and a neuron (in **D**).

with the pancreatic immune system (14, 46, 47), which could be involved in the development of autoimmune diabetes (48).

Sensory Innervation

The pancreas receives both vagal and spinal sensory innervation. Vagal sensory neurons have cell bodies in the nodose ganglion and their projections travel alongside parasympathetic efferent fibers in the vagus nerve. Spinal sensory neurons originating bilaterally in the T9-T13 dorsal root ganglia travel alongside sympathetic fibers in splanchnic and mesenteric nerves. Substance P- and CGRP-positive sensory fibers are found throughout exocrine tissue and in the majority of pancreatic islets. Vagal sensory fibers project preferentially to pancreatic islets, indicating that the exocrine sensory component is primarily of spinal origin (**Figure 2**), although a contribution of spinal afferents to islet innervation has also been reported (49–51). Pathologies of the exocrine tissue such as cancer and pancreatitis are usually perceived as very painful and associated with increases in sensory innervation (52, 53). Diabetes and insulinomas, by contrast, seem to develop without significant sensory awareness. Moreover, vagal afferents in the pancreas are chemosensors, while spinal afferents are preferentially mechanosensitive (14, 54). This supports the idea that vagal and spinal sensory pathways carry different sensory modalities: the vagal being more of homeostatic nature, while the spinal being more nociceptive. A small percentage of intrinsic pancreatic neurons in mice and human pancreas are substance P-positive, suggesting that the intrinsic pancreatic innervation might contain a sensory component. However, its sensory properties and physiological role remain elusive (11).

Enteric Innervation

The least studied and perhaps most intriguing neuronal input to the pancreas comes from the gut and is referred to as entero-pancreatic innervation. Tracing studies show that the neuronal plexus of the stomach antrum and proximal duodenum extends to the pancreas, sending cholinergic and serotonergic projections preferentially to intrinsic ganglia, and more sparsely to the acinar tissue, endocrine cells, vasculature, and ducts. While it is difficult to distinguish enteric cholinergic input from vagal parasympathetic and intrinsic cholinergic fibers, serotonergic terminals in the pancreas seem to originate exclusively from the enteric nervous system. The effect of serotonergic innervation on pancreatic neurons is not straightforward since the latter express both excitatory [5HT3R (55)], and inhibitory [5HT1 (55, 56)], receptors and intraluminal intestinal stimulation has been shown to elicit both excitatory (17, 57) and inhibitory (31) effects on pancreatic neurons and pancreas secretion. The enteric neuronal input to the endocrine pancreas has not been studied yet.

Intrinsic pancreatic neurons not only receive neuronal input from the gut (58), but also share anatomical similarities and embryonic origin with the enteric nervous system (8, 59, 60). Throughout her early work, Kirchgessner has been advocating for a continuity of the pancreatic network with the enteric nervous system (8, 59, 60). Moreover, vagotomy and sympathectomy have little effect on intrinsic pancreatic innervation (2), suggesting some degree of autonomy of the entero-pancreatic network from the central nervous system.

CHALLENGES FOR STUDYING PANCREATIC INNERVATION

In their early work on pancreatic innervation, Rudolf Heidenhein, Claude Bernard, and Ivan Pavlov acknowledged that studying pancreatic physiology and especially its innervation is by far a more challenging task than studying the innervation of other secretory glands (1, 61). They described the pancreas to be highly sensitive to surgical manipulations and experimental results to be extremely variable. Pavlov explained some of the experimental variability as a result of complex antagonistic interactions of innervation circuits and neuronal sensitivity to experimental conditions. Indeed, intrinsic pancreatic innervation receives multimodal input from all possible extrinsic innervation sources. Thus, output from intrinsic cholinergic neurons is a cumulative response to all extrinsic inputs, not a classical parasympathetic pathway. This is further complicated by the effects of extrinsic innervation on cardiovascular, exocrine, and endocrine systems, by the central nervous system feedback triggered by afferent innervation, and by local neuronal reflexes of the entero-pancreatic innervation.

The pancreas performs two very distinct yet essential functions: production of digestive enzymes by the exocrine compartment and secretion of the glucoregulatory endocrine hormones by its endocrine compartment. The pancreatic innervation is thus designed to control both exocrine and endocrine functions and target very distinct cell types. This heterogeneity, however, is very difficult to disentangle and make sense of.

The majority of axonal terminals inside the pancreas are non-myelinated axons that are difficult to visualize. For instance, in their work on sympathetic innervation of the pancreas, Alm et al. noticed that sympathetic terminals around small capillaries were very thin (under 0.2 um) and contained unusually low levels of catecholamines (at least 100 fold lower of what has been observed in other tissues), making visualization of such fibers only possible after catecholamine-increasing treatment with L-Dopa or dopamine (62). To improve visualization of axonal terminals, a wide range of transgenic reporter mice is now available along with advanced viral neuronal tracing techniques.

Neuronal fibers in the pancreas do not form classical synapses with well-defined pre- and post-synaptic structures. Instead, they contain neurotransmitter-rich varicosities along their path and release their contents into the surrounding space affecting nearby target cells with appropriate receptors. This makes innervation effective in its ability to affect multiple targets simultaneously and introduces another level of physiological complexity but hinders the identification of postsynaptic targets and physiological effects.

Despite a wide body of literature on pancreatic innervation, many physiological and even anatomical questions remain unanswered and need to be addressed. Modern neuronal labeling and imaging techniques introduce means for overcoming many technical challenges and tackling those questions (**Table 1**).

TABLE 1 | Open questions in the field of pancreatic innervation.

Innervation Branch	Open questions in the field
Intrinsic pancreatic innervation	• Differences in postganglionic cholinergic innervation of rodent and human endocrine pancreas raise many questions about postsynaptic targets, molecular mechanisms, and the physiological role of this innervation branch in different species. • The role of neuroinsular complexes and how they differ from other intrinsic ganglia that are not directly associated with endocrine islets remains unknown. • The anti-inflammatory effect of cholinergic innervation on resident macrophages has been proposed, but not confirmed.
Parasympathetic	• Although the vago-vagal reflex has been proposed to be involved in the regulation of glucose metabolism, the parts of the circuit have not been linked together. It has not been determined if the parasympathetic efferent output depends on vagal sensory input from the pancreas. • Hypothalamic and higher brain centers control of parasympathetic innervation in glucose metabolism is not fully understood. • The anti-inflammatory properties of parasympathetic innervation have been described systemically as well as in many visceral systems, but has been barely studied in the pancreas.
Sympathetic	Adrenergic neurons innervate pancreatic islets and draining lymph nodes and are suspected to be important players in the pathogenesis of autoimmune diabetes. The anatomical, physiological, and molecular properties of the interactions between sympathetic neurons and the local components of the immune system requires further research.
Enteric	Extensive tracing studies suggest that the enteric nervous system extends projections into the pancreas. The physiological significance of the entero-pancreatic network, however, is poorly understood.
Sensory	• Sensory transduction mechanisms and sensory modalities transmitted via spinal and vagal afferents are not well understood. • Although systemic manipulation of sensory innervation affects glucose metabolism, it is still not clear if and how pancreas-specific sensory pathways affect glucose metabolism and exocrine secretion, and whether the vagal sensory component is involved in the mediation of the vago-vagal reflex. • The etiology and pathogenesis of chronic pain in pancreatitis and pancreatic cancer is widely studied, but still not fully understood. • Sensory innervation is proposed to be an important mediator in pathogenesis of pancreatic cancers.

THE ARSENAL OF FLUORESCENT TOOLS TO STUDY PANCREATIC INNERVATION

A significant research effort focuses on developing non-invasive imaging approaches with the use of magnetic waves, ultrasound, and radiation. These techniques, unfortunately, are not sensitive enough to visualize peripheral innervation. Fluorescence microscopy is one of the most informative experimental approaches in neuroscience today as it has capacity not only for structural visualization but also for functional imaging and optical manipulation of delicate neuronal structures. Limited light penetration, however, requires tissue isolation or quite invasive *in vivo* preparations that restrict this technique to the experimental niche. Here we will discuss fluorescent neuronal labeling and existing approaches of optically accessing intrinsic and extrinsic pancreatic innervation.

The neuroscience field offers a wide variety of tools for neuronal labeling. These include antibody-dependent techniques, genetically encoded reporters, and neuronal dyes for structural and functional imaging (**Tables 2**–**4**). While most neuronal markers are shared between different neuronal types, several reporters allow to distinctively label major peripheral branches of innervation: cholinergic (vAChT, ChAT), adrenergic (TH), and sensory (SP, CGRP, TRPV1) fibers (**Table 2**). Some neurons can further be distinguished by placodal or neural crest embryonic origin markers (**Table 2**). Sequencing studies of peripheral neuronal ganglia identify unique markers for peripheral innervation providing deeper molecular and genetic characterization for various neuronal types (63, 64). These markers are then used as guides for developing neuronal antibodies and generating transgenic reporters of selective neural pathways.

Antibody dependent neuronal labeling is a classical immunohistochemical approach for structural delineation of neuronal pathways. It is, however, limited by antibody specificity, tissue penetration, and epitope availability. While few neuronal markers are abundantly expressed (Pgp9.5, b-Tubulin) throughout a neuron, localization of most neuronal epitopes can vary along the neural process (i.e. axon). Thus, antibodies do not label neuronal shafts uniformly and do not always allow delineating fine neuronal projections and terminals. Although labeling of living non-permeabilized neurons with antibodies against neuronal surface markers has been reported, it is very uncommon and only suitable to homogeneous neuronal cultures (65). Neuronal antibodies are preferentially suited for histology in fixed tissue.

Neurons can be targeted specifically by driving expression of fluorescent reporter proteins or transcriptional drivers under a neuron-specific promoter. This provides flexible access to neuronal populations for structural and functional imaging and for neuronal manipulations. Transgenic animal models that drive expression of either Cre-recombinase, fluorescent reporters, or Ca^{2+} indicators are available for the most common neuronal promoters (**Tables 2**, **3**). Work with transgenic animals, however, requires validation of gene expression specificity since transgene expression does not always reflect endogenous promoter activity. Wonderful reviews summarize currently existing transgenic tools for targeting central and peripheral innervation (66, 67). Transgenic labeling is widely used for structural imaging because it allows efficient labeling of neuronal projections that greatly complements antibody-dependent neuronal labeling. To allow physiological recording of neuronal activity *in vivo* and in living pancreatic slices, neuronal promoters and Cre-drivers can be coupled to expression of the genetically encoded calcium indicator GCaMP. Analogously, transgenic expression of optogenetic (channelrhodopsin), chemogenetic (DREADD), and magnetogenetic (TRPV1-ferritin) receptors provides access to neuronal manipulation.

TABLE 2 | Neuronal markers, antibodies, mouse transgenic lines, and promoters for neuronal labeling.

Innervation type	Marker	Antibodies validated in the pancreas	Promoters/Transgenic lines
Cholinergic (primary parasympathetic, primary sympathetic, intrinsic pancreatic)	ACh		N/A
	vAChT	139103, Synaptic Systems	SLC18A3-cre (PMID: 14502577)
	ChAT		ChAT-eGFP (Jax 007902)
			ChAT-Cre (Jax 006410)
Adrenergic (secondary sympathetic)	TH	AB152, Millipore	TH-Cre (Jax 008601)
Peptidergic-sensory (vagal afferents, spinal afferents, intrinsic sensory)	SP	MAB356, Millipore	Tac1-Cre (Jax 021877)
	CGRP	BML-CA1134, Enzo	CALCA-Cre/eGFP (Jax 033168)
	TRPV1	Alomone labs ACC-030	TRPV1-Cre (Jax 017769)
	5HT3R		5HT3R-GFP (PMID 19095802)
			5HT3R-Flpo (Jax 030755)
	Pirt		Pirt-GCaMP3 (JHU C13628)
			Pirt-Cre (JHU C13783)
Serotonergic (enteric)	5HT		N/A
Placodal-derived (vagal afferent and efferent)	Phox2b		Phox2b-Cre (Jax 016223)
Neural Crest-derived	Wnt1		Wnt1-Cre (Jax 022137)
Pan-neuronal markers	b3Tub	MRB-435P, Covance	TUBB3-eGFP (MGI:4847518)
	Pgp9.5	#233003, Synaptic Systems	UCHL1-eGFP (Jax 022476)
	Thy1		Thy1-Cre (Jax 006143)
	Snap25		Snap25-GCaMP6 (Jax 025111)
	Synaptophysin (Syp)		Syp promoter
			RC::FPSit (Jax 030206)
			Ai34D (Jax 012670)
	Synapsin (Syn)	Cell Signaling Technology 5297	Syn1-Cre (Jax 003966)
		#106011C5, Synaptic Systems	hSyn - most common AAV promoter on AddGene
	Acetylated tubulin	T6793, Sigma	TUBA1A promoter
	NeuN		RBFOX3 promoter
	S100	ab52642, Abcam	S100b-Cre (Jax 014160)
	NF200	Sigma-Aldrich N4142	
	cFos	#226003, Synaptic Systems	TRAP2 (Jax 030323)

TABLE 3 | Examples of Cre-dependent reporter mouse lines for neuronal labeling.

	Reporter line	Stock number	Use
Structural reporters	ROSA26-eGFP	Jax 004077	eGFP reporter
	Ai6	Jax 007906	Ubiquotous expression of ZsGreen1 reporter throughout dendrites and long axons
	Ai14	Jax 007914	Ubiquotous expression of tdTomato reporter throughout dendrites and long axons
Functional reporters	Ai95	Jax 028865	Ca^{2+} indicator GCaMP6f (fast response kintetics)
	Ai96	Jax 028866	Ca^{2+} indicator GCaMP6s (slow response kinetics)
	TRAP2	Jax 030323	Cre-dependent reporter expression in active neurons expressing immediate early gene cFos
Neuro-modulators	Ai32	Jax 012569	Channelrhodosin-2/eYFP fusion protein for optogenetic stimulation
	RC::FPDi	Jax 029040	Inhibitory DREADD-mCherry fusion protein for pharmacogenetic inhibition
	RC::L-hM3Dq	Jax 026943	Excitatory DREADD-mCherry fusion protein for pharmacogenetic stimulation

Viral delivery of transgenes allows targeting neurons specifically with improved spatial and temporal resolution (68). Pancreatic neurons can be transfected by injecting the virus into the pancreatic parenchyma (69), infusing the pancreas with the virus through the common bile duct (70), or by less specific injections into extrinsic neuronal ganglia. Viruses are excellent for long range neuronal tracing and neuronal manipulation *in vivo* and can potentially be used with pancreatic slices *in vitro*. Because pancreatic tissues are very heterogeneous, neuronal specificity of viral transfection requires the use of neuron-specific or Cre-dependent viral vectors and viral particles with increased neuronal tropism.

Being replaced by transgenic animal models and viral tracing approaches, conventional neuronal dyes are unjustly placed on the sideline of neuroscience research today. Compared to transgenic reporters, neuronal dyes are relatively inexpensive and allow acute neuronal labeling across different species, which can be especially advantageous for assessing innervation in human tissues (e.g. in living pancreas slices from human pancreatic donors). Cytoplasmic and membrane dyes are useful tools for structural assessment of innervation and can be used for long-range neuronal tracing *in vivo*, local neuronal labeling in living pancreatic tissue slices, and even in fixed tissues (in the case of DiI, **Table 4**). Functional neuronal dyes allow to

TABLE 4 | Conventional dyes for neuronal labeling.

	Neuronal dye	Labeling properties	Cell loading
Cytoplasmic	Hydrazides and Biocytins	Intracellular bidirectional tracer Assesment of gap junctions	enter cells by microinjection and iontophoresis, may cross gap junctions
	Dextran conjugates	Intracellular bidirectional tracer	enter cells by microinjection and through resected neuronal terminals
Membrane-bound	Choleratoxin subunit B (CTB)	membrane-bound bidirectional tracer	Binds to plasma membrane glycosphingolipids
	Lectins (WGA, Phaseolus Vulgaris, DBA, GS)	membrane-bound bidirectional tracer have limited trans-synaptic labeling capacity (WGA)	Bind various plasma membrane carbohydrates
	DiI	Lateral diffusion in plasma membrane Bidirectional tracer Can be used in live or fixed tissue	Lipohilic dye, incorporates into lipid bilayer
Functional	AM and FM dyes	Non-fluorescent in aqueous solution, become fluorescent upon internalization	Enter cells by endocytosis or through non-selective ion channels Internalization can be activity-dependent
	Calcium indicator dyes (Fluo-4, Fura-2)	Become fluorescent upon Ca^{2+} binding, Activity-dependent	Esterified dyes are membrane permeable, trapped inside cells after cytoplasmic de-esterification
	Voltage-sensetive dye (FluoVolt, ANEP)	Become fluorescent upon changes in electrical potential	Bind plasma membranes (FluoVolt), membrane-permeable (ANEP)

monitor neuronal activity either by binding intracellular signaling molecules (Ca^{2+} and cAMP indicators), responding to changes in electrical potential (membrane voltage dyes), or by activity-dependent internalization of the dye (AM and FM dyes, **Table 4**). The majority of conventional dyes, however, have limited neuronal specificity and thus must be applied locally.

STRUCTURAL IMAGING OF INNERVATION IN FIXED PANCREAS TISSUES

In the field of islet biology, the most common histological approach for studying endocrine cells involves widefield imaging of thin tissue sections (<10 μm). This, however, is not suitable for studying neuronal projections that with elaborate three-dimensional terminal trees. Thicker pancreatic cryo-sections (40-60 μm) allow sufficient antibody penetration, excellent access to confocal imaging, and easy histological processing on the slide without harsh clearing protocols (**Figures 2**, **3**). Confocal imaging of thick pancreatic cryo-sections allowed delineating parasympathetic and sympathetic innervation, reconstructing axonal terminals in 3D in human and mouse pancreatic tissues with excellent spatial resolution, and identifying their potential postsynaptic targets (19, 22).

The now popular technique of organ clearing allowed whole pancreas imaging and 3D reconstruction of entire pancreatic innervation. This technique is especially informative in understanding innervation continuity and heterogeneity throughout the whole pancreas and gives a better perspective on connectivity between endocrine and exocrine compartments (9, 11, 71–74). While advantageous for studying neuronal connectivity and histology of large neuronal structures such as neuronal ganglia and large neurites, this approach is not always adequate for analyzing fine neuronal terminals and their postsynaptic targets due to limited subcellular resolution. Moreover, tissue clearing involves use of harsh organic compounds which may interfere with epitope preservation, and usually requires lengthy incubations (days to weeks).

LIVE IMAGING OF PANCREATIC INNERVATION

Live imaging of innervation requires making target tissues visually accessible without significantly interfering with tissue physiology. Intrinsic pancreatic innervation and extrinsic neuronal terminals can be imaged at the level of the pancreas either in the intact pancreas or in living pancreatic slices. Extrinsic pancreatic innervation can also be imaged outside of the pancreas in corresponding extrinsic ganglia. Innervation of pancreatic islets can be studied longitudinally after transplantation into the anterior chamber of the eye. To avoid all the hurdles of exposing innervation in rodent models, pancreatic innervation can be studied in transparent animal models such as zebra fish. And finally, islet innervation can be studied in artificial setting of co-culture of pancreatic islets and primary neurons.

In Vivo Imaging of Intact Pancreas (Exteriorized Pancreas and Intravital Window)

The pancreas can be partially exteriorized and imaged acutely in anesthetized animals (46, 75–77). For gaining longitudinal optical access to the pancreas, several recent studies report the use of an intravital window installed into the abdominal wall. Unlike a very stable cranial window attached to the scull, the abdominal window is attached to the muscle, is more prone to movement and requires additional fixation of the pancreas to stabilize the field of view. Pancreas exteriorization and abdominal window provide access for imaging superficial structures at cellular resolution. Although innervation has never been imaged at the level of the intact pancreas *in vivo*, several studies report effective imaging of pancreatic endocrine cells, immune cells, and vasculature (46, 75–77), suggesting that this approach can potentially be used for imaging superficial large neuronal structures such as pancreatic ganglia and neuroinsular complexes. However, due to limitations of optical tissue penetration and residual tissue movement, this technique is not ideally suited for imaging fine neuronal projections and terminals.

Living Pancreatic Slices

Mouse and human pancreatic tissue slices are becoming a common tool for studying endocrine, exocrine, and vascular physiology (78–81). Living pancreatic slices provide optical access to deep pancreatic structures with a partially preserved native microenvironment. Slices with a thickness of 120-150 um can be almost entirely visualized with confocal microscopy, allowing high resolution imaging of fine neuronal terminals [**Figure 4** (14)]. Many neuronal terminals in the slice, however, end up being cut from their neuronal soma and therefore might maintain their responsiveness for a short period of time or change their physiological properties. Moreover, labeling efficiency of fine neuronal projections in the pancreas remains problematic. In our experience, animals expressing a knock in GCaMP3 gene under the Pirt promoter have strongly labeled pancreatic terminals (**Figure 4**), while terminals could not be visualized in Pirt-Cre-GCaMP6 mice (14). Despite these challenges, this approach has proven itself effective for imaging various pancreatic cell types, including neuronal terminals, and holds a lot of potential for functional imaging of pancreatic innervation.

Functional imaging of living tissue slices from human donors is an invaluable resource for studying physiology of human pancreas. Although functional studies of human pancreatic innervation have not been reported yet, we assume it is possible but challenging due to difficulties in neuronal labeling and the high neuronal vulnerability to ischemia with its associated anoxia.

Eye Model for Studying Islet Transplants

A creative attempt that is complementary to imaging the intact pancreas and pancreatic tissue slices is the "eye model" of noninvasive longitudinal imaging of pancreatic islets (82, 83). In this approach, islets isolated from the donor (mouse or human) are transplanted into the anterior chamber of the eye of a recipient mouse. Islets engraft on the iris of the eye, vascularize and establish innervation (**Figure 5**). The eye, in this case, plays a role as a natural imaging chamber and allows noninvasive longitudinal imaging with minimal movement artifacts in head-fixed anesthetized animals. Interestingly, once engrafted, the iris' autonomic nerves innervate the islet. The newly developed islet

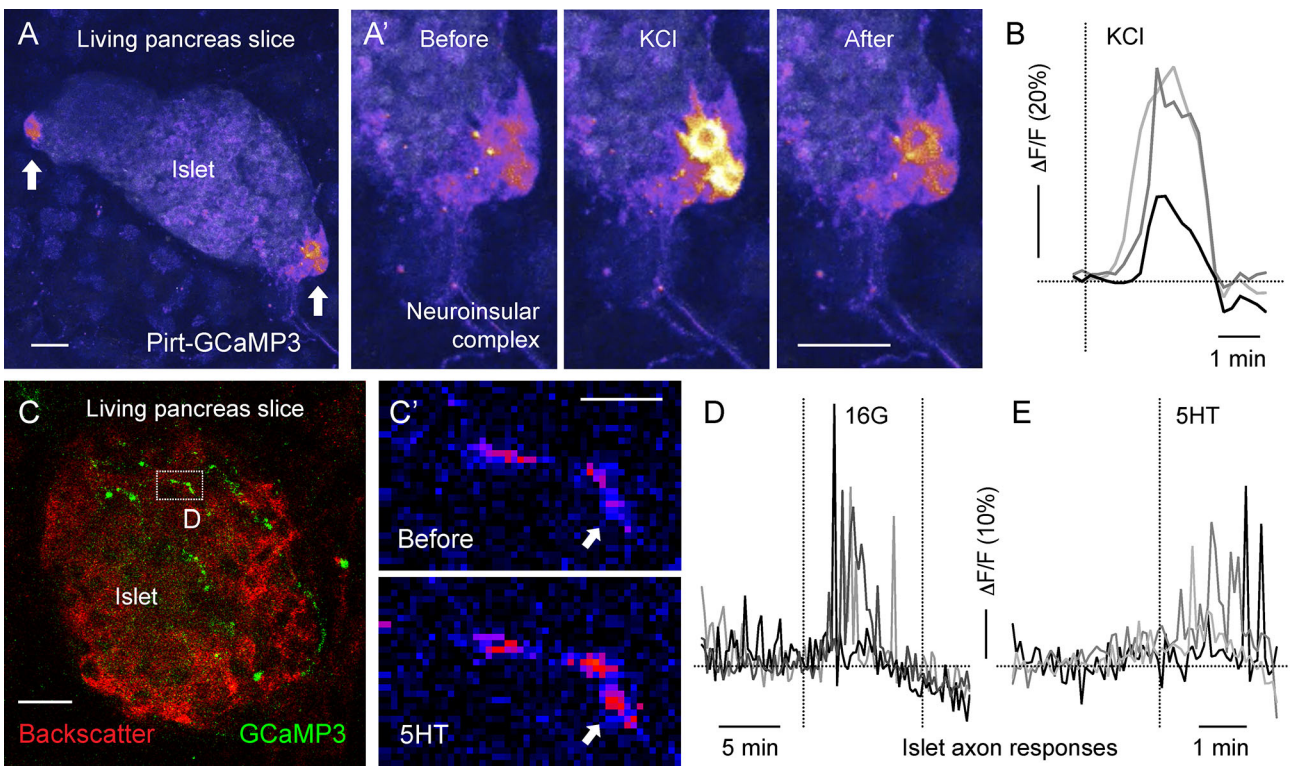

FIGURE 4 | Living mouse pancreatic slices for imaging Ca^{2+} activity in neuroinsular ganglia and in sensory axonal terminals [photomicrographs are from experiments conducted by Dr. Jonathan Weitz, **(A, B)** unpublished data, **(C–F)** adapted and modified from Figure 6 in Makhmutova et al, 2020]. **(A, C)** Z-stacks of confocal images of living pancreatic slices from Pirt-GCaMP3 mice. **(A)** A representative islet containing neuroinsular ganglia (*arrows*), with GCaMP3 fluorescence and islet backscatter shown in pseudocolor scale; scale bar 10 µm. (A') Sequential images of the neuroinsular ganglion shown in A, displaying a Ca^{2+} response to KCl (25 mM). **(B)** Representative traces of mean fluorescence intensity changes over baseline (δF/F) in the neuroinsular ganglion shown in **(A')**, demonstrating neuronal responses to KCl stimulation. **(C)** Representative islet containing GCaMP3-expressing sensory axonal terminals (green). Islet backscatter is shown in red; scale bar 20 µm. **(C')** Sequential images of the sensory fiber shown in C (box), displaying a Ca^{2+} response to 5-HT (50 µM). The *arrow* points to a region showing an increase in GCaMP3 fluorescence (pseudocolor scale); scale bar 5 µm. **(D, E)** Representative traces of mean fluorescence intensity changes over baseline (δF/F) in sensory fibers, demonstrating responses to an increase in glucose concentration from 3 mM to 16 mM (16G, **D**) and to 5-HT (50 µM) stimulation **(E)**.

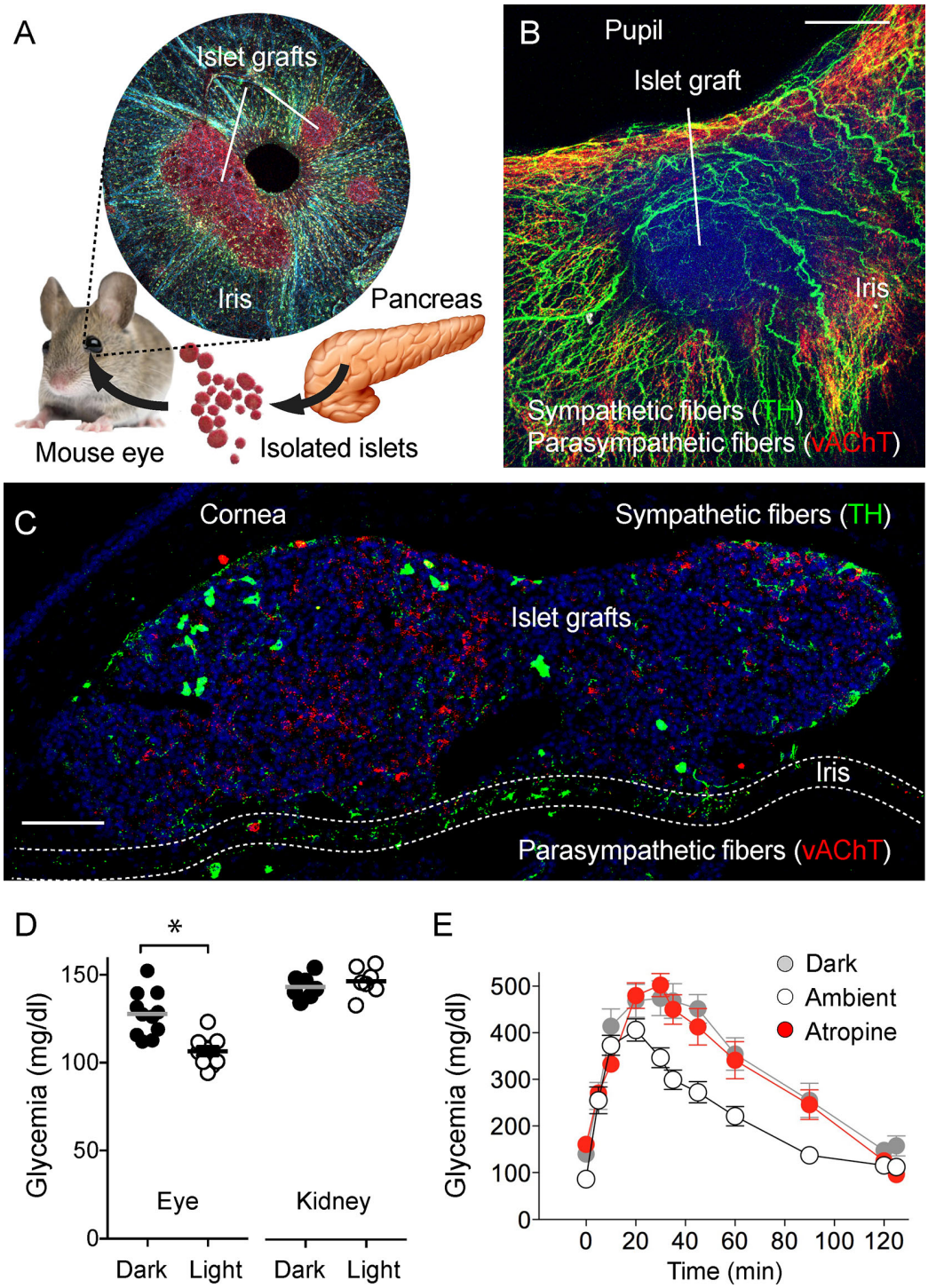

FIGURE 5 | Eye model for imaging innervation of pancreatic islet grafts [photomicrographs are from experiments conducted by Dr. Rayner Rodriguez-Diaz (**A–C**, unpublished data], data in **(D)** and **(E)** adapted and modified from Figure 4 in Rodriguez-Diaz et al., 2012). **(A)** Schematic representation of islet transplantation into the anterior chamber of the eye. Islets isolated from the pancreas are transplanted into the mouse eye. Microphotograph of an iris wholemount with islet grafts. **(B)** Z-stack of confocal images of a wholemount of the mouse iris with an islet graft immunostained for TH (green) and vAChT (red); scale bar 50 µm. **(C)** Confocal image of a cross-section of the mouse eye showing two islet grafts, stained for TH (green), vAChT (red), and DAPI (blue); scale bar 50 µm. **(D)** Plasma glucose levels in mice transplanted with islets in the anterior chamber of the eye or under the kidney capsule, in ambient light or in the dark (*$p < 0.05$, paired Student's t-test). **(E)** Glucose excursion during an IPGTT of transplanted mice performed in the dark (gray symbols), ambient light (open symbols), or in ambient light after topical application of the muscarinic receptor antagonist atropine (red symbols).

innervation thus becomes dependent on the pupillary light reflex. When the light is on, parasympathetic stimulation triggers pupillary constriction and induces insulin secretion in engrafted islets. In dark ambient conditions, sympathetic activation triggers the pupil to dilate, and insulin secretion returns back to baseline levels (84). While the peripheral innervation of the islet graft and responses of the graft to neuronal stimulation are physiologically accurate, the neuronal pathways are not linked to the autonomic centers innervating the pancreas.

Imaging Extrinsic Nuclei and Ganglia That Send Neuronal Projections to the Pancreas

Axonal terminals of extrinsic innervation can be studied at the level of the pancreas using the approaches listed above. Extrinsic innervation can also be examined at the level of the neuronal cell bodies that reside in brain nuclei or peripheral ganglia outside of the pancreas.

The dorsal vagal complex of the brainstem includes dorsal motor nucleus of vagus (DMV), composed of primary parasympathetic neurons, and the nucleus of the solitary tract (NTS), the region that receives sensory input from vagal sensory neurons. This site is believed to be an integral part of the vago-vagal reflex. Although the existence of this reflex has been confirmed for the exocrine pancreas (85), and has been proposed for the endocrine pancreas, a pancreas-specific pathway in the dorsal vagal complex remains to be described. Neurons of the dorsal vagal complex can be labeled by tracing from the pancreas (14, 69, 86) or by activity-dependent genetic labeling (87) induced by pancreas-specific stimulation. Once labeled, these neurons can be studied using imaging approaches *in vivo* or in brainstem slices (88, 89).

Celiac ganglia are the largest ganglia in the peripheral nervous system and are the major site of postganglionic sympathetic neurons innervating the pancreas (43, 90). Although sympathetic neurons have been extensively studied morphologically and electrophysiologically (91), a characterization of sympathetic subpopulations based on innervation targets is still lacking. Perhaps investigators were not motivated to do so because of the common notion that sympathetic stimulation induces a uniform inhibitory effect on digestion. Recent studies, however, are revealing

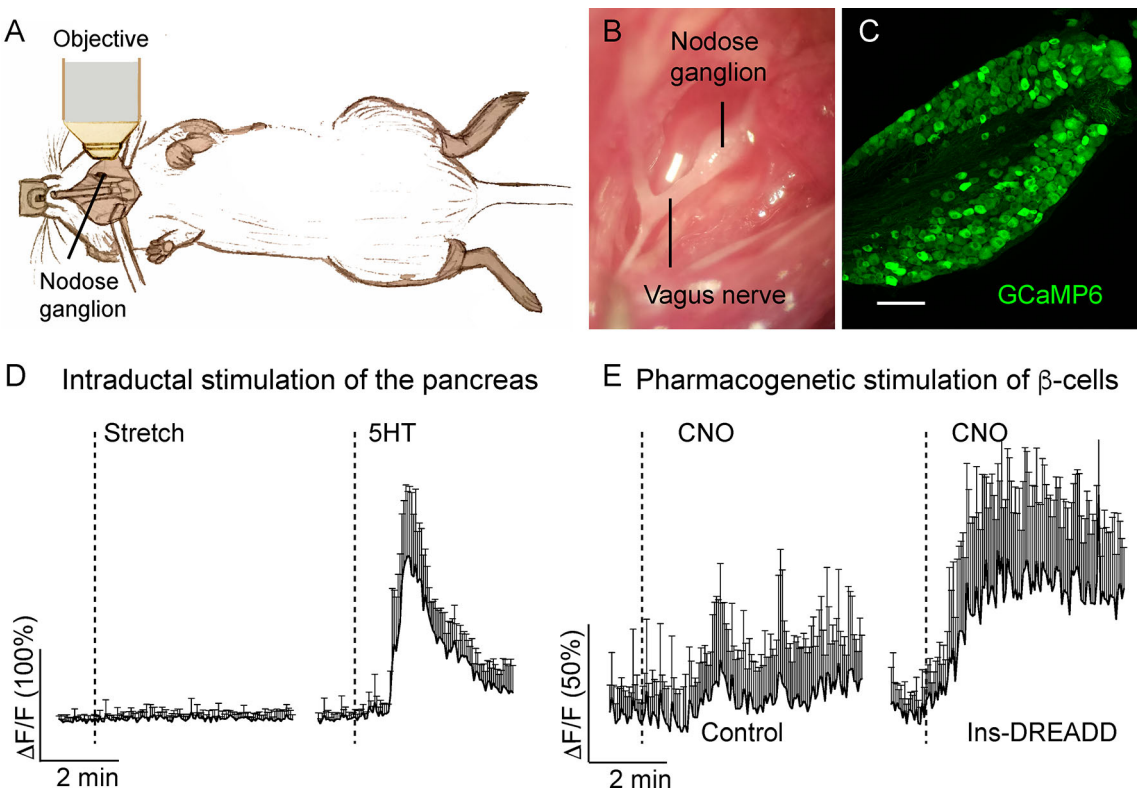

FIGURE 6 | *In vivo* imaging of the mouse nodose ganglion (figure adapted and modified from Figures 3, 4 in Makhmutova et al, 2020). **(A)** Drawing illustrates the experimental set up, where the intact nodose ganglion is exposed for Ca^{2+} imaging under a confocal microscope. **(B)** Photomicrograph of the exposed nodose ganglion. **(C)** Section of the nodose ganglion from a Pirt-GCaMP6 mouse. **(D)** Average traces of fluorescence intensity changes over baseline (δF/F) in nodose ganglion neurons, demonstrating neuronal responses to stretch (intraductal pancreatic infusion with saline, 300 µl/min) or intraductal application of 5-HT (1 mM, 150 µl/min). **(E)** Average traces of fluorescence intensity changes over baseline (δF/F) in nodose ganglion neurons, demonstrating neuronal responses to pharmacogenetic stimulation of β-cells by i.p. injection of clozapine nitric oxide (CNO, 5 mg/kg) in control mice or in mice expressing designer receptor activated by designer drug (DREADD) exclusively in β-cells. Shown is the mean trace of 10 neurons (+/- SEM).

an important interaction of sympathetic nerves with the immune system, particularly with immune cells of lymph nodes associated with the pancreas (14, 46, 47). A characterization of postganglionic sympathetic neurons therefore becomes physiologically and even clinically relevant. Although *in vivo* imaging approaches of the celiac ganglia have not been developed yet due to its inaccessible anatomical localization, explants of the ganglia can be studied morphologically and physiologically using immunohistochemical and calcium imaging approaches in combination with retrograde tracing from the pancreas.

Nodose and dorsal root ganglia (DRGs) are respectively the sensory ganglia of the vagal and spinal sensory pathways that receive input from the pancreas (50). Because sensory innervation has been attributed a role in the maintenance of glucose homeostasis (49, 92, 93), decoding the signals at the level of the primary sensory neuron becomes an essential step in understanding the type of information the pancreas is transmitting to the brain *via* autonomic nerves. By recording activity of nodose ganglion neurons *in vivo*, we showed that these neurons are pancreatic chemosensors, responsive to selective stimulation of β-cells, presumably *via* serotonin-dependent mechanism, and are not sensitive to mechanical stimulation of the pancreas (**Figure 6**) (14) The sensory modality transmitted through the DRG remains to be discovered, but *in vivo* imaging of the DRG is technically challenging (94).

In Vivo Imaging of Pancreatic Innervation in Zebra Fish (PMID: 29916364)

The zebra fish is an experimental model that has been used for studying multiple aspects of pancreas biology including pancreatic development, endocrine cell regeneration, vascularization and innervation (95–97). Its transparency during larval stages makes the zebra fish a great model for functional live imaging. Easy access for genetic manipulations allows efficient multi transgenic labeling of neurons and other pancreatic cell types simultaneously. Also, a short lifespan facilitates studies on development. Time-lapse *in vivo* imaging of zebra fish allowed delineating the sequence of events that leads to parasympathetic innervation of the pancreatic islet and measuring in real time changes in the endocrine cell mass in response to targeted neuronal ablation (97). Although advantageous for imaging pancreatic innervation and having multiple physiological and morphological similarities to the mammalian systems, processes learned in the zebra fish model need to be analyzed through the prism of interspecies differences.

Co-Culture of Neurons and Pancreatic Cells

Studying synaptic transmission between a neurite and its postsynaptic target is a challenging task in the *in vivo* experimental setting. It is very difficult to access and manipulate the selected individual synaptic interaction. Furthermore, the local physiological mechanism cannot be uncoupled from the confounding systemic effects innervation has. The interactions between nerves and its targets can be better addressed *in vitro* (**Figure 7**). A beautiful example of synapse formation *in vitro* has been shown by culturing trigeminal sensory neurons with intestinal enteroendocrine cells (98). An example closer to islet biologist are studies showing that sympathetic neurons cultured with pancreatic islets triggered changes in islet cytoarchitecture inducing β-cell migration (99). Co-culture experiments might be challenging as culturing conditions need to accommodate the needs of very distinct cell types, and primary neuronal cultures are famous for being difficult to maintain *in vitro*.

CONCLUDING REMARKS

Pancreatic tissues and their innervation have been studied for decades using classical histology in combination with electrophysiology. Those laborious methods are being replaced by modern optical imaging techniques combined with precise genetic cellular labeling. While the pancreas biology field has implemented the approaches needed to access the pancreas optically (e.g. exteriorized pancreas, living pancreas slices),

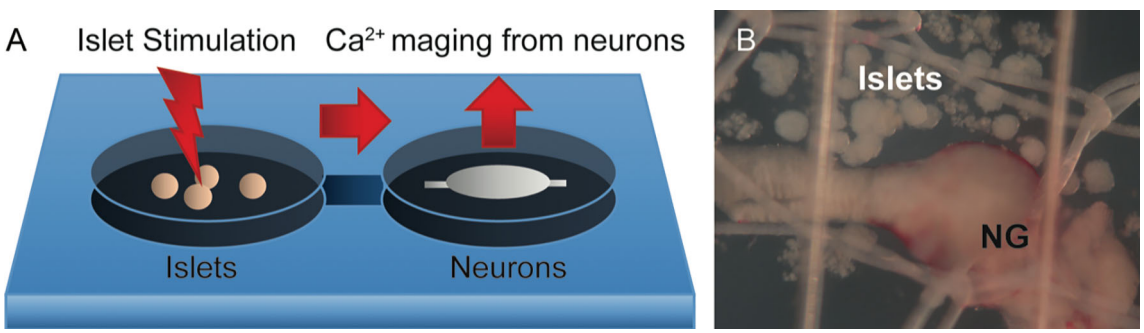

FIGURE 7 | Potential model for recording Ca^{2+} neuronal activity in response to islet stimulation *in vitro*. **(A)** Schematic representation of the proposed experimental setup, where islets are placed upstream of neurons in a perfusion chamber or a microfluidics device. Pharmacological or optogenetic stimulation of islets will induce release of substances that have a potential to act on downstream neurons. **(B)** Representative photomicrograph of islets placed in close proximity to the nodose ganglion (NG) in an imaging chamber.

the neuroscience field offers a variety of ready to use tools for neuronal labeling and manipulation (e.g. transgenic mice, genetically encoded reporters, optogenetics). Although the pancreas remains a difficult organ to study, we now can deploy an arsenal of tools that will allow us tackling many longstanding questions in the field of pancreatic innervation.

AUTHOR CONTRIBUTIONS

MM wrote the original draft of the manuscript. AC reviewed the original draft, edited and approved final version of the manuscript, and designed the figures. All authors contributed to the article and approved the submitted version.

FUNDING

This work was supported by the Diabetes Research Institute Foundation and National Institutes of Health grants R56DK084321 (AC), R01DK084321 (AC), R01DK111538 (AC), R01DK113093 (AC), U01DK120456 (AC) R33ES025673 (AC) and R21ES025673 (AC), F31DK112596 (MM), the Leona M. and Harry B. Helmsley Charitable Trust grants G-2018PG-T1D034 and G-1912-03552.

REFERENCES

1. Pavlov I. *Full Collection of Works*. USSR, Moscow: Academy of Sciences (1952).
2. Richins CA. The Innervation of the Pancreas. *J Comp Neurol* (1945) 83:223. doi: 10.1002/cne.900830303
3. Li W, Yu G, Liu Y, Sha L. Intrapancreatic Ganglia and Neural Regulation of Pancreatic Endocrine Secretion. *Front Neurosci* (2019) 13:21. doi: 10.3389/fnins.2019.00021
4. Rodriguez-Diaz R, Caicedo A. Neural Control of the Endocrine Pancreas. *Best Pract Res Clin Endocrinol Metab* (2014) 28:745–56. doi: 10.1016/j.beem.2014.05.002
5. Love JA, Yi E, Smith TG. Autonomic Pathways Regulating Pancreatic Exocrine Secretion. *Auton Neurosci* (2007) 133:19–34. doi: 10.1016/j.autneu.2006.10.001
6. Brunicardi FC, Shavelle DM, Andersen DK. Neural Regulation of the Endocrine Pancreas. *Int J Pancreatol* (1995) 18:177–95. doi: 10.1007/BF02784941
7. Havel PJ, Taborsky GJJr.. The Contribution of the Autonomic Nervous System to Changes of Glucagon and Insulin Secretion During Hypoglycemic Stress. *Endocr Rev* (1989) 10:332–50. doi: 10.1210/edrv-10-3-332
8. Kirchgessner AL, Pintar JE. Guinea Pig Pancreatic Ganglia: Projections, Transmitter Content, and the Type-Specific Localization of Monoamine Oxidase. *J Comp Neurol* (1991) 305:613–31. doi: 10.1002/cne.903050407
9. Tang SC, Baeyens L, Shen CN, Peng SJ, Chien HJ, Scheel DW, et al. Human Pancreatic Neuro-Insular Network in Health and Fatty Infiltration. *Diabetologia* (2018) 61:168–81. doi: 10.1007/s00125-017-4409-x
10. Persson-Sjogren S, Zashihin A, Forsgren S. Nerve Cells Associated With the Endocrine Pancreas in Young Mice: An Ultrastructural Analysis of the Neuroinsular Complex Type I. *Histochem J* (2001) 33:373–8. doi: 10.1023/A:1012439510709
11. Chien HJ, Chiang TC, Peng SJ, Chung MH, Chou YH, Lee CY, et al. Human Pancreatic Afferent and Efferent Nerves: Mapping and 3-D Illustration of Exocrine, Endocrine, and Adipose Innervation. *Am J Physiol Gastrointest Liver Physiol* (2019) 317:G694–706. doi: 10.1152/ajpgi.00116.2019
12. Berthoud HR, Powley TL. Morphology and Distribution of Efferent Vagal Innervation of Rat Pancreas as Revealed With Anterograde Transport of DiI. *Brain Res* (1991) 553:336–41. doi: 10.1016/0006-8993(91)90846-N
13. Wang J, Zheng H, Berthoud HR. Functional Vagal Input to Chemically Identified Neurons in Pancreatic Ganglia as Revealed by Fos Expression. *Am J Physiol* (1999) 277:E958–64. doi: 10.1152/ajpendo.1999.277.5.E958
14. Makhmutova M, Weitz J, Tamayo A, Pereira E, Boulina M, Almaca J, et al. Pancreatic Beta-Cells Communicate With Vagal Neurons. *Gastroenterology* (2021) 160(3):875–88.e11. doi: 10.1053/j.gastro.2020.10.034
15. Yi E, Smith TG, Baker RC, Love JA. Catecholamines and 5-Hydroxytryptamine in Tissues of the Rabbit Exocrine Pancreas. *Pancreas* (2004) 29:218–24. doi: 10.1097/00006676-200410000-00007
16. Berthoud HR, Patterson LM, Zheng H. Vagal-Enteric Interface: Vagal Activation-Induced Expression of c-Fos and p-CREB in Neurons of the Upper Gastrointestinal Tract and Pancreas. *Anat Rec* (2001) 262:29–40. doi: 10.1002/1097-0185(20010101)262:1<29::AID-AR1008>3.0.CO;2-B
17. Kirchgessner AL, Gershon MD. Innervation of the Pancreas by Neurons in the Gut. *J Neurosci* (1990) 10:1626–42. doi: 10.1523/JNEUROSCI.10-05-01626.1990
18. Sharkey KA, Williams RG, Dockray GJ. Sensory Substance P Innervation of the Stomach and Pancreas. Demonstration of Capsaicin-Sensitive Sensory Neurons in the Rat by Combined Immunohistochemistry and Retrograde Tracing. *Gastroenterology* (1984) 87:914–21. doi: 10.1016/0016-5085(84)90088-X
19. Rodriguez-Diaz R, Abdulreda MH, Formoso AL, Gans I, Ricordi C, Berggren PO, et al. Innervation Patterns of Autonomic Axons in the Human Endocrine Pancreas. *Cell Metab* (2011) 14:45–54. doi: 10.1016/j.cmet.2011.05.008
20. van Westerloo DJ, Giebelen IA, Florquin S, Bruno MJ, Larosa GJ, Ulloa L, et al. The Vagus Nerve and Nicotinic Receptors Modulate Experimental Pancreatitis Severity in Mice. *Gastroenterology* (2006) 130:1822–30. doi: 10.1053/j.gastro.2006.02.022
21. Weitz J, Diaz RR, Almaca J, Makhmutova M, Caicedo A. Anti-Inflammatory Cholinergic Signals Inhibit Islet Resident Macrophage Responses to ATP in Living Pancreatic Tissue Slices. *Diabetes* (2018) 67:197–OR. doi: 10.2337/db18-197-OR
22. Reinert RB, Cai Q, Hong JY, Plank JL, Aamodt K, Prasad N, et al. Vascular Endothelial Growth Factor Coordinates Islet Innervation Via Vascular Scaffolding. *Development* (2014) 141:1480–91. doi: 10.1242/dev.098657
23. Scott MM, Williams KW, Rossi J, Lee CE, Elmquist JK. Leptin Receptor Expression in Hindbrain Glp-1 Neurons Regulates Food Intake and Energy Balance in Mice. *J Clin Invest* (2011) 121:2413–21. doi: 10.1172/JCI43703
24. Bloom SR, Edwards AV. Pancreatic Endocrine Responses to Stimulation of the Peripheral Ends of the Vagus Nerves in Conscious Calves. *J Physiol* (1981) 315:31–41. doi: 10.1113/jphysiol.1981.sp013730
25. King BF, Love JA, Szurszewski JH. Intracellular Recordings From Pancreatic Ganglia of the Cat. *J Physiol* (1989) 419:379–403. doi: 10.1113/jphysiol.1989.sp017877
26. Kirchgessner AL, Liu MT. Immunohistochemical Localization of Nicotinic Acetylcholine Receptors in the Guinea Pig Bowel and Pancreas. *J Comp Neurol* (1998) 390:497–514. doi: 10.1002/(SICI)1096-9861(19980126)390:4<497::AID-CNE4>3.0.CO;2-W
27. Love JA. Electrical Properties and Synaptic Potentials of Rabbit Pancreatic Neurons. *Auton Neurosci* (2000) 84:68–77. doi: 10.1016/S1566-0702(00)00187-9
28. Nishi S, Seino Y, Ishida H, Seno M, Taminato T, Sakurai H, et al. Vagal Regulation of Insulin, Glucagon, and Somatostatin Secretion In Vitro in the Rat. *J Clin Invest* (1987) 79:1191–6. doi: 10.1172/JCI112936
29. Sha L, Love JA, Ma RC, Szurszewski JH. Cholinergic Transmission in Pancreatic Ganglia of the Cat. *Pancreas* (1997) 14:83–93. doi: 10.1097/00006676-199701000-00013
30. Stagner JI, Samols E. Modulation of Insulin Secretion by Pancreatic Ganglionic Nicotinic Receptors. *Diabetes* (1986) 35:849–54. doi: 10.2337/diab.35.8.849
31. Kirchgessner AL, Gershon MD. Presynaptic Inhibition by Serotonin of Nerve-Mediated Secretion of Pancreatic Amylase. *Am J Physiol* (1995) 268:G339–45. doi: 10.1152/ajpgi.1995.268.2.G339
32. Ma RC, Szurszewski JH. 5-Hydroxytryptamine Depolarizes Neurons of Cat Pancreatic Ganglia. *J Auton Nerv Syst* (1996) 57:78–86. doi: 10.1016/0165-1838(95)00100-X

33. Sha L, Miller SM, Szurszewski JH. Nitric Oxide is a Neuromodulator in Cat Pancreatic Ganglia: Histochemical and Electrophysiological Study. *Neurosci Lett* (1995) 192:77–80. doi: 10.1016/0304-3940(95)11614-3
34. Yi E, Love JA. Alpha-Adrenergic Modulation of Synaptic Transmission in Rabbit Pancreatic Ganglia. *Auton Neurosci* (2005) 122:45–57. doi: 10.1016/j.autneu.2005.07.008
35. Yi E, Love JA. Short-Term Synaptic Plasticity in Rabbit Pancreatic Ganglia. *Auton Neurosci* (2005) 119:36–47. doi: 10.1016/j.autneu.2005.03.001
36. Buijs RM, Chun SJ, Niijima A, Romijn HJ, Nagai K. Parasympathetic and Sympathetic Control of the Pancreas: A Role for the Suprachiasmatic Nucleus and Other Hypothalamic Centers That are Involved in the Regulation of Food Intake. *J Comp Neurol* (2001) 431:405–23. doi: 10.1002/1096-9861(20010319)431:4<405::AID-CNE1079>3.0.CO;2-D
37. Daniel PM, Henderson JR. The Effect of Vagal Stimulation on Plasma Insulin and Glucose Levels in the Baboon. *J Physiol* (1967) 192:317–27. doi: 10.1113/jphysiol.1967.sp008302
38. Frohman LA, Ezdinli EZ, Javid R. Effect of Vagotomy and Vagal Stimulation on Insulin Secretion. *Diabetes* (1967) 16:443–8. doi: 10.2337/diab.16.7.443
39. Meyers EE, Kronemberger A, Lira V, Rahmouni K, Stauss HM. Contrasting Effects of Afferent and Efferent Vagal Nerve Stimulation on Insulin Secretion and Blood Glucose Regulation. *Physiol Rep* (2016) 4(4):e12718. doi: 10.14814/phy2.12718
40. Niebergall-Roth E, Singer MV. Central and Peripheral Neural Control of Pancreatic Exocrine Secretion. *J Physiol Pharmacol* (2001) 52:523–38.
41. Rohner-Jeanrenaud F, Bobbioni E, Ionescu E, Sauter JF, Jeanrenaud B. Central Nervous System Regulation of Insulin Secretion. *Adv Metab Disord* (1983) 10:193–220. doi: 10.1016/B978-0-12-027310-2.50012-8
42. Streefland C, Maes FW, Bohus B. Autonomic Brainstem Projections to the Pancreas: A Retrograde Transneuronal Viral Tracing Study in the Rat. *J Auton Nerv Syst* (1998) 74:71–81. doi: 10.1016/S0165-1838(98)00047-2
43. Quinson N, Robbins HL, Clark MJ, Furness JB. Locations and Innervation of Cell Bodies of Sympathetic Neurons Projecting to the Gastrointestinal Tract in the Rat. *Arch Histol Cytol* (2001) 64:281–94. doi: 10.1679/aohc.64.281
44. Dunning BE, Taborsky GJ Jr. Neural Control of Islet Function by Norepinephrine and Sympathetic Neuropeptides. *Adv Exp Med Biol* (1991) 291:107–27. doi: 10.1007/978-1-4684-5931-9_10
45. Dunning BE, Ahren B, Veith RC, Taborsky GJJr. Nonadrenergic Sympathetic Neural Influences on Basal Pancreatic Hormone Secretion. *Am J Physiol* (1988) 255:E785–92. doi: 10.1152/ajpendo.1988.255.6.E785
46. Christoffersson G, Ratliff SS, von Herrath MG. Interference With Pancreatic Sympathetic Signaling Halts the Onset of Diabetes in Mice. *Sci Adv* (2020) 6(35):eabb2878. doi: 10.1126/sciadv.abb2878
47. Guyot M, Simon T, Ceppo F, Panzolini C, Guyon A, Lavergne J, et al. Pancreatic Nerve Electrostimulation Inhibits Recent-Onset Autoimmune Diabetes. *Nat Biotechnol* (2019) 37:1446–51. doi: 10.1038/s41587-019-0295-8
48. Mundinger TO, Mei Q, Foulis AK, Fligner CL, Hull RL, Taborsky GJ Jr. Human Type 1 Diabetes is Characterized by an Early, Marked, Sustained, and Islet-Selective Loss of Sympathetic Nerves. *Diabetes* (2016) 65:2322–30. doi: 10.2337/db16-0284
49. Bou Karam J, Cai W, Mohamed R, Huang T, Meng L, Homan EP, et al. TRPV1 Neurons Regulate Beta-Cell Function in a Sex-Dependent Manner. *Mol Metab* (2018) 18:60–7. doi: 10.1016/j.molmet.2018.10.002
50. Fasanella KE, Christianson JA, Chanthaphavong RS, Davis BM. Distribution and Neurochemical Identification of Pancreatic Afferents in the Mouse. *J Comp Neurol* (2008) 509:42–52. doi: 10.1002/cne.21736
51. Neuhuber WL. Vagal Afferent Fibers Almost Exclusively Innervate Islets in the Rat Pancreas as Demonstrated by Anterograde Tracing. *J Auton Nerv Syst* (1989) 29:13–8. doi: 10.1016/0165-1838(89)90015-5
52. Hameed M, Hameed H, Erdek M. Pain Management in Pancreatic Cancer. *Cancers (Basel)* (2010) 3:43–60. doi: 10.3390/cancers3010043
53. Pasricha PJ. Unraveling the Mystery of Pain in Chronic Pancreatitis. *Nat Rev Gastroenterol Hepatol* (2012) 9:140–51. doi: 10.1038/nrgastro.2011.274
54. Schloithe AC, Sutherland K, Woods CM, Blackshaw LA, Davison JS, Toouli J, et al. A Novel Preparation to Study Rat Pancreatic Spinal and Vagal Mechanosensitive Afferents In Vitro. *Neurogastroenterol Motil* (2008) 20:1060–9. doi: 10.1111/j.1365-2982.2008.01141.x
55. Sha L, Ou LL, Miller SM, Ma R, Szurszewski JH. Cat Pancreatic Neurons: Morphology, Electrophysiological Properties, and Responses to 5-HT. *Pancreas* (1996) 13:111–24. doi: 10.1097/00006676-199608000-00001
56. Kirchgessner AL, Liu MT, Raymond JR, Gershon MD. Identification of Cells That Express 5-hydroxytryptamine1A Receptors in the Nervous Systems of the Bowel and Pancreas. *J Comp Neurol* (1996) 364:439–55. doi: 10.1002/(SICI)1096-9861(19960115)364:3<439::AID-CNE5>3.0.CO;2-5
57. Kirchgessner AL, Liu MT, Gershon MD. In Situ Identification and Visualization of Neurons That Mediate Enteric and Enteropancreatic Reflexes. *J Comp Neurol* (1996) 371:270–86. doi: 10.1002/(SICI)1096-9861(19960722)371:2<270::AID-CNE7>3.0.CO;2-#
58. Kirchgessner AL, Gershon MD. Innervation and Regulation of the Pancreas by Neurons in the Gut. *Z Gastroenterol Verh* (1991) 26:230–3. doi: 10.1523/JNEUROSCI.10-05-01626.1990
59. Kirchgessner AL, Adlersberg MA, Gershon MD. Colonization of the Developing Pancreas by Neural Precursors From the Bowel. *Dev Dyn* (1992) 194:142–54. doi: 10.1002/aja.1001940207
60. Tharakan T, Kirchgessner AL, Baxi LV, Gershon MD. Appearance of Neuropeptides and NADPH-diaphorase During Development of the Enteropancreatic Innervation. *Brain Res Dev Brain Res* (1995) 84:26–38. doi: 10.1016/0165-3806(94)00142-M
61. Heidenhain R. Beiträge Zur Kenntniss Des Pancreas. *Archiv Für Die Gesamte Physiol Des Menschen Und Der Tiere* (1875) 10:557–632. doi: 10.1007/BF01639951
62. Alm P, Cegrell L, Ehinger B, Falck B. Remarkable Adrenergic Nerves in the Exocrine Pancreas]. *Z Zellforsch Mikrosk Anat* (1967) 83:178–86. doi: 10.1007/BF00362399
63. Furlan A, La Manno G, Lubke M, Haring M, Abdo H, Hochgerner H, et al. Visceral Motor Neuron Diversity Delineates a Cellular Basis for Nipple- and Pilo-Erection Muscle Control. *Nat Neurosci* (2016) 19:1331–40. doi: 10.1038/nn.4376
64. Kupari J, Haring M, Agirre E, Castelo-Branco G, Ernfors P. An Atlas of Vagal Sensory Neurons and Their Molecular Specialization. *Cell Rep* (2019) 27:2508–2523 e4. doi: 10.1016/j.celrep.2019.04.096
65. Glynn MW, McAllister AK. Immunocytochemistry and Quantification of Protein Colocalization in Cultured Neurons. *Nat Protoc* (2006) 1:1287–96. doi: 10.1038/nprot.2006.220
66. Daigle TL, Madisen L, Hage TA, Valley MT, Knoblich U, Larsen RS, et al. A Suite of Transgenic Driver and Reporter Mouse Lines With Enhanced Brain-Cell-Type Targeting and Functionality. *Cell* (2018) 174:465–480 e22. doi: 10.1016/j.cell.2018.06.035
67. Udit S, Gautron L. Molecular Anatomy of the Gut-Brain Axis Revealed With Transgenic Technologies: Implications in Metabolic Research. *Front Neurosci* (2013) 7:134. doi: 10.3389/fnins.2013.00134
68. Davidson BL, Breakefield XO. Viral Vectors for Gene Delivery to the Nervous System. *Nat Rev Neurosci* (2003) 4:353–64. doi: 10.1038/nrn1104
69. Rosario W, Singh I, Wautlet A, Patterson C, Flak J, Becker TC, et al. The Brain-to-Pancreatic Islet Neuronal Map Reveals Differential Glucose Regulation From Distinct Hypothalamic Regions. *Diabetes* (2016) 65:2711–23. doi: 10.2337/db15-0629
70. Xiao X, Guo P, Prasadan K, Shiota C, Peirish L, Fischbach S, et al. Pancreatic Cell Tracing, Lineage Tagging and Targeted Genetic Manipulations in Multiple Cell Types Using Pancreatic Ductal Infusion of Adeno-Associated Viral Vectors and/or Cell-Tagging Dyes. *Nat Protoc* (2014) 9:2719–24. doi: 10.1038/nprot.2014.183
71. Alvarsson A, Jimenez-Gonzalez M, Li R, Rosselot C, Tzavaras N, Wu Z, et al. A 3D Atlas of the Dynamic and Regional Variation of Pancreatic Innervation in Diabetes. *Sci Adv* (2020) 6(41):eaaz9124. doi: 10.1126/sciadv.aaz9124
72. Hara M, Dizon RF, Glick BS, Lee CS, Kaestner KH, Piston DW, et al. Imaging Pancreatic Beta-Cells in the Intact Pancreas. *Am J Physiol Endocrinol Metab* (2006) 290:E1041–7. doi: 10.1152/ajpendo.00365.2005
73. Hsueh B, Burns VM, Pauerstein P, Holzem K, Ye L, Engberg K, et al. Pathways to Clinical CLARITY: Volumetric Analysis of Irregular, Soft, and Heterogeneous Tissues in Development and Disease. *Sci Rep* (2017) 7:5899. doi: 10.1038/s41598-017-05614-4
74. Tang SC, Shen CN, Lin PY, Peng SJ, Chien HJ, Chou YH, et al. Pancreatic Neuro-Insular Network in Young Mice Revealed by 3D Panoramic Histology. *Diabetologia* (2018) 61:158–67. doi: 10.1007/s00125-017-4408-y

75. Ahl D, Eriksson O, Sedin J, Seignez C, Schwan E, Kreuger J, et al. Turning Up the Heat: Local Temperature Control During In Vivo Imaging of Immune Cells. *Front Immunol* (2019) 10:2036. doi: 10.3389/fimmu.2019.02036
76. Frikke-Schmidt H, Arvan P, Seeley RJ, Cras-Meneur C. Improved In Vivo Imaging Method for Individual Islets Across the Mouse Pancreas Reveals a Heterogeneous Insulin Secretion Response to Glucose. *Sci Rep* (2021) 11:603. doi: 10.1038/s41598-020-79727-8
77. Reissaus CA, Pineros AR, Twigg AN, Orr KS, Conteh AM, Martinez MM, et al. Portable Intravital Microscopy Platform for Studying Beta-Cell Biology In Vivo. *Sci Rep* (2019) 9:8449. doi: 10.1038/s41598-019-44777-0
78. Almaca J, Weitz J, Rodriguez-Diaz R, Pereira E, Caicedo A. The Pericyte of the Pancreatic Islet Regulates Capillary Diameter and Local Blood Flow. *Cell Metab* (2018) 27:630–44.e4. doi: 10.1016/j.cmet.2018.02.016
79. Marciniak A, Cohrs CM, Tsata V, Chouinard JA, Selck C, Stertmann J, et al. Using Pancreas Tissue Slices for in Situ Studies of Islet of Langerhans and Acinar Cell Biology. *Nat Protoc* (2014) 9:2809–22. doi: 10.1038/nprot.2014.195
80. Panzer JK, Hiller H, Cohrs CM, Almaca J, Enos SJ, Beery M, et al. Pancreas Tissue Slices From Organ Donors Enable in Situ Analysis of Type 1 Diabetes Pathogenesis. *JCI Insight* (2020) 5(8):e134525. doi: 10.1172/jci.insight.134525
81. Weitz JR, Makhmutova M, Almaca J, Stertmann J, Aamodt K, Brissova M, et al. Mouse Pancreatic Islet Macrophages Use Locally Released ATP to Monitor Beta Cell Activity. *Diabetologia* (2018) 61:182–92. doi: 10.1007/s00125-017-4416-y
82. Speier S, Nyqvist D, Cabrera O, Yu J, Molano RD, Pileggi A, et al. Noninvasive In Vivo Imaging of Pancreatic Islet Cell Biology. *Nat Med* (2008) 14:574–8. doi: 10.1038/nm1701
83. Speier S, Nyqvist D, Kohler M, Caicedo A, Leibiger IB, Berggren PO. Noninvasive High-Resolution In Vivo Imaging of Cell Biology in the Anterior Chamber of the Mouse Eye. *Nat Protoc* (2008) 3:1278–86. doi: 10.1038/nprot.2008.118
84. Rodriguez-Diaz R, Speier S, Molano RD, Formoso A, Gans I, Abdulreda MH, et al. Noninvasive In Vivo Model Demonstrating the Effects of Autonomic Innervation on Pancreatic Islet Function. *Proc Natl Acad Sci USA* (2012) 109:21456–61. doi: 10.1073/pnas.1211659110
85. Singer MV, Solomon TE, Wood J, Grossman MI. Latency of Pancreatic Enzyme Response to Intraduodenal Stimulants. *Am J Physiol* (1980) 238:G23–9. doi: 10.1152/ajpgi.1980.238.1.G23
86. Rinaman L, Miselis RR. The Organization of Vagal Innervation of Rat Pancreas Using Cholera Toxin-Horseradish Peroxidase Conjugate. *J Auton Nerv Syst* (1987) 21:109–25. doi: 10.1016/0165-1838(87)90014-2
87. DeNardo LA, Liu CD, Allen WE, Adams EL, Friedmann D, Fu L, et al. Temporal Evolution of Cortical Ensembles Promoting Remote Memory Retrieval. *Nat Neurosci* (2019) 22:460–9. doi: 10.1038/s41593-018-0318-7
88. Schwenkgrub J, Harrell ER, Bathellier B, Bouvier J. Deep Imaging in the Brainstem Reveals Functional Heterogeneity in V2a Neurons Controlling Locomotion. *Sci Adv* (2020) 6(49):eabc6309. doi: 10.1126/sciadv.abc6309
89. Stein LM, Lhamo R, Cao A, Workinger J, Tinsley I, Doyle RP, et al. Dorsal Vagal Complex and Hypothalamic Glia Differentially Respond to Leptin and Energy Balance Dysregulation. *Transl Psychiatry* (2020) 10:90. doi: 10.1038/s41398-020-0767-0
90. Furuzawa Y, Ohmori Y, Watanabe T. Anatomical Localization of Sympathetic Postganglionic and Sensory Neurons Innervating the Pancreas of the Cat. *J Vet Med Sci* (1996) 58:243–8. doi: 10.1292/jvms.58.243
91. Jobling P, Gibbins IL. Electrophysiological and Morphological Diversity of Mouse Sympathetic Neurons. *J Neurophysiol* (1999) 82:2747–64. doi: 10.1152/jn.1999.82.5.2747
92. Razavi R, Chan Y, Afifiyan FN, Liu XJ, Wan X, Yantha J, et al. TRPV1+ Sensory Neurons Control Beta Cell Stress and Islet Inflammation in Autoimmune Diabetes. *Cell* (2006) 127:1123–35. doi: 10.1016/j.cell.2006.10.038
93. Riera CE, Huising MO, Follett P, Leblanc M, Halloran J, Van Andel R, et al. TRPV1 Pain Receptors Regulate Longevity and Metabolism by Neuropeptide Signaling. *Cell* (2014) 157:1023–36. doi: 10.1016/j.cell.2014.03.051
94. Chen C, Zhang J, Sun L, Zhang Y, Gan WB, Tang P, et al. Long-Term Imaging of Dorsal Root Ganglia in Awake Behaving Mice. *Nat Commun* (2019) 10:3087. doi: 10.1038/s41467-019-11158-0
95. Field HA, Dong PD, Beis D, Stainier DY. Formation of the Digestive System in Zebrafish. *II Pancreas Morphogen Dev Biol* (2003) 261:197–208. doi: 10.1016/S0012-1606(03)00308-7
96. Matsuda H. Zebrafish as a Model for Studying Functional Pancreatic Beta Cells Development and Regeneration. *Dev Growth Differ* (2018) 60:393–9. doi: 10.1111/dgd.12565
97. Yang YHC, Kawakami K, Stainier DY. A New Mode of Pancreatic Islet Innervation Revealed by Live Imaging in Zebrafish. *Elife* (2018) 7:e34519. doi: 10.7554/eLife.34519
98. Bohorquez DV, Shahid RA, Erdmann A, Kreger AM, Wang Y, Calakos N, et al. Neuroepithelial Circuit Formed by Innervation of Sensory Enteroendocrine Cells. *J Clin Invest* (2015) 125:782–6. doi: 10.1172/JCI78361
99. Borden P, Houtz J, Leach SD, Kuruvilla R. Sympathetic Innervation During Development is Necessary for Pancreatic Islet Architecture and Functional Maturation. *Cell Rep* (2013) 4:287–301. doi: 10.1016/j.celrep.2013.06.019

Conflict of Interest: The authors declare that the research was conducted in the absence of any commercial or financial relationships that could be construed as a potential conflict of interest.

frontiers in Endocrinology

MINI REVIEW
published: 10 May 2021
doi: 10.3389/fendo.2021.602620

In Vivo and *In Situ* Approach to Study Islet Microcirculation: A Mini-Review

Michael P. Dybala and Manami Hara *

Department of Medicine, The University of Chicago, Chicago, IL, United States

The pancreas is regarded as consisting of two separate organ systems, the endocrine and exocrine pancreas. While treatment of a disease with either an endocrine or exocrine pathogenesis may affect the function of the entire pancreas, the pancreatic diseases have been treated by clinicians in different medical disciplines, including endocrinologists and gastroenterologists. Islet microcirculation has long been considered to be regulated independently from that of the exocrine pancreas. A new model proposes that pancreatic islet blood flow is integrated with the surrounding exocrine capillary network. This recent model may provide revived or contrasting hypotheses to test, since the pancreatic microcirculation has critical implications for the regulation of islet hormones as well as acinar pancreas functions. In this mini-review, practical applications of *in vivo* and *in situ* studies of islet microcirculation are described with a specific emphasis on large-scale data analysis to ensure sufficient sample size accounting for known islet heterogeneity. For *in vivo* small animal studies, intravital microscopy based on two-photon excitation microscopes is a powerful tool that enables capturing the flow direction and speed of individual fluorescent-labeled red blood cells. Complementarily, for structural analysis of blood vessels, the recent technical advancements of confocal microscopy and tissue clearing have enabled us to image the three-dimensional network structure in thick tissue slices.

Keywords: beta cell (β-Cell), islet, capillary, microcirculation, intravital 2-photon microscopy, 3D image analysis

OPEN ACCESS

Edited by:
Amelia K. Linnemann, Indiana University, United States

Reviewed by:
Barak Blum, University of Wisconsin-Madison, United States
Sarah Tersey, University of Chicago, United States
Guy A. Rutter, Imperial College London, United Kingdom

***Correspondence:**
Manami Hara
mhara@uchicago.edu

Specialty section:
This article was submitted to Diabetes: Molecular Mechanisms, a section of the journal Frontiers in Endocrinology

Received: *03 September 2020*
Accepted: *26 April 2021*
Published: *10 May 2021*

Citation:
Dybala MP and Hara M (2021) In Vivo and In Situ Approach to Study Islet Microcirculation: A Mini-Review. Front. Endocrinol. 12:602620. doi: 10.3389/fendo.2021.602620

INTRODUCTION

In 1869, Paul Langerhans as a medical student first described the islet cells from rabbit pancreas as "small irregularly polygonal structures" that "gathered in rounded masses, 0.12-0.24 mm in diameter, distributed at regular intervals in the parenchyma". Interestingly, Langerhans made these observations through the simple use of a primitive light microscope and multi-day fixation in Müller's fluid (1). In the early 20th century, islet morphology studies were performed using hematoxylin and eosin staining, which allowed researchers to appreciate islet morphology but not distinguish individual islet cell populations (2). Early descriptions of pancreatic beta- and alpha-cells were made using dye injections, since little was known about the functional differences of the endocrine cells (3). Lane was likely the first to differentiate alpha- and beta-cells in 1907, by

Abbreviations: GFP, green fluorescent protein; IHC, Immunohistochemistry; MIP, mouse insulin I promoter; RBC, red blood cell.

observing morphological differences in islet cells when stained with aqueous-chrome-sublimate (beta-cells) versus alcohol-chrome-sublimate (alpha-cells). Approximately three decades later, Bloom described a method of differentiating beta-, alpha- and delta-cells using a single stain, the Mallory-Heidenhain azan trichrome technique, based on differential colors of cytoplasm and intracellular granules size and color (4). Elucidation of the function of islet endocrine cells allowed for implementation of a variety of histochemical methods to identify islet endocrine cells, including the Gömöri trichrome stain, pseudoisocyanin, and zinc and cobalt crystallization. Immunohistochemical (IHC) techniques were first described in 1942 as a method of detecting pneumococcal antigens using chemically-labeled antibodies (5). The use of IHC to identify pancreatic endocrine cells followed shortly after (6–8), though the IHC technique was not immediately widely adopted due to a lack of access to experimental tools such as antibody development and fluorescence microscopes (9). The development of IHC techniques allows for more specific and reproducible islet imaging as well as providing means of cell identification based on endocrine hormone production (e.g. insulin) rather than a chemical profile. Furthermore, fluorescent immunostaining for specific cellular products allows for simultaneous identification of multiple endocrine cell types within the same islet thus becoming a powerful tool for observing islet cell changes in both the healthy and pathological state. Parallel to the rapid development of unique staining techniques has been the rise of advanced microscopy, which allows for high resolution, multi-fluorescent, and even live-organism imaging (10).

Until recently, the pancreatic islet has mostly been studied using two-dimensional (2D) imaging even though the earliest trials of three-dimensional (3D) islet imaging took place as early as 1989 (11). 3D immunohistochemical microscopy has permitted visualization of the islet in its entire microenvironment and has provided new insight into islet architecture, such as the lack of a mantle consisting of non-beta-cells in rodent islets when observed in 3D (12). Such 3D techniques involve imaging of ~600-800μm thick slices of pancreatic tissue, whereas traditional 2D techniques use sections ~5μm thick, making the former more reasonable to visualize whole islets simultaneously since the vast majority of islets tend to be less than 200μm in diameter (13). Large-scale imaging of pancreatic tissue slices also permits adequate sampling of islets which are known to be heterogeneous in size, cellular arrangement, and cellular composition both within individuals and across individuals, particularly in humans. Limitations in interpretation of 2D imaging studies have been acknowledged, especially with consideration to the challenge posed by reconstructing 2D information into 3D and how such interpretation might have influenced how we would understand islet biology (14). Furthermore, the development of *in vivo* imaging has allowed us to visualize the dynamic pancreatic microenvironment in real-time. In this Mini Review, we will discuss the implementation of intravital islet imaging in mice and subsequent analysis of a large sample of data. Additionally, a procedural description of 3D imaging of thick pancreatic tissue slices and ensuing computer-assisted visualization and analysis will be presented. Overall, the rapid development of novel imaging techniques have allowed investigators to further their understanding of pancreatic and islet physiology. As such technological advances continue to change, though, precautions should be taken to understand potential limitations of contemporary techniques when interpreting experimental results.

CONVENTIONAL METHODS USED FOR STUDYING ISLET MICROCIRCULATION

The three previously discussed models of islet microcirculation, in which blood flows from non-beta-cells to beta-cells (model 1), beta-cells to non-beta-cells (model 2), or unidirectional *via* a gated portal system (model 3), were developed using distinct experimental methods (15). Proponents of model 1 used scanning electron microscopy to examine corrosion cast images of islet vasculature. Analysis of corrosion casts allowed for fine observation of microvascular details but failed to account for directionality of individual vessels, possibly contributing to the development of the insulo-acinar portal system hypothesis, in which efferent blood from the islets drains to the surrounding exocrine tissue. Furthermore, model 1 was built on studies of *in vivo* microscopy of ink-perfused islets under ultraviolet illumination. In these experiments, a fluorescent dye, either fluorescein isothiocyanate conjugated to bovine serum albumin or sulfoflavin S was injected into anesthetized rats. While *in vivo* imaging captures directionality of blood flow, the use of a dye makes it difficult to capture directionality of individual intra- and extra-islet blood flow. Model 2 was developed using corrosion casts and india-ink perfusion of rat islets followed by immunostained sections. Additionally, model 2 ascertained that afferent arterioles penetrated the islet core through gaps in the non-beta-cell mantle that help comprise the non-beta-cell mantle/beta-cell core structure that is necessary for the ordered perfusion of islets in this model. As we have previously shown, 3D reconstruction of a stack of 2D optical slices are necessary to appreciate the unique cytoarchitecture of the human islet. Analysis of immunostained 2D sections may lead to the perception of structural components, such as "composites of mantle-core cellular structures or subunits", that are not seen when imaged in 3D (14). The researchers supporting model 3 utilized intravenous or intra-arterial infusions of fluorescent markers with subsequent examination under fluorescent light. They observed a "wave" of fluorescent markers move across islets under *in vivo* analysis, but a lack of highly specific tracking of individual cells may have contributed to interpretation of islet blood flow as afferent-to-efferent rather than recognizing the heterogeneous directionality of intra- and extra-islet pancreatic blood flow. Over a decade after the presentation of three models, Nyman and colleagues examined the proportion of these three models in mice using live imaging of islets with rhodamine-labeled dextran injection. They reported that all three models of blood flow were observed in mouse islets, with varying frequencies: model 2 > model 3 > model 1. Thus, this decades-long debate surrounding patterns of islet microcirculation

remained unresolved, as the authors noted that the functional significance of finding multiple models of islet blood flow would require further study (16). It is noted that these previous models and the newly proposed one are mutually exclusive.

FLUORESCENT RED BLOOD CELL (RBC) LABELING

In order to label and track individual RBCs in live mice, we used a similar method to one used to visualize fluorescent-labeled erythrocytes and leukocytes in mouse retinas (17). In transgenic mice in which beta cells expressed GFP under the control of the mouse insulin I promoter [MIP-GFP mice; (18)], the animals were anesthetized with ketamine (100mg/kg) and xylazine (5 mg/kg). Following anesthetization, 10^8 fluorescent DiI-labeled RBCs were injected retro-orbitally, and the mouse pancreas was exteriorized following depilation. Intravital microscopy was conducted using the Leica TCS SP5 MP confocal microscope (**Figure 1A**). Advanced use of an abdominal imaging window for longitudinal studies of intravital imaging is described by Reissaus et al. (19).

RBC FLOW ANALYSIS

Data from *in vivo* imaging are stored as .lif files and imported into Imaris image analysis software (Bitplane, Switzerland). Prior to performing RBC tracking analysis, the data must be stabilized, as perturbations from the mouse respirations can cause back-and-forth oscillations that will distort detected RBC flow patterns. In Imaris, such data can be modified for more accurate analysis using the drift correction tool, in which a stable reference point (e.g. the islet of interest) is used to modify the time series such that oscillations are reduced. Once drift has been corrected, RBC fluorescent signal is processed for easier flow analysis, using background subtraction and Gaussian blur features (**Figures 1B.a-b**). Using the Spots tool, individual RBCs can be tracked as individual objects, which provides detailed physical data, such as speed, velocity, acceleration, and displacement, among other measurements (**Figure 1B.c**). Specifically, when performing spot tracking analysis of mouse RBCs *in vivo*, we estimated the RBC diameter to be 6-8μm, which was confirmed with the measurement tool, and selected autoregressive motion tracking algorithm with a max distance between spots in subsequent frames of ~25μm. Imaris recommends that users only track spots in successive frames that can be distinguished with the human eye. That is, any uncertainty in the frame-to-frame identity of a single RBC, which may result from a low frame rate or extremely high RBC speeds, will make it difficult to precisely and reliably collect tracking data. Once RBC spot analysis has been completed, physical data can be collected for individual spots as well as for the paths on which the RBCs travel (length, straightness, average speed along track, maximum/minimum speed along track, etc.) (**Figure 1B.d**). Additionally, data can be filtered to only include RBC paths/tracks of a certain length, straightness, average speed, or physical location, as well as other variables.

OPTICAL TISSUE CLEARING

Successful 3D imaging requires optical tissue clearing, which allows for increased tissue transparency and the ability to image thick tissue slices with cellular resolution. Since the development of one of the most popular methods for tissue clearing, "CLARITY" (20), numerous other methods have been developed (21–23) to allow investigators to prepare tissues in a manner that aligns with their experimental goals. Many of these procedures are complex, requiring special devices and days to weeks of preparation. For example, CLARITY, which was coined from "Clear Lipid-exchanged Acrylamide-hybridized Rigid Imaging/Immunostaining/*In situ* hybridization-compatible Tissue-hYdrogel", is based on hydrogel-tissue hybridization featuring lipid extraction by passive thermal diffusion and electrophoresis (20). Therefore, it requires a custom-designed chamber and continuous exchange of detergent (SDS solution) with the controlled gradual increase of the temperature. In the original protocol, relatively expensive solution FocusClear® (CelExplorer Labs, Hsinchu, Taiwan) is used for refractive index matching. This sophisticated method takes considerably long time from tissue preparation to imaging. We adapted the T3 method (24), which clears thick human pancreatic tissues in 1 day. The versatility of our method further stems from the use of primary antibodies conjugated with fluorescent dyes, which allows any combinations of primary antibodies regardless of their species-specific affinities. Our modified T3 method begins with washing antibody-incubated tissues slices for 30 minutes in PBS at 4°C. After washing, up to two tissue slices are sequentially incubated in 20, 50, 80, and 100% (v/v) solutions consisting of D-fructose in phosphate buffer with an additional 0.3% of α-thioglycerol for two hours each. Tissues are incubated using 10mL of solution in small glass vials wrapped in tin foil under gentle agitation at 36°C. Following incubation in the 100% D-fructose solution, cleared tissue samples can be stored at -20°C for several months based on our experience.

ANTIBODY CONJUGATE PREPARATION

Primary antibodies are first conjugated with secondary dyes overnight in a 1.5mL tube. The amount of primary antibody conjugated can vary depending on the volume needed for pancreatic tissue preparation but tends to fall in the range of 0.1-0.5mL. A 30:1 ratio of molar mass of antibody to mass of dye is used, which determines the required amount of dye for a given antibody volume (depending on the antibody's concentration). Roughly 1-5μL of dye is required per 100μL of primary antibody. Following overnight conjugation *via* gentle agitation away from light at 4°C, the antibody conjugation is dialyzed in 1L of PBS at 4°C by injecting the conjugated antibody into a small dialysis

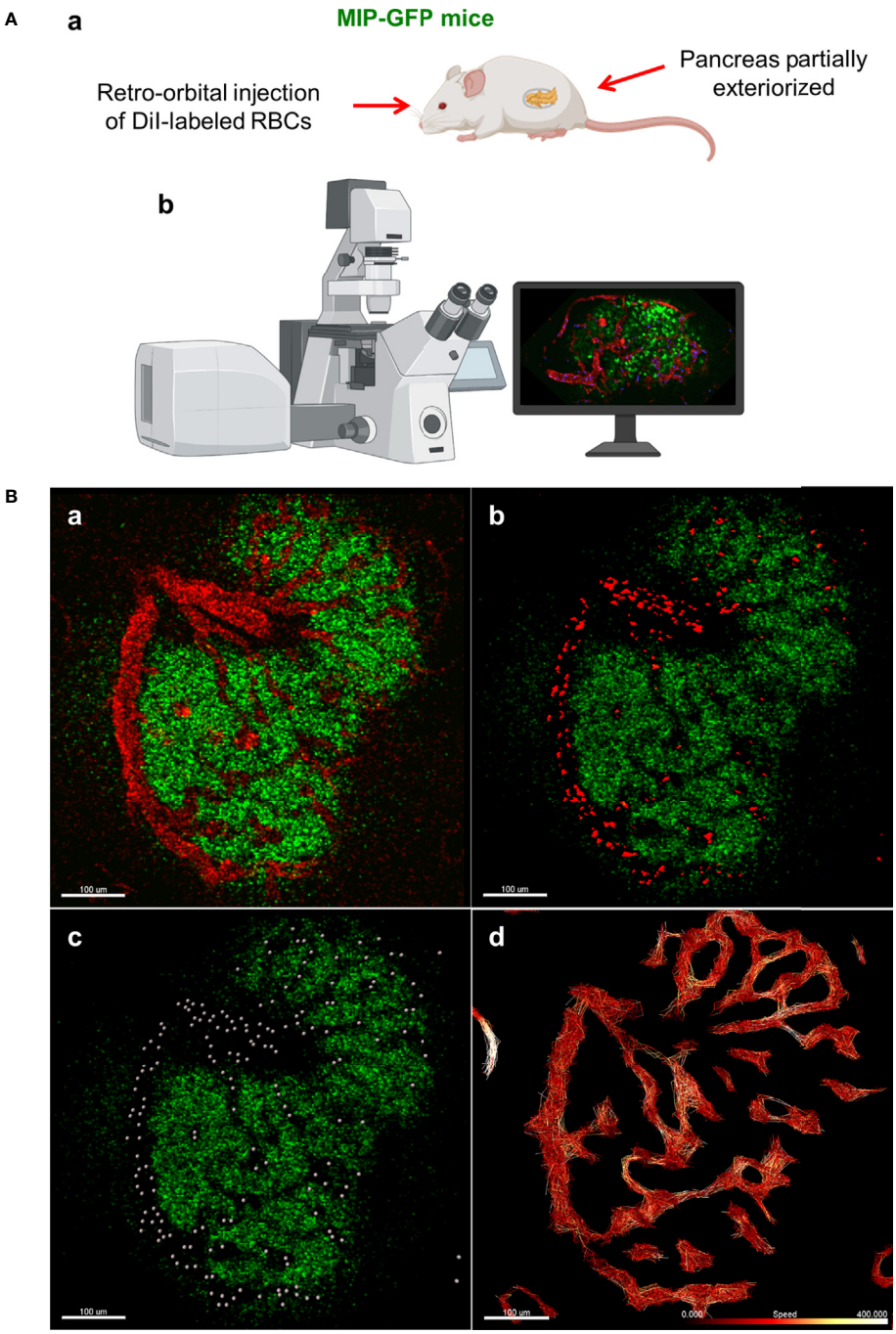

FIGURE 1 | *In vivo* approach to study islet microcirculation in mice. **(A) a.** MIP-GFP mice are anesthetized with ketamine (100 mg/kg) (Fort Dodge AnimalHealth, Fort Dodge, IA) and xylazine (5 mg/kg) (Ben Venue Laboratories, Bedford, OH). After depilation, a pancreas is exteriorized. To visualize the blood flow, 10^8 RBCs stained with DiI (Thermo Fisher Scientific, Waltham, MA) and/or tetramethylrhodamine (TMRD)-labeled dextran (2,000,000 MW) (Thermo Fisher Scientific) are injected intravenously in the mice just before imaging. **b.** Intravital microscopy is conducted using Leica TCS SP5 MP confocal microscope (Leica Microsystems, Mannheim, Germany). Images are recorded and analyzed using Leica LAS-AF as well as Fiji (http://imagej.net/Fiji). (Created with BioRender.com) **(B) a.** Fluorescent signal of dextran in mouse islet vasculature. **b.** Fluorescent signal of labeled individual RBCs in mouse islet vasculature. Scale bar: 100 µm. **c.** Computer-generated spheres representing tracked RBCs. **d.** Heatmap of RBC speed within the islet (fast to slow, white to red). Scale bar: 100 µm. (Adopted from 12).

cassette (Slide-A-Lyzer, Thermo-Fisher). The dialysis cassette should be spun on a low-speed setting throughout the dialysis process using a magnetic stir bar. The PBS solution is to be replaced with fresh solution three times: once in the afternoon of the same day as the start of dialysis, once the following morning, and once the following afternoon. Two days from the beginning

of dialysis, the conjugate can be withdrawn and stored away from light in a tube at 4°C for up to six months.

3D IMAGING

It is important to note that although we describe specific step-by-step methods for 3D modeling using a particular microscope and software, the same general principle of imaging and reassembling data points in 3D can be readily applied in other commonly-used and freely available software such as Fiji. Confocal 3D microscopy is performed using the Leica SP8 microscope in conjunction with Leica's LASX imaging software (Wetzlar, Germany). Thick pancreatic tissue slices are examined under a 10x objective magnification. Specific features of the LASX software used to enhance imaging include increasing the bit depth from 8 (default) to 12, which captures finer details of the image. Additionally, the Super-Z mode is used to allow for visualization of up to 1.5mm of tissue, compared to the default range of 500µm. Multiple channel lasers and detectors are used (up to eight channels, where currently five are more optimal) in combinations of sequence bits such that the lasers in each sequence are on opposite ends of the emission spectra. Islets may be captured as part of a larger tile-scan, in which LASX stitches together a user-defined region of image tiles to capture an entire section of pancreatic tissue containing hundreds of islets. Additionally, single-tile images of a selected region may allow for higher quality analysis of an area containing several islets and their local environment. Importantly, adjusting certain parameters will markedly enhance or reduce the quality of image capture. First, reducing the z-step size in LASX will increase resolution of image details by capturing z-slices at smaller z-intervals, allowing for a more continuous structure when observed later in 3D (**Figure 2A**). We have imaged islets using z-step intervals as small as 0.5µm. Additionally, line averaging is a method used in which each X-line is scanned a user-defined number of times, and the result is averaged. Increasing the line averaging value is the most effective method for reducing noise in the resulting image. However, reducing z-step size and increasing the line averaging value will consequently result in longer scan times and larger file sizes. Generally, small z-step sizes and higher line averaging values can be used for imaging small regions of tissue, whereas large z-step sizes and lower line averaging values are required for whole-section tile-scans. For imaging small regions, we generally use z-step sizes of 1-2µm and line averaging values of 32-64. For larger whole-tissue sections, z-step sizes range from 6-10µm and line averaging values are generally 8-16.

3D SURFACE RENDERING AND 3D PRINTS

Files in ".lif" format can be loaded into Imaris for 3D surface rendering and analysis. Data from a tile-scan performed on the SP8 is imported into Imaris with all fluorescent channels available for analysis individually or simultaneously. For more specific analysis, such as analyzing a small region containing several islets and their associated vasculature, the Crop 3D function reduce the area of analysis. To process and clean the data, background signal/noise can be reduced by using the Thresholding-Baseline Subtraction function. Once background is reasonably reduced, the fluorescent signal for the structure of interest (islet, vasculature, beta-cells, alpha-cells, smooth muscle actin, etc.) can be transformed into a 3D structure using the Surfaces tool. First, the source channel must be specified for the structure of interest. Then, smoothing function within the Surfaces tool applies a Gaussian filter to the generated 3D surface, which can be useful in order to create smooth islet and vascular surfaces. In the next step, the user will manually select a threshold value to reasonably reduce background noise while including as much signal and structure of the desired object as possible. Once the algorithm completes, the user will have a set of surfaces that represent their fluorescent signal as well as accompanying data, which includes volume, surface area, sphericity, and x-y location, among others. Importantly, created surfaces can be used to "mask" another fluorescence within the same dataset, which allows for the capturing of fluorescent channels (and subsequent surface creation if desired) exclusively within or exterior to another surface. For instance, we have used the masking feature to measure the relative volume of capillaries within islets compared to the volume of each individual islet by masking the vasculature channel within a surface created for the islets (**Figure 2B**) (25). Furthermore, surfaces created in Imaris can be exported for 3D printing. The surface can be saved in Imaris as .vmrl file, which can then be imported into a free, open-source 3D mesh processing software (Meshlab) where the surface can be saved as a file compatible with 3D printing software (.ply and .stl, etc.) (**Figures 2C–E**).

DISCUSSION

Optical tissue clearing has been a key for successful 3D imaging of thick tissues. Among many reagents, we have chosen a sequential use of increasing concentrations of D-fructose supplemented with 0.3% α-thioglycerol to prevent browning (Maillard reaction) and autofluorescence (21). The refractive index of high-concentration D-fructose is higher than other water-based clearing reagents. Unlike sucrose, it does not cause tissue shrinkage. With this simple method, sufficient clearing of the pancreatic tissue is achieved in 1 day. Pre-conjugation of primary antibodies with an NHS ester-activated form of fluorescent dyes also accelerates the procedure, at the same time allowing for any combinations of primary antibodies without a concern of species-specific affinities. In terms of 3D imaging, a tile-scan of an entire tissue slice is useful for a large-scale unbiased analysis by capturing hundreds of islets at a time. Surface rendering is a powerful tool that includes many functions of Imaris such as panoramic views of islets and surrounding microenvironment as well as targeted transparency (e.g. intra-islet views). For *in vivo* studies of islet microcirculation in

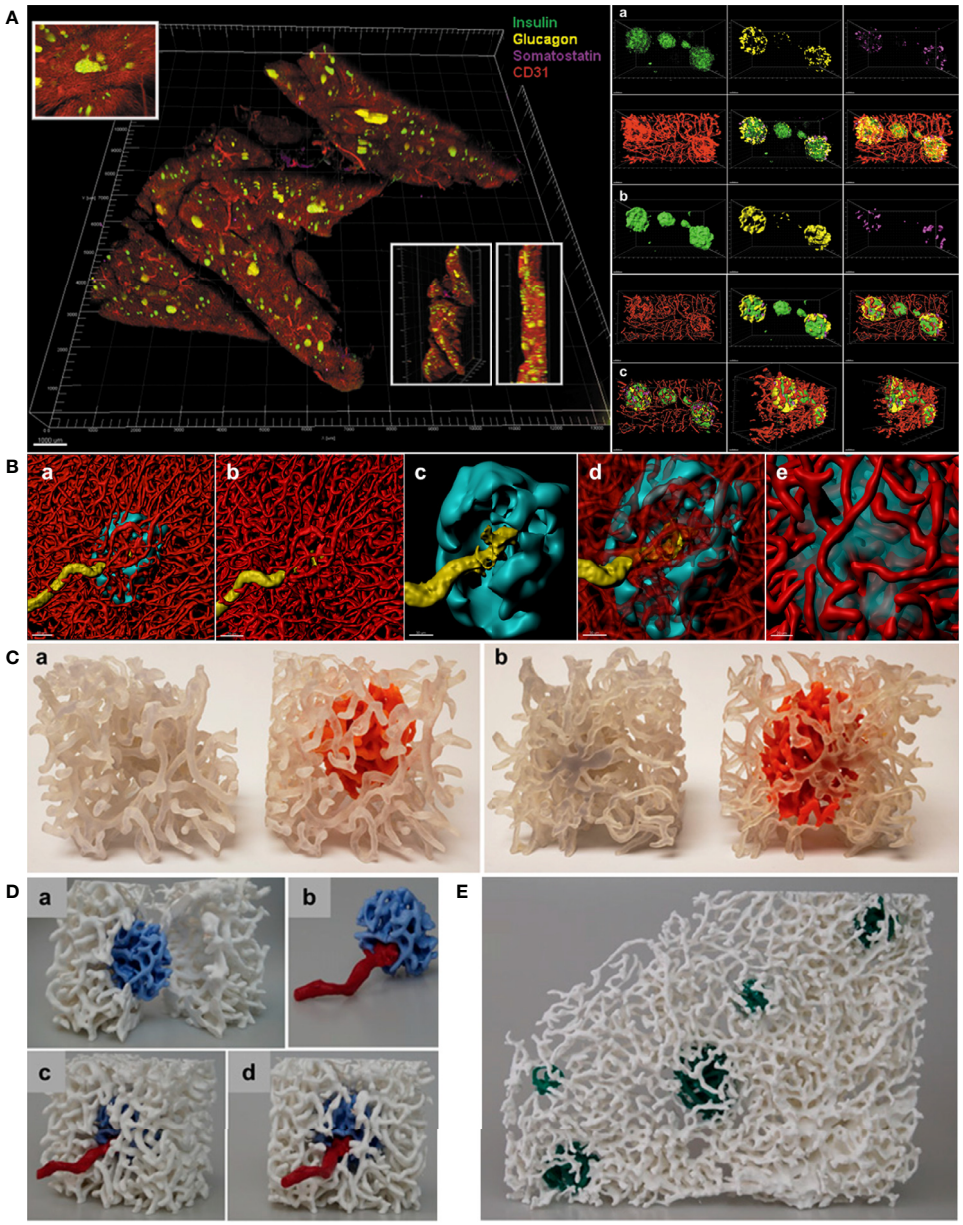

FIGURE 2 | *In situ* approach to study the capillary network. **(A)** *Left*. Full scan of a 600 µm pancreatic slice immunostained for insulin (green), glucagon (yellow), somatostatin (magenta) and CD31 (red). Three insets for detailed islet resolution and displaying depth with different angles. Scale bar: 1000 µm. *Right*. **a.** Cluster of islets in the sample with individual fluorescent channel images and merged ones. **b.** Same cluster of islets converted to a computer-generated surface rendering with multiple angles displayed for 3D viewing. c. Coronal slice of all islets in the cluster and a sagittal slice of the leftmost islet visualized by use of a computer-generated clipping plane to reveal the intraislet blood vessels. Scale bars: all 50 µm. (Adopted from 25) **(B) a.** 3D-rendered view of a human islet integrated in the pancreatic capillary network. Islet (HPi1, a human pan-endocrine cell marker in cyan), blood vessels (CD31 in red), and an afferent arteriole (α-SMA in yellow). Scale bar: 50 µm. **b.** Blood vessels only, displaying the continuity of capillaries in the islet as well as exocrine tissue. **c.** The aforementioned feeding arteriole penetrating the center of the islet. Scale bar: 30 µm. **d.** Vasculature partially made transparent. **e.** Close-up view of the interface of capillaries entering and exiting the islet. Scale bar: 20 µm. **(C)** 3D prints of a human islet. **a.** Side-by-side comparison of the same region of pancreas with exocrine and endocrine (intraislet) capillaries printed the same color (left, clear) and the exocrine capillaries in clear and endocrine capillaries in orange (right). **b.** Opposite side. **(D)** A more expansive view of the endocrine/exocrine vascular network with feeding arteriole shown in **(B)** Blood vessels within the islet (light blue) are integrated with those in the exocrine tissue (white). A feeding arteriole (red) penetrates the center of the islet. **a.** A cross-sectional view of the islet capillary network within the exocrine tissue vasculature. **b.** Islet capillaries with a feeding arteriole. Note the markedly larger size of the feeding arteriole compared with endocrine blood vessels. **c.** Side view of the endocrine and exocrine vascular network. **d.** Front view of the endocrine and exocrine vascular network. **(E)** Human islet vascular network embedded in the exocrine vasculature. Blood vessels in five human islets (dark green) integrated with the pancreatic vascular network (white). (**B–D**, adopted from 12).

mice,direct RBC labeling with fluorescent dye and particle tracking functions of Imaris have enabled us to perform quantitative analyses.

The use of imaging modalities including both real-time *in vivo* microscopy of mouse tissues and 3D analysis of thick pancreatic tissue slices from various species enables investigators to study the endocrine and exocrine pancreas in an environment that more closely mimics the living organism. *In vivo* microscopy allows us to see movements within the tissue, but the recording of these motions occurs in one 2D plane, limiting our view of tissue depth. Whereas, the *in situ* approach provides an in-depth view of the 3D structure of the tissue, despite lacking a view of movements within the tissue. Together, these imaging modalities complement one another and help us integrate our observations by incorporating complex visual characteristics obtained from different modalities into a better understanding of islets and the pancreas. We further propose that there are still gaps in our knowledge of the evolutionary relationships among different species in terms of the distinct pancreas structures including islet architecture and vascular, neuronal and ductal networks. For example, intra-islet capillary is believed to be significantly less dense in humans than mice (26, 27). When islet size distribution is similar in these two species (13, 28), functional implications of this inverted intra-islet capillary density are unknown. Expanding the application of these methods to various species, particularly relevant to 3D imaging, such studies may shed light on some unanswered questions and further elucidate similarities and differences of the pancreatic structures among diverse species and the underlying evolutionary adaptations.

Along with the progression of methods from islet cell identification, as in the studies performed in the early 20th century, to modern 3D rendering and real-time visualization, our interpretation of novel findings must also be adapted. We are looking at the same pancreas, but how we look at it has changed, which may provide us with a unique appreciation for pancreatic architecture and physiology that have not been recognized before.

Our understanding of the physiology and biology of the pancreas has been continually enhanced with the advancement of technology as described above. Interestingly, though, it is the human mind that could hamper such progress. Retrospectively, we may see something that does not exist, such as a non-beta-cell mantle of a rodent islet in 2D images that, we propose, may be due to our inherited visual perception, where Gestalt principles of continuity and closure are relevant (14). Inversely, we can fail to see something very new and unexpected that might have been right in front of us, especially when it challenges a gold standard that has dominated the field for a long time. In parallel with rapidly developing technology that allows us increasing resolution and maximal precision in our observations, it is important to remind ourselves to keep an open mind with good imagination.

AUTHOR CONTRIBUTIONS

MD and MH wrote, edited, and revised the manuscript. All authors contributed to the article and approved the submitted version.

ACKNOWLEDGMENTS

The study is supported by National Institutes of Health, DK117192, DK127786, DK020595 to the University of Chicago Diabetes Research and Training Center (Physiology Core), and a gift from the Kovler Family Foundation to MH.

REFERENCES

1. Morrison H. Contributions to the Microscopic Anatomy of the Pancreas. *Bull Inst Hist Med* (1937) 5:259–97. doi: 10.1038/1411038c0
2. Baskin DG. A Historical Perspective on the Identification of Cell Types in Pancreatic Islets of Langerhans by Staining and Histochemical Techniques. *J Histochem Cytochem* (2015) 63(8):543–58. doi: 10.1369/0022155415589119
3. Lane MA. The Cytological Characters of the Areas of Langerhans. *Am J Anat* (1907) 7:409–22. doi: 10.1002/aja.1000070304
4. Bloom W. A New Type of Granular Cell Inthe Islets of Langerhans of Man. *Anat Rec* (1931) 49:363–71. doi: 10.1002/ar.1090490406
5. Coons AH, Creech HJ, Jones RN, Berliner E. The Demonstration of Pneumococcal Antigen in Tissues by the Use of Fluorescent Antibody. *J Immunol* (1942) 45:159–70.
6. Lacy PE, Davies J. Preliminary Studies on the Demonstration of Insulin in the Islets by the Fluorescent Antibody Technic. *Diabetes* (1957) 6(4):354–7. doi: 10.2337/diab.6.4.354
7. Lacy PE, Davies J. Demonstration of Insulin in Mammalian Pancreas by the Fluorescent Antibody Method. *Stain Technol* (1959) 34(2):85–9. doi: 10.3109/10520295909114654
8. Baum J, Simoms BE Jr, Unger RH, Madison LL. Localization of Glucagon in the Alpha Cells in the Pancreatic Islet by Immunofluorescent Technics. *Diabetes* (1962) 11:371–74.
9. Coalson RE. Pseudoisocyanin Staining of Insulin and Specificity of Empirical Islet Cell Stains. *Stain Technol* (1966) 41(2):121–9. doi: 10.3109/10520296609116291
10. Wollman AJM, Nudd R, Hedlund EG, Leake MC. From Animaculum to Single Molecules: 300 Years of the Light Microscope. *Open Biol* (2015) 5 (4):150019. doi: 10.1098/rsob.150019
11. Brelje TC, Scharp DW, Sorenson RL. Three-Dimensional Imaging of Intact Isolated Islets of Langerhans With Confocal Microscopy. *Diabetes* (1989) 38 (6):808–14. doi: 10.2337/diab.38.6.808
12. Dybala MP, Kuznetsov A, Motobu M, Hendren-Santiago BK, Philipson LH, chervonsky AV, et al. Integrated Pancreatic Blood Flow: Bidirectional Microcirculation Between Endocrine and Exocrine Pancreas. *Diabetes* (2020) 69(7):1439–50. doi: 10.2337/db19-1034
13. Dybala MP, Hara M. Heterogeneity of the Human Pancreatic Islet. *Diabetes* (2019) 68(6):1230–9. doi: 10.2337/db19-0072
14. Dybala MP, Butterfield JK, Hendren-Santiago BK, Hara M. Pancreatic Islets and Gestalt Principles. *Diabetes* (2020) 69(9):1864–74. doi: 10.2337/db20-0304
15. Brunicardi FC, Stagner J, Bonner-Weir S, Wayland H, Kleinman R, Livingston E, et al. Microcirculation of the Islets of Langerhans. Long Beach Veterans Administration Regional Medical Education Center Symposium. *Diabetes* (1996) 45:385–92. doi: 10.2337/diab.45.4.385
16. Nyman LR, Wells KS, Head WS, McCaughey M, Ford E, Brissova M, et al. Powers AC. Real-Time, Multidimensional in Vivo Imaging Used to

Investigate Blood Flow in Mouse Pancreatic Islets. *J Clin Invest* (2008) 118:3790–7. doi: 10.1172/JCI36209
17. Agrawal R, Balne PK, Tun SBB, Sia Wey Y, Khandelwal N, Barathi VA. Fluorescent Dye Labeling of Erythrocytes and Leukocytes for Studying the Flow Dynamics in Mouse Retinal Circulation. *J Vis Exp* (2017) 125:55495. doi: 10.3791/55495
18. Hara M, Wang X, Kawamura T, Bindokas VP, Dizon RF, Alcoser Y, et al. Transgenic Mice With Green Fluorescent Protein-Labeled Pancreatic Beta-Cells. *Am J Physiol Endocrinol Metab* (2003) 284:E177–83. doi: 10.1152/ajpendo.00321.2002
19. Reissaus CA, Piñeros AR, Twigg AN, Orr KS, Conteh AM, Martinez MM, et al. A Versatile, Portable Intravital Microscopy Platform for Studying Beta-Cell Biology in Vivo. *Sci Rep* (2019) 9(1):8449. doi: 10.1038/s41598-019-44777-0
20. Chung K, Wallace J, Kim SY, Kalyanasundaram S, Andalman AS, Davidson TJ, et al. Structural and Molecular Interrogation of Intact Biological Systems. *Nature* (2013) 497(7449):332–7. doi: 10.1038/nature12107
21. Muntifering M, Castranova D, Gibson GA, Meyer E, Kofron M, Watson AM. Clearing For Deep Tissue Imaging. *Curr Protoc Cytom* (2018) 86(1):e38. doi: 10.1002/cpcy.38
22. Costantini I, Cicchi R, Silvestri L, Vanzi F, Saverio Pavone F. In-Vivo and Ex-Vivo Optical Clearing Methods for Biological Tissues: Review. *BioMed Opt Express* (2019) 10(10):5251–67. doi: 10.1364/BOE.10.005251
23. Wang H, Khoradmehr A, Tamadon A. FACT or PACT: A Comparison Between Free-Acrylamide and Acrylamide-Based Passive Sodium Dodecyl Sulfate Tissue Clearing for Whole Tissue Imaging. *Cell J* (2019) 21(2):103–14. doi: 10.22074/cellj.2019.5989
24. Lee SSY, Bindokas VP, Kron SJ. Multiplex Three-Dimensional Optical Mapping of Tumor Immune Microenvironment. *Sci Rep* (2017) 7(1):17031. doi: 10.1038/s41598-017-16987-x
25. Fowler JL, Lee SS, Wesner ZC, Olehnik SK, Kron SJ, Hara M. Three-Dimensional Analysis of the Human Pancreas. *Endocrinology* (2018) 159 (3):1393–400. doi: 10.1210/en.2017-03076
26. Brissova M, Shostak A, Fligner CL, Revetta FL, Washington MK, Powers AC, et al. Human Islets Have Fewer Blood Vessels Than Mouse Islets and the Density of Islet Vascular Structures is Increased in Type 2 Diabetes. *J Histochem Cytochem* (2015) 63(8):637–45. doi: 10.1369/0022155415573324
27. Cohrs CM, Chen C, Jahn SR, Stertmann J, Chmelova H, Weitz J, et al. Vessel Network Architecture of Adult Human Islets Promotes Distinct Cell-Cell Interactions in Situ and is Altered After Transplantation. *Endocrinology* (2017) 158:1373–85. doi: 10.1210/en.2016-1184
28. Kilimnik G, Kim A, Jo J, Miller K, Hara M. Quantification of Pancreatic Islet Distribution in Situ in Mice. *Am J Physiol Endocrinol Metab* (2009) 297(6): E1331–8. doi: 10.1152/ajpendo.00479.2009

Conflict of Interest: The authors declare that the research was conducted in the absence of any commercial or financial relationships that could be construed as a potential conflict of interest.

The reviewer ST declared a shared affiliation with the authors, to the handling editor, at time of review.

frontiers in Endocrinology

ORIGINAL RESEARCH
published: 26 May 2021
doi: 10.3389/fendo.2021.641722

Imaging Beta-Cell Function in the Pancreas of Non-Human Primates Using a Zinc-Sensitive MRI Contrast Agent

Veronica Clavijo Jordan[1,2†], Catherine D. G. Hines[3†], Liza T. Gantert[3], Shubing Wang[4], Stacey Conarello[5], Christian Preihs[2,6], Sara Chirayil[2], Michael Klimas[3], Jeffrey L. Evelhoch[3] and A. Dean Sherry[2,6,7,8]*

[1] Athinoula A. Martinos Center for Biomedical Imaging, Massachusetts General Hospital, Harvard Medical School, Charlestown, MA, United States, [2] Advanced Imaging Research Center, The University of Texas Southwestern Medical Center, Dallas, TX, United States, [3] Translational Biomarkers, Merck & Co., Inc., Kenilworth, NJ, United States, [4] Biometrics Research, Merck & Co., Inc., Kenilworth, NJ, United States, [5] Pharmacology, Merck & Co., Inc., Kenilworth, NJ, United States, [6] VitalQuan, LLC, Dallas, TX, United States, [7] Department of Radiology, The University of Texas Southwestern Medical Center, Dallas, TX, United States, [8] Department of Chemistry & Biochemistry, The University of Texas at Dallas, Richardson, TX, United States

Non-invasive beta cell function measurements may provide valuable information for improving diabetes diagnostics and disease management as the integrity and function of pancreatic beta cells have been found to be compromised in Type-1 and Type-2 diabetes. Currently, available diabetes assays either lack functional information or spatial identification of beta cells. In this work, we introduce a method to assess the function of beta cells in the non-human primate pancreas non-invasively with MRI using a Gd-based zinc(II) sensor as a contrast agent, Gd-CP027. Additionally, we highlight the role of zinc(II) ions in the paracrine signaling of the endocrine pancreas *via* serological measurements of insulin and c-peptide. Non-human primates underwent MRI exams with simultaneous blood sampling during a Graded Glucose Infusion (GGI) with Gd-CP027 or with a non-zinc(II) sensitive contrast agent, gadofosveset. Contrast enhancement of the pancreas resulting from co-release of zinc(II) ion with insulin was observed focally when using the zinc(II)-specific agent, Gd-CP027, whereas little enhancement was detected when using gadofosveset. The contrast enhancement detected by Gd-CP027 increased in parallel with an increased dose of infused glucose. Serological measurements of C-peptide and insulin indicate that Gd-CP027, a high affinity zinc(II) contrast agent, potentiates their secretion only as a function of glucose stimulation. Taken in concert, this assay offers the possibility of detecting beta cell function *in vivo* non-invasively with MRI and underscores the role of zinc(II) in endocrine glucose metabolism.

Keywords: beta cell function, imaging, primate, diabetes, pancreas

OPEN ACCESS

Edited by:
Guy A. Rutter, Imperial College London, United Kingdom

Reviewed by:
Marcia Hiriart, Universidad Nacional Autonoma de Mexico, Mexico
Guoqiang Gu, Vanderbilt University, United States

***Correspondence:**
A. Dean Sherry
dean.sherry@utsouthwestern.edu

†These authors have contributed equally to this work

Specialty section:
This article was submitted to Diabetes: Molecular Mechanisms, a section of the journal Frontiers in Endocrinology

Received: *14 December 2020*
Accepted: *26 April 2021*
Published: *26 May 2021*

Citation:
Clavijo Jordan V, Hines CDG, Gantert LT, Wang S, Conarello S, Preihs C, Chirayil S, Klimas M, Evelhoch JL and Sherry AD (2021) Imaging Beta-Cell Function in the Pancreas of Non-Human Primates Using a Zinc-Sensitive MRI Contrast Agent. Front. Endocrinol. 12:641722. doi: 10.3389/fendo.2021.641722

INTRODUCTION

Glucose metabolism is tightly controlled by a systemic feedback-loop mechanism comprised of communication between beta cells in the pancreas and insulin-sensitive tissues (1). The disturbance of glucose homeostasis as a result of immunologically-induced loss of pancreatic beta cells ultimately leads to symptoms of type 1 diabetes mellitus (T1DM). This disease usually presents itself in young individuals, and common treatment options include self-injected doses of long-acting and short-acting insulin derivatives, mechanical monitoring of glucose and insulin dosing *via* pumps, and pancreatic islet transplantation (2, 3). In contrast, Type 2 diabetes mellitus (T2DM), responsible for approximately 90% of all diabetes cases (4), represents a systemic disease characterized by hyperglycemia either in the context of insulin resistance in peripheral tissues or lack of insulin secretion from the pancreas (1, 5). The treatment paradigm for T2DM includes initial lifestyle changes to attempt to reduce insulin resistance often supplemented with oral metformin, a biguanide-class drug whose primary mechanism of action is to reduce hepatic glucose production while simultaneously increasing insulin uptake in insulin-sensitive tissues (6). Although effective at reducing hyperglycemia, metformin has not been proven to prevent the conversion from impaired glucose tolerance to frank T2DM, only slowing the progression of disease while maintaining the rate of beta cell function deterioration when compared to other treatment options such as sulfonylureas or insulin injections (7). The pathophysiology of the disease is vastly heterogeneous across patients and this creates uncertainties in the optimal treatment regimen (1). While therapeutic outcomes may be predicted by knowing the state of beta-cell functionality (8), at this time there is no accurate way to measure beta-cell function directly from the pancreas in a non-invasive fashion.

Beta cell function is currently assessed by measuring blood glucose, proinsulin, insulin and C-peptide levels, or clamping experiments (9–12). However, blood levels lack information on the volume of beta cells (beta cell mass) or recruitment of cells (beta cell dynamics) needed to maintain blood glucose levels. While beta cell mass loss is well-known to parallel pancreatic function (13), it does not provide a complete picture of beta cell failure that is also attributable to beta cell dysfunction (14). Spatial or dynamic beta cell function information could be helpful to investigate the relationship of beta cell function to mass loss, where the latter can be measured invasively (15, 16) or non-invasively (17, 18). Both beta cell mass and function deficits contribute to T2DM (13) although some data suggests that beta cell function is more relevant and elusive in this disease (13, 14), particularly when beta cells are present but not viable (19). Thus, the means to non-invasively and longitudinally measure beta-cell function would be highly advantageous to determine the time course of T2DM development and for monitoring interventions to preserve beta-cell function.

Magnetic Resonance Imaging (MRI) is routinely used in abdominal diagnoses, particularly those related to the structural integrity of the pancreas. This includes ductal anatomy, presence of cysts, or acute pancreatitis, and diagnosis of lesions (20). Standard extracellular contrast agents are routinely used in abdominal MRI exams for tumor identification and staging. However, most if not all, currently conducted pancreatic radiological exams offer no direct information about beta cell mass or function. Zinc(II) is known to be co-released with insulin from beta cells in response to an increase in blood glucose. This ion is then dispersed into the islet extracellular space where it is taken up by neighboring alpha cells serving as an inter-cellular messenger ion signaling for glucagon secretion (21). The secreted zinc(II) can then be used as an indirect indicator of insulin release (i.e., beta cell function) by use of a zinc(II) responsive contrast agent. A number of MRI zinc(II)-responsive agents have been reported (22–25) with designs largely based upon formation of a ternary complex with serum albumin in the presence of excess zinc(II). Upon co-release of zinc(II) and insulin from pancreatic beta-cells, these agents form a complex with the excess zinc(II) and subsequently bind with albumin to form a high-relaxivity complex that ultimately translates into hyperintense voxels in a T_1-weighted MRI image. Studies in rodents have demonstrated that this allows functional mapping of the insulin profile *in vivo* in healthy and diabetic rodents by MRI (22, 26, 27). However, it is generally appreciated that the rodent pancreas is an amorphous organ dispersed along the abdomen and interlaced between the intestines, stomach, liver, and spleen so it is exceedingly difficult to identify the endocrine lobes both accurately and consistently to monitor beta-cell function or loss in a longitudinal manner as a consequence of diabetes. As a result, a larger animal model in which the pancreas is a solid organ with easily identifiable lobes is paramount to further evaluate the use of such agents for functional imaging of glucose-stimulated insulin secretion.

A technique for imaging beta-cell function directly from different regions of the pancreas or other tissues could be quite useful for islet transplantation studies. Identification of dysfunctional islets in the pancreas along with accurate sorting of xenograft islets would most certainly benefit from an imaging method designed to assess beta-cell function in order to maximize the chances of graft success. In the treatment of T2DM, it would be beneficial to obtain beta-cell functional information to understand the pathogenesis of T2DM, treatment response and ultimately aid in the selection of improved T2DM therapies. In this work, we describe the use of the previously reported zinc(II) sensor (Gd-CP027) (22, 28) to measure beta-cell function in healthy non-human primates. In order to evaluate the sensitivity and specificity of this assay, we perform a modified graded glucose infusion (GGI) paradigm to initiate zinc(II)/insulin co-release in the presence of Gd-CP027 versus a control agent (gadofosveset) with similar albumin binding behavior and relaxivity but lacking in sensitivity to zinc(II).

MATERIALS AND METHODS

Animal Preparation

All procedures were performed in accordance with our institution's IACUC guidelines at the AALAC-accredited facility where the animals were housed. Adult, healthy male

and female (n = 2, each) rhesus macaques were used for this study; alternative large animal models (e.g. swine, canines) were not used because primates allow for easier translation to human studies. All four animals were imaged on two separate days, Study 1 and Study 2, which were approximately three weeks apart to allow for adequate recovery after anesthesia and blood sampling. Animals underwent a 16 hour fast prior to the day of the MRI exam, and water intake was restricted two hours prior to anesthesia to facilitate easier visualization of the pancreas.

The animals were fed a High Protein Monkey Diet 5045 and High Protein Monkey Diet Jumbo 5047 biscuits once a day, where daily intake was calculated and tailored to each animal as a function of age, weight, and body condition. The animals weighed 7.1 ± 1.1 kg (range, 6.3-9.7 kg) on both study days. To facilitate handling in preparation for MRI, animals were first anesthetized with 10 mg/kg ketamine hydrochloride (100 mg/mL) administered intramuscularly so intravenous catheters could be placed into the left and right saphenous veins and a cephalic vein for contrast agent, glucose infusion, and blood sampling, respectively. Animals were then administered 5 mg/kg of propofol intravenously *via* the cephalic vein to allow endotracheal intubation. Once placed on the scanning table, anesthesia was maintained using a mix of approximately 70:30 ratio of oxygen to isoflurane, which was then maintained between 1.5-3%. A temperature probe, pulse oximeter and end tidal CO_2 monitor were connected for continuous monitoring. Body temperature was maintained by a dorsal K-module warm water recirculating blanket. Fluid maintenance (10 mL/kg/hr Lactated Ringer's solution) was co-administered in conjunction with the GGI platform during the MRI exam, as described in main text.

Breath-hold imaging was also performed on the anesthetized animals during the dynamic 3D T1-weighted images only. Animals were pre-selected based on their ability to breath-hold during previous MRI exams. The gas lines to the ventilator were shut off when breath-holding was needed and was then opened five seconds before breath-holding needed to end. All breath-holds were less than 40 seconds, and at least three minutes were allowed for recovery between breath-holds, consistent with our animal protocol. Each animal was able to receive enough oxygen and remain physiologically stable while under anesthesia. SpO_2 was monitored for any irregularities. SpO_2 did not drop lower than 95, which would require longer recovery between breath-holds and adjustment of anesthesia, if necessary. Adjustments to the amount of air administered, ratio of oxygen to isoflurane, and percent of isoflurane were carried out as needed to maintain stable anesthesia and breath-holding under the supervision of a veterinarian.

MRI Acquisition

All imaging was performed using a Siemens 3T Trio and a four-channel flex coil. After a series of localizer images to position the region of the abdomen where the T1-weighted images would be acquired, T2-weighted axial and coronal single-shot turbo spin echo images were acquired with respiratory triggering to identify the pancreas. Using these spin echo images, higher resolution, fat-saturated T2-weighted turbo spin echo images of the pancreas were acquired with respiratory triggering in preparation for the T1-weighted 3D gradient echo dynamic sequence. For dynamic imaging, an axial, breath-held 3D T_1-weighted ("T1W") sequence was acquired with the following parameters: FOV = 20 cm x 20 cm, slice thickness = 1.0 mm, TE/TR = 2.32/5.75 ms, 1 average, 30 slices, parallel acceleration factor = 2, flip-angle = 10°, 192 x 192 matrix for a resolution of 1.0 mm x 1.0 mm x 1.0 mm, BW = 360 Hz/pixel, and a scan time of 25 seconds.

In Study 1, the animals were administered 50 mg/kg/hr Gd-CP027 intravenously. For comparison purposes, this amounts to ~2-3 fold less contrast agent that that typically administered as a single bolus (0.1 mmol/kg) in a clinical study. Lyophilized, research grade Gd-CP027 (VitalQuan, Dallas, TX) was reconstituted in 100 mM TRIS buffer, pH 7.40 (25.5 mg/mL) and filtered for sterility. In Study 2, gadofosveset trisodium was administered intravenously at 50 mg/kg/hr. Commercially available gadofosveset was diluted into 100 mM TRIS buffer, pH 7.40 (25.2 mg/mL) and filtered for sterility. The two imaging studies were performed at least three weeks apart.

Infusion of contrast agent was initiated after all anatomical images of the pancreas and an initial T1W image was acquired. Immediately after initiating the infusion, the first dynamic T1W, breath-held image was acquired ("-20 min"). The infusion was then continued for the entirety of the exam. After 20 minutes of waiting to ensure the contrast agent was well-distributed and in steady-state, dynamic T1-weighted images were acquired beginning at "0 min" over one hour ("60 min") at four-minute intervals (17 total time points). The 20 min pre-circulation time was established by imaging the kidneys every five minutes after infusion until constant enhancement was seen in the renal pelvis (data not shown).

Graded Glucose Infusion and Blood Sampling

To challenge the pancreas to co-release insulin and zinc(II), a modified 2-step graded glucose infusion (GGI) protocol, a standard paradigm for pancreas challenges (29–31), was performed during the MRI exam. Intermittent blood samples were also collected during the study for glucose, insulin, and C-peptide measurements. **Figure 1** summarizes the simultaneous MRI acquisition, blood sampling, and infusion paradigms. The GGI consisted of 20 min of saline infusion (0 min – 20 min) as an internal control, followed by 20 minutes of 8 mg/kg/min dextrose (20 min – 40 min), and then 20 minutes of 16 mg/kg/min dextrose (40 min – 60 min). Blood samples were taken every four minutes in EDTA tubes beginning at 0 min and continuing for one hour (60 min) at 4 min intervals.

MRI Analysis

All images were analyzed using both VivoQuant (v2.50, inviCRO, LLC, Boston, MA) and ImageJ (National Institutes of Health, Bethesda, MD). The pancreas was manually subdivided into body/head/neck and tail regions of interest (ROIs), with the plane containing the superior pole of the left kidney identified as the division between the body/head/neck and tail. Small circular or ellipsoid-shaped hyperintense regions, typically 15-20 pixels

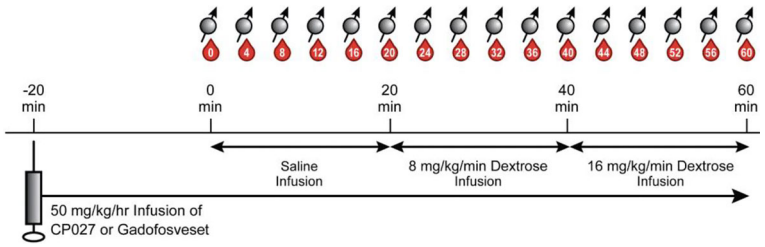

FIGURE 1 | Altered GGI paradigm. After animals were anesthetized and anatomical images were acquired, 50 mg/kg/hr of contrast agent was infused intravenously. After waiting 20 min for the agent to circulate, a separate saline infusion was administered for 20 min (0 min – 20 min), followed by 20 min of 8 mg/kg/min dextrose (20 min – 40 min), and then 20 min of 16 mg/kg/min of dextrose (40 min – 60 min). Blood sampling (denoted as red drops) and breath-held T1W images (spin symbols) were acquired every 4 min.

in size, were observed predominantly in the pancreatic tail region during infusion of Gd-CP027 ($n \geq 4$) and recorded. These regions are hereafter referred to as "hotspots". During infusion of gadofosveset, a largely albumin-bound vascular agent, fewer and less intense hotspots were also detected but these likely reflect small vascular regions of increased blood flow stimulated by insulin secretion (32, 33). To compare the signal intensities of these hotspots with nearby regions of lower intensity, 4 – 7 similarly sized and shaped ROIs on the same imaging slice adjacent to the identified hotspots were also measured in images collected during infusion of either Gd-CP027 of gadofosveset. These ROIs are hereafter referred to as "within-slice comparator"). The signal intensity at each time point in all ROIs in the pancreas (whole pancreas, tail, body/head/neck, hotspots, within-slice comparators) was normalized to the signal intensity in nearby muscle ROIs at the same time points. Using the normalized signal intensities in the pancreas ROIs, the percent change from 0 min (initiation of saline infusion; hereafter referred to as "% Signal Change") was calculated for each ROI at each time point.

Additionally, hotspots were categorized and clustered by size (area in mm^2) using the "Grow region" tool on Horos dicom viewing software. The pancreas prior to contrast agent infusion was segmented and the average and standard deviation in signal intensity of a 5 mm-thick slab was measured. The smart ROI selection tool was programmed to only select regions of interest that were 2-standard deviations above the average segmented pre-infusion pancreas signal intensity. Every imaging time point was analyzed in this manner and the ROIs were identified by average signal intensity, standard deviation, and size. This sequence was repeated for all animals in both studies. A K-means clustering algorithm was performed in order to determine hotspot clusters by size and change in contrast-to-noise ratio as a function of blood c-peptide, where the centroid of the clusters was identified by minimizing the sum of the squared distance between the centroid and each data point.

Blood Analysis

Plasma samples were analyzed for glucose, insulin, and C-peptide levels at each time point (In Vitro Sciences Laboratory, David H. Murdock Research Institute, Kannapolis, NC). Immediately after collection, blood was centrifuged at 1300 g at 4°C for 10 minutes. The plasma was removed, and frozen at -80°C for analysis. Glucose levels (mg/dL) were obtained using an Analox Glucose Analyzer (Analox Instruments Ltd, UK) from plasma samples and a commercially available glucose kit. Insulin levels (μIU/mL) and C-peptide levels (ng/mL) were obtained using a Meso Scale Discovery Sector Imager S 600 (Meso Scale Diagnostics, LLC, Rockville, MD) with commercially available insulin and C-peptide custom kits, respectively.

Statistical Analysis

A sequential statistical analysis was performed using two models (34). The first model estimated the slope of each parameter vs. time for each contrast agent to characterize agent and time interaction ("slope analysis") for C-peptide, glucose, insulin, and %signal change in the whole pancreas, head/body/neck, tail, hotspots, and comparator ROIs. Whenever the slope analysis identified differences between the two agents, a second analysis was performed. This second model used the means of each time point for each parameter and each agent to determine the time at which the two agents diverge ("time course analysis"). To avoid inflating false positives, rigorous multiplicity adjustments were performed and resulted in splitting the p-value between the slope analysis and the time course analysis. A p-value of 0.025 (=0.05/2) was used to determine statistical significance; a Bonferroni Correction for the multiple time point comparisons (n=15) in the time course analysis was applied using an adjusted significance level ~0.00167 (=0.05/2/15) to control the family-wise error rate at the 0.025 level.

RESULTS

Figure 2A depicts the rhesus pancreas in vivo and plane of MRI acquisition shown in **Figure 2B**. **Figure 2B** shows representative T_1-weighted MRI images acquired at the 16, 36, and 56-min time points corresponding to the end of the three different infusion blocks (i.e. saline, 8 mg/kg/min dextrose, and 16 mg/kg/min dextrose). In study 1, steady-state contrast enhancement was detected in the abdominal aorta and inferior vena cava by the end of the first infusion block (saline, 20 mins). Upon initiation of

dextrose infusion at 8 mg/kg/min, the image intensity of the pancreas was further enhanced and small regions of higher intensity "hot spots" were detected primarily in the tail region. Signal enhancement throughout the pancreas and the hotspots became even more prominent when the dextrose level was increased to 16 mg/kg/min. The bottom panel of **Figure 2B** (study 2) shows images of the pancreas of the same animal and the same time points as in Study 1 after infusion of gadofosveset. Here, less enhancement was evident in images of the pancreas either before (16 min image) or after infusion of glucose (images at 36 and 56 min). **Figure 2C** compares the changes in image enhancement over the entire time course within the regions identified as hotspots after infusion of Gd-CP027 plus glucose versus gadofosveset plus glucose. All animals fully recovered from anesthesia after each study.

The average image intensity within ROIs consisting of the entire pancreas, the tail alone, and body/head/neck alone for the 4 animals are compared in **Figures 3A, B**. The increase in MR signal intensity over time in study 1 versus study 2 did not differ significantly for any of the segmented regions but an analysis of the slopes of these curves indicate there are statistically significant differences for the whole pancreas segment *versus* the body/head/neck region (p = 5.29E-7 and 2.79E-6, respectively). Like the comparator ROI data shown in **Figure 2C**, the segmented whole pancreas and body/head/neck time course data did not diverge significantly at any point during the GGI (p ≥0.00167 for all). The slope analysis for the tail region showed no differences between agents (p = 0.92).

Figure 3 show plots of image intensity increase (± SD, n=4) for the segmented pancreas (**Figures 3B–D**) and for within-slice comparator ROIs (**Figure 3E**) and hotspot ROIs (**Figure 3F**) over the 60 min study. The hotspot ROIs showed a 3% increase in normalized signal intensity during infusion gadofosveset versus an 8% increase during infusion of Gd-CP027 over the first 16 min. These differences likely reflect differences in the extracellular distribution of gadofosveset (largely vascular) versus Gd-CP027 (both vascular and extracellular). However, after initiation of the GGI, these differences in ROI image intensity diverged even further with the gadofosveset data remaining near 5% at 60 min versus near 20% for Gd-CP027. These differences can only be attributed to responsiveness of Gd-CP027 to Zn(II) release in these well-defined regions of the pancreas. An analysis of slopes of these curves also reported significant differences [hotspot ROIs (p = 1.81E-12) versus comparator ROIs (p = 0.003)]. The hotspot data comparisons between the two studies diverged significantly at minute 44

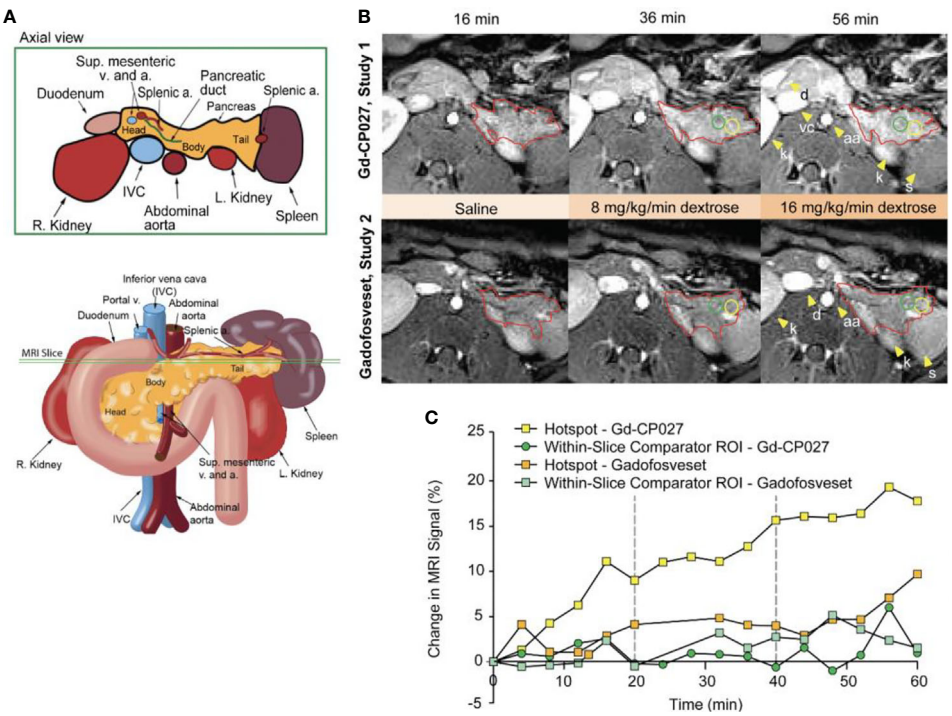

FIGURE 2 | **(A)** Schematic illustrating non-human primate abdominal anatomy, including organs surrounding the pancreas, and an axial cross-section indicating imaging slice used for MRI pancreas localization and quantification. **(B)** In vivo MR imaging of non-human primate after infusion of Gd-CP027 (Study 1), and gadofosveset (Study 2). Both studies received the altered GGI, and 3D T_1-weighted images were collected every four minutes. Axial images show the T_1-weighted scans at 16, 36, and 56 min time points, where each represent the scan after complete saline infusion, 8 mg/kg/min dextrose, and 16 mg/kg/min dextrose infusion, respectively. The tail of the pancreas is highlighted in both panels (red) and Gd-CP027 shows a more prominent enhancement in the pancreas, with focal signal enhancements intensifying over time. Hotsposts (yellow) and adjacent comparator ROIs (green) were identified and measured, and are plotted in **(C)** for the animal displayed in **(B)**.

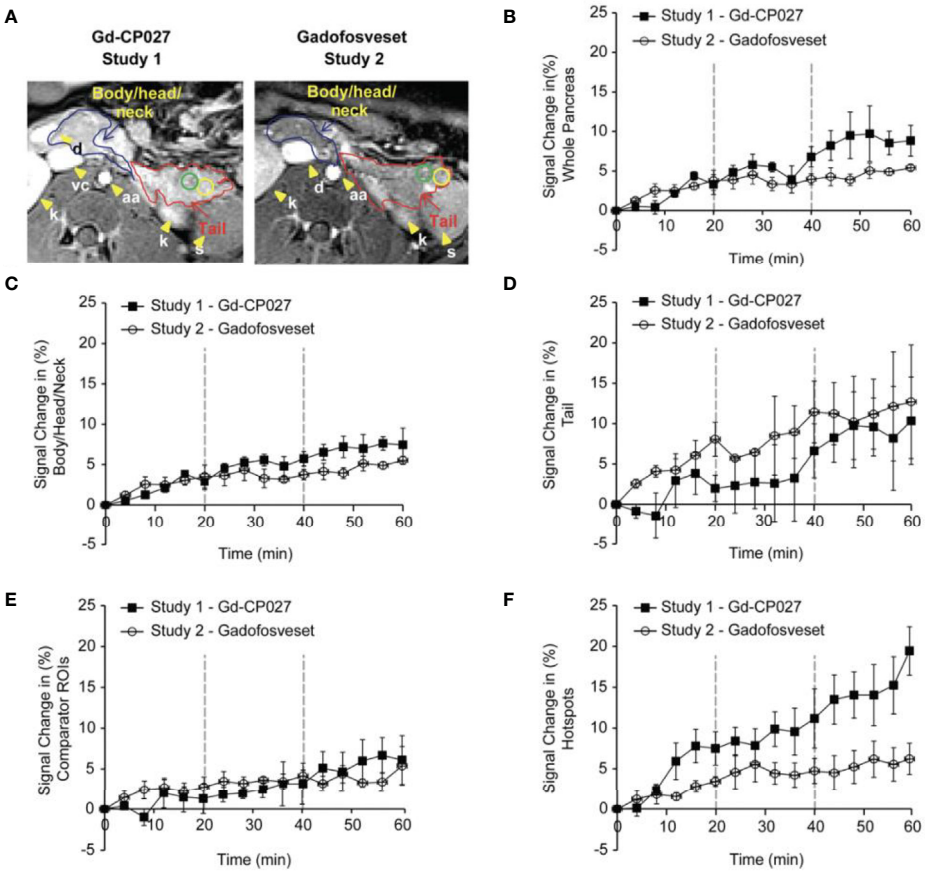

FIGURE 3 | **(A)** Non-human pancreas segmentation delineating the tail (red outline), body/head/neck (blue outline) and ROIs within the tail. Change in signal intensity (%) after infusion of each agent alone (0-20 min) and after graded increases in glucose (20-40 and 40-60 min). for **(B)** the entire pancreas, **(C)** Body/Head/Neck, and **(D)** Tail of the pancreas. The error bars reflect standard deviations for the 4 animals. **(E)** Change in MRI signal intensity (%) for within-slice comparator ROIs for the 4 animals. **(F)** Change in MRI signal intensity (%) within the regions identified as hotspots in the 4 animals.

(after infusion of glucose at the higher level) and remained divergent through the end of the GGI. The comparator ROI time courses did not diverge significantly at any time point during the GGI.

The blood measurements showed the expected increase in blood glucose during each dextrose infusion period in both studies (**Figure 4A**). An analysis of slopes of these curves showed no significant differences between study groups ($p = 0.07$). As expected, insulin and C-peptide increased in parallel with plasma glucose (**Figures 4B, C**) although, interestingly, both insulin and C-peptide were consistently higher in the Gd-CP027 study after infusion of glucose in comparison to the gadofosveset study. The slopes of these time-dependent increases were significantly different for both insulin ($p = 4.64E-5$) and C-peptide ($p = 3.29E-5$). These differences indicate that Gd-CP027 enhances insulin secretion above that initiated by glucose. By analyzing the area under the curve of the hotspot signal for both Gd-CP027 and Gadofosveset we observe that only Gd-CP027 corelates tightly to the blood measurements, in particular to insulin and C-peptide (**Figures 4D–F**).

To examine whether there are differences in the hotspot signal intensity and size patterns with respect to C-peptide levels in blood, plots of dCNR (increase in CNR compared to an equally-sized ROI in muscle) versus plasma C-peptide are shown in **Figures 5A, B**. Hotspots of various sizes were identified and included in this plot only if the average intensity was 2-standard deviations higher than the pre-infusion signal intensity. Further clustering of hotspot dCNR was done by using an algorithm to minimize the distance between the centroid of the clusters and each data point (K-means clustering). The same number of clusters ($k = 4$) was used in both plots. The average hotspot size in the Gd-CP027 group ranged from 12 - 50 mm^2 in comparison to an average size of 22 - 52 mm^2 in the gadofosveset group. One animal displayed hyper-physiological secretion of C-peptide/insulin in response to glucose as shown by the light blue colored cluster of 12 mm^2 in sized hotspots in **Figure 5A**. This illustrates that not all animals release the same amount of C-peptide when stimulated by a similar increase in plasma glucose. Nonetheless, this K-means cluster analysis showed a positive correlation between hotspot dCNR versus blood C-peptide levels in the Gd-CP027 group but not in the gadofosveset group.

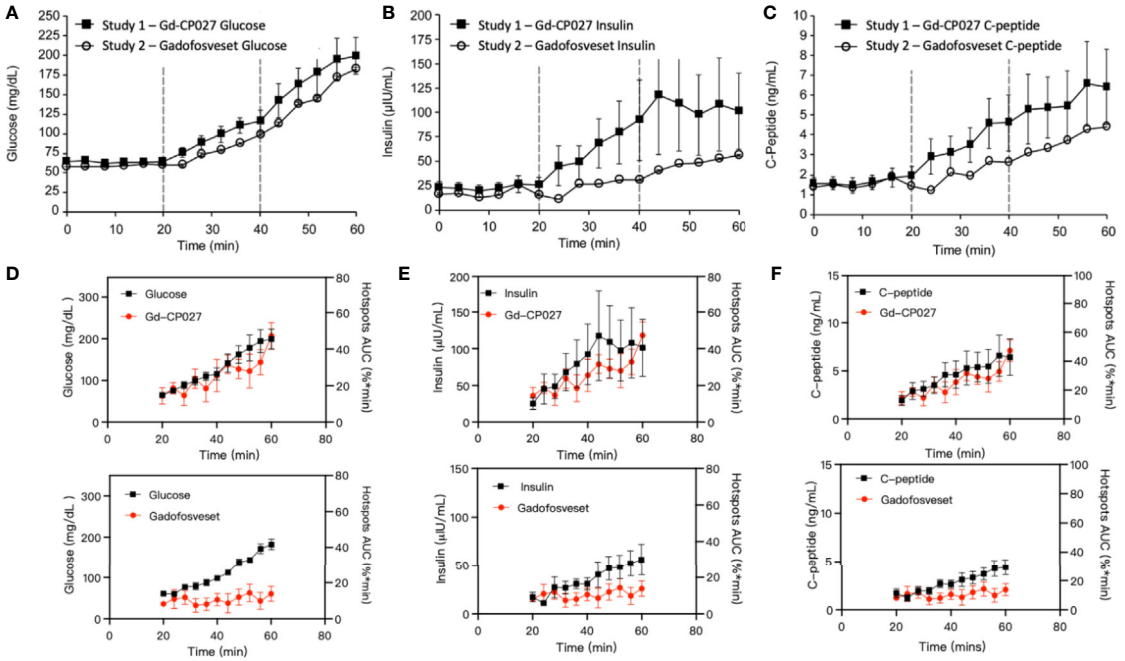

FIGURE 4 | **(A)** Blood glucose, **(B)** insulin, and **(C)** C-peptide levels collected during each GGI study (n = 4). Error bars represent standard error, and vertical dashed lines reflect each infusion period. Area under the curve for Gd-CP027 and Gadofosveset hotspots overlapped to blood measurements of **(D)** Glucose, **(E)** Insulin, and **(F)** C-peptide.

DISCUSSION

As demonstrated previously in isolated islets and in the rodent pancreas (26, 27), this imaging study of the non-human primate pancreas demonstrates that it may be feasible to assess β-cell function locally *in vivo* by glucose-stimulated zinc secretion (GSZS) and a Gd-based zinc(II) sensor as a contrast agent. Given that GSZS could also reflect β-cell mass, given the spatial resolution of MRI and the inability to resolve individual β-cells in this study it is deemed that this technology more accurately reflect β-cell function. Although MR signal enhancement was detected throughout the pancreas upon a graded glucose infusion (GGI) in the presence of either Gd-CP027 (zinc-sensitive agent) or gadofosveset (zinc insensitive), small regions previously referred to as "hotspots" (27) did show significant differences between the two agents during the highest GGI infusion period (44-60 min, **Figure 3F**). The blood plasma panel (**Figures 4A–C**) showed that glucose homeostasis was not significantly disturbed by infusion of either contrast agent (prior to initiation of the first glucose infusion) yet the insulin and C-peptide profiles suggest that Gd-CP027 may potentiate insulin secretion, especially at the highest level of glucose infusion. Since insulin secretion and potentiation by Gd-CP027 occurred only after infusion of glucose, the potentiation appears to be related to zinc(II) released in response to glucose and not the

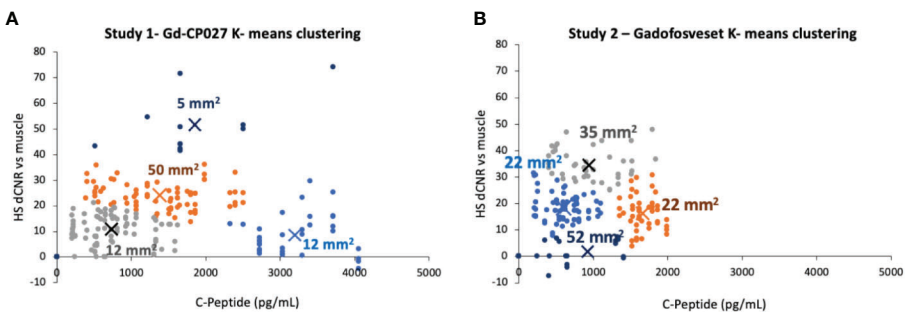

FIGURE 5 | K-means clustering (k = 4 for both studies) showing the change in contrast-to-noise ratio versus the corresponding blood C-peptide measurement for all animals and all hotspots, where "X" represents the centroid of each cluster labeled with its respective average hotspot area for animals receiving **(A)** Gd-CP027, or **(B)** Gadofosveset.

initial extracellular zinc(II) present in tissue. These observations are further confirmed in **Figures 4D–F** where the area under the curve (AUC) for the hotspots over the 20 – 60 minute infusion periods corelate tightly with insulin and c-peptide plasma profiles over time. However, further experiments will be necessary to understand the mechanism of Gd-CP027 potentiation, but it is important to note that neither Gd-CP027 nor gadofosveset are thought to enter cells so this potentiation likely reflects a disturbance in extracellular zinc (II) levels.

It is well known that zinc(II) plays a role in the correct function of many secretory organs including prostate, mammary glands, and the pancreas (21, 35–37). In the pancreas, co-secretion of zinc and insulin has been imaged using fluorescent probes (38, 39) and more recently by MRI (22, 24, 26). Given that MRI sensors detect insulin secretion indirectly by binding to excess Zn(II) released with insulin, it is important to consider the potential impact these agents have on other pancreatic secretory cell mechanisms. Secretory cells have distinct mechanisms to maintain tightly controlled Zn(II) homeostasis. This is mainly achieved by the expression of Zn(II) transporters of the ZnT and ZIP families (36). It has been shown that extracellular signals, such as exposure of prostate epithelial cells to an increase in plasma glucose (40), triggers a rapid redistribution of Zn(II) transporters between the plasma membrane and other cellular organelle membranes that results in also rapid redistribution of mobile Zn(II). Many other studies in multiple cell types have shown that alterations in various extracellular processes induces an immediate redistribution of intracellular Zn(II), a phenomenon referred to as "the zinc wave" (41). These and other studies showing that Zn(II) mimics the actions of hormones, growth factors, and cytokines have led to the concept that Zn(II) ions play a role as a second messenger capable of transducing extracellular stimuli into intracellular signaling pathways (42). Several different Zn(II) transporters are expressed in β-cells but the most highly abundant transporter, ZnT8, playing a key role in formation of zinc-insulin granules (43) and ZnT8 expression has been shown to positively correlate with circulating levels of insulin and glucagon (44). Although controversial, release of Zn(II) and insulin from β-cells has been reported to modulate glucagon secretion by uptake of Zn(II) ions into neighboring α-cells *via* ZIP transporters (21). Given that Gd-CP027 has a high affinity for Zn(II) (K_D ≈30 nM), infusion of this agent certainly must have an influence on the activity of Zn(II) transporters and likely could impact signaling of glucagon secretion (36, 45, 46). Although further studies will be required to determine the exact mechanism of insulin potentiation by Zn(II) chelating agents, we hypothesize that the origin of the observed potentiation of glucose-dependent insulin secretion by Gd-CP027 may reflect Zn(II) scavenging and subsequent calcium-mediated cell-membrane depolarization (21, 47). Although the plasma glucose levels tended to be higher in animals infused with Gd-CP027 versus gadofosveset (**Figure 4A**), these differences did not reach statistical significance. Nevertheless, this trend would be consistent with the hypothesis that a lower concentration of bioavailable Zn(II) in the extracellular space in animals exposed to Gd-CP027 could allow unabated glucagon secretion from α-cells.

One of the most interesting findings in this study was the focal nature of the normalized image enhancement in select regions of the pancreas. These focal hotspots, observed mostly in the tail, are consistent with clusters of islets as reported in previously published studies (27, 32, 33, 48). It is known that the regional distribution of pancreatic islets is uneven and clustered throughout the pancreas (32) and that this distribution varies among animal species (49, 50). The non-human primate, like the human pancreas, has insulin-secreting islets dispersed throughout the body of the pancreas, with higher β-cell density in the tail (50). Based on these prior reports, we expected to find significant differences in the segmented whole tail. An analysis of size and signal change clustering of hotspots (**Figure 5A**) showed that the smallest hotspots correlated with higher levels of C-peptide in blood even though there were no significant differences in image intensity in the entire segmented tail because of averaging with non-enhancing pancreas regions.

Although we observed that the change in signal intensity of hotspot clusters in the pancreas correlated with insulin and C-peptide secretion only in the Gd-CP027 group (**Figures 4D–F**), it was interesting to find observable hotspots in the pancreas in the gadofosveset group as well. These results indicate that these focal enhancements do not only reflect insulin and Zn(II) secretion but there must be an additional mechanism that contributes to these higher intensity regions in the gadofosveset study. Given that gadofosveset is a blood pool agent that extravasates into extracellular space more slowly than other low molecular weight Gd-based agents, it is reasonable to suggest that the focal enhancements observed in the gadofosveset study may reflect an increase in blood flow in those regions releasing the most insulin. It has been shown previously using fluorescence-labeled red blood cells that the apparent blood volume of the pancreas is greater during hyperglycemia than during hypoglycemia (51, 52) and this may be the origin of the effects observed here when using the vascular agent, gadofosveset.

The primary limitation of this study was the small number of animals available for study. Given the small cohort and the fact that one animal released more insulin and C-peptide while generating smaller changes in CNR in the Gd-CP027 study compared to the other animals, the differences between many of the parameters measured in this study did not reach statistical significance. Another potential limitation could be differences in pharmacokinetics and biodistribution of the two contrast agents. It was evident that uptake/clearance rates may differ, as seen in the 0-20 minute interval of **Figure 2C** and in the kidneys of **Figure 2B**, so the tissue biodistribution could contribute to local concentration differences at any given time point during the study. An analysis of slopes in the time-dependent data revealed significant differences between contrast agents for all measured parameters except the tail and glucose levels while the time course analysis revealed divergent responses at specific times only for the hotspot data. However, a consistent trend in the time course was evident in the plots (**Figures 3** and **4**) demonstrating different C-peptide and insulin release, as well as increased enhancement with Gd-CP027. This discrepancy between the sequential tests is due to a very conservative multiplicity adjustment as well as low power for the time course analysis due to the small sample size. Despite these limitations, this first study in the

non-human primate pancreas offers the possibility of imaging β-cell function *in vivo* (38, 47, 53).

DATA AVAILABILITY STATEMENT

The original contributions presented in the study are included in the article/supplementary material. Further inquiries can be directed to the corresponding author.

ETHICS STATEMENT

The animal study was reviewed and approved by the Institutional Animal Care and Use Committee at Merck & Co., Inc.

AUTHOR CONTRIBUTIONS

VCJ, AS, MK, JE, CH, and SCo conceived of the project. CH, LG, SW, VCJ, and JE carried out the experiments and analyzed the data. CP, SCh, and AS designed and prepared the zinc-sensitive imaging agent. All authors contributed to the article and approved the submitted version.

FUNDING

This work was supported in part by grants to ADS from the National Institutes of Health (DK-095416) and the American Diabetes Association (7-12-IN-42).

REFERENCES

1. Kahn SE, Cooper ME, Del Prato S. Pathophysiology and Treatment of Type 2 Diabetes: Perspectives on the Past, Present, and Future. *Lancet* (2014) 383 (9922):1068–83. doi: 10.1016/S0140-6736(13)62154-6
2. Bruni A, Gala-Lopez B, Pepper AR, Abualhassan NS, Shapiro AJ. Islet Cell Transplantation for the Treatment of Type 1 Diabetes: Recent Advances and Future Challenges. *Diabetes Metab Syndr Obes* (2014) 7:211–23. doi: 10.2147/DMSO.S50789
3. Atkinson MA, Eisenbarth GS, Michels AW. Type 1 Diabetes. *Lancet* (2014) 383(9911):69–82. doi: 10.1016/S0140-6736(13)60591-7
4. Shi Y, Hu FB. The Global Implications of Diabetes and Cancer. *Lancet* (2014) 383(9933):1947–8. doi: 10.1016/S0140-6736(14)60886-2
5. Melmed S, Polonsky K, Larsen PR, Kronenberg H. *Williams Textbook of Endocrinology*. *12*. Philadelphia, PA USA: Elsevier/Saunders (2011).
6. White JRJr. A Brief History of the Development of Diabetes Medications. *Diabetes Spectr* (2014) 27(2):82–6. doi: 10.2337/diaspect.27.2.82
7. Page KA, Reisman T. Interventions to Preserve Beta-Cell Function in the Management and Prevention of Type 2 Diabetes. *Curr Diabetes Rep* (2013) 13 (2):252–60. doi: 10.1007/s11892-013-0363-2
8. Nguyen KT, Billington CJ, Vella A, Wang Q, Ahmed L, Bantle JP, et al. Preserved Insulin Secretory Capacity and Weight Loss Are the Predominant Predictors of Glycemic Control in Patients With Type 2 Diabetes Randomized to Roux-en-Y Gastric Bypass. *Diabetes* (2015) 64(9):3104–10. doi: 10.2337/db14-1870
9. Lee SW, Lee S, Kim SH, Kim TH, Kang BS, Yoo SH, et al. Parameters Measuring Beta-Cell Function are Only Valuable in Diabetic Subjects With Low Body Mass Index, High Blood Glucose Level, or Long-Standing Diabetes. *Yonsei Med J* (2011) 52(6):939–47. doi: 10.3349/ymj.2011.52.6.939
10. U.K. Prospective Diabetes Study 16. Overview of 6 Years' Therapy of Type II Diabetes: A Progressive Disease. U.K. Prospective Diabetes Study Group. *Diabetes* (1995) 44(11):1249–58. doi: 10.2337/diabetes.44.11.1249
11. Festa A, Williams K, D'Agostino RJr., Wagenknecht LE, Haffner SM. The Natural Course of Beta-Cell Function in Nondiabetic and Diabetic Individuals: The Insulin Resistance Atherosclerosis Study. *Diabetes* (2006) 55(4):1114–20. doi: 10.2337/diabetes.55.04.06.db05-1100
12. Sjaarda L, Lee S, Tfayli H, Bacha F, Bertolet M, Arslanian S. Measuring Beta-Cell Function Relative to Insulin Sensitivity in Youth: Does the Hyperglycemic Clamp Suffice? *Diabetes Care* (2013) 36(6):1607–12. doi: 10.2337/dc12-1508
13. Meier JJ, Bonadonna RC. Role of Reduced Beta-Cell Mass Versus Impaired Beta-Cell Function in the Pathogenesis of Type 2 Diabetes. *Diabetes Care* (2013) 36 Suppl 2:S113–9. doi: 10.2337/dcS13-2008
14. Leahy JL, Hirsch IB, Peterson KA, Schneider D. Targeting Beta-Cell Function Early in the Course of Therapy for Type 2 Diabetes Mellitus. *J Clin Endocrinol Metab* (2010) 95(9):4206–16. doi: 10.1210/jc.2010-0668
15. Reiner T, Thurber G, Gaglia J, Vinegoni C, Liew CW, Upadhyay R, et al. Accurate Measurement of Pancreatic Islet Beta-Cell Mass Using a Second-Generation Fluorescent Exendin-4 Analog. *Proc Natl Acad Sci USA* (2011) 108 (31):12815–20. doi: 10.1073/pnas.1109859108
16. Rahier J, Guiot Y, Goebbels RM, Sempoux C, Henquin JC. Pancreatic Beta-Cell Mass in European Subjects With Type 2 Diabetes. *Diabetes Obes Metab* (2008) 10 Suppl 4:32–42. doi: 10.1111/j.1463-1326.2008.00969.x
17. Blomberg BA, Codreanu I, Cheng G, Werner TJ, Alavi A. Beta-Cell Imaging: Call for Evidence-Based and Scientific Approach. *Mol Imaging Biol* (2013) 15 (2):123–30. doi: 10.1007/s11307-013-0620-4
18. Jodal A, Schibli R, Behe M. Targets and Probes for non-Invasive Imaging of Beta-Cells. *Eur J Nucl Med Mol Imaging* (2016) 44(4):712–27. doi: 10.1007/s00259-016-3592-1
19. Gotthardt M, Eizirik DL, Cnop M, Brom M. Beta Cell Imaging - a Key Tool in Optimized Diabetes Prevention and Treatment. *Trends Endocrinol Metab* (2014) 25(8):375–7. doi: 10.1016/j.tem.2014.02.002
20. Zamboni G, Gourtsoyianni S. MDCT and MRI of Liver, Bile Ducts and Pancreas. Italy: Springer (2015). p. 121. doi: 10.1007/978-88-470-5720-3_26
21. Kelleher SL, McCormick NH, Velasquez V, Lopez V. Zinc in Specialized Secretory Tissues: Roles in the Pancreas, Prostate, and Mammary Gland. *Adv Nutr* (2011) 2(2):101–11. doi: 10.3945/an.110.000232
22. Yu J, Martins AF, Preihs C, Clavijo Jordan V, Chirayil S, Zhao P, et al. Amplifying the Sensitivity of Zinc(II) Responsive MRI Contrast Agents by Altering Water Exchange Rates. *J Am Chem Soc* (2015) 137(44):14173–9. doi: 10.1021/jacs.5b09158
23. De Leon-Rodriguez LM, Lubag AJ, Lopez JA, Andreu-de-Riquer G, Alvarado-Monzon JC, Sherry AD. A Second Generation MRI Contrast Agent for Imaging Zinc Ions *In Vivo*. *Medchemcomm* (2012) 3(4):480–3. doi: 10.1039/c2md00301e
24. Esqueda AC, Lopez JA, Andreu-de-Riquer G, Alvarado-Monzon JC, Ratnakar J, Lubag AJ, et al. A New Gadolinium-Based MRI Zinc Sensor. *J Am Chem Soc* (2009) 131(32):11387–91. doi: 10.1021/ja901875v
25. Major JL, Parigi G, Luchinat C, Meade TJ. The Synthesis and *In Vitro* Testing of a Zinc-Activated MRI Contrast Agent. *Proc Natl Acad Sci USA* (2007) 104 (35):13881–6. doi: 10.1073/pnas.0706247104
26. Lubag AJ, De Leon-Rodriguez LM, Burgess SC, Sherry AD. Noninvasive MRI of Beta-Cell Function Using a Zn2+-responsive Contrast Agent. *Proc Natl Acad Sci USA* (2011) 108(45):18400–5. doi: 10.1073/pnas.1109649108
27. Martins AF, Clavijo Jordan V, Bochner F, Chirayil S, Paranawithana N, Zhang S, et al. Imaging Insulin Secretion From Mouse Pancreas by MRI is Improved by Use of a Zinc-Responsive Mri Sensor With Lower Affinity for Zn(2+) Ions. *J Am Chem Soc* (2018) 140(50):17456–64. doi: 10.1021/jacs.8b07607
28. Clavijo Jordan MV, Lo ST, Chen S, Preihs C, Chirayil S, Zhang S, et al. Zinc-Sensitive MRI Contrast Agent Detects Differential Release of Zn(II) Ions From the Healthy vs. Malignant Mouse Prostate. *Proc Natl Acad Sci USA* (2016) 113(37):E5464–71. doi: 10.1073/pnas.1609450113
29. Wang X, Hansen BC, Shi D, Fang Y, Du F, Wang B, et al. Quantification of Beta-Cell Insulin Secretory Function Using a Graded Glucose Infusion With C-peptide Deconvolution in Dysmetabolic, and Diabetic Cynomolgus Monkeys. *Diabetol Metab Syndr* (2013) 5(1):40. doi: 10.1186/1758-5996-5-40

30. Lin JD, Wu CZ, Tang WH, Kuo FC, Pei D, Liang YJ, et al. Comparison of Second-Phase Insulin Secretion Derived From Standard and Modified Low-Dose Graded Glucose Infusion Tests. *Can J Diabetes* (2016) 40(6):529–34. doi: 10.1016/j.jcjd.2016.03.007
31. Kim SH, Liu A, Ariel D, Abbasi F, Lamendola C, Grove K, et al. Effect of Salsalate on Insulin Action, Secretion, and Clearance in Nondiabetic, Insulin-Resistant Individuals: A Randomized, Placebo-Controlled Study. *Diabetes Care* (2014) 37(7):1944–50. doi: 10.2337/dc13-2977
32. Ionescu-Tirgoviste C, Gagniuc PA, Gubceac E, Mardare L, Popescu I, Dima S, et al. A 3D Map of the Islet Routes Throughout the Healthy Human Pancreas. *Sci Rep* (2015) 5:14634. doi: 10.1038/srep14634
33. Zhu S, Larkin D, Lu S, Inouye C, Haataja L, Anjum A, et al. Monitoring C-Peptide Storage and Secretion in Islet Beta-Cells In Vitro and In Vivo. *Diabetes* (2016) 65(3):699–709. doi: 10.2337/db15-1264
34. Pinheiro JC, Bates DM. *Mixed-Effects Models in S and s-PLUS*. New York: Springer (2004).
35. Liu Y, Batchuluun B, Ho L, Zhu D, Prentice KJ, Bhattacharjee A, et al. Characterization of Zinc Influx Transporters (Zips) in Pancreatic Beta Cells: Roles In Regulating Cytosolic Zinc Homeostasis and Insulin Secretion. *J Biol Chem* (2015) 290(30):18757–69. doi: 10.1074/jbc.M115.640524
36. Chimienti F. Zinc, Pancreatic Islet Cell Function and Diabetes: New Insights Into an Old Story. *Nutr Res Rev* (2013) 26(1):1–11. doi: 10.1017/S0954422412000212
37. Haase H, Rink L. Functional Significance of Zinc-Related Signaling Pathways in Immune Cells. *Annu Rev Nutr* (2009) 29:133–52. doi: 10.1146/annurev-nutr-080508-141119
38. Li D, Chen S, Bellomo EA, Tarasov AI, Kaut C, Rutter GA, et al. Imaging Dynamic Insulin Release Using a Fluorescent Zinc Indicator for Monitoring Induced Exocytotic Release (ZIMIR). *Proc Natl Acad Sci USA* (2011) 108 (52):21063–8. doi: 10.1073/pnas.1109773109
39. Qian WJ, Aspinwall CA, Battiste MA, Kennedy RT. Detection of Secretion From Single Pancreatic Beta-Cells Using Extracellular Fluorogenic Reactions and Confocal Fluorescence Microscopy. *Anal Chem* (2000) 72(4):711–7. doi: 10.1021/ac991085t
40. Lo ST, Parrott D, Jordan MVC, Joseph DB, Strand D, Lo UG, et al. The Roles of ZnT1 and ZnT4 in Glucose-Stimulated Zinc Secretion in Prostate Epithelial Cells. *Mol Imaging Biol* (2021) 23(2):230–40. doi: 10.1007/s11307-020-01557-x
41. Yamasaki S, Sakata-Sogawa K, Hasegawa A, Suzuki T, Kabu K, Sato E, et al. Zinc is a Novel Intracellular Second Messenger. *J Cell Biol* (2007) 177(4):637–45. doi: 10.1083/jcb.200702081
42. Beyersmann D, Haase H. Functions of Zinc in Signaling, Proliferation and Differentiation of Mammalian Cells. *Biometals* (2001) 14(3-4):331–41. doi: 10.1023/A:1012905406548
43. Lemaire K, Chimienti F, Schuit F. Zinc Transporters and Their Role in the Pancreatic Beta-Cell. *J Diabetes Investig* (2012) 3(3):202–11. doi: 10.1111/j.2040-1124.2012.00199.x
44. Cauchi S, Del Guerra S, Choquet H, D'Aleo V, Groves CJ, Lupi R, et al. Meta-Analysis and Functional Effects of the SLC30A8 rs13266634 Polymorphism on Isolated Human Pancreatic Islets. *Mol Genet Metab* (2010) 100(1):77–82. doi: 10.1016/j.ymgme.2010.01.001
45. Ravier MA, Rutter GA. Glucose or Insulin, But Not Zinc Ions, Inhibit Glucagon Secretion From Mouse Pancreatic Alpha-Cells. *Diabetes* (2005) 54(6):1789–97. doi: 10.2337/diabetes.54.6.1789
46. Franklin I, Gromada J, Gjinovci A, Theander S, Wollheim CB. Beta-Cell Secretory Products Activate Alpha-Cell ATP-dependent Potassium Channels to Inhibit Glucagon Release. *Diabetes* (2005) 54(6):1808–15. doi: 10.2337/diabetes.54.6.1808
47. MacDonald PE, Rorsman P. Oscillations, Intercellular Coupling, and Insulin Secretion in Pancreatic Beta Cells. *PLoS Biol* (2006) 4(2):e49. doi: 10.1371/journal.pbio.0040049
48. Stefan Y, Meda P, Neufeld M, Orci L. Stimulation of Insulin Secretion Reveals Heterogeneity of Pancreatic B Cells *In Vivo*. *J Clin Invest* (1987) 80(1):175–83. doi: 10.1172/JCI113045
49. Wang X, Misawa R, Zielinski MC, Cowen P, Jo J, Periwal V, et al. Regional Differences in Islet Distribution in the Human Pancreas–Preferential Beta-Cell Loss in the Head Region in Patients With Type 2 Diabetes. *PLoS One* (2013) 8(6):e67454. doi: 10.1371/journal.pone.0067454
50. Kim A, Miller K, Jo J, Kilimnik G, Wojcik P, Hara M. Islet Architecture: A Comparative Study. *Islets* (2009) 1(2):129–36. doi: 10.4161/isl.1.2.9480
51. Nyman LR, Ford E, Powers AC, Piston DW. Glucose-Dependent Blood Flow Dynamics in Murine Pancreatic Islets *In Vivo*. *Am J Physiol Endocrinol Metab* (2010) 298(4):E807–14. doi: 10.1152/ajpendo.00715.2009
52. Carlbom L, Espes D, Lubberink M, Eriksson O, Johansson L, Jansson L, et al. Pancreatic Perfusion and Subsequent Response to Glucose in Healthy Individuals and Patients With Type 1 Diabetes. *Diabetologia* (2016) 59 (9):1968–72. doi: 10.1007/s00125-016-4016-2
53. MacDonald PE, Braun M, Galvanovskis J, Rorsman P. Release of Small Transmitters Through Kiss-and-Run Fusion Pores in Rat Pancreatic Beta Cells. *Cell Metab* (2006) 4(4):283–90. doi: 10.1016/j.cmet.2006.08.011

Conflict of Interest: CH, LG, SW, SC, MK, and JE were employed by Merck & Co., Inc. CP, one of the inventors of Gd-CP027, was employed by VitalQuan, LLC during the study. VitalQuan LLC licensed Gd-CP027 from the University of Texas and supplied the compound to Merck & Co., Inc.

The remaining authors declare that the research was conducted in the absence of any commercial or financial relationships that could be construed as potential conflict of interest.

Advantages of publishing in Frontiers

OPEN ACCESS
Articles are free to read for greatest visibility and readership

FAST PUBLICATION
Around 90 days from submission to decision

HIGH QUALITY PEER-REVIEW
Rigorous, collaborative, and constructive peer-review

TRANSPARENT PEER-REVIEW
Editors and reviewers acknowledged by name on published articles

Frontiers
Avenue du Tribunal-Fédéral 34
1005 Lausanne | Switzerland

Visit us: www.frontiersin.org
Contact us: frontiersin.org/about/contact

REPRODUCIBILITY OF RESEARCH
Support open data and methods to enhance research reproducibility

DIGITAL PUBLISHING
Articles designed for optimal readership across devices

FOLLOW US
@frontiersin

IMPACT METRICS
Advanced article metrics track visibility across digital media

EXTENSIVE PROMOTION
Marketing and promotion of impactful research

LOOP RESEARCH NETWORK
Our network increases your article's readership